2011

STUDIES RELATED TO COULOMBIC FISSIONS OF CHARGED DROPLETS AND HYGROSCOPIC BEHAVIOR OF MIXED PARTICLES

Harry Cook Hunter III
University of Kentucky, HHunter_01@yahoo.com

ABSTRACT OF DISSERTATION

Harry Cook Hunter, III

The Graduate School

University of Kentucky

2011

STUDIES RELATED TO COULOMBIC FISSIONS OF CHARGED DROPLETS AND HYGROSCOPIC BEHAVIOR OF MIXED PARTICLES

ABSTRACT OF DISSERTATION

A dissertation submitted in partial fulfillment of the
requirements for the degree of Doctor of Philosophy in the
College of Engineering
at the University of Kentucky

By
Harry Cook Hunter, III

Lexington, Kentucky

Director: Dr. Asit K. Ray, Professor of Chemical Engineering

Lexington, Kentucky

2010

ABSTRACT OF DISSERTATION

STUDIES RELATED TO COULOMBIC FISSIONS OF CHARGED DROPLETS AND HYGROSCOPIC BEHAVIOR OF MIXED PARTICLES

This dissertation describes two independent studies related to charged aerosols. The first study examines the role of electrical conductivity on the amounts of charge and mass emitted during the break-up of charged droplets via Coulombic fission. The second study examines the hygroscopic behavior of mixed particles. The results from both studies are presented here in detail along with an in-depth discussion of pertinent literature and applications in modern technologies.

Charged droplets break-up via a process termed Coulombic fission when their charge density reaches a certain level during which they emit a portion of their charge and mass in the form of progeny microdroplets. Although Rayleigh theory can be used to predict the charge level at which break-ups occur, no equivocal theory exists to predict the amounts of charge or mass emitted or the characteristics of the progenies. Previous investigations have indicated that the electrical conductivity of a charged droplet may determine how much charge and mass are emitted during its break-up via Coulombic fission. To further examine this supposition, charged droplets having known electrical conductivities were observed through multiple break-ups while individually levitated in an electrodynamic balance. The amounts of charge and mass emitted during break-ups were determined using a light scattering technique and changes in the DC null point levitation potentials of the charged droplets. Here, electrical conductivity was found to increase and decrease the amounts of charge and mass emitted, respectively, while having no effect on the charge level at which break-ups occurred. The findings of this investigation have significant bearing in nanoparticle generation and electrospray applications.

The hygroscopic behavior of atmospherically relevant inorganic salts is essential to the chemical and radiative processes that occur in Earth's atmosphere. Furthermore, studies have shown that an immense variety of chemical species exist in the atmosphere which inherently mix to form complex heterogeneous particles with differing morphologies. However, how such materials and particle morphologies affect the hygroscopic behavior of atmospherically relevant inorganic salts remains mostly

unknown. Therefore, the effects of water insoluble materials, such as black carbon, on the hygroscopic behavior of inorganic salts were examined. Here, water insoluble solids were found to increase the crystallization relative humidities of atmospherically relevant inorganic salts when internally mixed. Water insoluble liquids however, were found to have no effect on the hygroscopic behavior of atmospherically relevant inorganic salts. The findings of this investigation have significant bearing in atmospheric modeling.

KEYWORDS: charged droplets, Coulombic fission, hygroscopic behavior, electrodynamic balance, light scattering

Harry Hunter, III
Student's Signature

_____
Date

STUDIES RELATED TO COULOMBIC FISSIONS OF CHARGED DROPLETS AND HYGROSCOPIC BEHAVIOR OF MIXED PARTICLES

By

Harry Cook Hunter, III

Asit_Ray_____
Director of Dissertation

Stephen_Rankin_____
Director of Graduate Studies

_____

RULES FOR THE USE OF DISSERTATIONS

Unpublished dissertations submitted for the Doctor's degree and deposited in the University of Kentucky Library are as a rule open for inspection, but are to be used only with due regard to the rights of the authors. Bibliographical references may be noted, but quotations or summaries of parts may be published only with the permission of the author, and with the usual scholarly acknowledgments.

Extensive copying or publication of the dissertation in whole or in part also requires the consent of the Dean of the Graduate School of the University of Kentucky.

A library that borrows this dissertation for use by its patrons is expected to secure the signature of each user.

Name Date

_____

_____

_____

_____

_____

_____

_____

_____

_____

_____

_____

DISSERTATION

Harry Cook Hunter, III

The Graduate School

University of Kentucky

2011

STUDIES RELATED TO COULOMBIC FISSIONS OF CHARGED DROPLETS AND HYGROSCOPIC BEHAVIOR OF MIXED PARTICLES

DISSERTATION

A dissertation submitted in partial fulfillment of the
requirements for the degree of Doctor of Philosophy in the
College of Engineering
at the University of Kentucky

By
Harry Cook Hunter, III

Lexington, Kentucky

Director: Dr. Asit K. Ray, Professor of Chemical Engineering

Lexington, Kentucky

2011

Dedicated in the loving memory of my father

Harry Cook Hunter, Jr.

(November 19, 1945 – May 5, 2005)

and the recent birth of my daughter

Catherine Marie Hunter

(June 26, 2010)

ACKNOWLEDGMENTS

I would like to foremost extend my gratitude to my advisor Dr. Asit K. Ray for his guidance and support. I would like to thank the continual help provided by Mr. Jerry Vice, Mr. Bruce Cole, Dr. John Anthony, and the faculty, staff, and my fellow classmates at the department of Chemical and Materials Engineering at the University of Kentucky. I am appreciative of the support of my coworkers, past and present, Fred Li, Zhiqiang Gao, Michael Cusick, Venkat Rajagopalan, and Mark Warren. Most of all I want to thank my wife Margaret, my mother Charlotte, and my son Mason for their love and support as well my remaining relatives and all my friends. I would like to thank Matthew and Michelle Vincent and their family for opening their home to my wife, my son, and myself time and time again. I would like to thank my buddies Packer and Maverick for always listening. Finally, I would like to thank Robert and Larry Srygler and their families in Bonnieville, Kentucky, my true home, for teaching me that not all knowledge comes from a book and to never outsmart my common sense. Thank you all!

TABLE OF CONTENTS

LIST OF TABLES

LIST OF FIGURES

Chapter 1: Introduction

1.1 General Introduction

Aerosols play an indispensible role in both atmospheric processing and modern technology. As such, research in this field has found no shortage of relevance, interest, or application. Although aerosols can be simply defined as solid particles or liquid droplets suspended in a gaseous medium, their behaviors are immensely complex and still not fully understood. This dissertation examines two specific areas of aerosol research that remain unknown. First, what are the physical properties of charged droplets that determine how much charge and mass are emitted during their break-up via Coulombic fission and how do such properties affect the characteristics of the progeny microdroplets formed during break-ups? Furthermore, can these properties be manipulated to improve current industrial applications such as electrostatic spraying? Second, how is the hygroscopic behavior of atmospherically relevant inorganic salt particles affected when they are mixed with non-volatile, hydrophobic compounds? Also, how do the individual components within mixed particles combine and do different morphologies exhibit different behaviors? The work presented here is a continued effort to resolve such questions.

In Chapter 2, a detailed background of current and previous research and modern technological applications is given providing a basis for the focus of this dissertation. Chapter 3 describes in detail the equipment used for data collection to better understand the fission and growth processes of single particles. Chapter 4 discusses the theories underlying the research performed here and their application in analyzing collected data. Chapters 5 and 6 are devoted to the results obtained from the Coulombic fissions of charged droplets and the hygroscopicity of mixed particles, respectively. Chapters 5 and 6 also include discussions related to pertinent literature and conclusions for the corresponding subjects. Finally, Chapter 7 provides general conclusions to the work presented in this dissertation and its impacts on modern technology and future research.

1.2 Introduction to the Study of Charged Droplets

Over a century ago, Lord Rayleigh (Rayleigh, 1882) theoretically determined the charge level at which a purely conductive, spherical droplet would break-up via Coulombic fission given by

$$q_R = 8\pi\sqrt{\varepsilon_0 \gamma a^3} \tag{1.1}$$

where ε_0, γ, and a are the permittivity of free space, the surface tension of the droplet, and the droplet radius, respectively. Although Rayleigh's limit has been repeatedly validated (Duft et al., 2002; Manil et al., 2003; Li et al., 2005; Hogan et al., 2009), even for dielectric droplets (Richardson et al., 1989; Grimm and Beauchamp, 2002; Li et al., 2005; Nakajima, 2006), no equivalent theory has been developed to explain the disparity reported for the amounts of charge and mass emitted during the break-up of charged droplets via Coulombic fission. For example, droplets of sulfuric acid have been observed to emit 50% of their charge while emitting no detectable mass (Richardson et al., 1989) whereas droplets of diethyl phthalate have been observed to emit only 21% of their charge, but over 2% of their mass (Li et al., 2005) even though both types of droplets were observed to proceed through break-ups via Coulombic fission at their corresponding Rayleigh limits and both were studied using comparable electrodynamic balances. Furthermore, the numerous hypotheses that exist for predicting the characteristics of progeny microdroplets often rely on assumed values for the amounts of charge and mass emitted during a break-up (Roth and Kelly, 1983; Tang and Smith, 1999) or the charge level of the primary droplet after a break-up (Li et al., 2005) and none have been experimentally substantiated. In order to more fully understand the factors pertaining to the amounts of charge and mass emitted by charged droplets during their break-ups at the Rayleigh limit and the characteristics of the progeny microdroplets formed, experiments were conducted on dielectric droplets containing various amounts of ionic dopants. This dissertation details the work performed, results discovered, and a discussion of pertinent literature related to the break-up of charged droplets via Coulombic fission at the Rayleigh limit.

1.3 Introduction to the Study of Mixed Particles

Hilding Kohler (1936) was the first to use thermodynamics to explain how the size and number density of droplets found in fogs and frosts were directly related to the amount of NaCl located within the droplets. Since Kohler's seminal paper, an immense variety of compounds have been identified in Earth's troposphere (Saxena and Hildemann, 1996; Kanakidou et al., 2005) and observed to exist as mixed particles composed of multiphase mixtures of organic and inorganic components (Posfai et al., 1999; Semeniuk et al., 2007a,b; Wise et al., 2007; Adachi and Buseck, 2008; Eichler et al., 2008). Although certain hygroscopic properties of some mixed particles can typically be ascertained from their bulk solution counterparts (Tang, 1976; Tang et al., 1978; Cohen et al., 1987b; Tang and Munkelwitz, 1993), and several predictive models have been developed that provide reasonable estimates of particle properties such as composition and phase (Clegg, 1992;1997;1998a,b; Carslaw et al., 1995; Clegg and Brimblecombe, 1995; Chan et al., 1997), no widespread theory currently exists that can completely and accurately predict the hygroscopic behavior of mixed particles even though numerous mixed particle systems have been investigated (Martin, 2000). Furthermore, many questions persist regarding how the individual components within mixed particles combine and how different particle morphologies may affect hygroscopic behavior. For example, Colberg et al. (2004) have proposed eight different morphologies for mixed particles formed from various ratios of H_2SO_4, NH_3, and H_2O and reported that ascertaining the correct morphology is "…not easily predictable." Also, inorganic salt particles have been observed to still deliquesce and exhibit hygroscopic growth despite being completely externally coated by a non-volatile, hydrophobic compound (Otani and Wang, 1984; Hansson et al., 1990;1998; Hameri et al., 1992; Xiong et al., 1998). In an effort to better understand how the hygroscopic behavior of mixed particles is affected by their individual components and morphologies, experiments were conducted on atmospherically relevant inorganic salts mixed with non-volatile, hydrophobic materials. This dissertation details the work performed, results discovered, and a discussion of pertinent literature related to the hygroscopic behavior of mixed particles.

Chapter 2: Background

2.1 Characteristics of Charged Droplet Break-ups via Coulombic Fission

2.1.1 Introduction

The characteristics of charged droplets are vital to many current technologies as nearly every droplet generation process, even those in the absence of an external electric field, imparts a certain amount of positive or negative charge on a droplet. The most familiar of these is likely the use of electrospray mass spectrometry for the ionization of large biomolecules. However, many modern applications of charged droplets are likely implemented without realization. The charging of insect repellent sprays used in agriculture allows farmers to extend protection to the underside of the leaves on their crops (Law, 2001). Current electrostatic spray painting systems create less waste and provide a more even distribution since the paint molecules are charged opposite to the corresponding structure (Hines, 1966). The charge to mass ratio of pharmaceutical ingredients can be manipulated to affect mixing kinetics (Lachiver et al., 2006) and determine their deposition in either the throat or lungs (Ali et al., 2009). The developments of anti-static fuel additives and better grounding techniques have nearly eliminated hydrocarbon related explosions corresponding to static discharge (Bustin and Dukek, 1983). Electrostatic precipitators filter industrial plumes as well as our homes by charging and then attracting unwanted contaminants (Constable and Somerville, 2003).

Although charged droplets have become indispensible to modern life, the processes through which they are formed and eventually become gas phase ions remain an enigma. In the remainder of this chapter, the current state of literary knowledge related to the break-up of charged droplets is discussed. Of primary interest here is the break-up of charged droplets via Coulombic fission at their Rayleigh limit, the factors pertaining to the amounts of charge and mass emitted during a break-up, and the characteristics of the progeny microdroplets formed.

2.1.2 Coulombic Fission

A Coulombic fission occurs according to Rayleigh theory as given by (1.1) when the charge density of a droplet increases to a certain level during the loss of neutral solvent molecules through evaporation. As the droplet volume is reduced during evaporation, the net charges of like sign residing on the droplet surface are subsequently forced into a tighter proximity thereby increasing their combined electrostatic repulsion in opposition to the cohesive force of the droplet's surface tension. At a certain point, the electrostatic repulsion begins to disrupt the spherical geometry and the droplet is forced into a more elliptical shape similar to that of a lemon or a football (Duft et al., 2003; Achtzehn et al., 2005; Giglio et al., 2008). When the opposing forces of electrostatic repulsion and surface tension become equal, the droplet emits a portion of its charge and mass through the apices of conical shaped tips, termed cone-jets, located at the opposing ends of the ellipsoidal shaped droplet via a stream of monodisperse progeny microdroplets (Duft et al., 2003; Achtzehn et al., 2005; Giglio et al., 2008).

The formation and structure of these cone-jets have been extensively studied using liquids charged to a sufficiently high electrical potential at the end of a capillary needle (Taylor, 1964;1966;1969; Melcher and Taylor, 1969). Taylor (1964) has reported that a specific conical structure, currently termed a Taylor cone, having a semi-vertical angle of 49.3° results from the balance of electrostatic and capillary forces on the liquid surface. However, Cloupeau (1986a,b) and Cloupeau and Prunet-Foch (1989;1990;1994) later described a wide variety of cone-jets and Giglio et al. (2008) has recently purported that the cone-jets are significantly narrower with an angle of 39° and are more 'lemon-like' in shape.

After emitting a certain portion of its charge and mass, the droplet then returns to a spherical geometry and the evaporation process continues. The processes of evaporation and Coulombic fission continue for both the primary and progeny microdroplets until only gas phase ions remain. Such charged droplets which break-up

via Coulombic fission at their Rayleigh limit are investigated and discussed in this dissertation.

Figure 2.1 depicts the processes of evaporation, Coulombic fission, and progeny microdroplet formation for a droplet of diethyl phthalate (DEP). For simplicity, the deformation of the droplet into an elliptical shape is omitted from the figure. The droplet is shown with an initial radius of a = 15 μm and a charge of $q = 4.5 \times 10^{-13}$ C. For a Coulombic fission to occur, the droplet must evaporate via loss of neutral solvent molecules until it has a radius of a = 10 μm assuming a surface tension of γ = 36.1 mN/m (Li et al., 2005). At the instant prior to its break-up, the droplet's charge corresponds to only a single elementary charge per 4.5×10^{6} molecules of DEP. This exemplifies why even the slightest change in a droplet's charge can affect the fission process. Assuming such a droplet emits 20.8% of its charge and 2.28% of its mass during a fission (Li et al., 2005), the droplet's charge and radius are reduced to $q = 3.56 \times 10^{-13}$ C and a = 9.92 μm, respectively. Li et al. (2005) have purported that such a droplet of DEP would form three progeny microdroplets having equal charge and size. Therefore, the charge and radius of an individual progeny droplet would be $q = 3.12 \times 10^{-14}$ C and a = 1.97 μm, respectively. After a fission, the primary droplet must continue to evaporate until its radius is reduced to a = 8.56 μm for another Coulombic fission to occur. In order for the size of the primary droplet to be reduced to that of the progeny microdroplets first produced, it must undergo ten additional fissions at which point its radius will have been reduced to a = 1.79 μm.

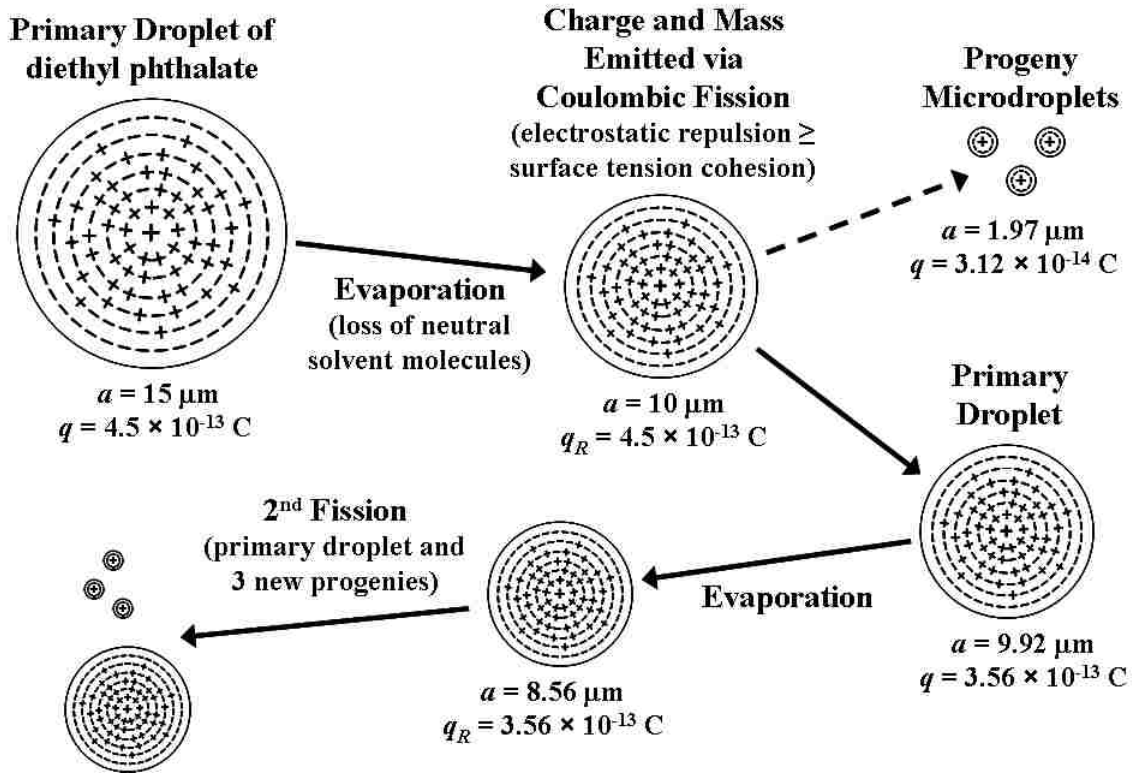

Figure 2.1 Illustration of the evaporation, Coulombic fission, and progeny droplet formation for a droplet of diethyl phthalate.

2.1.3 Validity of Rayleigh Theory

A common theme in the literature pertaining to the break-up of charged droplets is the validity of Rayleigh theory. Specifically, investigators typically report the charge levels at which they observed break-ups to occur respective of the charge limits predicted by Rayleigh theory. Most initial investigators reported they observed charged droplets to break-up via Coulombic fission at their respective Rayleigh limits (Doyle et al., 1964; Abbas and Latham, 1967; Schweizer and Hanson, 1971; Roulleau and Desbois, 1972) even though the droplets studied were not purely conductive as required under Rayleigh theory. Several investigators however, have reported they observed charged droplets to break-up at charge levels from as low as 3% (Widmann et al., 1997) to as high as 200% (Li and Ray, 2004) of their respective Rayleigh limits. However, the most recent and accurate investigations have shown Rayleigh theory to hold true (Duft et al., 2002; Manil et al., 2003; Li et al., 2005; Nakajima, 2006; Hogan et al., 2009), even for charged droplets as small as 40 nm in diameter (Hogan et al., 2009).

In fact, most of the instances where non-Rayleigh break-ups have been observed have since been explained. Duft et al. (2002) have asserted that even trace amounts of a contaminant can noticeably reduce the surface tension of a charged droplet and thereby lower the charge level at which break-ups occur. Taflin et al. (1988) had previously suggested that the surface tensions of their droplets were possibly affected by contamination. However, they stated that the surface tension of their dodecanol droplets would have to be reduced from 19.14 $mN \cdot m^{-1}$ to 13.3 $mN \cdot m^{-1}$ for break-ups to occur precisely at the Rayleigh limit. They concluded that such a significant lowering in surface tension was unlikely and that the sub-Rayleigh break-ups they observed were valid. In a later study by Taflin et al. (1989), they again acknowledged that contamination of the droplet surface could be responsible for their observations of sub-Rayleigh break-ups. They also purported that the applied electric fields could have affected the charge levels at which break-ups occurred. However, Davis and Bridges (1994) have examined the role of the electric field and concluded that it did not affect droplet stability. Only in the case of field-induced droplet ionization, where very high

electrical fields are applied, have the break-up of charged droplets been proven to occur at sub-Rayleigh charge levels. Li et al. (2005) have also commented on the sub-Rayleigh break-ups reported by Taflin et al. (1989) and suggested that either the geometric balance constant they used was incorrect or their sizing technique used was inadequate. Gomez and Tang (1994) have suggested that aerodynamic effects may have contributed to their observations of sub-Rayleigh break-ups.

Widmann et al. (1997) have purported the sub-Rayleigh charge levels they observed at break-up resulted from the photosensitive nature of the halogenated compounds in their droplets. They purport that decomposition of the compounds may have led to gas formation within the droplet or that Marangoni instability resulted from the polymerization of the monomer. Their presumption may in fact be correct as Donaldson et al. (2001) have theoretically discussed the ability of droplets to spontaneously divide into equal fragments under certain thermodynamic conditions. Namely, they have discussed droplets coated with a thin film of a long-chain fatty acid that collapses in on itself causing droplet break-up to occur. Donaldson et al. (2001) concluded that the same type of droplet break-up would be possible for droplets with surface active species that could undergo polymerization on the droplet surface.

Shrimpton (2005) has proposed an extension to Rayleigh's theory that incorporates the dielectric nature of some charged droplets in an attempt to explain sub-Rayleigh limit break-ups. He suggests that dielectric droplets contain an internal electric field that causes polarization and aligns the molecules within charged droplets according to the applied electric field. The polarization is purported to induce a charge on the droplet surface which increases the total charge on one side and reduces it on the other such that one side of the droplet is always unstable relative to the other. This effect is purported to be more prominent for larger size droplets and was found to be the case for low permittivity droplets. The results from his model show that the droplet charge varies with $a^{3/2}$ whereas the induced charge varies with a^2, where a is the droplet radius, and that droplet break-up will always occur when the surface tangent is normal to the direction of the electric field.

Li and Ray (2004) have shown that charged droplets containing a precipitate will not break-up until they reach as much as twice their Rayleigh limit. Their work explains why Cederfelt et al. (1990) and Smith et al. (2002) have both observed that charged droplets of various compounds containing NaCl experienced break-ups well above their respective Rayleigh limits. The results by Li et al. (2004) were later supported by the findings of Bakhoum and Agnes (2005) who reported that droplets of water and water/glycerol containing either a NaCl precipitate or 20 nm fluospheres did not undergo Coulombic fission until the Rayleigh limit was significantly exceeded.

The instances where charged droplets have been reported to break-up at charge levels other than predicted by Rayleigh theory have been shown to be the result of droplet contamination or an incorrectly determined charge level. As such, Rayleigh theory is currently held as valid for charged droplets that are purely liquid in phase and are stably levitated. This assertion is later shown to be true for the charged droplets studied as part of this dissertation.

2.1.4 Charge and Mass Emissions during Coulombic Fission

Although Rayleigh theory can be used to predict the charge level at which a charged droplet will break-up via Coulombic fission, no equivocal theory exists that can predict how much charge and mass will be emitted during fission. The disparity between how much charge and mass is emitted by charged droplets during a Coulombic fission persists even where they have been observed to break-up precisely at their Rayleigh limit. This is clearly shown by the results of Li et al. (2005) who have observed that charged droplets of triethylene glycol emitted over 40% of their charge and less than 0.03% of their mass, whereas charged droplets of diethyl phthalate emitted 21% of their charge and 2.3% of their mass, even though both droplet types were observed to break-up via Coulombic fission precisely at their Rayleigh limits. In fact, the disparity between how much charge and mass is emitted by charged droplets found in recent literature ranges from 7% to 49% for the amount of charge emitted (Nakajima, 2006; Richardson et al., 1989) and from less than 0.03% to over 2% for the amount of mass emitted (Li et al., 2005) for pure

component droplets, and a wider disparity has been purported for other droplet conditions (Taflin et al., 1989) and in older literature (Abbas and Latham, 1967).

Table 2.1 lists the charge and mass emissions from charged droplets found in literature. The table lists the droplet compounds in alphabetical order, gives the amounts of charge and mass emitted by each droplet compound, the corresponding droplet size and equipment used, and the literature source. When available, the diameter of the droplet immediately prior to fission was listed. Also, several investigators were unable to measure the amount of mass emitted during a fission as it was below the detectable limit of their equipment. These instances and others have been identified and explained with a corresponding tag number. The equipment used for a particular investigation has been listed within the table using a set of corresponding initials which are expounded below it. The range of data values presented in the table exemplifies the need for a more thorough understanding of the droplet factors that determine how much charge and mass will be emitted during the break-up of a charged droplet via Coulombic fission.

Table 2.1 List of droplet compounds and corresponding charge and mass emissions observed by previous investigators. (Table 2.1 continues on pages 13 and 14.)

Compound	Charge Emitted during a Fission (%)	Mass Emitted during a Fission (%)	Droplet Diameter μm	Experimental Setup	Investigators
acetonitrile	15 - 20	[3]	5 – 40	PDI	Smith et al., 2002
analine	~ 25	~ 25	60 - 400	EDB	Abbas & Latham, 1967
analine	~ 30	[3]	60 - 250	EDB	Doyle et al., 1964
bromo-dodecane	12	N/A	43.48[1]	EDB	Taflin et al., 1989
BTD / IDD[9]	20.9 & 74.0[2]	24.3 & 75.4[2]	30.5 & 27.8	EDB	Widmann et al., 1997
dibromo-octane	14 - 18	1.55 - 2.23	27.722 - 38.474[1]	EDB	Taflin et al., 1989
dibutyl phthalate[8]	1 - 63.1	2 – 75	12.8 - 21.2[1]	EDB	Taflin et al., 1989
dibutyl phthalate	10 - 27	3 – 18	3 – 18	LDV	Nakajima, 2006
diethylene glycol	37.7	<0.03	30	EDB	Li et al., 2005
diethyl phthalate	20.8	2.28	30	EDB	Li et al., 2005
dioctyl phthalate	~ 30	[3]	60 - 250	EDB	Doyle et al., 1964
dioctyl phthalate	15.0	2.25	1 – 10	EDB	Richardson et al., 1989
dodecanol	17.7	3.9	8.724[1]	EDB	Taflin et al., 1988
dodecanol	13 - 17	2.0	32.26 - 35.56[1]	EDB	Taflin et al., 1989
1-dodecanol	N/A	1.65 & 2.35[2]	22.40 & 20.76[1]	EDB	Davis & Bridges, 1994
ethylene glycol	25	[3]	~ 25.5[4]	EDB	Duft et al., 2002
ethylene glycol	33	0.30	24[1]	EDB	Duft et al., 2003
ethylene glycol	25	[3]	100	EDB	Manil et al., 2003

[Table 2.1 continued]

ethylene glycol	28 - 35	[3]	3 - 18	LDV	Nakajima, 2006
heptadecane	9.5 - 14	0.98 - 2.3	29.072 - 36.144[1]	EDB	Taflin et al., 1989
n-heptane[6]	19	[3]	3 - 60	PDA	Grimm & Beauchamp, 2002
hexadecane	15.3	1.48	30	EDB	Li et al., 2005
hexadecane	14 - 18	1.5 - 1.6	29.12 - 65.16[1]	EDB	Taflin et al., 1989
isopropyl benzene	~ 30	[3]	60 - 250	EDB	Doyle et al., 1964
methanol	81	~ 55[5]	84	EDB	Feng et al., 2001
methanol[7]	15 - 30	[3]	5 - 40	PDI	Smith et al., 2002
n-octane[6]	17	[3]	3 -60	PDA	Grimm & Beauchamp, 2002
n-octanol	23	5	15 - 40	EDB	Schweizer & Hanson, 1971
pentadecane	7 - 13	0.7 - 1	3 - 18	LDV	Nakajima, 2006
sulfuric acid	49.4	< 0.1%	1 - 10	EDB	Richardson et al., 1989
toluene	~ 25	~ 25	60 - 400	EDB	Abbas & Latham, 1967
triethylene glycol	41.1	<0.03	30	EDB	Li et al., 2005
water	~ 30	[3]	60 - 250	EDB	Doyle et al., 1964
water	~ 25	~ 25	60 - 400	EDB	Abbas & Latham, 1967
water	16 - 40	[3]	50 - 200	EDB	Roulleau & Desbois, 1972
water	20 - 40	[3]	5 - 40	PDI	Smith et al., 2002
p-xylene[6]	17	[3]	3 - 60	PDA	Grimm & Beauchamp, 2002

[Table 2.1 continued]

N/A	not available

EDB	electrodynamic balance
PDA	phase Doppler anemometer
PDI	phase Doppler interferometer
LDV	laser Doppler velocimeter

[1]	droplet diameter at fission
[2]	respective to order of corresponding droplet diameters given
[3]	below the detectable limit
[4]	estimated from Fig. 1 in Duft et al. (2002)
[5]	calculated from data given in Table 2 in Feng et al. (2001)
[6]	a small concentration of Stadis-450 was added to control droplet size
[7]	some droplets were reported to contain up to 10^{-4} M NaCl
[8]	droplets were exposed to gas ionized via β emission from C^{14}-tagged dibutyl phthalate
[9]	1-bromotetradecane (BTD) with 33% by volume iododecane (IDD)

The disparity between how much charge and mass is emitted by charged droplets during a Coulombic fission has been previously noted and discussed by some investigators. Schweizer and Hanson (1971) have acknowledged the variances observed between different droplet compounds during droplet break-ups and asserted that "…it is not inconceivable that the charge and mass of the mother [primary droplet] could depend on the substance used." Li et al. (2005) have stated that "…the amounts [of charge and mass emitted during Coulombic fission] are related to the droplet properties, such as the surface tension, dielectric constant, and electrical conductivity." Their findings mirror those of Richardson et al. (1989) who have observed that droplets with higher electrical conductivity emitted more charge and less mass than droplets that were relatively dielectric. Shrimpton (2005) has also commented on the matter stating that, "It is notable that the measured critical charge for a particular liquid was similar, even for different sized droplets, and that it was different for each liquid which may suggest the critical charge depends in some way on the material properties." The comments by the aforementioned investigators and the data presented in Table 2.1 suggest that certain droplet properties may in fact determine how much charge and mass are emitted by a charged droplet during a break-up via Coulombic fission. This assertion is later shown to be true for the charged droplets studied as part of this dissertation.

2.1.5 Characteristics of Progeny Microdroplet Formation

The lack of understanding pertaining to the disparity observed for the amounts of charge and mass emitted by charged droplets during their break-ups via Coulombic fission is directly extended to the characteristics of the progeny microdroplets formed during such break-ups. Here too, no proven, comprehensive theory exists that can predict the size, charge density, or number of progeny droplets formed during the break-up of charged droplets. As such, some investigators have assumed values for the amounts of charge and mass emitted by a droplet during break-up to predict the characteristics of the progeny microdroplets formed (Roth and Kelly, 1983; Tang and Smith, 1999). Moreover, the number of progeny droplets predicted to be formed is found to range from a maximum of seven (Roth and Kelly, 1983) to several thousand (Li et al., 2005). Investigators have

also developed models that assert the progeny microdroplets are of equal size (Pfeifer and Hendricks, 1967; Li et al., 2005). Such assumption is not without merit as photographs have long shown that progeny microdroplets are formed approximately equal in size (Macky, 1931; Duft et al, 2003). Some investigators have also asserted that such progenies would be of equal charge (Li et al., 2005), although Konermann (2009) has recently developed a model suggesting that the charge on each successive progeny microdroplet formed is slightly reduced to the previous one. Investigators have also developed predictive models that assume a relationship between the charge on the primary droplet and the charge on the progeny microdroplets (Li et al., 2005) rely on the surface and kinetic energies of the primary droplet (Storozhev and Nikolaev, 2004) and use scaling laws to relate the formation of progeny microdroplet from charged droplets to those formed from the tips of electrified capillary tubes (de la Mora, 1996; Gu et al., 2007).

De la Mora (1996) has purported that the sizes of the progeny microdroplets formed by the charge and mass emitted during the break-ups of charged droplets are determined by the charge relaxation length, d_m, of the primary droplet according to

$$d_m = \left(\frac{\gamma \varepsilon^2 \varepsilon_0^2}{K^2 \rho} \right)^{1/3} \tag{2.1}$$

where ε_0 is the permittivity of free space, and γ, ρ, ε, and K are the surface tension, density, dielectric constant, and electrical conductivity of the liquid, respectively. He suggests that progeny microdroplets are formed through either 'rough fission' or 'fine fission' modes where the latter occurs only when d_m is much smaller than the diameter of the primary droplet. During a rough fission, the progeny microdroplets that are formed are purportedly few in number and have sizes and charge densities that are comparable to that of the primary droplet. For a fine fission however, a vast multitude of highly charged progenies having almost no mass, even collectively, are purported to be formed. According to de la Mora (1996), rough and fine fissions are likely to occur for droplets of dielectric and electrically conductive compounds, respectively. His assertion is qualitatively supported by a previous study by Richardson et al. (1989) and has been more recently validated by the findings of Li et al. (2005). In both studies, the

investigators found that relatively dielectric droplets emitted a small fraction of their charge and a noticeable amount of their mass, whereas more electrically conductive droplets were found to emit a large portion of their charge, but no detectable amount of mass.

Figure 2.2 illustrates the two modes of fission purported by de la Mora (1996). The two droplets shown at the bottom of the figure have the same initial size and charge. However, the droplet on the left represents a dielectric droplet whereas the droplet on the right is more electrically conductive. The dielectric droplet is shown to undergo a 'rough' fission. It produces only a few progeny microdroplets having sizes and charge densities that are comparable to the primary droplet. The electrically conductive droplet is shown to undergo a 'fine' fission. It produces a multitude of highly charged progenies and significant charge, but almost no mass.

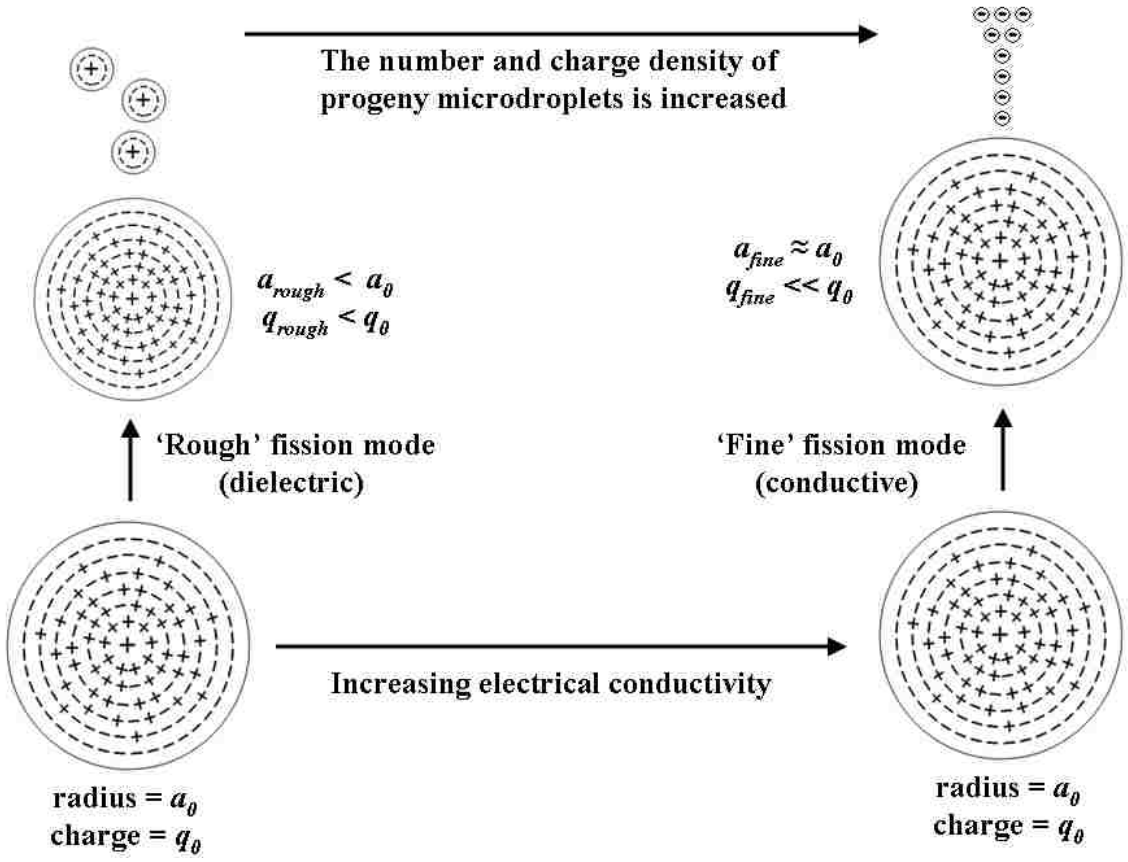

Figure 2.2 Illustration of the 'rough' and 'fine' fission modes purported by de la Mora (1996).

Recently, Gu et al. (2007) have added a constant to de la Mora's (1996) charge relaxation length given by (2.1) and purport that the radius of a progeny microdroplet, a_p, can be determined using

$$a_p = \left(\frac{3 \cdot 2^8 \gamma \varepsilon^2 \varepsilon_0^2}{\pi^6 \rho K^2} \right)^{1/3} = \left(\frac{3\pi}{2^8} \right)^{1/3} r_{jet} \tag{2.2}$$

where γ, ε_0, ρ, K, and r_{jet} are the surface tension, permittivity of free space, density, electrical conductivity, and initial cone-jet radius, respectively. The investigators suggest however, that the relationships provided in their publication should be used as scaling laws rather than exact equations.

The findings of the aforementioned authors all strongly indicate that the electrical conductivity of the primary droplet plays a critical role in the determining the characteristics of progeny microdroplets. From here, the logical point of departure is to more closely examine the effects of electrical conductivity on the amounts of charge and mass emitted by charged droplets during their break-ups at the Rayleigh limit and the characteristics of the progeny microdroplets formed during such break-ups.

2.1.6 Formation of Gas Phase Ions

The process by which a charged droplet eventually forms gas phase ions has been a source of dispute for nearly half of a century now and has culminated in two distinct ideologies. The first of these was originally proposed by Dole et al. (1968) and has since been termed the charge residue model. Here gas phase ions are formed after all neutral solvent molecules have evaporated. Nearly a decade later, Iribarne and Thomson (1976) proposed a competing view for ion formation termed the ion evaporation model. Here, an ion is emitted from a group of molecules. It is important to note however, that the ion evaporation model does not necessarily contradict the charge residue model in that the hypothesis supporting the ion evaporation model is only valid so long as enough electrostatic energy is provided and that the critical size of the group of molecules is larger than the subsequent solid residue and the size corresponding for the Rayleigh limit.

Rollgen et al. (1987) and Schmelzeisen-Redeker et al. (1989) have disputed the validity of the ion evaporation model. Rollgen et al. (1987) claimed "…that ion evaporation is unlikely to occur for most solute/solvent systems and of no significance in the formation of gaseous ions." However, Rollgen et al. (1987) did acknowledge that such mechanism could take place for ions with surface active properties. Schmelzeisen-Redeker et al. (1989) stated that, "The mechanism of field induced ion evaporation is shown to depend on some rather unrealistic assumptions and should not contribute to the desolvation of ions." Still, Fenn (1993) has commented that "…most investigators now believe that the IEM [ion evaporation model] of Iribarne and Thomson is more widely applicable than the CRM [charge residue model] of Dole", although the charged residue model had been previously validated by the work of Nohmi and Fenn (1992) for the analysis of polyethylene oxide oligomers with molecular weights of 5,000,000.

Loscertales and de la Mora (1995) have measured the charges and diameters of the particles from a monodisperse cloud of charged droplets and concluded that the resulting 'small' ions were produced via field-emission and could not be explained by the charge residue model. Labowsky et al. (2000) have developed a model to determine the solvated energy of an ion inside of a liquid droplet based on the physical properties of the droplet. They claim that their model, when applied with experimental data, predicts a small region where ion evaporation exists for small droplets charged near the Rayleigh limit having twelve or less individual charges. Their work was later supported by Ichiki and Consta (2006) who conducted constant temperature molecular dynamics simulations of small clusters of up to 1600 water molecules with up to eleven chloride ions and primarily observed that the clusters emitted single ions solvated by a shell of water molecules and that such emissions occurred when the charge on the cluster was at 87% of the Rayleigh limit. Hogan et al. (2009) have recently observed that mixed methanol-water droplets having diameters between 10 and 40 nm emitted ions and maintained a constant electric field of 1.1 $V \cdot nm^{-1}$ as predicted by Iribarne and Thomson (1976).

Disagreement still exists however as Rohner et al. (2004) have purported that the model proposed by Iribarne and Thomson (1976) underestimates the number of surface charges for droplets produced in an external electrical field. Recently, Consta (2010) has reported that single ions do not spontaneously escape droplets when a highly charged macroion is present, but form stable complexes, although only for brief time periods. Moreover, in such occurrences, the use of Rayleigh's model was found to no longer be valid to describe the droplet energy. The work by Consta (2010) is likely the first to begin bridging the gap between the charge residue model of Dole et al. (1968) and the ion evaporation model of Iribarne and Thomson (1976).

2.1.7 Summary

Although Rayleigh theory has been shown to be a valid means of predicting when a charged droplet will break-up via Coulombic fission, there are still no means by which to predict how much charge and mass will be emitted or the characteristics of the progeny microdroplets formed. A review of relevant literature has shown that droplets that are relatively more electrically conductive tend to emit more charge and less mass in the form of a multitude of highly charged progeny microdroplets, whereas relatively more dielectric droplets tend to emit less charge and more mass in the form of a few moderately charged progeny microdroplets. Furthermore, the means by which gas phase ions are produced has been shown to depend on the size of the charged molecules originally contained within a charged droplet. Here, literature suggests that small ions will be formed via the ion evaporation model, whereas extremely large ions will form via the charge residue model. The work presented in the remainder of this dissertation is an effort to better understand the role of electrical conductivity during the break-up of charged droplets via Coulombic fission at their Rayleigh limit.

2.2 Hygroscopic Behavior of Mixed Particles

2.2.1 Introduction

The hygroscopic behavior of atmospheric particles is directly related to the quality of life on Earth (Guenther et al., 1995; Raes et al., 2000; Kanakidou et al., 2005; Fuzzi et al., 2006). Therefore, a more complete understanding of such behavior is a truly important objective. The complexity of this objective however, is further complicated by mankind's impact on the atmosphere. Anthropogenic contaminants in the atmosphere have been shown to negatively impact the quality of the air we breathe (Posfai et al., 1999; Adachi and Buseck, 2008; Eichler et al., 2008), the water we drink (Rae et al., 2000), and the ability of our skies to protect us from harmful radiation (Hobbs et al., 1997; Haywood et al., 1999; Charlson et al., 2001). Global atmospheric investigations conducted at the turn of the millennia found that over 10×10^{12} $kg \cdot yr^{-1}$ of particulate matter were emitted into Earth's atmosphere, of which more than 50% was sea-salt from ocean spray and approximately 45% was mineral dust from wind-blown soils (Raes et al., 2000). The remainder of the annual global emission rate consisted of sulfates, organics, and black carbon primarily resulting from the intentional burning of biomass and fossil fuels (Raes et al., 2000). Yet, even though anthropogenic materials constituted only a minute fraction of the global emissions, they accounted for almost 25% of the radiative climate forcing observed in the troposphere during the same time period (Haywood et al., 1999).

However, the true impact of anthropogenic particulates is not fully portrayed by global emission rates. For example, the atmospheric concentration of black carbon over rural populated regions has been observed to be up to 40 times higher than over remote oceanic regions (Posfai et al., 1999) and biomass burning has been reported to account for over half of the organic fine particulate matter (= 2.0 μm) that was emitted into the lower troposphere at the end of the millennia (Jacobson et al., 2000). Furthermore, agricultural shifting via biomass burning continually exposes tens of thousands of square miles of land once covered by vegetation to the elements (Crutzen and Andreae, 1990;

Lauk and Erb, 2009) and therefore contributes to the emission rate of mineral dust. In addition, the effects of biomass burning are compounded since more than half of the land-based biomass is located underground and is gradually uncovered during burnings (Crutzen and Andreae, 1990).

Anthropogenic particles are not limited to geographic regions near populated areas, however. Atmospheric particles collected over remote parts of the Southern Ocean found that up to 45% contained soot inclusions that were directly linked to anthropogenic sources (Posfai et al., 1999). These types of particles have been observed to co-exist as heterogeneous mixtures of organic, inorganic, and carbonaceous materials (Semeniuk et al., 2007a,b; Wise et al., 2007; Adachi & Buseck, 2008; Eichler et al., 2008; Wex et al., 2008) and to significantly impact atmospheric chemistry (Crutzen and Andreae, 1990; Ellison et al., 1999; Jacobson et al., 2000; Raes et al., 2000; Donaldson et al., 2001; Kanakidou et al., 2005; Donaldson and Vaida, 2006; Fuzzi et al., 2006). However, the most significant effect of anthropogenic materials is possibly their effect on the hygroscopic behavior of atmospheric particles as it directly impacts the development, behavior, and lifetime of clouds (Kulmala et al., 1996; Charlson et al., 2001; Raymond and Pandis, 2003; Wex et al., 2008) and the radiative balance of Earth's atmosphere (Pilinis et al., 1995; Hobbs et al., 1997; Haywood et al., 1999; Raes et al., 2000; Kanakidou et al., 2005). Atmospheric chemistry involving organics has been found to affect rainwater acidification, NO_2 production, biogeochemical processing, and the formation of secondary organic aerosols (Jacobson et al., 2000). Furthermore, reactions occurring at the surface of organically coated particles can be significantly different than those of bulk phase reactions (Donaldson and Vaida, 2006). Surface active organics, such as surfactants, have been reported to affect the surface tension, diffusion, and solubility of particles (Latif and Brimblecombe, 2004) and to even cause the spontaneous division of particles through film collapse (Donaldson et al., 2001). As such, the presence of anthropogenic materials in the atmosphere immensely complicates the ability of investigators to accurately model atmospheric behavior (Jacobson et al., 2000; Raes et al., 2000; Ramanathan et al., 2001; Kanakidou et al., 2005; Fuzzi et al., 2006; Prather et al., 2008).

Although the presence of aerosols in our atmosphere is crucial to life on this planet, much remains unknown about their hygroscopic behavior. Namely, how are the naturally occurring inorganic salt particles found in Earth's atmosphere affected by the presence of anthropogenic materials, specifically those that are non-volatile and hydrophobic? Also, how do the individual components within these mixed particles combine and what effects do these differing particle morphologies have on hygroscopic behavior?

2.2.2 Hygroscopic Growth

When a solid particle of a water soluble compound is initially exposed to humid air, water molecules can adhere to sites on its surface such as steps, edges, and kinks where the incomplete cancellation of electrical fields make the particle surface more susceptible to adsorption (Ewing, 2005). As sufficient water becomes available on the particle surface, solute molecules begin to dissolve into the water thereby lowering its vapor pressure which in turn attracts additional gas phase water molecules to the liquid on the particle surface until equilibrium is regained. Depending on the chemical and physical properties of the particle and the partial pressure of water vapor in the atmosphere, the processes of solute dissolution and the absorption of water vapor will continue until the particle is transformed into a solution droplet. For some compounds, such as inorganic salts, this process occurs rapidly at a specific relative humidity (Cohen et al., 1987a) in a process termed deliquescence. For other compounds however, such as sugars, this process occurs gradually and in a completely reversible manner (Chan et al., 2008). The former of these two types of water soluble particles have been termed deliquescent, whereas the latter have been termed non-deliquescent (Chan et al., 2008) and are considered purely hygroscopic similar to water soluble liquids. Although both types of particles are relevant to atmospheric research, the focus of this portion of study is restricted to those particles that are considered deliquescent.

An interesting phenomenon of deliquescent particles is their ability to exist in a supersaturated state at relative humidities well below that at which they underwent deliquescence. If a deliquesced particle is exposed to a low enough relative humidity however, it will instantly shed nearly all its water and return to a solid state during a process termed crystallization. Here it is appropriate to note that many investigators commonly use the term efflorescence in place of crystallization (Ansari and Pandis, 1999; Lightstone et al., 2000; Martin, 2000; Colberg et al., 2004; Badger et al., 2005; Wise et al., 2005; Biskos et al., 2006a,b; Gao et al., 2007b,c,2008; Semeniuk et al., 2007a; Takahama et al., 2007; Woods et al., 2007). However, this term is typically used incorrectly as efflorescence is more accurately the loss of water of crystallization and not the process of crystallization itself. Simply explained, a supersaturated particle may crystallize, but still retain significant water in the form of hydrates which it may later lose via efflorescence. Once crystallization has occurred however, the water content of the particle is no longer related to the relative humidity of its surroundings until deliquescence again takes place. An important aspect of these particles is that the crystallization relative humidity is lower than the deliquescence relative humidity and therefore their hygroscopic growth patterns exhibit a hysteresis.

Figure 2.3 shows the hysteresis loop resulting from the deliquescence, water absorption and desorption, and crystallization of a NaCl particle observed as part of this study. The particle is initially completely dry and in a moisture-free environment. As the relative humidity of the air surrounding the particle is gradually increased, the particle retains its initial dry weight until the relative humidity is approximately 70%. Here, the water content of the particle begins to rapidly increase. By 75% relative humidity, the particle has taken on sufficient water to completely dissolve and has transitioned into a solution droplet. After deliquescing, the water mass fraction of the droplet is dependent on the relative humidity of the surrounding air. Here, the droplet can reversibly absorb and desorb water and can even exist in a supersaturated state at relative humidities below its deliquescence relative humidity. As seen in the figure, a solution droplet of NaCl will exist as a supersaturated droplet until the relative humidity is reduced to 45%, at which point the droplet instantly loses much or all of its remaining water content during

crystallization. After crystallization, the water mass fraction of the particle is no longer in equilibrium with its surroundings. However, particles may still possess a certain amount of water that has been 'trapped' during crystallization. This behavior has been reported by numerous investigators for similar types of particles (Choi and Chan, 2002a; Colberg et al., 2004; Badger et al., 2005; Rosenoern et al., 2008). This trapped water will typically remain with the particle even when all the moisture has again been removed from the environment.

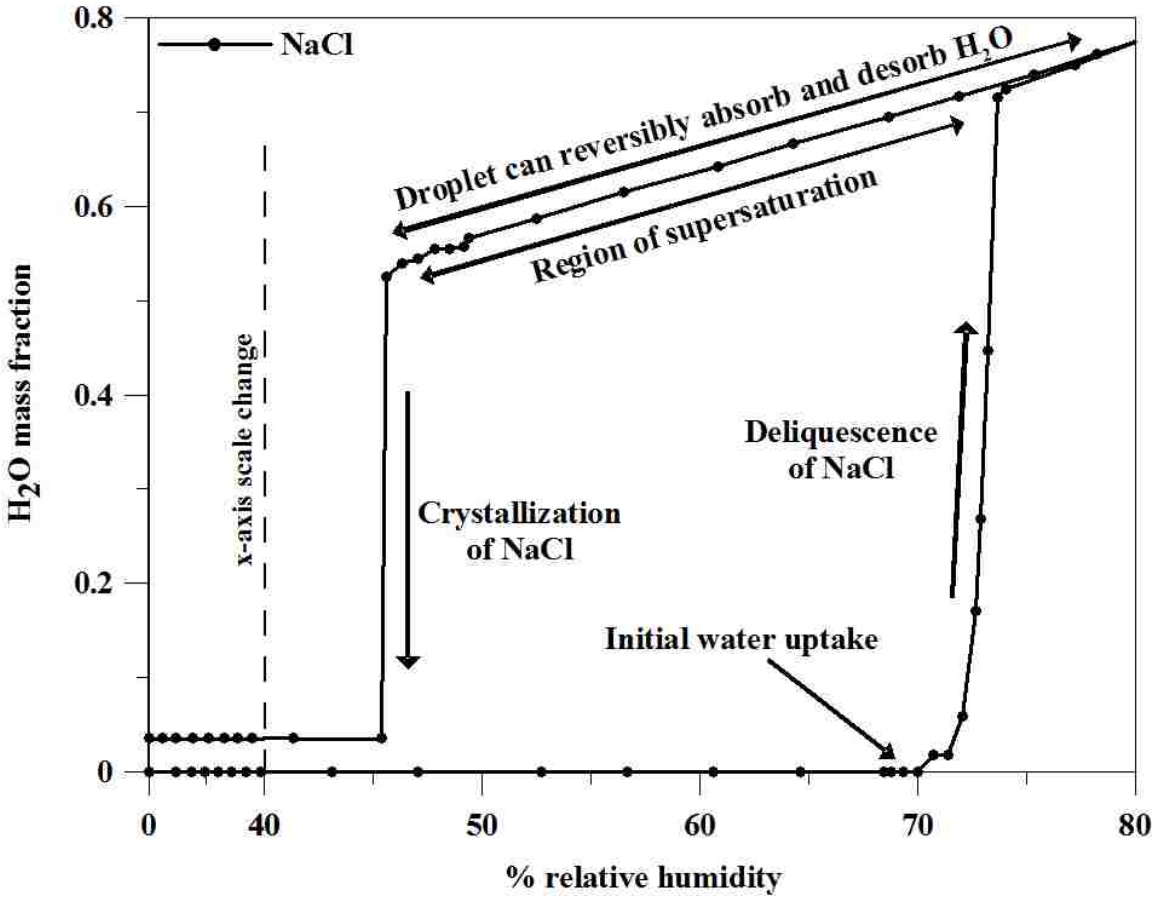

Figure 2.3 Hysteresis of a NaCl particle observed during this study.

2.2.3 Traditional and Modified Kohler theory

Kohler (1936) was the first to truly explain the role of hygroscopic particles in our atmosphere. By analyzing the chlorine content of frosts and the sizes of droplets observed during fogs he was able to determine a relationship between the water content of a saturated NaCl droplet and its surrounding vapor pressure. He used thermodynamics to explain the hygroscopic behavior that he observed and constructed graphical plots, currently termed Kohler curves, to predict the size and number density of NaCl particles under specific atmospheric conditions. Traditional Kohler theory is used to predict the droplet radius, *a*, at which a cloud condensation nuclei (CCN) can undergo spontaneous hygroscopic growth, or become 'activated' as termed in current literature, by the coalescence of atmospheric moisture. Kohler theory is typically expressed via the Kohler equation which relates relative humidity, *RH*, to the radius, *a*, of a solution droplet containing a water soluble inorganic salt through a combination of Raoult's law for water activity, a_w, and the Kelvin equation for curvature effect, given by

$$\frac{RH}{100} = \frac{P_{w,drop}}{P_{w,sat,flat}^{vap}} = a_w \exp\left(\frac{2M_w\gamma_{sol}}{RT\rho_{sol}a}\right) \tag{2.3}$$

where $P_{w,drop}$ is the equilibrium partial pressure of water above a solution droplet, $p_{w,sat,flat}^{vap}$ is the saturation vapor pressure of pure water over a flat surface of infinite extent, M_w is the molecular weight of water, γ_{sol} is the surface tension of the solution droplet, R is the universal gas constant, T is the absolute temperature, and ρ_{sol} is the density of the solution droplet. For solution droplets containing an electrolyte, a_w, can be expressed as

$$a_w = \exp\left(\frac{-M_w\nu\Phi m}{1000}\right) \tag{2.4}$$

where ν is the total number of dissociated ions from one molecule of solute, Φ is the osmotic coefficient of the solution, and m is the molality.

Expounding on Kohler's (1936) work, several authors have developed modified forms of Kohler theory. Laaksonen et al. (1998) have provided a simple algebraic form for this theory given by

$$S_w \approx 1 + \frac{a_w}{a} + \frac{b_s}{a^3} \tag{2.5}$$

where S_w is the saturation ratio, a_w incorporates the curvature effect given by the Kelvin equation, and b_s accounts for the reduction in the vapor pressure of water around the solution droplet due to dissolved solutes. Brechtel and Kreidenweis (200a,b) have modified Kohler theory to predict the critical supersaturations of binary mixtures by fitting two chemical and composition dependent parameters to corresponding experimental data. Petters and Kreidenweis (2007;2008) have further modified the work of Brechtel and Kreidenweis (200a,b) to require only a single hygroscopicity parameter that include solubility and is purported to better predict the hygroscopic behavior of solution droplets containing sparingly soluble or hydrophobic compounds given by

$$\frac{1}{a_w} = 1 + \kappa \frac{V_s}{V_w} \tag{2.6}$$

where a_w is the activity of water in a solution droplet, κ is the hygroscopicity parameter describing the effect on the water activity of the solution, and V_s and V_w are the volumes of the dry particle matter and the water, respectively. Kreidenweis (2008) has used the model developed by Petters and Kreidenweis (2007;2008) to predict the water content of atmospherically relevant particles from their dry volumes and tested the results against a more rigorous thermodynamic model over a wide range of stable and metastable solution droplets. Significant errors were reported for droplets observed below 85% relative humidity. Such findings however, are not unreasonable as the values suggested for κ by Petters and Kreidenweis (2007;2008) for use in (2.6) were specifically determined to predict the hygroscopic behavior of solution droplets above 90% relative humidity.

2.2.4 Hygroscopic Behavior of Single Component Particles

As traditional and modified Kohler theories require some a priori knowledge of the solute species, numerous investigators have examined the hygroscopic growth of particles

containing a single water soluble component, namely electrolytic compounds. The works of Robinson and Stokes (1949) and Hamer and Wu (1972) have been instrumental in predicting the behavior of water soluble inorganic salts. However, their studies were conducted using bulk solutions rather than individual particles. Regardless, they provided the osmotic and water activity coefficients for more than one hundred electrolytic compounds over a wide range of molalities that are still in use by investigators today. Although the thermodynamic data collected from studies using bulk solutions can be used to predict the deliquescence relative humidities and water content of post-deliquescent particles, the data fails to adequately predict the corresponding crystallization relative humidities. Orr et al. (1958) were among the first to express concern over this issue and commented that, "At present there are no good methods for predicting the point at which a supersaturated solution will crystallize." The comments of Orr et al. (1958) were later reiterated by Tang et al. (1986) after they observed that individual droplets of NaCl and KCl achieved much higher levels of supersaturation that predicted by Hamer and Wu (1972). Cohen et al. (1987a) have also commented on the subject stating that "…parameters estimated from low concentration data could not be reliably used to predict thermodynamic properties of the solution at high concentrations." In a later investigation, Cohen et al. (1987c) suggested that bulk solutions nucleate via heterogeneous due to impurities, whereas droplets proceed through homogenous nucleation at a much higher concentration. Such discrepancies had been previously discussed by Stokes and Robinson (1973) in an investigation that particularly examined very concentrated solutions of electrolytes. However, Stokes and Robinson (1973) were still unable to ascertain the hygroscopic behavior of supersaturated droplets since their investigation again pertained only to aqueous solutions.

Since data collected from bulk solutions often fails to adequately predict the behavior of individual particles (Tang et al., 1986; Cohen et al., 1987a), many investigators have specifically examined the hygroscopic properties of the particles themselves (Orr et al., 1958; Tang and Munkelwitz, 1984,1994; Tang et al., 1986; Cohen et al., 1987a,c; Brechtel and Kreidenweis, 2000a,b; Gysel et al., 2002; Wise et al., 2005,2008; Biskos et al., 2006a,b; Gao et al., 2007a,c; Petters and Kreidenweis,

2007,2008; Kreidenweis et al., 2008). Typical in many of these investigations is determining the relative humidities at which deliquescence and crystallization occur.

The investigations pertaining to the hygroscopic properties of single component particles have revealed that many factors contribute to their behavior. Cantrell et al. (2002) have shown that the crystalline surface of particles and their repeated exposure to humidification and dehumidification can affect the relative humidities at which deliquescence occurs. The work of Cantrell et al. (2002) is supported by that of Ewing (2005). He reported that the surface defects found at the steps, edges, and kinks of single NaCl crystals are more susceptible to adsorption and reactive processes due to the incomplete cancellation of electrical fields at such sites. Biskos et al. (2006a) and Gao et al. (2007c) have shown that the relative humidities at which deliquescence and crystallization occur in NaCl particles are related to their dry particle size. This behavior was also observed by Gao et al (2007c) to occur in $(NH_4)_2SO_4$ particles whereas Biskos et al. (2006b) have reported that $(NH_4)_2SO_4$ particles showed no dependence on dry particle size. In a separate study, Biskos et al. (2006c) have also reported that the size of dry NaCl particles affected their water uptake and Gao et al. (2007a) have reported that the deliquescence relative humidity of NaCl particles can be affected by the type of substrate supporting the particles. Gao et al. (2007a) have also reported that particle size, contact angles, and surface tension all affected the relative humidities at which particles deliquesced.

Although some disagreements persist regarding the hygroscopic behavior of single component particles, they typically pertain to the behavior of nanometer sized particles (Biskos et al., 2006b; Gao et al., 2007c). For the micrometer sized particles studied as part of this dissertation however, the relative humidities at which deliquescence and crystallization occur and the post-deliquescent water content of such particles have been well studied and accepted values exist in current literature (Cohen et al., 1987a; Tang and Munkelwitz, 1994; Martin, 2000; Wise et al., 2005; Biskos et al., 2006a). As such, it is not the focus of this study to determine such properties, but rather to examine how they are affected by the presence of additional components.

2.2.5 Hygroscopic Behavior of Multicomponent Particles

While the study of single component particles is fundamental to atmospheric research, it is essential to understand how the intermingling of different chemical species affects the hygroscopic behavior of the combined particle since atmospheric particles have been observed to exist as multiphase mixtures of organic and inorganic components (Posfai et al., 1999; Semeniuk et al., 2007a,b; Wise et al., 2007; Adachi and Buseck, 2008; Eichler et al., 2008). This area of study is made immensely complex when the vast number of currently identified atmospheric compounds is considered (Saxena and Hildemann, 1996; Kanakidou et al., 2005) and further compounded by the ability of some atmospheric particles to chemically react (Ellison et al., 1999; Kanakidou et al., 2005; Donaldson and Vaida, 2006). Moreover, some investigators have reported conflicting findings regarding the hygroscopic behavior of mixed particles collected directly from the atmosphere. Saxena et al. (1995) have reported that the organic fraction of particles collected from the skies above the Grand Canyon and Los Angeles affected the water content of the particles by as much as 40% in comparison to that estimated for the corresponding inorganic fraction. Semeniuk et al. (2007a) have reported however, that the hygroscopic behaviors of the particles they collected from various clean and polluted environments around the planet were dominated by the inorganic fraction.

Although the study of atmospherically collected particles has yielded valuable information about mixed particles, the time and expense required for such studies is not available to most investigators. As such, most studies involving mixed particles are conducted using laboratory generated particles. In addition to being a more feasible means of investigation, particles generated in the laboratory give investigators control over composition and the environment the particles are exposed to. Although some investigators have examined mixed particles composed of numerous components (Ming and Russell, 2001; Marcolli et al., 2004; Svenningsson et al., 2006; Moore and Raymond, 2008), most studies are limited to the hygroscopic behavior of particles containing two components. Here, the primary focus is typically to observe if and how one component affects the hygroscopic behavior of the other. More specifically, investigators have

routinely examined how both anthropogenic and naturally occurring organics affect the deliquescence, hygroscopic growth, and crystallization of atmospherically relevant inorganic salts; namely NaCl and $(NH_4)_2SO_4$ as they are the two dominant naturally occurring inorganic salts (Martin, 2000; Raes et al., 2000; Wise et al., 2007). As such, further discussion is restricted to this area as it is also pertains to the area of study discussed in this dissertation.

One type of commonly studied organics are the humic and fulvic acids isolated from the humus resulting from the decomposition of plant and animal matter (Brooks et al., 2004). These acids typically exist as heterogeneous mixtures, have been observed to have a wide range of solubilities, are reported to account for up to one-half of the dissolved organic matter in water, and are known to complex trace metals (Thruman and Malcolm, 1981; Chan and Chan, 2003; Brooks et al., 2004). When combined with inorganic salts, they have been found to have little effect on the amount of water absorbed by the inorganic fraction (Chan and Chan, 2003; Brooks et al., 2004), although they retain water at very low relative humidities (Chan and Chan, 2003; Badger et al., 2005). The two natural organics have been shown to have different effects on the hygroscopic properties of inorganics, however. Chan and Chan (2003) and Parsons et al. (2004) have both reported that fulvic acids had no noticeable effect on the deliquescence and crystallization relative humidities of micrometer-sized NaCl and $(NH_4)_2SO_4$ particles, whereas Badger et al. (2005) observed a significant decrease and increase in the deliquescence and crystallization relative humidities, respectively, for comparatively sized $(NH_4)_2SO_4$ particles containing humic acids.

Many investigators however, have examined the effects of simpler organic compounds that have better defined thermodynamic and hygroscopic properties. Disagreement persists here too, as several investigators have reported contradictory findings regarding the effects of these organics on the hygroscopic behavior of atmospherically relevant inorganic salts. The most common of these disagreements pertain to the effects on the deliquescence and crystallization relative humidities of a specific inorganic salt and the subsequent hygroscopic growth of the mixed particles.

Still, a closer inspection indicates that the solubility of the organic compounds studied may play a role in how they affect the deliquescence and crystallization relative humidities of inorganic salts. To aid the reader in the following discussion, Table 2.2 is presented to provide a list of the organic compounds to be later mentioned. The table lists the organic compounds in alphabetical order along with their chemical formula, molecular weight, and water solubility (when available). The solubilities of the individual organics were obtained from Lide (2004) in $g \cdot l^{-1}$ along with their associated temperatures in degrees Celsius unless otherwise stated. The solubility values are also given in units of $mol \cdot l^{-1}$ as calculated from the molecular weights of the corresponding compounds.

Table 2.2 List of water solubilities of the organic compounds studied by previous investigators. (Table 2.2 continues on page 36.)

Compound	Chemical Formula	Mol. Wt. $g \cdot mol^{-1}$	Solubility $mol \cdot l^{-1}$	Solubility $g \cdot l^{-1}$	Temp. °C
adipic acid	$C_6H_{10}O_4$	146.141	0.10	15.0	15
cetyl alcohol	$C_{16}H_{34}O$	242.440	1.2×10^{-7}	3×10^{-5}	25
citric acid	$C_6H_8O_7$	192.124	3.07	590	20
dioctyl phthalate	$C_{29}H_{38}O_4$	390.557	6.9×10^{-7}	2.7×10^{-4}	25
glutamic acid	$C_5H_9NO_4$	147.130	0.16[1] & 0.06[2]	23.5[1] & 8.5[2]	25
glutaric acid	$C_5H_8O_4$	132.116	4.4	582	25
Glycerol	$C_3H_8O_3$	92.094	fully miscible in water		
hexadecane	$C_{16}H_{34}$	226.441	2.6×10^{-8}	6×10^{-6}	25
lauric acid	$C_{12}H_{24}O_2$	200.320	2.7×10^{-4}	0.055	20
leucine	$C_6H_{13}NO_2$	131.173	0.17[3]	22.0[3]	25
levoglucosan	$C_6H_{10}O_5$	162.140	0.38 - 0.80[5]	62.3 - 128[5]	25
maleic acid	$C_9H_4O_4$	116.073	3.8	441	25
malic acid	$C_4H_6O_5$	134.088	4.4	590	26
malonic acid	$C_3H_4O_4$	104.062	4.1	424	20
norpinic acid	$C_8H_{12}O_4$	172.179	0.003[6]	0.47[6]	N/A
octadecane	$C_{18}H_{38}$	254.495	2.4×10^{-8}	6×10^{-6}	25
octanoic acid	$C_8H_{16}O_2$	144.212	0.0055	0.80	25
oleic acid	$C_{18}H_{34}O_2$	282.462	$< 1 \times 10^{-5}$[7]	< 0.003[7]	50
oxalic acid	$C_2H_2O_4$	90.035	1.06	95.1	20
palmitic acid	$C_{16}H_{32}O_2$	256.427	2.8×10^{-6}	0.0072	20
phthalic acid	$C_8H_6O_4$	166.132	0.042	6.977	25
pinic acid	$C_9H_{14}O_4$	186.206	~ 0.05[6]	~ 8.5[6]	N/A
pinonic acid	$C_{10}H_{16}O_3$	184.233	3.3×10^{-4}[4,6]	0.06[4,6]	N/A
pyruvic acid	$C_3H_4O_3$	88.062	fully miscible in water		
stearic acid	$C_{18}H_{36}O_2$	284.478	1.0×10^{-5}	0.0029	20
succinic acid	$C_4H_6O_4$	118.089	0.71	83.5	25
tetracosane	$C_{24}H_{50}$	338.654	1.2×10^{-8}	4×10^{-6}	22

[Table 2.2 continued]

Solubility values ($g \cdot l^{-1}$) were obtained from Lide (2004) unless otherwise noted.

N/A not available

[1] solubility of DL-glutamic acid

[2] solubility of L-glutamic acid

[3] solubility of L-leucine

[4] Cruz and Pandis, 2000

[5] range of solubility values obtained from http://mmcd.nmrfam.wisc.edu/test/cqsearch.py?cqid=cq_10725

[6] Raymond and Pandis, 2003

[7] Khuwijitjaru et al., 2004 (value given in mol/l and converted to g/l)

Hameri et al. (1997;1998;2002) have studied the effects of adipic, phthalic, succinic, and malonic acids on the hygroscopic behavior of 100 nm $(NH_4)_2SO_4$ particles. They observed that the relatively less water soluble organics, such as adipic and phthalic acids, acted as insoluble materials and did not affect the post-deliquescent water absorption and desorption by the inorganic salt, whereas the relatively more water soluble malonic acid made particles behave as a purely hygroscopic material. They also found that the relative humidity at which mixed particles deliquesced was reduced relative to the pure inorganic salt as the organic fraction was increased and that mixed particles exhibited water uptake prior to deliquescence.

Cruz and Pandis (2000) have studied the effects of pinonic and glutaric acids on the hygroscopic behavior of comparatively sized NaCl and $(NH_4)_2SO_4$ particles. They reported that increasing the organic fraction enhanced the water absorption of the particles, but did not affect the deliquescence relative humidities of the inorganic salts. However, Lightstone et al. (2000) have studied the effects of succinic acid on the hygroscopic behavior of 8 μm NH_4NO_3 particles and observed the organic fraction to increase the relative humidity at which crystallization occurred. Chen and Lee (2001) have studied the effects of glutaric and pyruvic acid on the hygroscopic behavior of 100 nm NaCl particles and found that increasing the organic fraction decreased the deliquescence relative humidity of the mixed particle.

Choi and Chan (2002a) have studied the effects of glycerol and succinic, malonic, citric, and glutaric acids on the hygroscopic behavior of micrometer sized NaCl and $(NH_4)_2SO_4$ particles. They observed that succinic acid increased the crystallization relative humidities of both inorganic salts, but had no effect on their deliquescence relative humidities. Particles containing malonic or citric acid were reported to absorb significant amounts of water at low relative humidities prior to deliquescence and those containing glutaric acid were reported to become more hygroscopic and no longer have a sharp deliquescence. However, particles containing succinic acid and glycerol were found to have no noticeable effect on the water absorption of either salt.

Prenni et al. (2003) have studied the effects of adipic, succinic, oxalic, malonic, and glutaric acids on the hygroscopic behavior of 100 nm $(NH_4)_2SO_4$ particles and reported agreement with Hameri et al. (1997;1998;2002) and Choi and Chan (2002a) for particles containing adipic or succinic acid, but they did not observe an increase in the crystallization relative humidity of the particles containing succinic acid as reported by Choi and Chan (2002a). Particles containing oxalic or malonic acid were observed to become fully hygroscopic in agreement with Hameri et al. (2002), while those containing glutaric acid did become fully hygroscopic as observed by Choi and Chan (2002a), but deliquesced at a slightly lower relative humidity than pure $(NH_4)_2SO_4$ particles. However, the water uptake of particles containing glutaric acid was in agreement with that of Choi and Chan (2002a).

Raymond and Pandis (2003) have studied the effects of leucine, glutamic, pinonic, pinic, and norpinic acids on the CCN activation of nanometer sized NaCl and $(NH_4)_2SO_4$ particles. Results from all particles, with one exception, containing 1% by mass of the selected organic were consistent with traditional Kohler theory. The exception noted was for a leucine particle with 1% NaCl. The investigators concluded that "…there were no strong interactions between inorganics and organics or among multiple organic species that would alter the CCN activation abilities of the constituent species of a multiple-component particle." This finding however, was in contradiction to a previous investigation by Cruz and Pandis (1998) that reported the CCN activations of comparatively sized $(NH_4)_2SO_4$ particles were increased when mixed with glutaric acid.

Braban and Abbatt (2004) have studied the effects of malonic acid on the hygroscopic behavior of nanometer and micrometer sized $(NH_4)_2SO_4$ particles. Particles containing malonic acid were observed to have reduced deliquescence and crystallization relative humidities, with some particles exhibiting no crystallization at all as previously observed by Prenni et al. (2003). Bilde and Svenningsson (2004) have studied the effects of adipic and succinic acid on the critical supersaturations and CCN activity of nanometer sized NaCl particles and found that even a slight amount of NaCl to significantly increased their CCN activity. Parsons et al. (2004) have studied the effects of malonic

acid, glycerol, and levoglucosan on the hygroscopic behavior of micrometer sized $(NH_4)_2SO_4$ particles deposited on the bottom surface of a flow cell and viewed with an optical microscope. They observed that the deliquescence and crystallization relative humidities of the particles decreased as the molar fraction of organic material was increased. Also, particles containing malonic acid were found to no longer crystallize once the mole fraction of the particles was > 0.5.

Sjogren et al. (2007) have studied the effects of adipic acid on the hygroscopic behavior of both nanometer and micrometer sized $(NH_4)_2SO_4$ particles. The larger particles were examined using an electrodynamic balance and observed to have a reduced deliquescence relative humidity, whereas no such effect was observed for the smaller particles examined using tandem differential mobility analyzers (TDMA). Zardini et al. (2008) have studied the effects of citric, glutaric, and adipic acids on the hygroscopic behavior of both nanometer and micrometer sized $(NH_4)_2SO_4$ particles in a manner similar to Sjogren et al. (2007). Here, the particles examined with an electrodynamic balance showed a distinct hysteresis, whereas those examined via TDMA appeared hygroscopic and did not crystallize. The investigators suggest that the partial crystallization observed for particles in the balance system was due to the rapid evaporation experienced by the solution droplet upon injection to the balance. Moreover, after the initial crystallization, the particles in the electrodynamic balance were no longer observed to crystallize upon subsequent humidification and dehumidification cycles. When the molar amount of citric acid was 50%, no deliquescence or crystallization was observed using either technique. However, particles containing glutaric or adipic acids were observed to still undergo deliquescence and crystallization similar to pure $(NH_4)_2SO_4$ particles.

What is evident from the aforementioned investigations is the ability of some organics to affect the hygroscopic behavior of atmospherically relevant salts. However, as many of these organics were water soluble, the expectation of such effects is not unreasonable. Moreover, Cruz and Pandis (2000) and Choi and Chan (2002a) have both reported they were able to accurately predict the overall water content of their mixed

particles using a group contribution method, although Sjogren et al. (2007) and Zardini et al. (2008) have reported significant deviations using the same method for mixed particles containing a large or undissolved organic fraction. Furthermore, as some of the organics studied have deliquescent and crystallization relative humidities other than those of the inorganic salts they were paired with, it is also not unreasonable that the mixed particles would deliquesce and crystallize at relative humidities other than those of the corresponding pure inorganic salts. Therefore, further discussion is restricted to those organic compounds which are considered water insoluble.

2.2.6 Effect of Water Insoluble Materials on the Hygroscopic Behavior of Inorganic Salts

Some investigators have specifically examined how water insoluble compounds affect the hygroscopic behavior of atmospherically relevant inorganic salts. A common misperception among these studies, however, was that the hygroscopic growth of inorganic salts could be prevented by externally coating the particles with layers of non-volatile, hydrophobic organics. Otani and Wang (1984) attempted and failed to prevent the hygroscopic growth of NaCl particles using cetyl alcohol. They were however, able to significantly reduce the growth rate. Similar studies were also conducted by Hansson et al. (1990;1998) and Hameri et al. (1992) wherein nanometer sized particles of NaCl and $(NH_4)_2SO_4$ were coated with dioctyl phthalate, octadecane, tetracosane, octanoic acid, or lauric acid. Here, the investigators applied a variety of coating techniques and even used scanning electron microscopy to insure that the particles were fully coated. Here too however, the particles were still observed to deliquesce and grow, even when coated with a solid layer of the designated organic applied as a liquid and allowed to solidify. Xiong et al. (1998) have specifically studied how lauric, stearic, and oleic acids effect the hygroscopic growth rate of nanometer sized H_2SO_4 particles. Here, particles were coated with up to 13 monolayers of the selected organic acid. They observe that increasing the number of monolayers could reduce the growth rate, but only in the time range of up to 6 s and that additional monolayers beyond the 6^{th} coating did not further reduce the growth rate.

Cruz and Pandis (1998) have studied the effects of dioctyl phthalate on the CCN activation of nanometer sized $(NH_4)_2SO_4$ particles and found that even a coating of 70% by mass of the organic could not prevent their activation at supersaturations of 0.5% and 1.0%. In a similar study, Raymond and Pandis (2003) have reported that the CCN activation of comparatively sized particles of $(NH_4)_2SO_4$ coated with up to 96% by mass of hexadecane were also unaffected at supersaturations of 0.3% and 1.0%.

Garland et al. (2005) have reported that coatings of palmitic acid had no effect on the crystallization relative humidity of nanometer and micrometer sized $(NH_4)_2SO_4$ particles. Here, it should be noted that the mixing procedure used by Garland et al. (2005) was stated to produce externally coated particles, but that "the internal mixing state of the aerosols is not known." Pictures of the particles taken by transmission electron microscopy indicate that some particles were in fact agglomerates of coated particles.

However, Chan and Chan (2007) have studied the effects of octanoic acid coatings on the hygroscopic behavior of 10 μm $(NH_4)_2SO_4$ particles and noticed an increase in the deliquescence relative humidity and decreased in the crystallization relative humidity of the coated particles relative to the pure inorganic salt, but suggested that such changes could be the result of the manner in which the relative humidity was related to the coated particles and not the addition of the organic.

From the previous discussion, it would appear that water insoluble organics have far less effect on the hygroscopic behavior of atmospherically relevant inorganic salts than water soluble organics, at least when externally coated. Furthermore, it is clear that water insoluble organics cannot prevent the hygroscopic growth of the inorganic salt fraction, but only reduce the rate at which such growth occurs, despite the amount of coating. However, as the inorganic salt particles in the aforementioned literature were externally coated, no conclusion can be drawn regarding the impact of such organics when internally mixed with inorganic salt fraction. Moreover, naturally collected aerosols have been shown to be internally mixed (Semeniuk et al., 2007a,b; Wise et al.,

2007; Adachi and Buseck, 2008). Therefore, the particles studied as part of this dissertation were not coated, but rather generated from a bulk solution containing both the organic and inorganic components to produce mixed particles where all components have some degree of external exposure.

2.2.7 Predicting the Hygroscopic Behavior of Multicomponent Particles

Although a wide variety of particles have been studied (Martin, 2000), specifically examining the hygroscopic properties of all the possible combinations of compounds currently identified in the atmosphere is unfeasible and impractical due to their immense number (Saxena and Hildemann, 1996; Kanakidou et al., 2005). As such, investigators typically rely on models to estimate the behaviors of mixed particles based on the thermodynamic properties of their individual components (Clegg, 1992;1997;1998a,b; Carslaw et al., 1995; Clegg and Brimblecombe, 1995; Chan et al., 1997). Ansari and Pandis (1999) have developed a model that incorporates the adjusted thermodynamic parameters of selected inorganic compounds and minimizes the Gibbs free energy to accurately predict the multistage growth, deliquescence point depression, and crystallization behavior of multicomponent inorganic particles.

Although each investigator may take a personalized approach towards their model development, most predictive models are modifications to Kohler theory (Laaksonen et al., 1998; Brechtel and Kreidenweis, 2000a,b) and utilize the Zdanovskii-Stokes-Robinson (ZSR) model (Zdanovskii, 1948a,b; Stokes and Robinson, 1966). The ZSR method provides a simple relationship between the activity coefficients and molalities of mixed systems to their individual counterparts at equilibrium. The ZSR method is typically used to predict the overall water content of a mixed particle (Cohen et al., 1987b, Wexler and Seinfeld, 1991; Ansari and Pandis, 1999; Cruz and Pandis, 2000; Choi and Chan, 2002a). Cohen et al. (1987b), Cruz and Pandis (2000), and Choi and Chan (2002a) have all reported good agreement using the ZSR method for particles mixtures, although Cohen et al. (1987b) only reported agreement when they assumed that a certain portion of water was ‘trapped’ by the particle during crystallization. However,

the assumption of Cohen et al. (1987b) is not unreasonable as particles have been observed to retain water after crystallization (Choi and Chan, 2002a; Colberg et al., 2004; Badger et al., 2005; Rosenoern et al., 2008). However, Sjogren et al. (2007) have reported that the ZSR model failed for mixed particles containing a large organic fraction and Zardini et al. (2008) have reported that the ZSR model failed for mixed particles containing an undissolved portion of the organic. Data from bulk multicomponent mixtures have also been shown to predict the behavior of corresponding mixed particles provided their diameters are such that the Kelvin effect is negligible and the particles are at relative humidities above their deliquescence point (Tang, 1976). Bulk mixtures have also been found to correctly predict multistage growth characteristics (Tang et al., 1978; Cohen et al., 1987b) and reductions in the deliquescence relative humidity for mixed inorganic particles (Tang et al., 1978), as well as composition and temperature dependencies (Tang and Munkelwitz, 1993).

However, several investigators have observed unique multicomponent particle behavior that is often difficult, if not currently impossible, to model. Finlayson-Pitts and Hemminger (2000) have discussed the importance of understanding tropospheric reactions of gases with NaCl and NaBr and the role of surface-adsorbed water. They have also discussed the role of hydroxyl and nitrate radicals and ozone in atmospheric chemistry and how heterogeneous chemistry must be included into atmospheric models. However, they did not mention a previous modification of Kohler theory by Laaksonen et al. (1998) that accounts for the inclusion of slightly soluble species and trace amounts of condensable gases. Gibson et al. (2007) have found that the chemical composition and inclusion of even trace quantities (< 1%) of soluble components can significantly alter the ability of mineral dust to form cloud condensation nuclei. Liu et al (2008) have found that atmospheric aging of mineral dust via reactive nitrogen species could significantly increase their hygroscopic properties. Wise et al. (2007) have observed that naturally collected specimens of soluble and insoluble inorganics would absorb water and either ‘engulf’ the insoluble portion or form a deliquescent ‘balloon’ adjacent to it. As such, it is imperative to continue the examination of mixed particles and their hygroscopic properties.

2.2.8 Summary

Despite the numerous studies that have been conducted into the hygroscopic properties of mixed particles and the improvements in predictive models, the complex behavior of the multiphase and multicomponent particles found in the atmosphere are still not acceptably understood. Moreover, given their ability to significantly impact life on Earth, a better understanding of how atmospheric particles behave is crucial. A review of the relevant literature has shown that the solubility of organics in water could possibly play a role in how they affect the hygroscopic behavior of mixed particles. Furthermore, it is not fully understood how different particle morphologies affect the hygroscopic behavior of mixed particles. The work presented in the remainder of this dissertation is an effort to better understand how non-volatile, hydrophobic organics affect the hygroscopic behavior of atmospherically relevant inorganic salts.

Chapter 3: Experimental

3.1 Experimental Setup

3.1.1 Introduction

Examining the properties and behavior of aerosols can be a daunting task considering their sizes are typically in the nanometer and micrometer range. As such, research in this field has led to the development and advancement of many current technologies that afford investigators the ability to examine a single particle suspended in air and to determine its chemical and physical characteristics with a high degree of both precision and accuracy. In this chapter, the equipment and methods used to study both charged droplets and mixed particles are described in detail.

3.1.2 Combined Experimental Setup

To examine the properties of the charged aerosols studied as part of this dissertation, an electrodynamic balance, thermal diffusion cloud chamber, and humid airflow system were all used collectively along with some additional accessories and a light scattering technique (van de Hulst, 1981; Bohren and Huffman, 1983; Kerker, 1983) based on Lorenz-Mie theory (Lorenz, 1890; Mie 1908). Davis (1997) has discussed in detail the development of the electrodynamic balance and corresponding use of light scattering techniques. In fact, many of the initial advancements and applications can be attributed to Davis and others in his group (Davis and Chorbajian, 1974; Davis and Ray, 1977;1978;1980; Davis and Ravindran, 1982; Davis, 1985; Davis and Periasamy, 1985).

Recent investigations have proven how accurate the combined application of the electrodynamic balance and light scattering technologies can be for determining the physical characteristics of charged droplets. Chylek et al. (1983) have shown that the diameter and refractive index of optically levitated particles can be simultaneously determined with relative errors of 5×10^{-5}. Taflin et al. (1988) used an electrodynamic

balance in conjunction with two forms of light scattering techniques and were able to determine the sizes of binary droplets to within 0.1% and those of pure component droplets to within 0.01%. Ray et al. (1991) also used an electrodynamic balance in conjunction with a light scattering technique and were able to determine the sizes and refractive indices of multicomponent and layered droplets with the same precision as Chylek et al. (1983). Huckaby et al. (1994) used an electrodynamic balance in conjunction with a light scattering technique to ascertain the size, refractive index, and dispersion of single droplets of Invoil 740, a silicon oil, with relative errors of 3×10^{-5}, 3×10^{-5}, and 2×10^{-5}, respectively. Ray and Nandakumar (1995) developed a technique using an electrodynamic balance in conjunction with a light scattering technique to simultaneously determine the size of the core, layer thickness, and refractive indices of single droplets of Santovac 5, a polyphenol ether, coated with an immiscible layer of Fomblin, a perfluorinated polyether. They were able to determine the size of the core, layer thickness, and refractive indices of both with relative errors of 3.5×10^{-4}, 4.5×10^{-2}, 2.3×10^{-4}, and 4.4×10^{-4} respectively. Recently, Nakajima (2006) has discussed a method to accurately determine the size and charge of individual charged particles with errors of less than 0.1% and 0.3%, respectively. His method incorporates a quasi-quadrupole levitator with a laser Doppler velocimeter and is a modified version of the electrical single particle aerodynamic relaxation time (E-SPART) analyzer proposed by Mazumder and Kirsch (1977) and Renninger et al. (1981).

The particular setup used as part of this dissertation has been previously described in detail by Tu (2000) and shown to be accurate to within 0.1% for determining droplet size by Tu and Ray (2001). Here, a description of the combined experimental system and how charged aerosols are generated, captured, observed, and measured is given. Figure 3.1 provides a top and side view of the combined setup. The electrodynamic balance is situated such that the center of the rings is aligned with the aerosol injection port on the top plate and the twin posts do not interfere with either the illumination or observation of a suspended aerosol. The polyethylene tubing for the saturated nitrogen gas feed is introduced through a port on the side of the chamber and winds around the inner circumference on the bottom of the chamber to acclimate the gas stream to the chamber

temperature before being connected to the manifold. The manifold is centered in the chamber surrounding the balance and also lies directly on the bottom plate. A tubing thickness of 3/8” O.D. was selected so that it would not interfere with the illumination or observation of suspended aerosols. The DC and AC coaxial wires connected to the balance rings are individually routed over the tubing and out of the chamber in such as manner as to not interfere with particle illumination or observation. The gas stream fed to the chamber is removed from a single 3/8” polyethylene tube that is attached to the post supporting the DC ring electrodes and exits through one of the chamber ports. The temperature and relative humidity of the nitrogen gas immediately surrounding a suspended aerosol are measured directly by a hygrometer probe. The tip of the probe is located only 1/2” from the center of the rings. The probe is connected to a hygrometer located outside the chamber via a power cord routed through a port on the side of the chamber. The hygrometer is a Traceable Digital Hygrometer with stated accuracies of ± 1.5% relative humidity and ± 0.4°C.

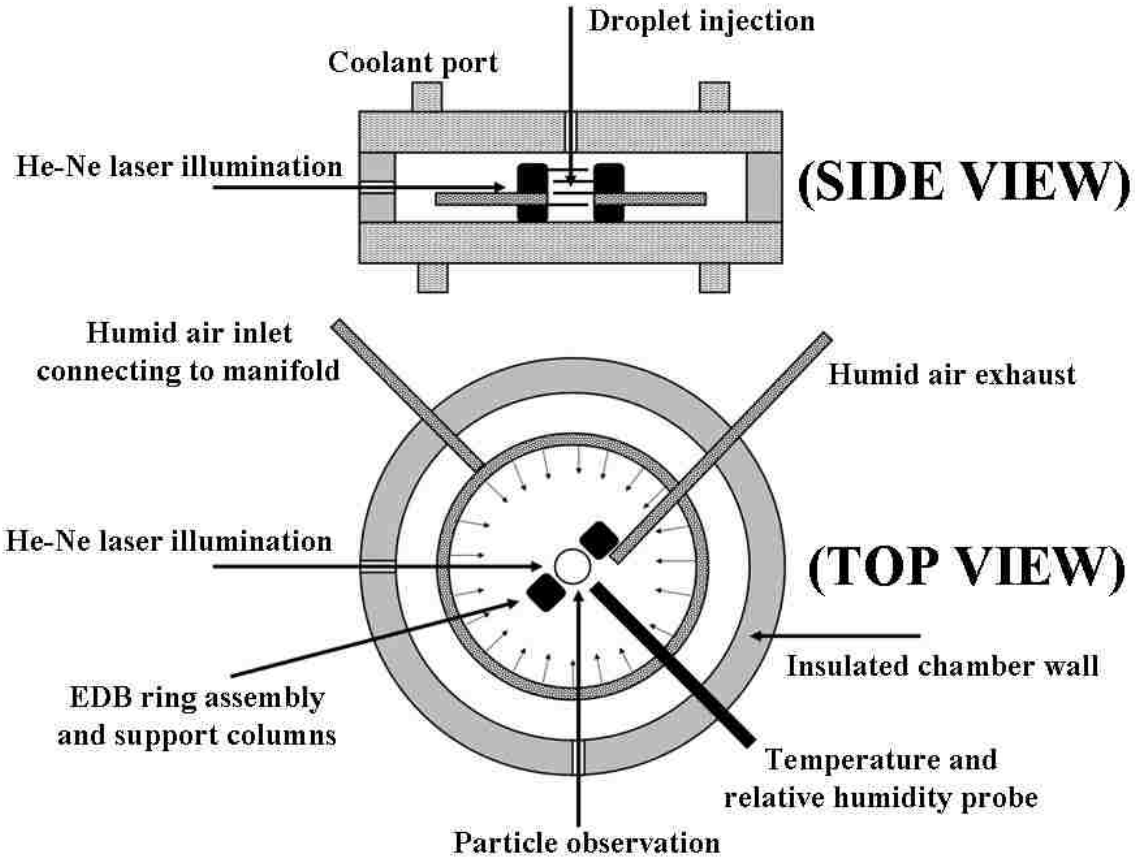

Figure 3.1 Side and top views of the combined experimental system.

For experiments involving the detection of scattered light intensity, two PMTs are incorporated into the experimental setup to observe the intensity of the light scattered by a levitated droplet. Both PMTs are positioned at scattering angles $\theta \sim p/2$ with respect to the polarization of the incident laser beam. One PMT is mounted on the side of the chamber opposite the port used for droplet observation. The side PMT detects the transverse electric (TE) mode resonances of the intensity of the light scattered by a droplet in the plane perpendicular to the polarization of the incident laser beam. The other PMT is attached over the port on the top plate of the chamber after a droplet has been captured. The top PMT detects the transverse magnetic (TM) mode resonances of the intensity of the light scattered by a droplet in the plane parallel to the polarization of the incident laser beam. The scattered intensity resonances observed in the two planes are independent of each other allowing two sets of data to be simultaneously collected from a single droplet. The PMTs are located behind apertures limiting their angular range of scattered light detection to $\Delta\theta \sim 0.05°$. They are type R374 and are manufactured by Hamamatsu. Both PMTs are situated in protective enclosures previously made in-house that are custom fit to the chamber. The PMTs are individually connected to intensity filters and amplifiers and adjustable power supplies also previously made in-house. Outputs from the PMTs are recorded as functions of time by a computer and saved to a data file. A detailed discussion of light scattering theory is provided in Chapter 4.

The ports used for laser illumination, visual observation, and the detection of scattered intensity are sealed externally using custom window ports to permit light transmission. When not being used for particle introduction, the port on the top chamber plate is also sealed in this manner. The ports through which the power cords and tubing pass are sealed internally using a silicone caulk. How well the chamber is sealed can be known by comparing the volumetric flowrates of the gas lines entering and exiting the chamber.

Charged droplets are generated from a high voltage pulse applied to a flat-tipped, 20 gauge, stainless steel needle containing a portion of the desired solution. During generation, the needle is housed in a Teflon apparatus situated over the port on the top of the chamber. The housing apparatus has been specifically designed to allow the needle to protrude through the center of the port so that its injection tip is slightly above the top ring electrode of the balance to allow for easier capture of charged droplets. The high voltage power supply is a Harrison 6525A DC power supply manufactured by Hewlett Packard and ranges from 0 – 4000 V and 0 – 50 mA. During use, it is operated at its maximum voltage and minimum amperage and the duration of the voltage pulse is typically about one second. The negative lead of the high voltage power supply is connected by a coaxial cable to a relay switch powered by a model LH 124 FM low voltage regulated power supply manufactured by Lambda Electronics Corp. The positive lead of the high voltage power supply is capped by a terminated coaxial lead. The relay switch was previously built in-house and operates by pressing a button which powers a relay via the low voltage power supply allowing for transmission of the high voltage power so long as the button is depressed. The relay is grounded to the chamber via the optical table and connected to the needle with an alligator clip. During droplet generation, the DC voltage applied to the balance rings is typically about 16 V and the AC voltage and frequency are about 1200 V and 400 hz, respectively.

Once a charged aerosol has been generated and then captured by the ring assembly, the droplet is illuminated by a vertically polarized, 20 mW, He-Ne laser beam (λ = 632.8 nm). The laser is a model 1135P manufactured by JDS Uniphase and is powered by a 115 v turn-key power supply. The laser beam is introduced to the chamber through a sealed window after making two 90° turns using optical mirrors. The beam is then passed through the vertical and horizontal centers of the chamber and exits through a light trap. The light trap is mounted to the side of the chamber opposite the incoming laser beam and deflects the path of the beam through a sealed tube to prevent backscattering of the laser light.

An illuminated aerosol can be visually observed either by the naked eye or through a 20X optical lens. The lens is fitted with a fine crosshair and is situated in a telescoping tube that is elevated and horizontally positioned to correspond with one of the sealed windows on the side of the chamber. The tube housing the lens can be precisely adjusted both vertically and horizontally so that a captured particle can be centered on the crosshairs of the lens. An additional sealed window provides the observer a quick glance to ensure particle introduction and droplet stability. The ability of the observer to clearly see the droplet in relation to the crosshair is crucial to acquiring an accurate levitation potential. Here, a Protek digital multimeter is connected to outlets in the DC power supply box by electrical leads and used to measure the potential difference between the top and bottom ring electrodes to within 0.001 V_{DC}. The potentials are recorded as functions of time by the observer during an experiment.

3.1.3 The Electrodynamic Balance

The electrodynamic balance has been routinely used for investigating the characteristics of individual aerosols since Robert Millikan's investigations into the charge on a single electron pioneered the observation of single charged droplets levitated in an electric field. During his observations of charged sprays of oil droplets, typically referred to as the Millikan oil drop experiment, Millikan (1910) found that a single charged droplet could be stably maintained by countering the gravitational force of the charged oil droplets with the repulsive and attractive electrostatic forces created by the potential applied between two metal plates vertically positioned above and below the droplet. His work provided the fundamental basis for the development of the quadrupole trap by Wolfgang Paul for use in mass spectrometry (Paul and Steinwedel, 1953; Paul and Raether, 1955) and the current configurations of the electrodynamic balance.

Although an electrical field is employed in nearly all balance systems, the physical application of such to stably levitate a charged aerosol may often vary from one research laboratory to another (Cohen et al., 1987a; Chan et al., 1997; Li et al., 2005). In general, an electrodynamic balance levitates an individual charged aerosol by applying an

electric potential between two conductive bodies, such as plates or rings, positioned vertically above and below the aerosol. The direction of the potential is determined by the sign of the charge on the aerosol, whether positive or negative. For instance, if a negatively charged aerosol is to be levitated, a negative potential is applied to the bottom electrode to counter the gravitational force of the aerosol. The vertical position of the droplet can then be manipulated by increasing or decreasing the applied potential. Typically, an AC power source is supplied to a central ring electrode to provide horizontal stability for the aerosol. The degree of horizontal stability is optimized by tuning the frequency. Davis (1997) has discussed in detail the evolution of the electrodynamic balance and provides a variety of balance configurations that were either in use or suggested for use at the time of publication. In Chapter 4, an in-depth discussion of the theory supporting the application of the electrodynamic balance is given.

Two electrodynamic balances of very similar configuration were used as part of this dissertation. The first balance used was previously constructed in-house and has been thoroughly described by Tu (2000) and Tu and Ray (2001). This balance was constructed of four ring electrodes constructed from molded copper wire and supported by a single polymer post. However, during the course of investigations this balance was found to occasionally arc between the AC and DC ring electrodes and destabilize a levitated droplet. As such, a new electrodynamic balance was constructed.

The currently used electrodynamic balance consists of four rings supported by two posts, where each post supports two ring electrodes connected to either the DC or AC circuits. Figure 3.2 provides a three-dimensional view of the four-ring electrodynamic balance used to levitate a charged aerosol. The right and left posts shown in the figure support the DC and AC ring electrodes attached to the corresponding posts. Two AC rings are used so that the particle can be illuminated, optically viewed, and the intensity of scattered light can be measured in the horizontal plane. For the type of ring electrodes used here, a single AC ring would impede such observational abilities as the levitated aerosol would be horizontally centered within the confines of the ring. The DC and AC

ring electrodes were placed on separate posts to reduce the electrical ‘leaking’ previously described between the DC and AC electrodes. Both posts are identically constructed from ultra-high temperature glass-mica ceramic and measure 3/4” in width by 3/4” in depth by 1” in height. They face each other squarely and are separated by 1 3/4" between their interior facing sides. The posts are coated in black liquid electrical tape to improve their electrical insulation and reduce unwanted backscattering of light during illumination of a levitated aerosol. Both posts have had four vertically aligned holes drilled completely through the center of one side. The holes measure ˜ 1/16” in diameter and are equally spaced ˜ 3/16” apart. The diameter of the holes is such to allow a single-conductor, 600 VAC, 12 AWG building wire through.

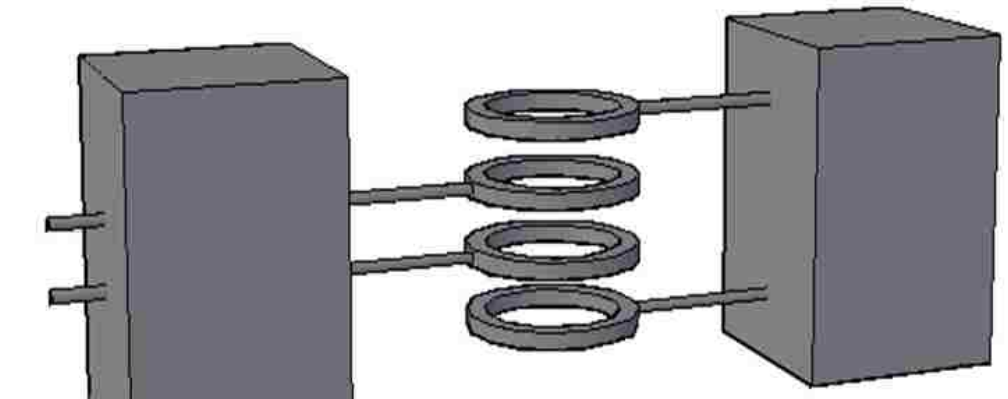

Figure 3.2 3D representation of the 4-ring electrodynamic balance.

Although each post is identically fitted with four holes, the solid copper wire is only run through two of the four holes on either post. Here, the left-hand side post is equipped with wires through the center two holes and the right-hand side post is equipped with wires through the top and bottom holes. The ends of each of the four wires are connected to a single, heavy duty ring terminal with a 1/2" interior diameter. All four rings are positioned horizontally so that their interior holes are aligned vertically. The rings have also been coated with a black, non-conductive paint to reduce unwanted backscattering and any electrical interference between the DC and AC rings. The coating material used on the rings was originally designed for coating cathode ray tubes in televisions.

The top and bottom endcap rings supported by the right post are individually connected to the positive and negative terminals of a DC power supply via coaxial cables attached to the ends of the corresponding solid copper wires on the opposite side of the post. The central two rings supported by the left post have both been connected to a high voltage AC power supply via a single coaxial cable attached to the ends of both the solid copper wires on the opposite side of the post. The connections between solid copper wires and coaxial cables are made using fully insulated quick connect terminals. The DC and AC power supplies are situated in a single enclosed structure previously made in-house. The combined power supply allows for each of the power types to be individually switched on or off. In addition, the DC power supply allows for coarse and fine adjustment of the potential from 0 to 40 V as well as the ability to reverse the potential. The combined power supply structure is fitted with coaxial connection ports for the output and monitoring of the DC potential and the input and output of the AC power supply. The voltage of the AC power supply is controlled using a Realistic model SA-150 integrated stereo amplifier and can be increased up to 1400 V and the frequency and wave type are established using a Dynascan 3010 function generator and typically operated in the region of 100 to 900 hz.

3.1.4 The Thermal Diffusion Cloud Chamber

A thermal diffusion cloud chamber was used as part of this study to aid in the stable levitation of individual droplets and particles by the electrodynamic balance and to allow for the control of the temperature, pressure, and relative humidity in their surrounding environment. The invention of the cloud chamber is credited to Langsdorf (1939) and a more modern version has since been employed for the study of levitated droplets by Tu and Ray (2001;2005) and Li et al. (2005). The chamber used here has been previously described in detail by Tu (2000). However, slight modifications have since been made and therefore it is further described in detail again here.

Figure 3.3 provides an expanded illustration of the primary components that make up the cloud chamber used as part of this dissertation. The chamber consists of three primary structures composed of 316 stainless steel; a top and bottom plate capable of coolant fluid circulation and a central ring containing a variety of ports. The top and bottom plates measure 13” in diameter and 1 1/8” in thickness and have 30 identically, equally spaced 1/2" holes along their outer circumference. Both plates have been machined to possess a hollow chamber for coolant fluid circulation. The coolant chambers in the plates measure 11” in diameter and 1” deep. The top and bottom plates both have removable covers to allow for cleaning. The covers are 11 1/2” in diameter and 1/8” thick and are secured to the corresponding top or bottom plate using 15 equally spaced 3/8” length, 6-32 thread, coated alloy steel socket head cap screws around the outer circumference. The covers have each been fitted with two straight thread tube adapters with o-ring connectors to permit coolant fluid circulation.

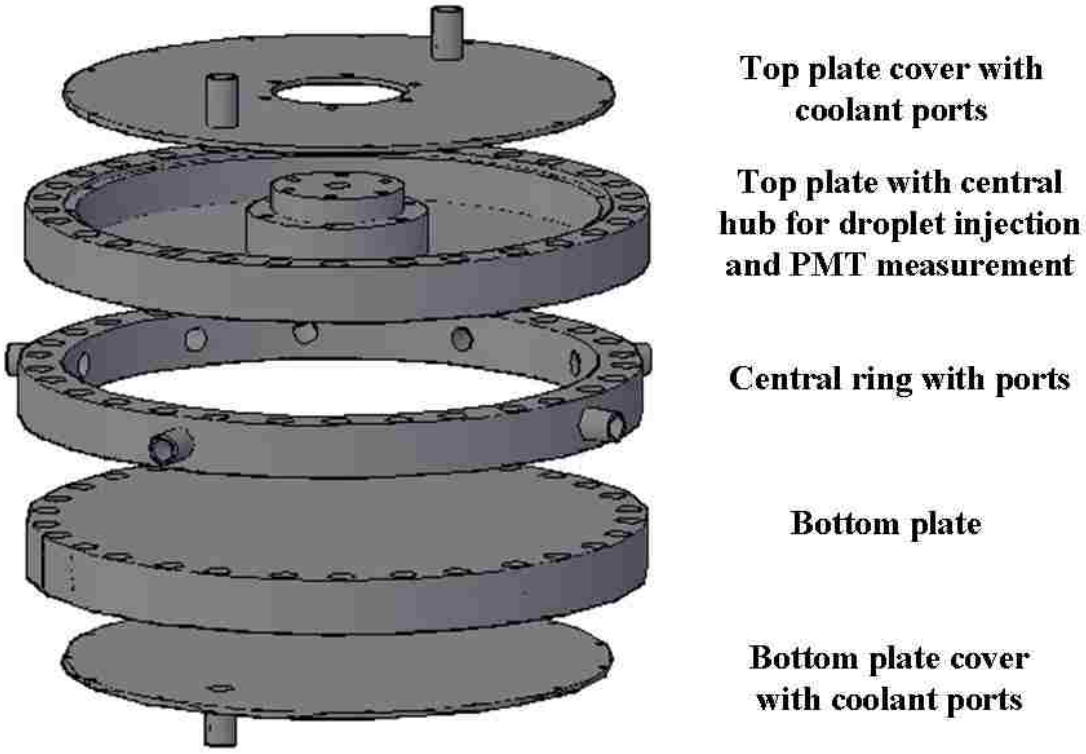

Figure 3.3 Expanded 3D view of the components of the thermal diffusion cloud chamber.

The top plate possesses a central port to allow for particle introduction into the chamber and detection of scattered light intensity via photomultiplier tubes (PMTs) whereas the bottom plate has a solid covering on both sides. The hub is located in the center of the top plate and is 3 1/2” in diameter and is capped with a 316 stainless steel fitting measuring 2 3/4” in diameter and 1/2" in height to allow the PMT to be secured during droplet observations. The fitting consists of 6 equally spaced 1/4" diameter threaded holes. The port located in the center of the hub measures 3/8” in diameter at the top and tapers to 1/4” diameter at the bottom of the plate which corresponds to the inside of the overall cloud chamber. The port has been coated with the same TV tube coating as the balance rings to reduce unwanted back-scattering of light when using the top PMT.

The central ring has the same diameter and outer bolt pattern as the corresponding top and bottom plates. The ring height and inside diameter measure 1 1/8” and 11”, respectively. The ring has been fitted with 9 ports which are selectively used for particle illumination and observation, detection of scattered light intensity, entrance and exit of an airflow system, temperature and relative humidity measurements, and the connection of the electrodynamic balance to the DC and AC power supplies.

The chamber is secured 10 1/2" above a vibration resistant optical table by three stainless steel posts. The chamber is attached to the post using 9 bolts through the outer bolt holes located on the chamber. The coolant fluid circulated through the top and bottom plates is a mixture of propylene glycol, water, and an algaecide. The coolant fluid is first introduced through one of the tube adapters on the top plate. It circulates through to the other top plate tube adapter before being directed to the bottom plate and finally returned to the coolant bath. The direction of this flow system helps reduce unwanted vertical temperature gradients within the chamber.

3.1.5 The Humid Airflow System

Investigations pertaining to hygroscopic materials typically involve observing a deliquescent salt or hygroscopic mixture at a particular relative humidity (RH). However, as the data obtained from these investigations is often directly related to the RH, ascertaining accurate RH values is essential. One option for precisely determining RH is to use saturated solutions of a well-characterized inorganic salt (Stokes and Robinson, 1949). However, this method can require days for equilibrium to occur and only provides a single RH data point. Choi and Chan (2002a) have described a humidity controlled system for use in conjunction with an electrodynamic balance they term the scanning electrodynamic balance (SEDB). Their procedure determines the solute mass fraction of a levitated particle as a function of relative humidity in the following manner. First, a particle is brought to equilibrium at a known relative humidity. Then, the relative humidity of the feed stream is stepped down to a known point. The solute mass fraction of the particle and corresponding relative humidity are observed as functions of time. The time dependence is calibrated using salts of known hygroscopic properties. Finally, the time dependent relationships between the solute mass fraction and relative humidity are equated to remove the time dependence. Although this procedure has been shown to produce reliable data (Choi and Chan, 2002a), it is only viable in regions where particle growth is reversible and is still on the time scale of an hour.

The humid airflow system used as part of this dissertation does not require the use of saturated salt solutions, allows equilibrium within minutes, and is viable over the full range of humidity. Simply described, the humid airflow system used here precisely combines a dry nitrogen gas stream with one saturated at a known temperature into a single stream with constant volumetric flow. This technique is routinely used to control the relative humidity in aerosol research (Cohen et al., 1987a,b,c; Andrews and Larson, 1993; Chan et al., 1997; Liu et al., 2008). The stream is introduced into the interior of the cloud chamber through a circular manifold constructed from 3/8” polyethylene tubing measuring 8” in diameter and having 16 equally spaced emission ports. The temperature and RH are measured by a probe placed in the immediate vicinity of the particle.

Figure 3.4 provides a schematic of the humid airflow system. Dry nitrogen gas is released from a cylinder of compressed nitrogen and passed through ¼" tubing. The initial dry stream is divided into two separate streams using a splitter shown by box 1 in the figure. Both of the streams leaving the splitter are routed through MKS mass airflow controllers, designated MAC 1 and 2, that are independently controlled by an interface. The stream passing through MAC 1 is maintained as dry nitrogen and sent directly to a merge point at box 2. The stream passing through MAC 2 is directed into a 500 ml round bottom flask containing de-ionized ultra-filtrated (DIUF) water. The flask is situated on top of a heater that maintains the water temperature at just below its boiling point. The saturated vapor stream leaving the flask is directed upwards through a liquid cooled reflux condenser located immediately above the flask and connected by a 24/40 glass fitting. The temperature of the humidified nitrogen gas stream leaving the reflux condenser is determined by the temperature of the coolant fluid circulated through the condenser and is measured by a probe attached to the top of the condenser. The coolant fluid enters the top of the condenser, travels downward, and is then sent to a temperature control bath at a desired temperature. After leaving the condenser, the humidified gas stream is at 100% relative humidity and is merged with the dry nitrogen gas stream shown by box 2 in the figure. The relative humidity of the combined gas stream is determined by the ratio of the dry stream to the humidified one. The flow rates of the two streams can be independently and precisely controlled (± 1 ml/min) by the mass airflow controller interface. However, their flow rates are manipulated in such as manner that the flow rate of their combined, humidified gas stream is constant at 1 l/min. The combined humid gas stream leaving box 2 is sent directly to the cloud chamber.

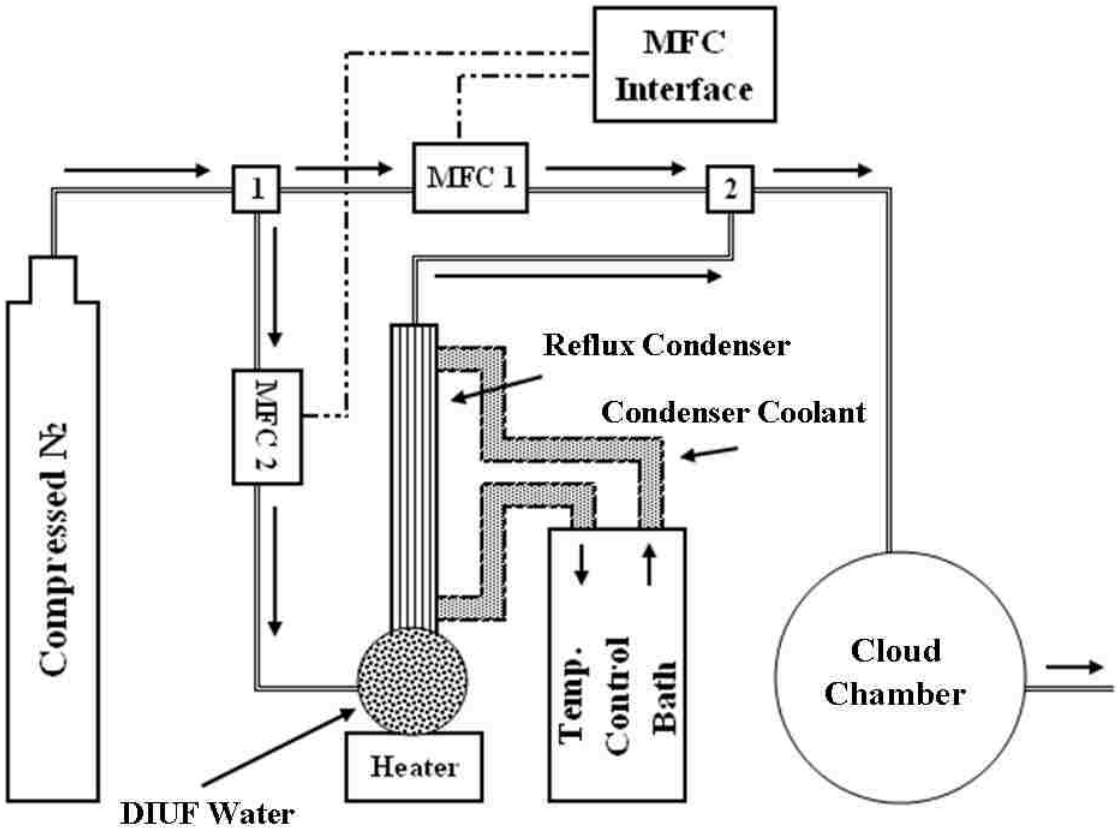

Figure 3.4 Schematic of the humid airflow system.

3.2 Experiments Pertaining to the Coulombic Fissions of Charged Droplets

3.2.1 Primary Focus of Investigation

The primary focus of this area of study was to investigate the role of electrical conductivity on the break-ups of charged droplets via Coulombic fission in response to findings in previous literature (de la Mora, 1996; Li et al., 2005; Gu et al., 2007). Here, the electrical conductivity of charged dielectric droplets has been manipulated via ionic dopants to observe the effects on their break-ups. The underlying assumption here is that the break-up characteristics of dielectric droplets can be made to resemble those of electrically conductive droplets. Specifically, by increasing the electrical conductivity of dielectric droplets, they should emit less mass and more charge during break-ups via Coulombic fission. How such an increase in electrical conductivity will affect the charge levels at which break-ups occur remains purely speculative.

3.2.2 Selection of Solvents

A critical aspect of this study was the selection of solvents from which charged droplets would be generated. As such, numerous solvents were initially evaluated against several criteria. First, the solvents needed to be relatively dielectric such that the resulting charged droplets would emit a considerable portion of mass during a break-up. Second, the solvents would have to be able to allow for the dissociation of the ionic dopants used. Finally, the evaporation rates of the solvents had to be considered. Here, the temperature at which experiments were conducted (25.0° C), the time required to begin monitoring the evaporation of the droplets (˜ 2 min), and an assumption of isothermal droplet evaporation all dictated the rate at which the droplets needed to evaporate.

Initially, ethylene glycol (EG), diethylene glycol (DEG), triethylene glycol (TEG), diethyl phthalate (DEP), and hexadecane (HXD) were selected as their amounts of charge and mass emitted during break-ups via Coulombic fission have been previously determined (Duft et al., 2002;2003; Manil et al., 2003; Li et al., 2005; Nakajima et al.,

2006). Tetraethylene glycol (T4EG) and dimethyl phthalate (DMP) were selected as they were currently available in the laboratory and were similar in nature to the glycol and phthalate solvents previously selected. Finally, nonanoic acid (NNA) and phenylnonane (PNN) were selected based on their dielectric nature and evaporation rates to add diversity to the types of solvents selected. All solvents were purchased from Sigma-Aldrich and used without further purification.

Not all the solvents originally selected for study however, were found to meet the required criteria. The ethylene glycol was observed to evaporate too rapidly under the desired temperature. When the temperature in the chamber was lowered sufficiently such that the evaporation rate was suitable, moisture was observed to condense inside the chamber. As ethylene glycol is very hygroscopic, the moisture present in the chamber at the lower temperature also was found to affect the evaporation rate. The solvent hexadecane was observed to evaporate suitably, but none of the observed intensity spectra were able to be correctly matched to corresponding theoretical spectra. Here, it was believed that the size of the hexadecane droplets being generated were very large at which point the intensity spectra become less unique.

3.2.3 Selection of Ionic Dopants

The selection of the ionic dopants posed a unique challenge to this study as almost no information is available in current literature regarding their use in association with charged droplets (Grimm and Beauchamp, 2002). As such, a wide variety of ionic dopants were selected and examined on a 'trial and error' basis. Two solid ionophores, tridodecylmethylammonium chloride (TDMAC) and tridodecylmethylammonium nitrate (TDMAN), and two ionic liquids, 1-ethyl-3-methylimidazolium dicyanamide [EMIM][$N(CN)_2$] and 1-methyl-3-octylimidazolium chloride [OMIM][Cl], were found to dissolve and increase the electrical conductivity in all of the phthalate and glycol solvents to some extent, but had no effect on the electrical conductivity of HXD, PNN, and NNA. Liquid hydrogen ionophore 1 and poly(3-hexylthiophene-2,5-diyl), regioregular (PHT), a conductive polymer, were also examined and found to be ineffective at increasing

electrical conductivity of HXD, PNN, and NNA. Only Stadis 450, a static dissipator containing dinonylnapthalene sulfonic acid, barium salt dissolved in toluene and isopropanol, was found to increase the electrical conductivity of HXD, PNN, and NNA. The ionophores and the conductive polymer were purchased from Sigma Aldrich and used without further purification. The ionic liquids were purchased from Solvent Innovation and also used without further purification. The static dissipator was currently available in the laboratory and made commercially available by Octel Stareon in Newark, New Jersey.

3.2.4 Experimental Procedure

Charged droplets of liquid solvents were observed both as pure components and when doped with a known concentration of a specified ionic material. Droplets having initial diameters between 35 and 50 μm were generated with a negative charge and studied using the electrodynamic balance, thermal diffusion cloud chamber, and light scattering equipment previously described. The temperature and pressure inside the chamber were constantly maintained at 25.0° C and 1 atm. Occasionally, more than one droplet was observed to be captured by the balance. When this situation occurred, the AC power supply to the central ring electrodes was rapidly switched off and on until only the most stable droplet remained. After visually verifying that only a single droplet exists, the DC potential was adjusted to position the droplet at its null point and the AC frequency was adjusted to center the droplet horizontally.

Once a droplet is properly centered and levitated, its mass, m, and charge, q, can be related through a force relation given by

$$mg = \frac{C_0 q V_{DC}}{z_0} \tag{3.1}$$

where g is the gravitational force acting on the droplet, C_0 is the geometric constant of the balance, V_{DC} is the potential required to levitate a charged droplet at is null point, and z_0 is the distance between the top and bottom electrodes. A stream of dry nitrogen gas was passed through the chamber to remove unwanted solvent vapor released by droplet

evaporation. The rate of the nitrogen gas flow was maintained at such a level to not alter the DC potential required to balance the droplet.

Once a charged droplet of a desired composition had been captured and properly balanced, the DC potentials required to periodically balance it at its null point were recorded as functions of time. The intensity of scattered light in the TE and TM modes were detected by the corresponding PMTs and recorded in arbitrary units as functions of time by a personal computer. The scattering intensities in the two modes were plotted in real time and could be continuously viewed on a monitor by the observer during an experiment. The ability to view the scattering intensities of a droplet in real time assists the observer in knowing when to record the balancing DC potentials. The data collected by the observer and the computer are used along with Mie theory and the refractive index of the droplet to determine the size and charge of a droplet immediately before and after droplet break-up via Coulombic fission and therefore the amounts of mass and charge emitted and the corresponding charge limit. The data analysis procedure is described in detail in Chapter 4.

3.3 Hygroscopic Growth of Mixed Particles

3.3.1 Primary Focus of Investigation

The primary focus of this area of study was to investigate how non-volatile, water insoluble materials affect the hygroscopic behavior of atmospherically relevant inorganic salts. Although similar studies have been previously conducted, disagreement persists on the hygroscopic effects of such materials (Garland et al., 2005; Chan and Chan, 2007). Furthermore, the inorganic salt particles in these studies were externally coated with the hydrophobic material (Otani and Wang, 1984; Hansson et al., 1990;1998; Hameri et al., 1992; Xiong et al., 1998; Cruz and Pandis, 1998; Raymond and Pandis, 2003; Garland et al., 2005; Chan and Chan, 2007). Here, the inorganic salt particles are internally mixed with the water insoluble material to also examine how different particle morphologies may impact the hygroscopic behavior.

3.3.2 Selection of Inorganic Salts

The two inorganic salts typically selected for this type of study are NaCl and $(NH_4)_2SO_4$ as they are the most dominant inorganic salts in the atmosphere (Martin et al., 2000; Raes et al., 2000; Wise et al., 2007). Here however, NaBr was selected in place of $(NH_4)_2SO_4$ since the deliquescence and crystallization relative humidities of NaCl and $(NH_4)_2SO_4$ are relatively similar (Tang and Munkelwitz, 1994; Wise et al., 2005; Biskos et al., 2006a,b; Gao et al., 2007a,c). Furthermore, the deliquescence and crystallization relative humidities and hygroscopic growth of NaBr particles are equally well studied and also occur as very sharp, distinct changes in the water content of the particles (Cohen et al., 1987a; Wise et al., 2005). Several additional inorganic salts were originally selected for study. They are $CaCl_2$, KCl, $NaClO_4$, NH_4Br, and NH_4Cl, and LiCl. $CaCl_2$ particles were observed to form various hydrates and to behave almost purely hygroscopic and therefore no further studies were conducted. Data from particles of KCl, $NaClO_4$, NH_4Br, and NH_4Cl and their mixtures with selected hydrophobic materials were taken using an old chilled optical mirror currently available in the laboratory. Later, and unfortunately, data from this piece of equipment was found to be unreliable. Due to time constraints, such experiments were not repeated using the newly acquired hygrometer. The inorganic salt LiCl was used solely as a supersaturated solution, along with corresponding solutions of NaBr and NaCl, to occasionally calibrate the hygrometer. All inorganics salts were purchased from Sigma-Aldrich and used without further purification.

3.3.3 Selection of Non-Volatile, Hydrophobic Additives

In previous relevant studies, only hydrophobic organics have been used (Otani and Wang, 1984; Hansson et al., 1990;1998; Hameri et al., 1992; Xiong et al., 1998; Cruz and Pandis, 1998; Raymond and Pandis, 2003; Garland et al., 2005; Chan and Chan, 2007). Here, some of these organics have been re-examined during this study. They are the dioctyl phthalate (DOP) and lauric acid (LA), which are liquid and solid, respectively, at the temperature studied (25° C). Two additional liquids, Invoil 704 silicone diffusion

pump fluid (SIL) and Santovac-5-oil, a polyphenyl ether (PPE), and two solids, anthracene (AN) and a carbon black (BC), were examined. Although SI and PPE have not been identified in the atmosphere, they serve as representative samples of non-volatile, hydrophobic materials. The PPE and SIL were currently available in the laboratory and used without further purification. The BC was provided by Contintental Carbon (lot N234, Phenix City, Al plant) and used as received. The DOP, LA, and AN were purchased from Sigma-Aldrich and used without further purification.

The liquid additives DOP, SI, and PPE and the solid additive LA used in this study were all found to be miscible in a solution of the selected inorganic salt, 200 proof ethanol, and de-ionized, ultra-filtrated water. Although the ratio of each of the solvents was unique to the particular additive, all the resulting solutions were completely homogeneous. Droplets generated from these solutions are assumed to be internally mixed as previous studies have employed an identical approach using water soluble organics and inorganic salts and have reported the formation of internally mixed particles (Chan et al., 1997; Cruz and Pandis, 2000; Lightstone et al., 2000; Bilde and Svenningsson, 2004; Braban and Abbatt, 2004; Parsons et al., 2004; Gao et al., 2007b).

The solid additives AN and BC had particle sizes below one micrometer and were mixed with a solution of the desired inorganic salt dissolved in de-ionized, ultra-filtrated water and 200 proof ethanol. The resulting heterogeneous mixtures were placed in a Branson model 1210 ultrasonic vibrator for at least an hour prior to particle generation to sufficiently disperse the solid in the solution. The water and ethanol were purchased from Sigma-Aldrich and used without further purification. Droplets generated from these solutions are also assumed to be internally mixed as previous studies have employed an identical approach using mineral dusts that are water insoluble or only slightly water soluble (Gibson et al., 2007; Liu et al., 2008).

Pure component particle of each of the water insoluble additives were exposed to increasing relative humidity and none showed any hygroscopic growth at relative humidities below 85%.

3.3.4 Experimental Procedure

Charged particles of inorganic salts were observed both as pure components and when internally mixed with a known concentration of a specified non-volatile, hydrophobic material. Particle having initial diameters between 35 and 50 μm were generated with a negative charge and studied using the electrodynamic balance, thermal diffusion cloud chamber, and humid airflow system previously described. The temperature and pressure inside the chamber were constantly maintained at 21.5° C, the ambient temperature of the laboratory, and 1 atm. The flow rate of the humid air entering the chamber was maintained at 1 $l \cdot min^{-1}$ and introduced by a circular manifold located inside the chamber. The relative humidity inside the chamber was controlled by adjusting the ratios of the water saturated and dry nitrogen gas streams as previously described. The temperature and relative humidity of the atmosphere surrounding a levitated particle were measured by the aforementioned hygrometer probe located immediately outside the balance rings. Again, more than one particle was occasionally observed to be captured by the balance and the situation was remedied in the manner previously described for charged droplets. Particles were balanced at their null point by adjusting the DC potential and radially centered by adjusting the AC frequency in an identical manner to charged droplets.

Prior to particle generation, all the humidity inside the chamber was removed by flushing with pure nitrogen gas. Upon generation, the ethanol and water were observed to nearly instantly evaporate and be flushed from the chamber leaving a solid particle. After being properly levitated, the particle was continually exposed to the stream of dry nitrogen until its levitation potential was observed to be constant. The relative humidity inside the chamber was then slowly increased to a desired point above the deliquescence relative humidity of the corresponding pure component inorganic salt and then decreased back to its starting point. The potentials required to levitate the particle at its null point, V_{DC}, were recorded as functions of relative humidity (RH) during the cycle. Upon completion of an experiment, the V_{DC} versus RH data was used to construct a hysteresis loop on an additive-free basis for comparison to the corresponding pure component inorganic salt. The data analysis procedure is described in detail in Chapter 4.

Chapter 4: Data Analysis

4.1 Theoretical Background

4.1.1 Stable Electrodynamic Levitation of an Individual Charged Droplet

The repulsion and attraction between charges of like and dislike signs, respectively, form the basis for the levitation of an individual droplet in an electrodynamic balance. To briefly explain the electrodynamic levitation of a charged droplet, consider a droplet with a fixed amount of negative charge as it is vertically introduced to the top center of the electrodynamic balance illustrated by figure 3.2 and where the top and bottom electrodes of the balance possess a positive and negative DC potential, respectively. The droplet is attracted vertically upwards to the top electrode, is repulsed vertically upwards away from the bottom electrode, and is pulled vertically downwards by gravity. For the droplet to be properly levitated at its null point, sufficient potential must be applied to completely cancel the gravitational force acting upon the droplet. In order to verify that the proper potential has been applied, the power supplied to the central AC rings of the balance is temporarily removed. If the droplet is not properly levitated, it will instantly move either vertically upwards or downwards depending on whether there is too much or too little DC potential, respectively. If the droplet is properly levitated at its null point however, it will not be observed to move for a brief period of time, after which it will eventually begin to lose its radial stability. Adornato and Brown (1983) and Tsamopoulos et al. (1985) have provided an in-depth analysis of the shape and stability of charged droplets levitated in an electrical field. Charged droplets examined as part of this study were observed while properly levitated and continuously maintained at their null point.

This process of levitating a charged droplet in an electrical field is physically explained by first summing the individual forces acting on a spherical droplet having an overall force, *F*, given by

$$F = F_G + F_E + F_D \tag{4.1}$$

where F_G, F_E, and F_D are the forces acting on the droplet due to gravity, the applied electric field, and drag from a vertically applied airflow, respectively, and are each further defined as

$$F_G = -mg \tag{4.2}$$

$$F_E = qE \tag{4.3}$$

$$F_D = -\frac{1}{2} C_D \rho_f U^2 A \tag{4.4}$$

where E is the applied electric field, C_D is the drag coefficient, U is the characteristic velocity of a droplet moving through a fluid of density ρ_f, A is the projected area of a spherical droplet, g is the gravitational force acting on the droplet, and m and q are the mass and charge of the droplet, respectively. Assuming the airflow past a levitated droplet is well within the laminar flow region (Re = 0.1) so as not cause destabilization, the drag force, F_D, given by (4.4) can be evaluated using Stokes law given by

$$F_D = -6\pi a \mu U \tag{4.5}$$

where μ is the dynamic viscosity of the fluid surrounding the droplet and a is the droplet radius. For the charged droplets investigated during this dissertation however, the airflow was reduced sufficiently low enough that the drag force term, F_D, could be neglected entirely. Therefore, the resulting force, F, on a levitated droplet applicable to the work here can be given by

$$F = -mg + qE \tag{4.6}$$

where E is further defined as

$$E = C_0 \frac{V}{z} \tag{4.7}$$

where V is the potential applied across two electrodes separated by a vertical distance z and C_0 is a geometrical constant determined by the balance configuration. To properly levitate a charged droplet at its null point, the total force acting on the droplet must be zero. Therefore, (4.6) is rewritten as

$$mg = qC_0 \frac{V}{z} \tag{4.8}$$

and is identical to (3.1) when V is V_{DC}, the DC potential required to levitate the droplet at its null point, and z is z_0, the distance between the top and bottom DC electrodes.

Davis (1985) and Hartung and Avedisian (1992) have discussed in detail the theory pertaining to the stability of a charged droplet while levitated in an electrodynamic balance of a known configuration. Stability theory assumes that the motion of a particle in an electrodynamic balance can be determined by Newton's second law and requires knowledge of the electromagnetic force on the droplet. The resulting equations for droplet motion in the radial and axial directions as given by Davis (1985) are recapitulated here by

$$m\frac{d^2r}{dt^2} = F_{D,r} + qE_{1,r} + qE_{2,r} \tag{4.9}$$

$$m\frac{d^2z}{dt^2} = F_{D,z} + qE_{1,z} + qE_{2,x} - mg \tag{4.10}$$

where the subscripts r and z refer to the radial and axial directions, respectively, t is time, z is the axial position of the droplet, m and q have been previously defined, F_D is given by (4.5), and E_1 and E_2 are the electrical field vectors for the AC and DC fields, respectively, and are given by

$$E = -\Delta V \tag{4.11}$$

where V is the superposition of the time-dependent ring potential, V_1, and the DC potential across the top and bottom electrodes, V_2, given by

$$V = V_1 + V_2 \tag{4.12}$$

Furthermore, V must satisfy Laplace's equation and is given in cylindrical coordinates by

$$\left(\frac{(1/r)\partial(r\,\partial V/\partial r)}{\partial r}\right) + \frac{\partial^2 V}{\partial z^2} = 0 \tag{4.13}$$

The resulting equations for the AC electrical field in the radial and axial directions are given by

$$E_{1,r} = \frac{-(V_b + V_{AC}\cos(\Omega t))r}{2z_0^2} \tag{4.14}$$

$$E_{1,z} = \frac{(V_b + V_{AC}\cos(\Omega t))z}{z_0^2} \tag{4.15}$$

where V_b is the DC bias potential, z_0 is the distance between the top and bottom DC electrodes, and Ω is given by

$$\Omega = 2\pi f_{AC} \tag{4.16}$$

where f_{AC} is the AC frequency. The resulting equations for the DC electrical field in the radial and axial positions are given by

$$E_{2,r} = \frac{C_1(r,z)V_0}{z_0} \tag{4.17}$$

$$E_{2,z} = \frac{C_2(r,z)V_0}{z_0} \tag{4.18}$$

where V_0 is the DC potential required to properly levitate a charged droplet at its null point, and C_1 and C_2 are radial and axial dependent geometric balance constants.

The resulting solutions to the equations of motion have been previously given by Davis (1985) and Hartung and Avedisian (1992). Therefore, further discussion is restricted to the determination of the geometric balance constant. This procedure has been previously discussed in detail by several investigators (Ataman and Hanson, 1969; Schweizer and Hanson, 1971; Davis, 1985) and involves manipulating either the AC frequency, the AC voltage, or a combination of both until the droplet begins to vertically oscillate at its null point. The point at which a charged droplet begins to oscillate is determined by the marginal stability envelope determined by relating the field strength parameter, β, to the drag parameter, δ, for a particular V_{DC}/V_{AC} where V_{AC} is the AC potential applied to the central balance rings and β and δ are given by

$$\beta = \frac{2gV_{AC}}{\pi^2 C_0 z_0 f_{AC}^2 V_{Dc}} \tag{4.19}$$

$$\delta = \frac{9\mu}{2\pi a^2 \rho f_{AC}} \tag{4.20}$$

where ρ is the droplet density, μ is the viscosity of the surrounding gas, and the remaining terms have been previously defined. Davis (1985;1997) and Hartung and Avedisian (1992) have provided figures showing up to the first four stability envelopes including the changes in the marginal stability limits when $V_b/V_{AC} = \pm 0.1$.

For this study, C_0 was determined using negatively charged droplets of diethyl phthalate properly levitated at their null point. The droplets were allowed to evaporate in a vapor-free environment while being maintained at their null point until enough

scattering intensity versus time data was acquired to accurately determine droplet size at a specific time. The AC potential was held constant at 1200 V and the AC frequency applied to the central balance rings was quickly reduced over a few seconds until the droplet was observed to oscillate. The AC frequency at which the oscillation was observed was recorded along with the corresponding DC potential and the time. The time was then used to determine the droplet diameter at the instant the oscillation occurred. Using this method, a single droplet could be used to provide numerous data sets since the droplet could be re-stabilized and the process repeated. After sufficient data points were collected, a series of values for δ were determined using (4.20). Next, corresponding values for β were determined using an equation developed from data located in Table 2 given by Ataman and Hanson (1969) that relates the two parameters. Using (4.19), a corresponding series of C_0 values were obtained, the average of which was used as C_0. As more than one electrodynamic balance configuration was used during this dissertation to examine charged droplets, and the rings of each balance were occasionally replaced due to miscellaneous reasons, three different balance constants were determined for use and were 0.49, 0.55, and 0.84. Figure 4.1 provides a plot of the individual data points used to calculate C_0 for the electrodynamic balance constructed as part of this dissertation and described in detail in Chapter 3. The solid line and corresponding equation were fitted to the data points (solid circles) obtained from Ataman and Hanson (1969) and used to develop the marginal stability curve relating δ and β. Here it should be noted that the equation fitted to the data given by Ataman and Hanson (1969) is a numerical fit only valid for the parameter ranges given within the figure. The experimental data from charged droplets of diethyl phthalate are given by solid triangles. Here, C_0 was determined from the average of 39 data points and found to be 0.55 ± 0.02. A density of 1118 kg·m-3 was used for diethyl phthalate (Li et al., 2005), a viscosity of 175.44 μP (Stephan et al., 1987) was used for nitrogen gas at 25.0 °C, and a value of 0.01945 m was used for z_0. Droplets had diameters in the range of 20 to 40 μm, DC potentials in the range of 2 to 40 V, and AC frequencies in the range of 80 to 450 hz.

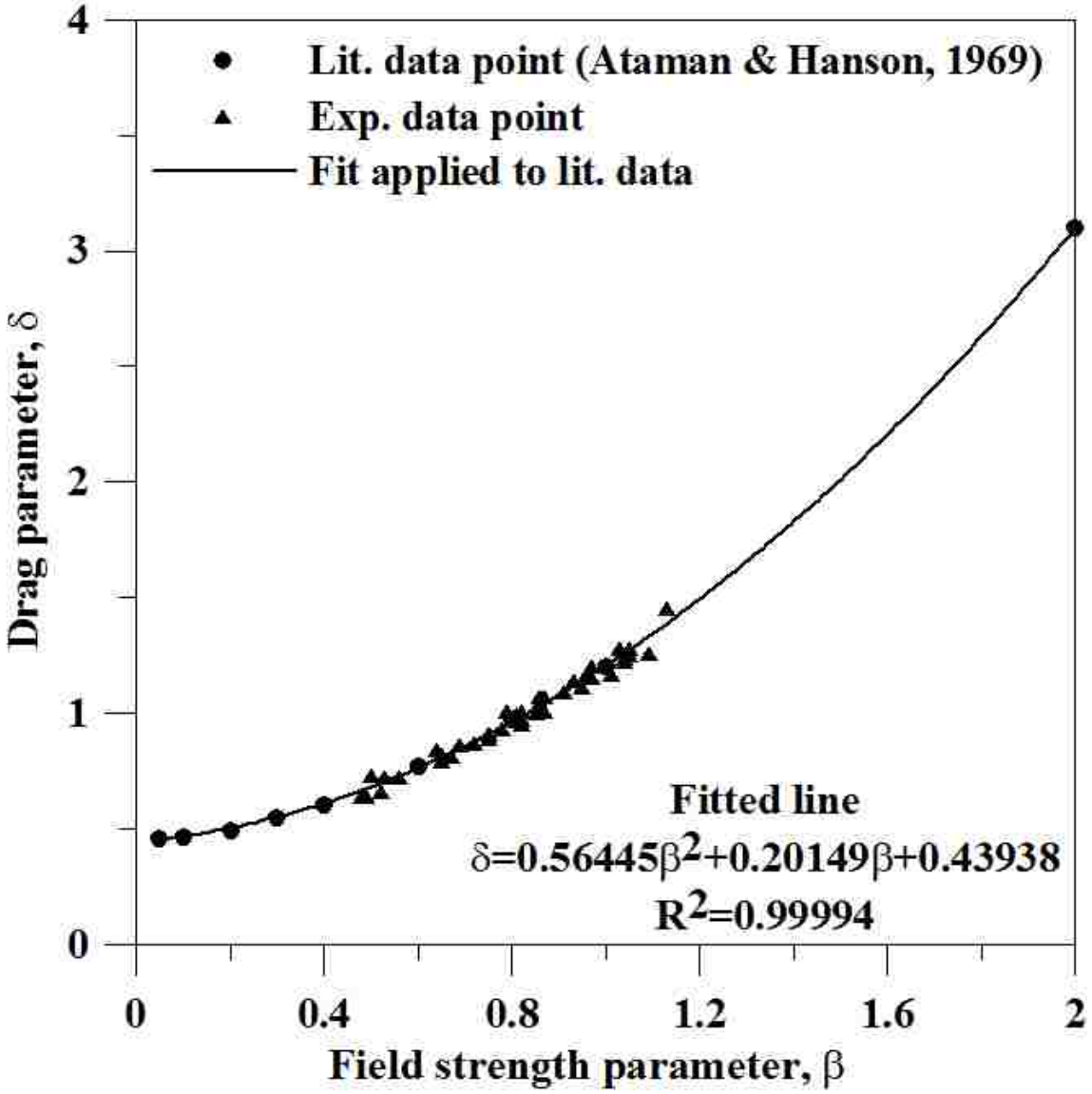

Figure 4.1 Plot of the marginal stability envelope and experimental data points used to determine C_0.

4.1.2 Evaporation of an Isolated Spherical Droplet

The evaporation or growth of an isolated spherical droplet is affected by both its own characteristics and those of its immediate environment. Here, the evaporation of an individual, homogenous, spherical, liquid droplet of component *A* having an initial radius, *a*, levitated in a stagnant, gaseous medium of component *B* is considered. Furthermore, it is assumed that the flux of the solvent molecules evaporating radially outwards from the surface of the droplet is dependent only on the radial position *r*, where $r=0$ at the center of the droplet, and is independent of azimuth and inclination.

Assuming quasi-steady state, a one-dimensional material balance over a spherical shell between *r* and Δr where $r>a$ gives

$$\frac{d}{dr}\left(N_{Ar}\,4\pi r^{2}\right)=0 \tag{4.21}$$

Integrating (4.21) gives

$$N_{Ar}\,4\pi r = W_{A} \tag{4.22}$$

where W_A is an unknown constant. The flux term, N_{Ar}, can be expressed by combining the diffusive flux and flux due to the bulk motion caused by diffusion given by

$$N_{Ar} = J_{Ar} + \left(N_{Ar} + N_{B,r}\right)y_{A} \tag{4.23}$$

where y_A is the vapor mole fraction of *A* and J_{Ar} is Fick's first law of diffusion. The flux of component *B*, $N_{B,r}$, can be equated to zero since it is assumed to be stagnant. Assuming components *A* and *B* behave solely as ideal gases, J_{Ar} can be given by

$$J_{Ar} = -D_{AB}C\frac{dy_{A}}{dr} \tag{4.24}$$

where D_{AB} is the diffusion coefficient of *A* in *B* and *C* is the molar concentration of an ideal gas given by

$$C=\frac{P}{RT_{\infty}} \tag{4.25}$$

where *P* and T_∞ are the total pressure and temperature, respectively, and *R* is the ideal gas constant. For $r>a$, it is assumed that the temperature and pressure of the surrounding gas

are independent of radial position and therefore C can be treated as a constant. Incorporating (4.22) and (4.24) into (4.23) and separating the variables gives

$$\frac{W_A}{4\pi}\frac{dr}{r^2} = -D_{AB}C\frac{dy_A}{(1-y_A)} \tag{4.26}$$

Integrating (4.26) between the surface of the droplet, a, and some value of r sufficiently far way from the surface of the droplet such that y_A becomes zero and solving in terms of W_A gives

$$W_A = -4\pi a D_{AB} C \ln(1-y_{AS}) \tag{4.27}$$

where y_{AS} is the mole fraction of A at the surface of the droplet given by

$$y_{AS} = \frac{P_A(T_S)}{P_\infty} \tag{4.28}$$

where P_A and T_S are the vapor pressure of A and temperature at the surface of the droplet. For relatively non-volatile droplets where $y_{AS} \ll 1$, as is applicable for the charged droplets investigated during this dissertation, (4.27) can be simplified to

$$W_A = 4\pi a D_{AB} C y_{AS} \tag{4.29}$$

Taking a time-dependent material balance at the surface of the droplet gives

$$-W_A = \frac{d}{dt}\left(\frac{4\pi a^3 \rho}{3M_A}\right) \tag{4.30}$$

where M_A is the molecular weight of A, ρ is the density of the droplet, and t is time. Incorporating (4.29) into (4.30) and cancelling redundant terms gives

$$-aD_{AB}Cy_{AS} = \frac{d}{dt}\left(\frac{a^3\rho}{3M_A}\right) \tag{4.31}$$

Taking the derivative on the right-hand side of (4.31), removing the constant terms ρ and M_A from the derivative, and cancelling redundant terms gives

$$-D_{AB}Cy_{AS} = \frac{a\rho}{M_A}\frac{da}{dt} \tag{4.32}$$

Separating the variables and integrating from t=0 where the radius of the droplet, a, has an initial radius, a_0, to some arbitrary time, t, where $0 < a < a_0$ gives

$$-D_{AB}Cy_{AS}t = \frac{\rho}{2M_A}\left(a^2 - a_0^2\right) \tag{4.33}$$

Rearranging (4.33) in terms of a^2 gives the surface evaporation rate of the droplet as a function of time given by

$$a^2 = a_0^2 - \frac{2D_{AB}Cy_{AS}M_A}{\rho}t \tag{4.34}$$

Incorporating (4.25) and (4.28) into (4.34) gives

$$a^2 = a_0^2 - \frac{2D_{AB}V_A P_A\left(T_S\right)}{RT_S}t \tag{4.35}$$

where V_A is the molar volume of the droplet given by

$$V_A = \frac{M_A}{\rho} \tag{4.36}$$

The relatively non-volatile solvents used as part of this study evaporate at a sufficiently low rate such that they can be considered to remain isothermal with respect to the surrounding temperature and T_S can be very closely approximated by T_∞. Therefore, an analysis of the heat transfer by the droplets is not required to accurately model their evaporation.

4.1.3 Light Scattering by a Homogeneous Sphere

When an object is illuminated by electromagnetic waves, discrete electric charges within the object become oscillatory resulting in the scatter and absorption of the electromagnetic energy (Bohren and Huffman, 1983). The theory of electromagnetism was first postulated by Maxwell (1865) wherein he showed that electricity, magnetism, and light were all interrelated. Although the processes of electromagnetic scattering and absorption cannot be mutually excluded, one from the other, hereafter only the scattering of electromagnetic energy, specifically that of light in the visible spectrum, will be discussed. Moreover, the following discussion will be restricted to the scattering of light by a homogeneous, spherical droplet as only this aspect of electromagnetic scattering is relevant to this dissertation.

From here, the logical point of departure is the solution of the Maxwell equations for microspheres having diameters slightly larger than the wavelength of light. Several authors have published the solutions to Maxwell's equations given by Lorenz (1890) and Mie (1908) for spheres (Born, 1980; van de Hulst, 1981; Bohren and Huffman, 1983; Kerker, 1983; Barber, 1990). Furthermore, these solutions have been discussed in great detail by previous investigators (Chylek, 1973; Conwell et al., 1984; Probert-Jones, 1984; Johnson, 1993) and have also been applied to the observation of levitated droplets (Chylek et al., 1983; Ray and Huckaby, 1993; Huckaby et al., 1994; Huckaby and Ray, 1995; Ray and Nandakumar, 1995). Therefore, only the pertinent aspects of these solutions will be given corresponding to the light scattered by a homogenous, spherical droplet. Here, the nomenclature and format used by Huckaby et al. (1994) will be repeated except that the term for refractive index, *m*, will be replaced by ω, to avoid confusion as *m* has been previously defined as a mass term.

According to Lorenz-Mie theory, a homogenous, spherical body illuminated by a polarized light with wavelength, λ, scatters light with intensities I_1 and I_2, respectively, into the planes perpendicular (TE mode) and parallel (TM mode) to the plane of incident light given by

$$I_1 = \frac{I_i \lambda^2}{4\pi^2 r^2}\left[\sum_{n=1}^{\infty} \frac{2n+1}{n(n+1)}\left(a_n \pi_n + b_n \tau_n\right)\right]^2 \tag{4.37}$$

$$I_2 = \frac{I_i \lambda^2}{4\pi^2 r^2}\left[\sum_{n=1}^{\infty} \frac{2n+1}{n(n+1)}\left(b_n \pi_n + a_n \tau_n\right)\right]^2 \tag{4.38}$$

where *r* is the radial distance out from the center of the sphere and must be much greater than λ and the angular functions p_n and t_n are given by

$$\pi_n = \frac{P_n^1(\cos\theta)}{\sin\theta} \tag{4.39}$$

$$\tau_n = \frac{d}{d\theta} P_n^1(\cos\theta) \tag{4.40}$$

where θ is the scattering angle and $P_n^1(\cos\theta)$ is a 1st order Legendre function of degree *n*. The scattering coefficients for the TM and TE modes are, respectively, a_n and b_n and are given by

$$a_n = \frac{A_n(x,\omega)}{A_n(x,\omega) + iC_n(x,\omega)} \tag{4.41}$$

$$b_n = \frac{B_n(x,\omega)}{B_n(x,\omega) + iD_n(x,\omega)} \tag{4.42}$$

where i is the imaginary unit, ω is the refractive index of the droplet, x is the size parameter given by

$$x = \frac{2\pi a}{\lambda} \tag{4.43}$$

and A_n, B_n, C_n, and D_n are given by

$$A_n(x,\omega) = \psi_n(x)\psi_n'(\omega x) - \omega\psi_n(\omega x)\psi_n'(x) \tag{4.44}$$

$$B_n(x,\omega) = \omega\psi_n(x)\psi_n'(\omega x) - \psi_n(\omega x)\psi_n'(x) \tag{4.45}$$

$$C_n(x,\omega) = \chi_n(x)\psi_n'(\omega x) - \omega\psi_n(\omega x)\chi_n'(x) \tag{4.46}$$

$$D_n(x,\omega) = \omega\chi_n(x)\psi_n'(\omega x) - \psi_n(\omega x)\chi_n'(x) \tag{4.47}$$

where ψ_n and χ_n are the n^{th} order Ricatti-Bessel functions of the 1st and 2nd kinds, respectively.

The intensities of light scattered by a homogeneous, spherical droplet in the TE and TM modes are dependent on the wavelength of incident light, λ, the refractive index, ω, and the droplet radius, a, and can be independently altered by each variable. From here, further discussion is restricted to droplets of a known ω that are illuminated by a polarized light source with a constant λ and are observed at a specific θ in both the perpendicular and parallel planes as is relevant to this dissertation. Therefore, all effects on the scattering intensities in the both the TE and TM modes can be attributed to the reduction in the radius of an evaporating droplet. Furthermore, when $\theta \sim 90°$, the angular functions given by (4.39) and (4.40) can be expressed with acceptable accuracy using the asymptotic relationships (Tu, 2000) given by

$$\pi_n = c_{(n-1)}\cos\left((n-1)\theta\right) \tag{4.48}$$

$$\tau_n = nc_{(n)}\cos\left(n\theta\right) \tag{4.49}$$

where $c_{(n)}$ is given by

$$c_{(n)} = \frac{(n+1)!}{2^n \left(\frac{n}{2}!\right)^2} \tag{4.50}$$

when *n* is zero or an even integer and

$$c_{(n)} = \frac{2n+3}{2n+2} \frac{n!}{2^{n-1} \left(\frac{n-1}{2}!\right)^2} \tag{4.51}$$

when n is an odd integer. As a result, (4.37) and (4.38) can be simplified and given by

$$I_1 = \frac{I_i \lambda^2}{4\pi^2 r^2} \left| \sum_{i=1}^{\infty} c_{(n)} \frac{2n+1}{n+1} b_n \cos(n\theta) \right|^2 \tag{4.52}$$

$$I_2 = \frac{I_i \lambda^2}{4\pi^2 r^2} \left| \sum_{i=1}^{\infty} c_{(n)} \frac{2n+1}{n+1} a_n \cos(n\theta) \right|^2 \tag{4.53}$$

The importance of (4.52) and (4.53) is that the scattering amplitudes of a_n and b_n can be mutually excluded from each other by independently observing the scattering intensities in the TE and TM modes.

Tu (2000) has previously described in detail the manner in which intensities are numerically calculated for a homogeneous, spherical droplet. For this study, three Fortran programs labeled TT1, TT2, and TT3 previously developed in-house were used to compute the intensities of scattered light in both the TE and TM modes. The first program, TT1, returns the scattered intensities as a function of the droplet size. The second program, TT2, returns the scattered intensities as a function of time and is discussed later in this chapter. The third program, TT3, returns the scattered intensities as a function of the refractive index.

Figure 4.2 provides an example of the intensity spectra in both the TE (lower spectrum) and TM (upper spectrum) modes for a homogeneous, spherical droplet of pure DEP (ω=1.4972) illuminated by a vertically polarized He-Ne laser (λ=632.8 nm) during evaporation as a function of the square of the droplet radius from 15.0^2 to 14.0^2 μm^2. The scattering intensities I_1 and I_2, respectively, in the TE and TM modes were both determined at a scattering angle exactly 90° using Fortran program TT1. Evident in both intensity spectra are very sharp intensity 'spikes' known as morphology dependent resonance (MDRs) that occur when the wavelength of incident light is totally, internally reflected within the sphere and correspond to when the imaginary parts of the denominators of the scattering coefficients, a_n and b_n, become zeros. The intensity spikes may appear as peaks or troughs or may not appear at all. To retain consistency when describing a particular optical resonance, investigators have classified each MDR by its polarization, TE or TM, by the mode number, n, of the scattering coefficient, and by an order number, l, where l=1 corresponds to the first positive root of $C_n(x,\omega)$=0 or $D_n(x,\omega)$=0 (Huckaby et al., 1994). Chylek et al. (1983) and Huckaby et al. (1994) have shown that light scattering theory can be used to precisely determine the size of a droplet with a relative error of 5×10^{-5} by relating the intensity spectra and MDRs obtained from a levitated droplet to corresponding theoretically generated spectra. More recently, this technique has been used by Li et al. (2005) to determine the amount of mass ejected by charged, levitated droplets during Coulombic fissions within a relative error of 1 part in 10^4.

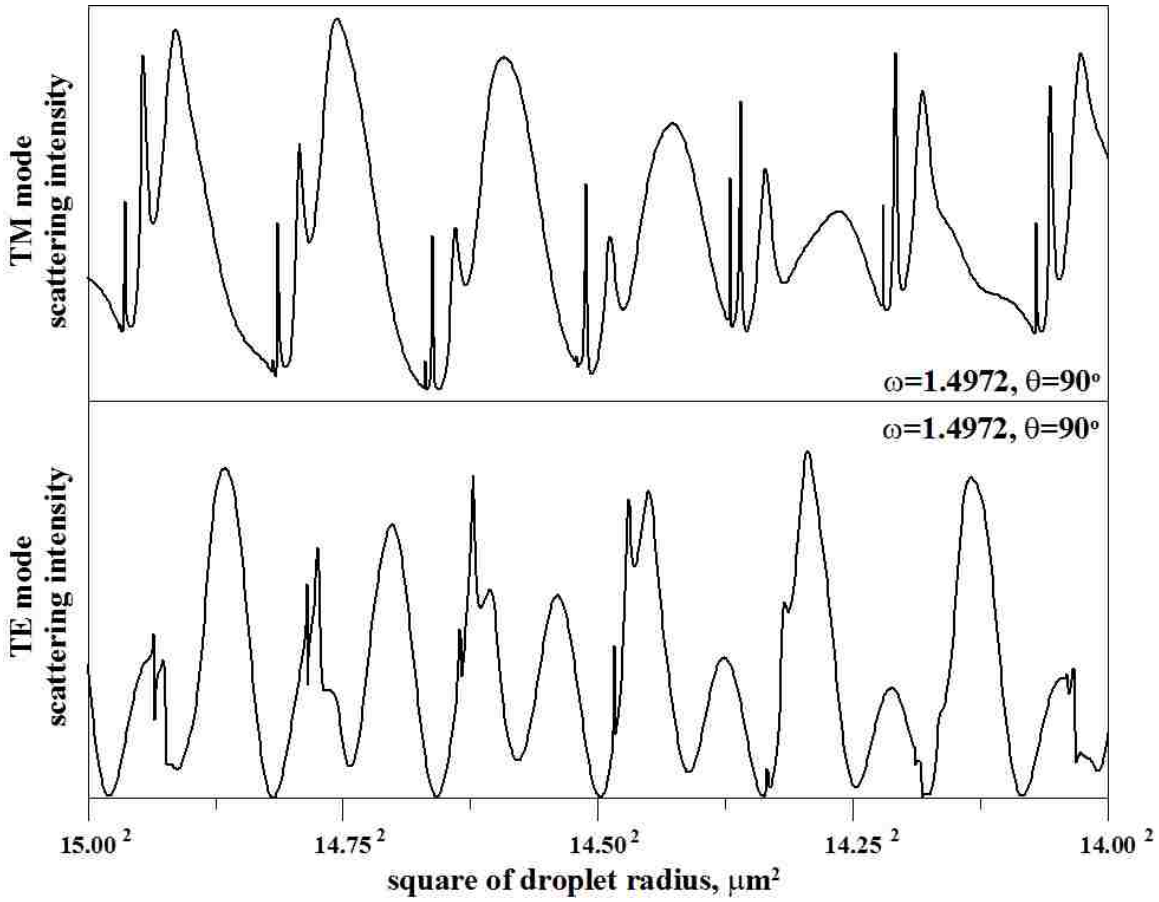

Figure 4.2 Example of the scattering intensity versus square of the droplet radius spectra for the TE and TM modes.

4.2 Analysis of Droplet Break-up Data

4.2.1 Analysis of Scattering Intensity Versus Time Data

During experiments involving a charged, levitated droplet, the intensities of the light scattered in the TE and TM modes were each independently measured by two PMTs and recorded as functions of time at a specified time interval by a personal computer. Typically, charged droplets were observed over a time interval of 30 minutes to two hours, depending on the evaporation rate of the droplet. The time interval between two successive data points for all experiments was set at 1/100 of a second. The interval was determined from initial experiments by evaluating the quality of the scattering intensity versus time data for various time intervals. Here, slower time intervals produced intensity spectra that lacked the detail necessary to observe the sharp MDR peaks and faster time intervals failed to improve spectra resolution while also decreasing the computational efficiency of subsequent data analysis.

Concluding the observation of a droplet, the intensity versus time data recorded for the TE and TM modes were used to construct intensity spectra using Grapher 3 software. Here, a number, *N*, of sharp MDR peaks or troughs, typically between 20 and 40, are selected from each of the spectra that will be used to independently determine both the initial size of the droplet and its evaporation rate. Tu and Ray (2001) have previously discussed the selection of MDR peaks suitable for further analysis. At this point, the experience of the investigator can be very beneficial in correctly ascertaining which peaks or troughs to select. To precisely identify the exact times at which the selected MDR peaks and troughs had their highest or lowest intensities, respectively, the times immediately before and after each selected MDR were recorded using an application with the Grapher 3 software. The recorded pairs of times were then inputted into a Fortran program previously developed in-house labeled ResonfinderA. The program compares the inputted time pairs for each MDR selected to the raw intensity versus time data file and returns the exact time at which each selected MDR had it highest or lowest intensity. When finished, the program provides an output data file

containing times, t_i, corresponding to each of the selected MDRs for both the TE and TM modes.

The output data file from the ResonfinderA program for the TE and TM modes are then input into a corresponding pair of Fortran programs previously developed in-house labeled TimalignaTE and TimalignaTM, respectively, to independently determine the initial size and evaporation rate of the droplet using a procedure previously described in detail by Tu and Ray (2001) and Li et al. (2005) and shown to determine droplet size within 0.1%. Both the TimalignaTE and TimalignaTM programs also require the user input an estimate for the size parameter range in which the MDRs occurred and to specify the refractive index. The estimated size parameter range should reasonably encompass that observed for the droplet. Here, the experience of the investigator is again very beneficial in estimating the correct size parameter range. However, the size parameter for a particular time in an intensity spectrum can be reasonably estimated in the following manner. First, (3.1) is expressed in terms of the droplet radius, a, given by

$$a = \left[\frac{3C_0 q V_{DC}}{4\pi\rho g z_0} \right]^{1/3} \tag{4.54}$$

Next, (4.54) is incorporated with (4.43) and rearranged in terms of x to give

$$x = kV_{DC}^{1/3} \tag{4.55}$$

assuming that q remains constant and where k is given by

$$k = \left[\frac{6C_0 q \pi^2}{\lambda^3 \rho g z_0} \right]^{1/3} \tag{4.56}$$

Next, (4.55) is applied to two successive MDRs having the same order and mode and recast as

$$\frac{x_1 - x_2}{x_1} = \frac{\Delta x}{x_1} = \frac{V_1^{1/3} - V_2^{1/3}}{V_1^{1/3}} \tag{4.57}$$

where the subset numbers 1 and 2 correspond the 1st and 2nd successive MDRs selected and where Δx can be approximated according to Huckaby et al. (1994) as

$$\Delta x \cong \frac{\tan^{-1}(\eta)}{\eta} \tag{4.58}$$

where η is given by

$$\eta = \left(\omega^2 - 1\right)^{1/2} \tag{4.59}$$

The potentials V_1 and V_2 corresponding to x_1 and x_2 can be related via the times at which the selected MDRs occurred. The relationship between the DC levitation potential and time is discussed in detail later in this chapter.

To correctly determine the initial size and evaporation rate of a droplet, each of the N selected MDRs occurring at a time, t_i, are aligned with one of M theoretical MDRs, where $M > N$, occurring at a size parameter, x_i, for a particular mode. The estimated size parameter range input by the user dictates the number, M, of theoretical MDR peaks having a specific width range that will be generated by the program. Furthermore, it is assumed that the refractive index of the droplet remains constant during evaporation. The times corresponding to the array of N selected MDRs and the size parameters corresponding to the array of M theoretically generated MDRs are arranged such that when properly aligned the earliest time corresponds to the largest size parameter. To relate the size parameter to time, (4.43) is incorporated into (4.35) and recast as

$$x_i^2 = x_0^2 - \kappa_1 t_i + \kappa_2 t_i^2 \tag{4.60}$$

where κ_1 and κ_2 are constants and the second order term has been included to account for slight errors in the evaporation rate due to the presence of trace impurities within the droplet and partial saturation of the vapor immediately surrounding the droplet (Tu and Ray, 2001; Li et al., 2005). Next, each of the x_i versus t_i data are regressed to compute the alignment error $Y(\omega)$ using

$$Y(\omega) = \sum_{i=1}^{N} \left(x_i^2 - x_0^2 + \kappa_1 t_i - \kappa_2 t_i^2\right)^2 \tag{4.61}$$

The alignment procedure is then repeated with a corresponding error analysis for all logical alignments between the selected and theoretical MDRs. The computer program then returns to the user the values for x_0, κ_1, and κ_2 that yielded a minimum in alignment error for each specified refractive index. A range of refractive indices is typically selected based on the droplet material selected or an a priori knowledge and inputted to the computer program along with a specific interval at which to implement (4.61). The

refractive index that returns the alignment with the best error is assumed correct. The ability to simultaneously determine both the size and refractive index of a droplet with a high degree of accuracy has previously been proven using this method (Chylek et al., 1983; Huckaby et al., 1994; Ray and Nandakumar, 1995; Tu and Ray, 2001). The refractive index and surface evaporation rates obtained from the TE and TM modes are then compared as each mode provides an independent set of results that should be identical for a correct alignment. Although the results from the two modes are rarely identical, their differences are nearly always negligible and only noticeable in the second order term corresponding to the error in the evaporation rate due to surface impurities on a droplet or some localized vapor saturation.

Table 4.1 provides an example of the output from the TimalignaTM program for a negatively charged droplet of pure DEP with an assumed refractive index of ω=1.4972. The program returns to the user the number of selected MDRs and the size parameter range originally inputted by the user along with the surface evaporation rate with the corresponding average time and size parameter errors and a breakdown of the individual times, size parameters, mode and order numbers, and time and size parameter errors for each of the x_i versus t_i data for the alignment producing the minimum error. The average time error and the value of κ_2 are typically the defining values used by the observer to determine the validity of the experiment. Here, an average time error greater than 0.4 s or a κ_2 value greater than 1×10^{-4} warrants repeating the experiment as they correspond to an unsteady droplet evaporation rate and add significant difficulty in further data analysis. Here, N=24 MDR peaks were selected from the observed time versus intensity spectrum obtained in the TM mode and their corresponding occurrence times, t_i, used as input. {As a note to the reader, the TM mode typically produces a more distinct selection of sharp MDRs. This can be easily seen by re-examining Figure 4.2 wherein the top portion (TM mode) of the figure has very sharp and distinct MDRs that appear with a regular periodicity as compared to the lesser distinguishable MDRs found in the lower portion (TE mode) of the figure.} To generate the array of theoretical MDRs, a size parameter range of $x_{initial}$=300 to $_{xfinal}$=100 was inputted from which M=715 theoretical MDR peaks occurring at size parameters, x_i, were calculated.

Table 4.1 Example of the output from the TimalignaTM program for a droplet of pure DEP observed in the TM mode.

Number of selected MDRs: N=24
Size parameter range: $x_{initial}$=300 to x_{final}=100
Number of theoretically generated MDRs: M=715

Surface evaporation rate: $x^2 = 3.00405 \times 10^4 - 7.49412t + (6.11880 \times 10^{-6})t^2$

Average time error: 0.04407 s
Average size parameter error: 0.001087

Observed Times (t_i in s)	**Theoretical Size Parameter (x_i)**	**Mode Number (n)**	**Order Number (l)**	**Time Error s**	**Size Parameter Error**
47.280	172.29704	182	13	-0.00819	-0.00018
115.870	170.79859	180	13	0.01301	0.00029
183.985	169.29841	178	13	-0.00409	-0.00009
246.700	167.90334	180	12	0.07468	0.00167
313.255	166.41405	178	12	-0.01160	-0.00026
379.220	164.92325	176	12	-0.02660	-0.00060
444.660	163.43087	174	12	-0.03429	-0.00079
509.550	161.93685	172	12	-0.00865	-0.00020
573.930	160.44111	170	12	0.01123	0.00026
637.860	158.94359	168	12	-0.03396	-0.00080
701.295	157.44422	166	12	-0.09896	-0.00235
759.990	156.04006	168	11	0.01293	0.00031
821.720	154.55237	166	11	0.01977	0.00048
882.915	153.06309	164	11	0.04127	0.00101
943.580	151.57215	162	11	0.07342	0.00181
1003.780	150.07947	160	11	0.05224	0.00130
1063.490	148.58497	158	11	0.00369	0.00009
1122.690	147.08856	156	11	-0.05146	-0.00131
1181.330	145.59018	154	11	-0.06286	-0.00161
1239.395	144.08977	152	11	-0.01573	-0.00041
1293.020	142.68918	154	10	0.06720	0.00176
1349.505	141.20172	152	10	0.05187	0.00137
1405.515	139.71250	150	10	-0.00938	-0.00025
1460.990	138.22143	148	10	-0.05552	-0.00150

The refractive index and surface evaporation rate from the alignment with the minimum error are then used as input into the Fortran program TT2 to generate a theoretical scattered intensity spectrum as a function of time for each mode. The user is also required to input a time period and range of scattering angles at a corresponding interval for which to generate the intensity spectra. The theoretical intensity spectra generated by the computer program are then plotted versus the corresponding observed intensity spectrum to visually determine the correct theoretical spectrum and thus the scattering angle of the observed spectrum. Here more than ever, the experience of the investigator is possibly the best tool for correctly determining the scattering angle of the observed spectrum as an incorrect scattering angle can lead to misalignment of the two spectra and therefore an inaccurate determination of droplet size.

Figure 4.3 provides an example of how a theoretical intensity spectrum can be misaligned with a corresponding observed intensity spectrum. Here, both spectra were theoretically generated for a droplet of pure DEP with ω=1.4972 and are in terms of scattering intensity (arbitrary units) versus the square of the size parameter. The lower spectrum was generated for a scattering angle, θ=94.55°, over the range, x^2=49,551 to x^2=43,098. The upper spectrum was generated for a scattering angle, θ=95.20°, over the range, x^2=52,900 to x^2=46,225. To the untrained eye, the two spectra appear strikingly similar, and differ only by minute details. However, such minute details are crucial in determining the correct scattering angle. Since both the scattering angle and droplet size are not known a priori, figure 4.3 highlights how one may incorrectly match a theoretically generated spectrum to an observed spectrum and therefore incorrectly determine the droplet size at a particular location in the intensity spectrum. Moreover, this dilemma is not resolved by analysis of the TM spectra assuming the same scattering angles and size parameter range as the same similarities will again be observed. An incorrect alignment is typically the result of using data from an alignment with too much associated error however, and illustrates why such tight restrictions are used in the aforementioned procedure pertaining to the TimalignaTE and TimalignaTM programs. Fortunately, the similarities only exist for a finite size parameter range. Therefore, by

comparing the observed and theoretical spectra over a sufficient size parameter range, the correct scattering angle and therefore correct droplet size can be determined.

When an observed intensity spectrum is correctly matched with its theoretical counterpart however, the two spectra are typically so well aligned that they cannot be distinguished, one from the other, when overlapped. Figure 4.4 provides an example of observed and theoretical spectrums that have been correctly aligned. The intensities of all spectra are in arbitrary units. Here, a scattering intensity spectrum observed in the TE mode for a droplet of pure DEP over a time range of 400 s is shown at the bottom of the figure. The matching theoretical scattering intensity spectrum for a sphere in the TE mode with a refractive index, ω=1.4972, scattering angle, θ=95.400°, and over the range of the square of the size parameter from x^2=27,044 to x^2=30,045 is shown at the top of the figure. The scattering intensity spectrum shown in the middle of the figure is an overlapping of the observed and theoretical spectra and illustrates the precision of a correctly determined scattering angle.

Once the correct TE and TM mode scattering intensity angles have been determined, the theoretical intensity spectra are used to independently and precisely determine the squares of the size parameters that correspond to the times immediately before and after each droplet break-up. Since a portion of droplet mass is emitted during break-up, the size of the droplet is instantly reduced and therefore a discontinuity in both the observed TE and TM intensity spectra exist where each break-up occurred. No discontinuity however, will exist for the corresponding theoretical intensity spectra. When properly aligned with the corresponding theoretical intensity spectra, the discontinuities appear as ‘gaps’ in the observed spectra. Furthermore, the sections of an observed intensity spectrum occurring before a break-up typically lack detail due to the geometric distortion experienced by a droplet immediately prior to a break-up via Coulombic fission. The sections of an observed intensity spectrum occurring after a break-up are nearly identical to that of a theoretical spectrum however, since the droplet has returned to a spherical shape.

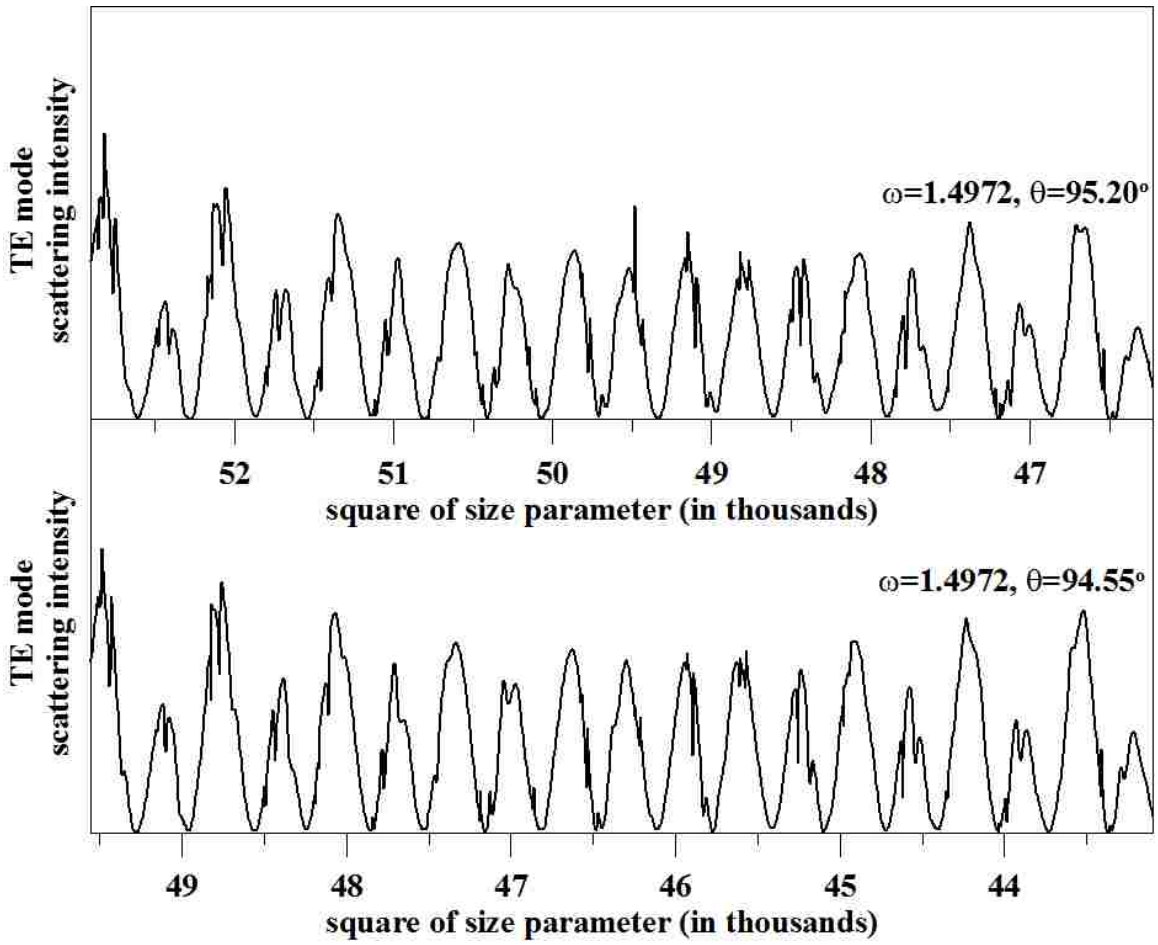

Figure 4.3 Example portraying the similarities between two different scattering intensity versus size the square of the parameter spectra.

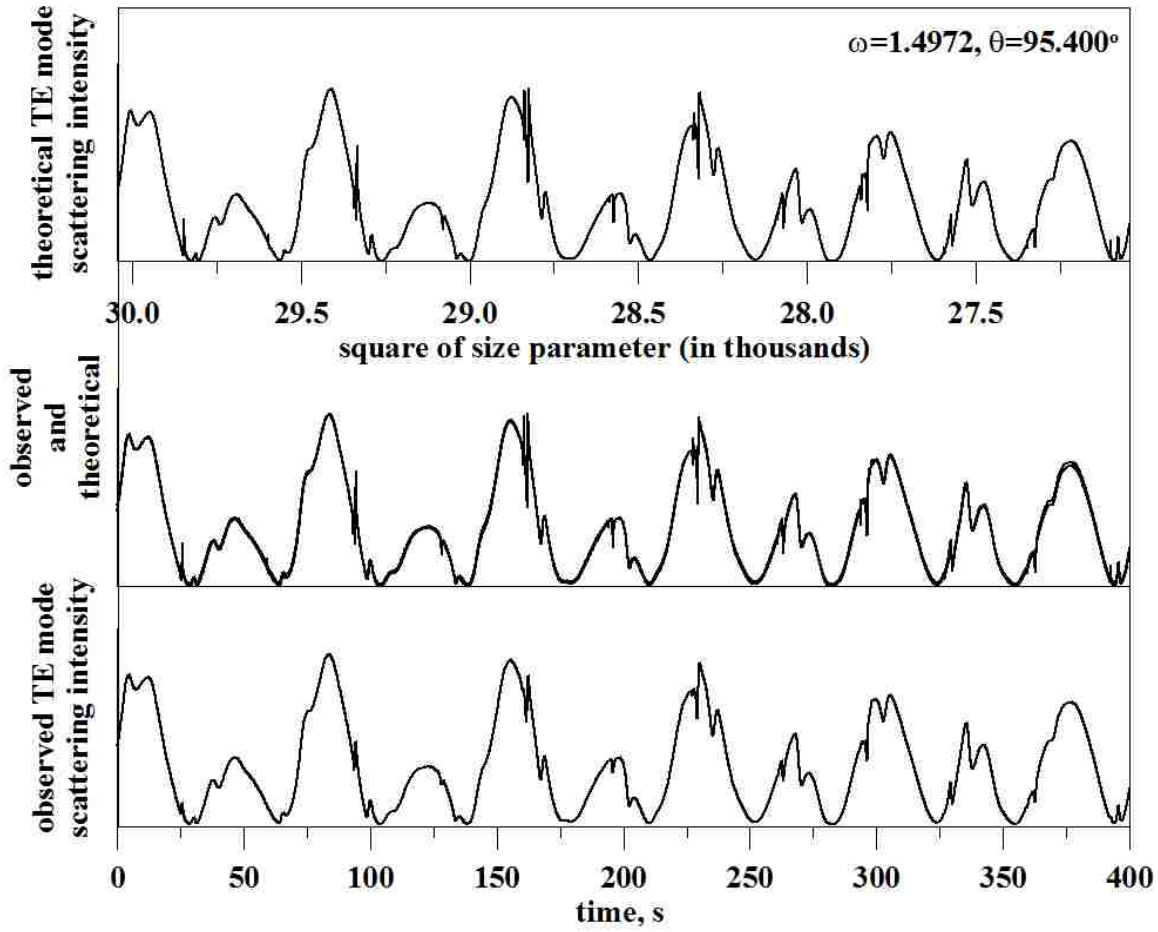

Figure 4.4 Example of a correct alignment between the theoretical (top) and observed (bottom) intensity spectrums. Middle spectrum is an overlapping of the top and bottom spectra.

Figure 4.5 provides an example for a properly aligned theoretical and observed intensity spectra in the TE mode in the region where a break-up via Coulombic fission has occurred during the evaporation of a negatively charged droplet of pure DEP. Due to the instantaneous emission of mass during a break-up, a discontinuity results in the observed intensity spectrum from the rapid change in the droplet radius. When the observed (bottom) and theoretical (top) intensity spectra are aligned, the discontinuity in the observed spectrum appears as a 'gap' since the theoretical spectrum does not account for a break-up. Here, the refractive index of the DEP droplet was ω=1.4972 and the scattering angle was found to be θ=95.400°. The scattering intensities of both spectra are given in arbitrary units. After aligning the theoretical and observed intensity spectra, the times immediately before and after the break-up were determined to be t_i=1899.14 s and t_f=1899.70 s, respectively. The corresponding squares of the size parameters immediately before and after the break-up were determined to be $(x_i)^2$=15663.5 and $(x_f)^2$=15837.2, respectively.

After determining the squares of the size parameters that correspond to the times immediately before and after a droplet break-up via Coulombic fission, the percentage of mass emitted by the droplet, f_m, can be calculated using

$$f_m(\%) = 100 \times \frac{x_i^3 - x_f^3}{x_i^3} \tag{4.62}$$

Using the values for x_i and x_f given in figure 4.5, f_m is calculated to be 1.64% which is just below the range of f_m =2.28% ± 0.45 for a pure DEP droplet given by Li et al. (2005).

The procedure just described for determining the percentage of mass emitted by a charged droplet during its break-up via Coulombic fission was repeated for all break-ups observed during the evaporation of a charged droplet. The aforementioned procedures used for droplet observation, data collection, data analysis, the generation of theoretical scattering intensity spectra, and the correct alignment of theoretical and observed spectra were repeated for all charged droplets.

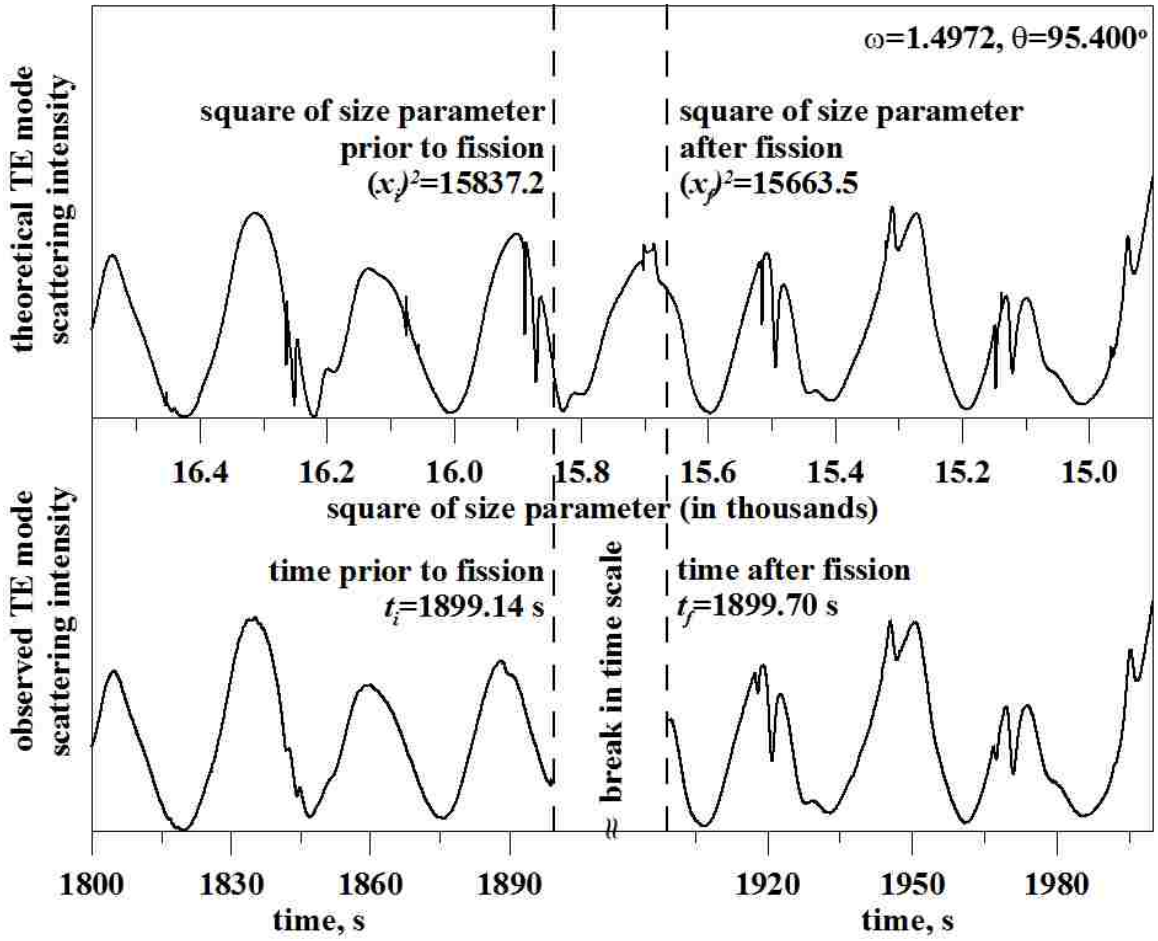

Figure 4.5 Example of a properly aligned theoretical and observed intensity spectra in the TE mode in which a break-up via Coulombic fission has occurred during the evaporation of a negatively charged droplet of pure DEP.

4.2.2 Analysis of DC Levitation Potential Versus Time Data

During the evaporation of a charged droplet, the observer manually records the change in the DC potential required to levitate a charged droplet at its null point as a function of time. Since the droplet mass is reduced during evaporation, the DC potential must by periodically adjusted to insure the droplet remains at its null point. To verify the position of the droplet in relation to its null point, the AC power is temporarily shut off for about a second by the observer. Depending on the response of the droplet in the absence of the AC voltage and frequency, an experienced observed can correctly and quickly return the droplet to its null point with minimal impact on the droplet. By precisely maintaining a droplet at its null point, the scattering angles in the TE and TM modes will remain constant and therefore subsequent data analysis will be more accurate. The time interval at which the DC potential is adjusted depends on the evaporation rate of the droplet, and can range from a few seconds to a few minutes. An additional effort is made to record the DC potentials immediately after a break-up has been observed.

To relate the change in the DC potential to time, (4.54) is incorporated into (4.35) to give

$$\left(\frac{3C_0 q}{4\pi\rho g z_0}\right)^{2/3} V_{DC}^{2/3} = a_0^2 - \left(\frac{2D_{AB}V_A P_A(T_S)}{RT_S}\right)t \tag{4.63}$$

which is simplified into

$$V_{DC}^{2/3} = \sigma t + V_{DC,0}^{2/3} \tag{4.64}$$

where V_{DC} is the DC potential required to levitate a charged droplet precisely at its null point and σ is a constant assuming the charge on a droplet remains constant between break-ups. Here, it is important to note that the times recorded by the observer are in sync with the times recorded by the personal computer used to record the intensities of scattered light in the TE and TM modes. To synchronize the two times, the observer maintains a stop watch that is started at the instant the computer is keyed to begin recording. This is critical in accurately determining the DC levitation potential at the times immediately before and after a droplet break-up. The times immediately before, t_i, and after, t_f, each break-up are precisely determined from the times corresponding to the

beginning and ending of the 'gap' in the observed intensity spectrum after being properly aligned with the correct theoretical intensity spectrum. Note the times recorded along with null point levitation potentials are only used to determine the corresponding relationships between $V_{DC}^{2/3}$ and t. The times t_i and t_f are then inputted to the corresponding equations determined for $V_{DC}^{2/3}$ as a function of t and used to extrapolate the DC levitation potentials of a droplet immediately before and after a break-up. In this manner, a DC null point levitation potential, $V_{DC,i}$, at a specific time, t_i, can be accurately related to a corresponding x_i. The ability to relate V_{DC} to x is critical in determining the amount of charge emitted by a droplet during its break-up via Coulombic fission.

Figure 4.6 provides an example of the $V_{DC}^{2/3}$ versus time data for a negatively charged droplet of pure DEP. Here, the droplet of DEP is the same droplet that was observed to produce Figure 4.5. Moreover, the timescale used in this figure directly corresponds to that used in Figure 4.5. The solid diamonds represent the raw data points recorded by the observer. The data points before and after the break-up were fitted to (4.64) to determine the values for σ and $V_{DC,0}^{2/3}$ for Fit 1 and Fit 2, respectively. The times, t_i and t_f, given in Figure 4.5 are inputted into the equations given by Fit 1 and Fit 2, respectively, to determine the corresponding values of $V_{DC,i}$ and $V_{DC,f}$. Here, the DC levitation potentials immediately before and after the droplet break-up were determined to be $V_{DC,i}$ =4.91 V and $V_{DC,f}$ =5.45 V using the corresponding times, t_i=1899.14 s and t_f=1899.70 s, obtained from Figure 4.5.

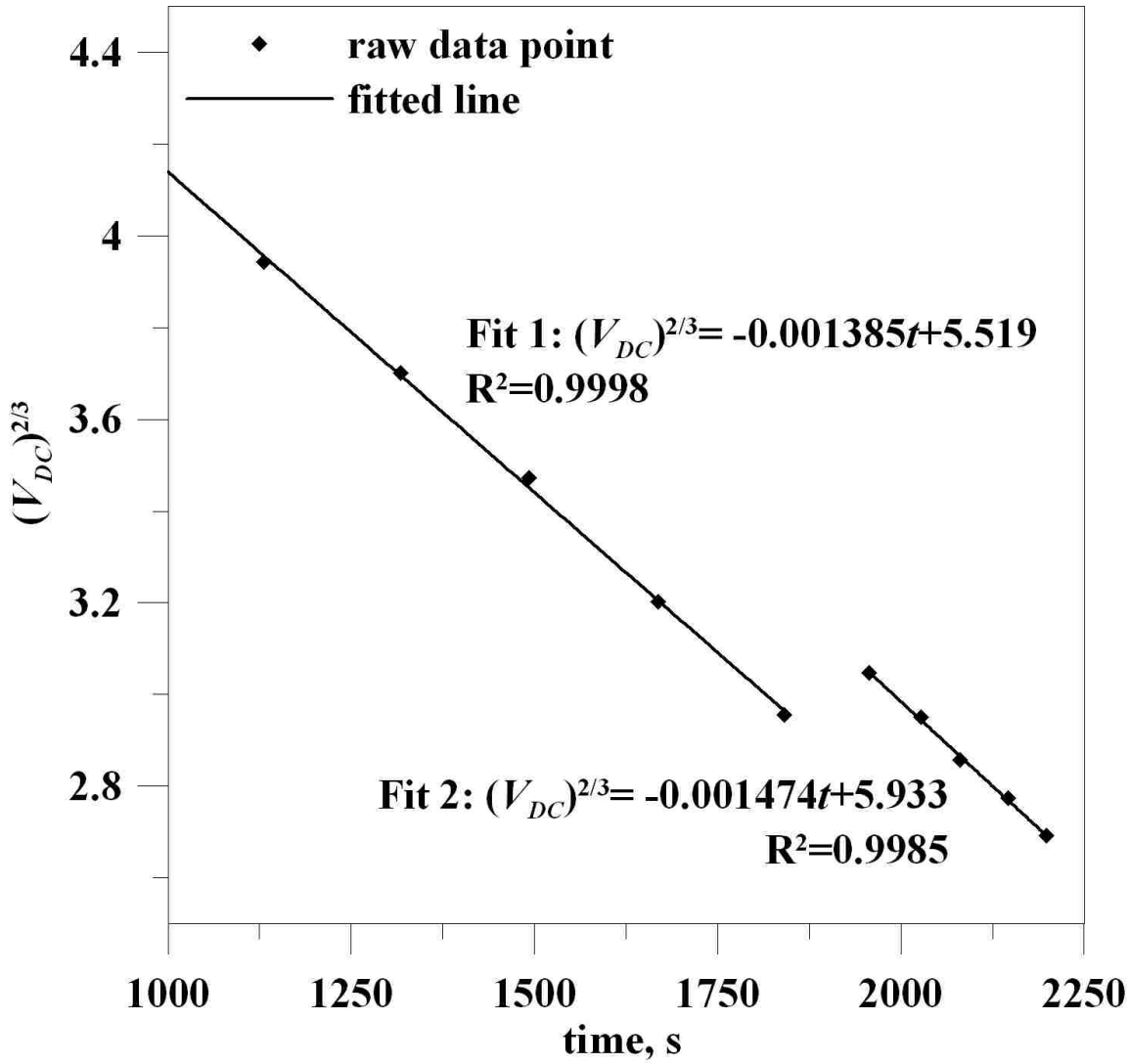

Figure 4.6 Example of $V_{DC}^{2/3}$ versus time plot for a droplet of pure DEP.

After determining the DC levitation potentials, $V_{DC,i}$ and $V_{DC,f}$, of a droplet immediately before and after a droplet break-up via Coulombic fission, the percentage of charge emitted, f_q, can be calculated using

$$f_q(\%) = 100 \times \left(1 - \frac{x_f^3 V_{DC,i}}{x_i^3 V_{DC,f}} \right) \tag{4.65}$$

Using the values of x_i, x_f, $V_{DC,i}$, and $V_{DC,f}$ obtained from Figures 4.5 and 4.6, f_q is calculated to be 11.4% which is below the range of f_q =20.8% ± 4.9 for a pure DEP droplet given by Li et al. (2005).

After ascertaining the values for the size and DC levitation potential of a droplet immediately before its break-up via Coulombic fission, the charge limit, q, and corresponding Rayleigh limit, q_R, at which the droplet break-up occurred can be calculated using (3.1) and (1.1), respectively, and expressed as a percentage of the Rayleigh limit, f_R, using

$$f_R = 100 \times \left(\frac{q}{q_R} \right) = \frac{mgz_0}{8\pi C_0 V_{DC,i} \left(\varepsilon_0 \gamma a_i^3 \right)^{1/2}} \tag{4.66}$$

Using (4.43) to determine the droplet radius, a_i, from the size parameter, x_i, occurring at the time t_i=1899.14 s in Figure 4.5 and the corresponding value of the DC levitation potential, $V_{DC,i}$, from Figure 4.6, the resulting values for q and q_R are 6.456×10^{-13} C and 6.411×10^{-13} C, respectively, where m=9.534×10^{-12} kg, g=9.81 m·s^{-2}, z_0=0.01664 m, C_0=0.491, $V_{DC,i}$=4.91 V, e_0=8.8542×10^{-12} s^4·A^2·m^{-3}·kg^{-1}, γ=0.0361 N·m^{-1}, and a_i=1.2674×10^{-5} m. The result of (4.66) is a value of f_R=100.7%. Therefore, the assumptions previously made regarding the data analysis procedure are validated as the break-up of the pure DEP droplet occurred via Coulombic fission precisely at its Rayleigh limit. Moreover, the values determined for f_m and f_q, although below the ranges given by Li et al (2005), can also be assumed to be valid.

4.2.3 Relating Ionic Dopant Concentration to Electrical Conductivity

To determine the role of electrical conductivity on the amounts of mass and charge emitted during a break-up via Coulombic fission and the charge limit at which the break-up occurred, droplets were generated from solutions doped with a known amount of an ionic additive. In order to determine the electrical conductivity of a droplet containing a specified amount of ionic dopant, a series of solutions were prepared from the desired solvent and known amounts of the selected ionic dopant. The electrical conductivity of each solution was then measured using a YSI 3200 Conductivity Instrument equipped with a model 3256 glass probe. For a particular series of solvent-dopant solutions, a plot of electrical conductivity versus dopant concentration was developed. For each solvent-dopant pair, an equation was fitted to the data that gave the best R^2 value. This equation was then used to calculate the electrical conductivity for a known concentration of ionic dopant.

Figure 4.7 provides an example of an electrical conductivity versus molar ionic dopant concentration plot developed from 10 solutions of DEP doped with TDMAC. The solid diamonds represent the raw data points. Here, the electrical conductivity, *K*, of pure DEP was measured to be 0.69 $\mu S \cdot m^{-1}$ and incorporated into the equation fitted to the data. The form of the fitted equation given by Fit 1 was chosen solely on its ability to best fit the data.

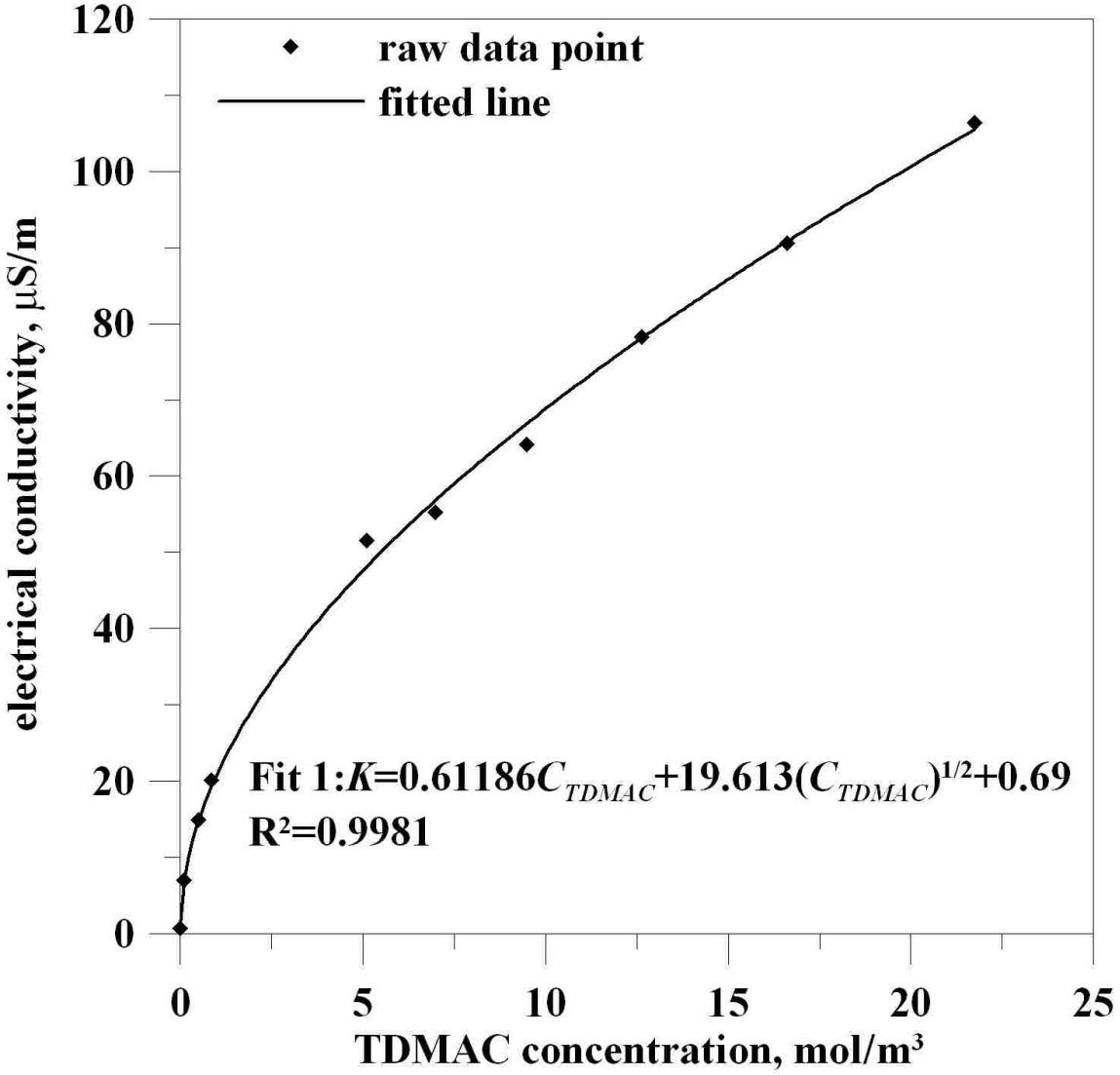

Figure 4.7 Example of an electrical conductivity versus molar ionic dopant concentration for mixtures of DEP and TDMAC.

To apply the relationship determined for a particular solvent-dopant pair to a charged droplet, it was assumed that the concentration of ionic dopant in a droplet at generation was equal to that of the corresponding bulk solution. For droplets experiencing multiple break-ups, it was also assumed that the amount of dopant emitted during a break-up was negligible. This assumption is later shown to be valid since droplets having noticeable mass emissions had very low dopant concentrations and droplets with high dopant concentrations had negligible mass emissions. Therefore, the concentration, C_i, of a droplet at a particular size, x_i, could be determined using

$$C_i = C_{i,0} \frac{x_0^3}{x_i^3} \tag{4.67}$$

where $C_{i,0}$ and x_0 are the droplet concentration and size at generation.

Given the underlying assumption pertaining to (4.67), it is important to note that there is a period of approximately four minutes that elapses between the instant a droplet is generated and when data collection begins. This 'gap' in the time arises from using the same location on the top of the cloud chamber to position both the electrified needle used for droplet generation and the PMT used to detect the intensities of scattered light in the TM mode. After a droplet is generated, the needle assembly must be carefully removed and the port sealed. Next, the PMT and its housing assembly are installed and covered in the same location. Finally, the signal strength of both PMTs is checked before data collection can begin.

Due to the time lapse between the generation and observation of charged droplets, the initial droplet size calculated from the fitted surface evaporation rate cannot be used to determine the concentration of ionic dopant in the droplet relative to its concentration at generation. Therefore, the amount of time elapsed prior to observation is precisely measured and used to extrapolate the true droplet size at the instant of generation, x_0, from the surface evaporation rate equation.

4.3 Analysis of Hygroscopic Particle Growth Data

4.3.1 Analysis of Pure Component Hygroscopic Growth

To construct a hysteresis loop for the pure component inorganic salt particles studied as part of this dissertation required only a simple analysis procedure. An example of a hysteresis loop for a particle of pure NaCl exposed to relative humidities from 0% to 80% and back to 0% has been previously provided by Figure 2.3 in Chapter 2. To develop a hysteresis loop requires knowledge of how the water mass fraction of a particle changes as it is exposed to a cycle of humidification and dehumidification. Since the water mass fraction of a particle at a specific relative humidity, $f_{water,i}$, could not be directly measured during its observation, it was determined from the change in its DC null point levitation potential relative to its DC null point levitation potential at a relative humidity of zero using

$$f_{water,i} = \frac{V_{DC,i} - V_{DC,0}}{V_{DC,i}} \tag{4.68}$$

where $V_{DC,i}$ and $V_{DC,0}$ are the DC null point levitation potentials of the particle at a specific relative humidity and at a relative humidity of zero, respectively. Here, two basic assumptions were made. First, the charge on the particle was assumed to remain constant. Therefore, the mass of the particle can be directly related to its DC null point levitation potential by a simplified form of (3.1) given by

$$m = \alpha V_{DC} \tag{4.69}$$

where the terms g, C_0, q, and z_0 have been grouped into the constant a. Second, it was assumed that the only changes in mass by the particle are due to the changes in its water content.

The value of $V_{DC,0}$ was obtained by exposing a properly levitated particle to dry nitrogen gas until its levitation potential remained constant. Here, it was assumed that the particle was completely dry. The values for $V_{DC,i}$ were obtained from the DC levitation potentials of a particle at specific relative humidities. The values of $V_{DC,i}$ were typically recorded in intervals of 5% relative humidity, but were taken at much shorter intervals in

the regions where deliquescence and crystallization were known to occur. After determining $V_{DC,0}$ and the $V_{DC,i}$ values over a complete cycle of humidification and dehumidification, (4.68) was used to calculate $f_{water,i}$ for each relative humidity at which the DC levitation potential was recorded. Finally, all $f_{water,i}$ versus relative humidity values were plotted to construct the hysteresis loop for a pure component particle.

4.3.2 Analysis of Mixed Particle Hygroscopic Growth

The analysis procedure for constructing a hysteresis loop for the mixed particles studied as part of this dissertation was similar to that described for pure component particles. Here however, the addition of the hydrophobic material had to be accounted for so that the mixed particles could be qualitatively compared to their pure component counterparts. To assess the impact of the hydrophobic material on the hygroscopic behavior of the inorganic salt, the water mass fraction of the particle at a specific relative humidity was determined on an additive-free basis, as compare to the hygroscopic growth of the whole particle. To determine the mass of the inorganic salt portion of a mixed particle, it was first assumed that the ratio of the hydrophobic additive to the inorganic salt in the particle was equal to that of the bulk solution from which the particle was generated. Second, it was assumed that the additive is completely hydrophobic and non-volatile. This assumption was tested by observing pure component particles of the hydrophobic materials and none were observed to have any hygroscopic growth for relative humidities up to 95% or to exhibit any mass loss when continually exposed to a relative humidity of zero. Finally, it was again assumed that the only changes in mass by the particle are due to the changes in its water content and that the particle charge remained constant.

As with a pure component particle, a mixed particle was initially exposed to dry nitrogen until its DC null point levitation potential remained constant to obtain a value for $V_{DC,0}$ and its $V_{DC,i}$ values were obtained from the its DC levitation potentials at specific relative humidities. The difference between the two values was taken to be the change in mass by a mixed particle due to the hygroscopic growth of the inorganic salt. The water mass fraction of a mixed particle at a specific relative humidity was then calculated using

$$f_{water,i} = \frac{V_{DC,i} - V_{DC,0}}{V_{DC,i} - X_{add} V_{DC,0}} \tag{4.70}$$

where X_{add} is the mass fraction of the water insoluble additive of the mixed particle when completely dry. Since all additives were assumed to be completely hydrophobic, (4.70) was valid regardless if the additive was liquid or solid. After determining $V_{DC,0}$ and the $V_{DC,i}$ values over a complete cycle of humidification and dehumidification, (4.70) was used to calculate $f_{water,i}$ for each relative humidity at which the DC levitation potential was recorded. Finally, all $f_{water,i}$ versus relative humidity values were plotted to construct the hysteresis loop for a mixed particle.

By attributing all the hygroscopic growth of the mixed particle to the inorganic salt, the hysteresis loops of corresponding pure and mixed particles could be directly compared to ascertain the effects of the hydrophobic additive on the hygroscopic behavior of the mixed particle. Figure 4.8 provides an example of the comparison of the hysteresis loops of a mixed particle containing 32% SIL and 68% NaCl and a pure component particle of NaCl. The mixed particle clearly shows a significant increase in its water content prior to deliquescence and that its water uptake began at a much lower relative humidity. Here, the mixed particle begins to absorb water at a relative humidity of ˜ 57% whereas the pure component particle does not begin its water uptake until just prior to its deliquescence at a relative humidity of ˜ 70%. However, the deliquescence relative humidities (DRH) of both particles are nearly identical and their post deliquescent water absorptions and desorptions are indistinguishable. Prior to its crystallization relative humidity (CRH), the mixed particle is observed to remain in a highly supersaturated state slightly longer than its pure component counterpart.

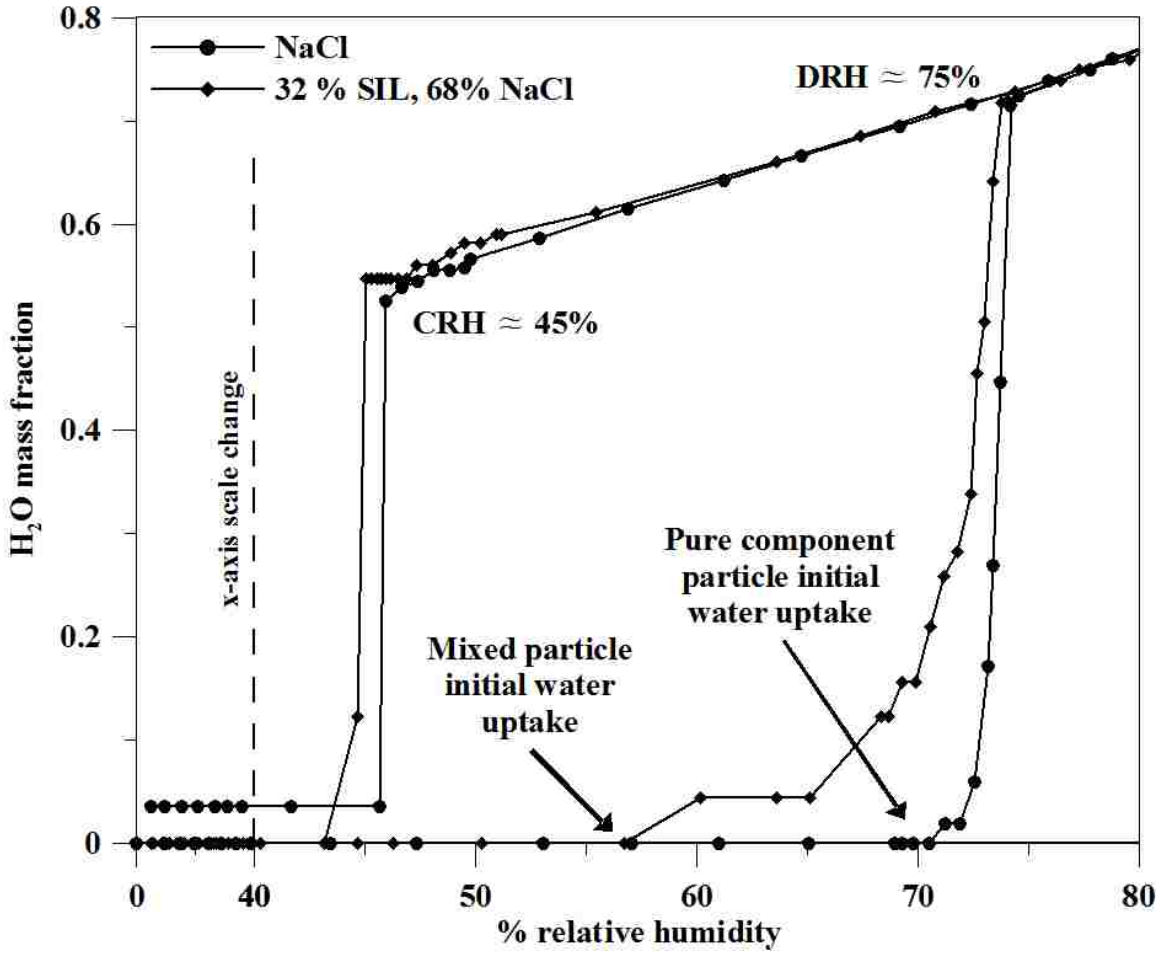

Figure 4.8 Example of the comparison of the hysteresis loops of a mixed particle and its pure component counterpart.

Chapter 5: Role of Electrical Conductivity on the Break-up of Charged Droplets via Coulombic Fission

5.1 Results and Discussion

5.1.1 Pure Component Droplets

Charged droplets of diethylene glycol (DEG), triethylene glycol (TEG), tetraethylene glycol (T4EG), dimethyl phthalate (DMP), diethyl phthalate (DEP), nonanoic acid (NNA), and phenylnonane (PNN) were each individually levitated in an electrodynamic balance and observed until a break-up via Coulombic fission had occurred. Typically, more than one break-up was observed for a single droplet during its evaporation. Using the data analysis procedure described in Chapter 4, the percentages of mass, f_m, and charge, f_q, emitted by each of the charged droplets and the percentage of the Rayleigh limit, f_R, at which break-ups occurred were determined. These values are given in Table 5.1 for each of the droplet compounds. The droplet compounds are listed in the column labeled 'Compound' by a set of abbreviated capital letters that have previously been assigned to them. Each break-up is identified by a pair of numbers given in the column labeled 'ID' where the first number corresponds to the droplet that was observed and the second number corresponds to the order in which break-ups occurred. For example, an ID number pair of (5,2) for DEP would equate to the second break-up of the fifth charged droplet of diethyl phthalate. The next two columns provide the densities and surface tensions of each of the droplet compounds when available. Superscripted numbers are used to reference the literature source used to obtain the values and are provided at the bottom of the table. The last three columns provide the values of f_m, f_q, and f_R that were determined for each of the droplet break-ups except for PNN. The values listed in the f_R column for PNN represent a constant value calculated using an alternate method to assess the charge limit at which break-ups occurred since no value for the surface tension of PNN could be found in literature. Also, the averages and standard deviations for the f_m, f_q, and f_R of DMP, DEP, NNA, and PNN are given.

Table 5.1 Results for the values of f_m, f_q, and f_R obtained from the break-ups of pure component droplets examined as part of this study. (Table 5.1 continues on page 107.)

Compound	ID	Density $kg \cdot m^{-3}$	Surface Tension $N \cdot m^{-1}$	f_m(%)	f_q(%)	f_R(%)[6]
DEG	1,1	1118[1]	0.0448[1]	0.66	37.24	96.9
	1,2			0.48	40.69	98.6
TEG	1,1	1125[1]	0.0451[1]	0.15	43.67	100.8
T4EG	2,1	1124[2]	0.044[2]	<0.10	40.83	N/A
	2,2			<0.10	51.68	N/A
DEP	4,1	1118[1]	0.0361[1]	1.65	12.97	100.5
	4,2			1.95	16.05	99.9
	4,3			2.60	17.28	99.5
	4,4			2.70	18.21	98.9
	5,1			1.97	16.21	100.6
	5,2			1.77	12.67	99.6
	5,3			1.79	15.86	101.1
	5,4			2.63	19.52	102.4
	6,1			2.32	19.39	102.3
	6,2			1.95	17.61	100.5
	6,3			2.24	19.29	101.1
	Average			2.14	16.82	100.6
	Standard Deviation			0.37	2.38	1.1
DMP	1,1	1175[3]	0.0405[3]	2.23	17.12	99.7
	1,2			1.92	14.43	96.8
	3,1			2.07	19.50	103.2
	3,2			2.50	18.65	100.5
	3,3			2.59	19.24	99.6
	Average			2.26	17.79	100.0
	Standard Deviation			0.28	2.09	2.3
NNA	2,1	921[4]	0.0331[4]	2.07	17.73	100.2
	2,2			1.52	14.91	102.9
	2,3			1.48	11.84	105.0
	4,1			1.08	11.95	113.0
	4,2			1.35	14.27	114.7
	4,3			1.92	16.36	117.7
	Average			1.57	14.51	108.9
	Standard Deviation			0.37	2.35	7.1

[Table 5.2 continued]

PNN	3,1	858[5]	N/A	0.61	7.22	N/A
	3,2			0.72	8.31	N/A
	3,3			0.89	10.20	N/A
	3,4			0.80	6.85	N/A
	3,5			1.15	11.01	N/A
	4,1			1.21	11.83	N/A
	4,2			1.09	10.81	N/A
	4,3			1.27	15.26	N/A
	4,4			1.37	15.54	N/A
	4,5			1.66	15.06	N/A
	Average			1.08	11.21	N/A
	Standard Deviation			0.32	3.25	N/A

N/A not available

[1] Li et al., 2005

[2] http://www.dow.com/ethyleneglycol/about/properties.htm

[3] http://www.thegoodscentscompany.com/data/rw1018891.html

[4] http://www.thegoodscentscompany.com/data/rw1012131.html

[5] http://www.chemcas.com/AnalyticalDetail.asp?pidx=1&id=16438&cas=1081-77-2&page=411

[6] values for PNN are not f_R, but a constant related to charge limit

The average values of f_m, f_q, and f_R for DEP and the values for f_q and f_R for DEG and TEG agree well with the corresponding values reported by Li et al. (2005). However, the average values for f_m for DEG and TEG are higher than those given by Li et al. (2005), especially for DEG which was observed here to have a noticeable amount of emitted mass whereas Li et al. (2005) reported that the amounts mass emitted were below their detectable limit. No literature data exist to compare the values obtained for the remainder of the droplet compounds.

Charged droplets of NNA were observed to increase the percentage of the Rayleigh limit, f_R, at which break-ups occurred with each successive break-up. This type of behavior has only been previously reported to occur for charged droplets containing a precipitate (Li and Ray, 2004). This suggests that the NNA may have become contaminated. However, no tests were conducted to verify this assertion.

The percentage of the Rayleigh limit, f_R, at which break-ups occurred for charged droplets of PNN could not be directly determined as no value was found in literature for its surface tension. Therefore, an alternate analysis procedure was used to evaluate the charge limit at which break-ups occurred. This method has previously been described and used by Li et al. (2005). Here, (1.1), (3.1), and (4.43) are combined to give a constant, c, according to

$$c = \frac{6C_0}{\rho g z_0}\sqrt{\frac{\pi^3 \varepsilon_0 \gamma}{\lambda^3}} = \frac{x_b^{3/2}}{V_{DC,b}} \tag{5.1}$$

assuming the charge on the droplet remains constant during evaporation and where x_b and $V_{DC,b}$ are the size parameter and DC null point levitation potential of the charged droplet immediately before a break-up via Coulombic fission. Assuming that the break-ups observed for PNN droplet occurred via Coulombic fission precisely at the Rayleigh limit, a value for the surface tension of PNN was estimated to be γ=0.0297 N·m^{-1} ± 0.0019.

The amounts of mass and charge emitted during the break-up of charged droplets of pure DEP and DMP via Coulombic fission were analyzed to determine their relationship to the corresponding mass and charge, respectively, of the droplets

immediately before break-up. Figure 5.1 shows the relationship between both the amount of mass emitted and the percentage of mass emitted during a break-up to the mass of the droplet immediately before a break-up. The solid diamonds and solid circles represent the data from charged droplets of pure DEP and pure DMP, respectively. Here, the amount of mass emitted during a break-up is clearly shown to decrease as the mass of the droplet decreases (bottom half of figure) whereas the percentage of the mass emitted by the droplet during its break-up shows no relationship to the droplet mass whatsoever (top half of figure). A nearly identical finding was reported by Richardson et al. (1989) for droplets of dioctylphthalate.

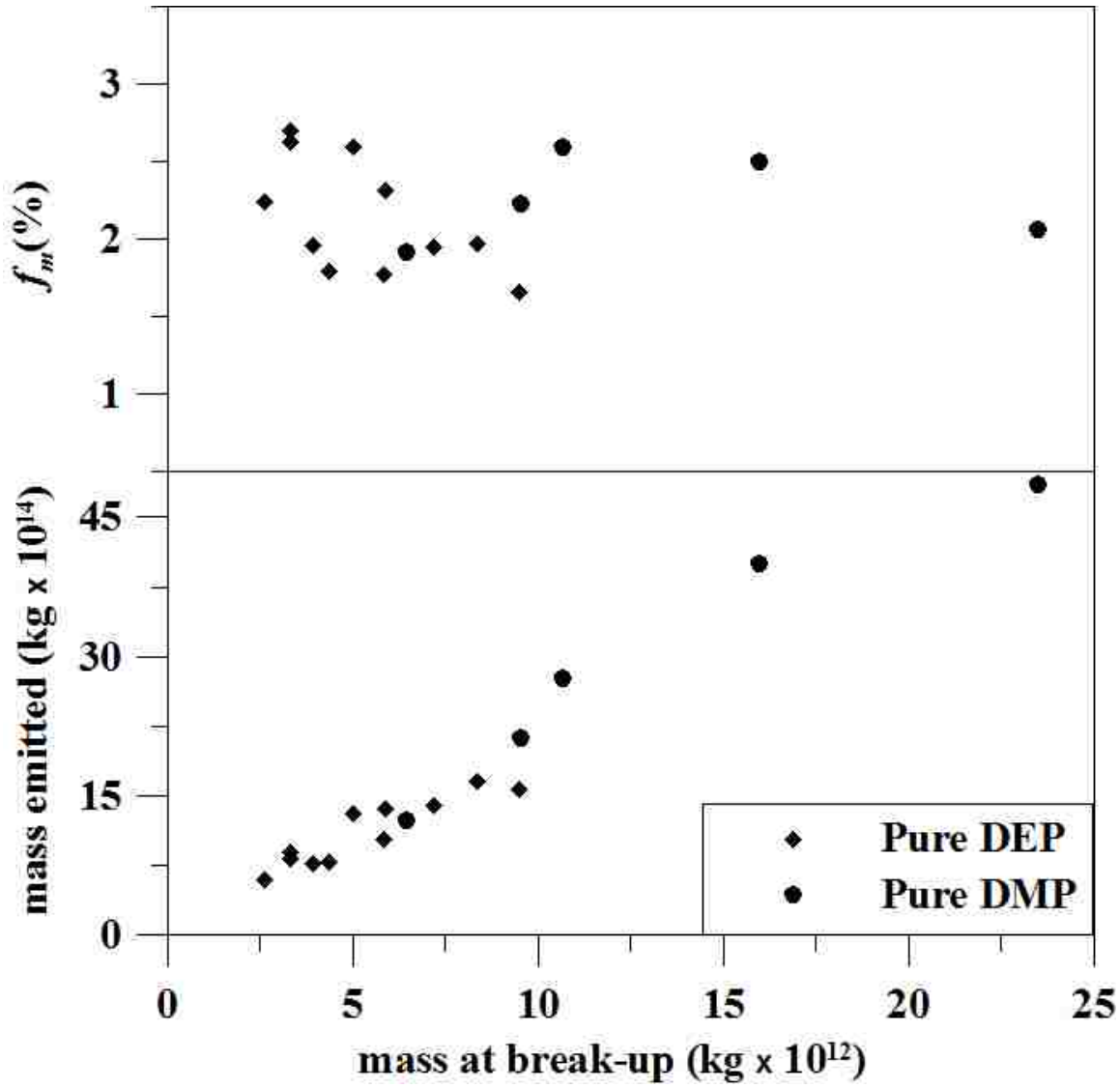

Figure 5.1 The relationship between both the amount of mass emitted and the percentage of mass emitted during a break-up to the mass of the droplet immediately before a break-up.

Figure 5.2 shows the relationship between both the amount of charge emitted and the percentage of charge emitted during a break-up to the charge of the droplet immediately before a break-up. The solid diamonds and solid circles represent the data from charged droplets of pure DEP and pure DMP, respectively. Here, the amount of charge emitted during a break-up is clearly shown to decrease as the charge of the droplet decreases (bottom half of figure) whereas the percentage of the charge emitted by the droplet during its break-up shows no relationship to the droplet charge whatsoever (top half of figure). A nearly identical finding was reported by Richardson et al. (1989) for droplets of sulfuric acid.

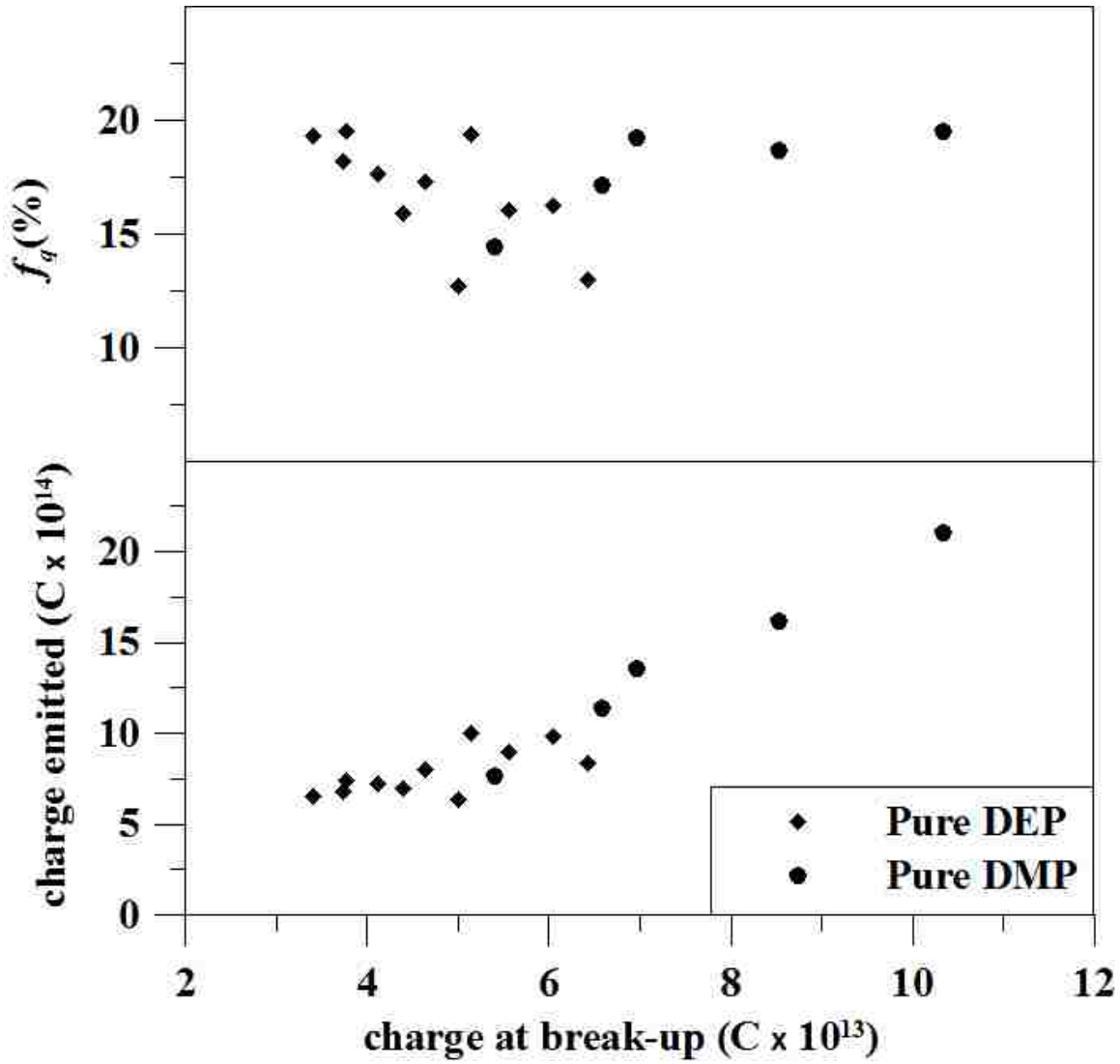

Figure 5.2 The relationship between both the amount of charge emitted and the percentage of charge emitted during a break-up to the charge of the droplet immediately before a break-up.

5.1.2 Droplets Containing an Ionic Dopant

To evaluate the role of electrical conductivity on the characteristics of charged droplet break-ups via Coulombic fission, charged droplets were generated from solutions containing a dielectric solvent and a known quantity of an ionic dopant. Here, only the solvents TEG, DMP, DEP, and PNN were combined with ionic dopants for further study. The ionic dopants used during this area of investigation were tridodecylmethylammonium chloride (TDMAC), tridodecylmethylammonium nitrate (TDMAN), 1-ethyl-3-methylimidazolium dicyanamide (IL1), 1-methyl-3-octylimidazolium chloride (IL2), and Stadis 450. Moreover, each of the solvents was only combined with some of the ionic dopants.

The solvent DEP was chosen as the prime candidate for ionic doping as it has been previously observed as a pure component (Li et al., 2005) and the amounts of charge and mass emitted during a Coulombic fission are sufficient enough that any changes due to an increased electrical conductivity can be more readily determined. The ionic dopants TDMAC, IL1, and IL2 were each independently combined with DEP in various known concentrations to increase its electrical conductivity. Negatively charged droplets from each of the solutions were individually observed through one or more break-ups via Coulombic fission. Using the data analysis procedure described in Chapter 4, the percentages of mass and charge emitted by each of the charged droplets and the percentage of the Rayleigh limit at which break-ups occurred were determined. These values were plotted versus the electrical conductivities, K, determined for each droplet immediately before a break-up.

The data collected from the break-ups of charged droplets of DEP containing and ionic dopant are given in Figure 5.3. The raw data points are indicated by a hollow square for pure DEP, a solid diamond for DEP-TDMAC, a solid circle for DEP-IL1, and a solid square for DEP-IL2. Here, the effects of electrical conductivity on f_m, f_q, and f_R are given by the lower, middle, and upper plots, respectively. The corresponding values of f_m, f_q, and f_R for pure DEP have also been included for comparison and are those given

in Table 5.1. The electrical conductivity of pure DEP was measured to be 0.69 $\mu S \cdot m^{-1}$ during this study and therefore all pure DEP values appear to reside on the y-axis. The raw data points given for droplets of DEP-TDMAC represent 39 break-ups from 14 droplets generated from 8 different initial concentrations. The raw data points given for droplets of DEP-IL1 represent 8 break-ups from 7 droplets generated from 7 different initial concentrations. The raw data points given for droplets of DEP-IL2 represent 5 break-ups from 3 droplets generated from 3 different initial concentrations.

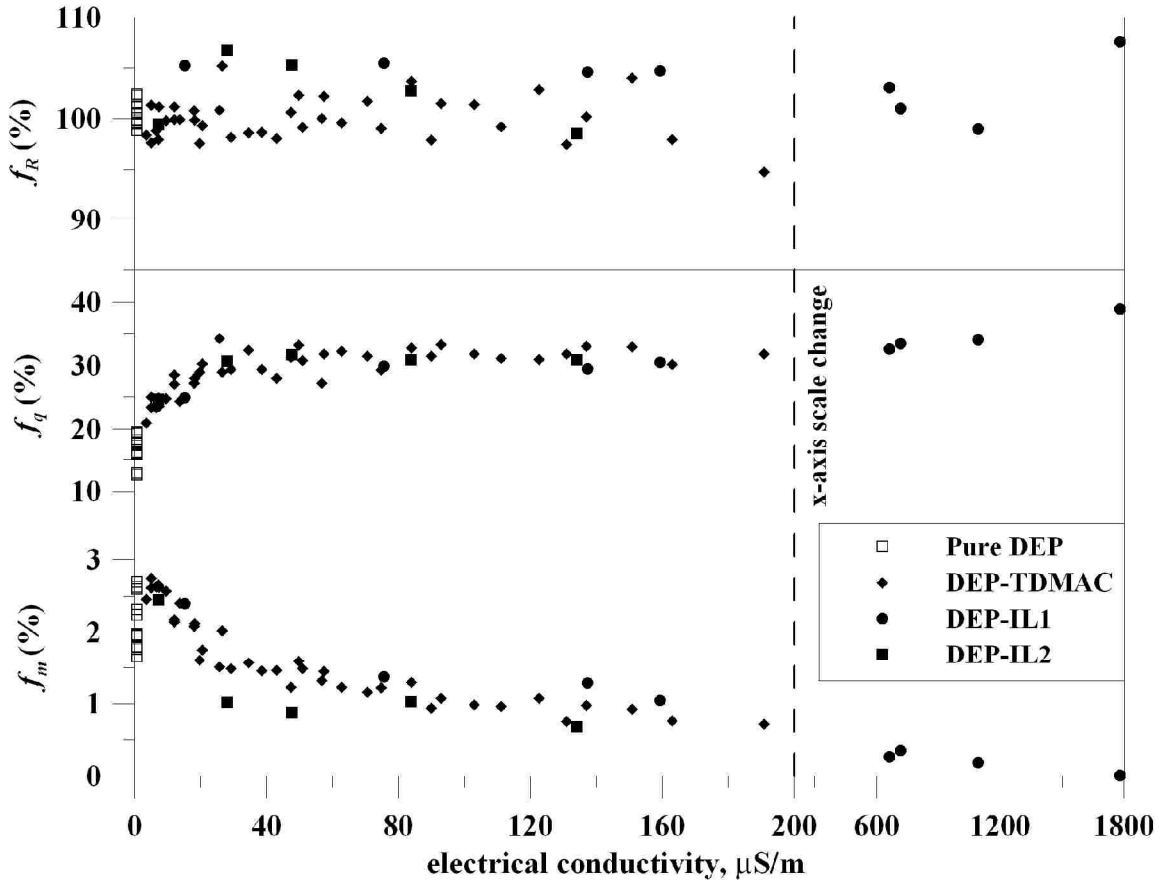

Figure 5.3 The effects of electrical conductivity on f_m, f_q, and f_R for charged droplets of DEP doped with either TDMAC, IL1, or IL2.

The data presented in Figure 5.3 clearly indicate that increasing the electrical conductivity of a dielectric droplet effects the percentages of mass and charge emitted during break-ups via Coulombic fission, but has no observable effect on the corresponding charge limits at which the break-ups occurred. Here, an increase in the electrical conductivity of a dielectric droplet is seen to decrease the percentage of mass emitted and increase, to a point, the amount of charge emitted during a break-up via Coulombic fission, regardless of the type of ionic dopant used. The percentage of mass emitted is decreased from 2.14 ± 0.37% (pure DEP average) to below the detectable limit of the equipment (<0.1%) and the percentage of charge emitted is increased from 16.82 ± 2.38% (pure DEP average) to over 35%.

Similar effects were observed for charged droplets of DMP that contained various amounts of TDMAC or TDMAN. The data collected from charged droplets of DMP containing an ionic dopant are given in Figure 5.4. The raw data points are indicated by a hollow square for pure DMP, a solid diamond for DMP-TDMAC, and a solid circle for DEP-TDMAN. Here, the effects of electrical conductivity on f_m, f_q, and f_R are given by the lower, middle, and upper plots, respectively. The corresponding values of f_m, f_q, and f_R for pure DMP have also been included for comparison and are those given in Table 5.1. The electrical conductivity of pure DMP was measured to be 0.50 $\mu S \cdot m^{-1}$ during this study and therefore all pure DMP values appear to reside on the y-axis. The raw data points given for droplets of DMP-TDMAC represent 4 break-ups from 3 droplets generated from 2 different initial concentrations. The raw data points given for droplets of DMP-TDMAN represent 2 break-ups from 2 droplets generated from 1 initial concentration.

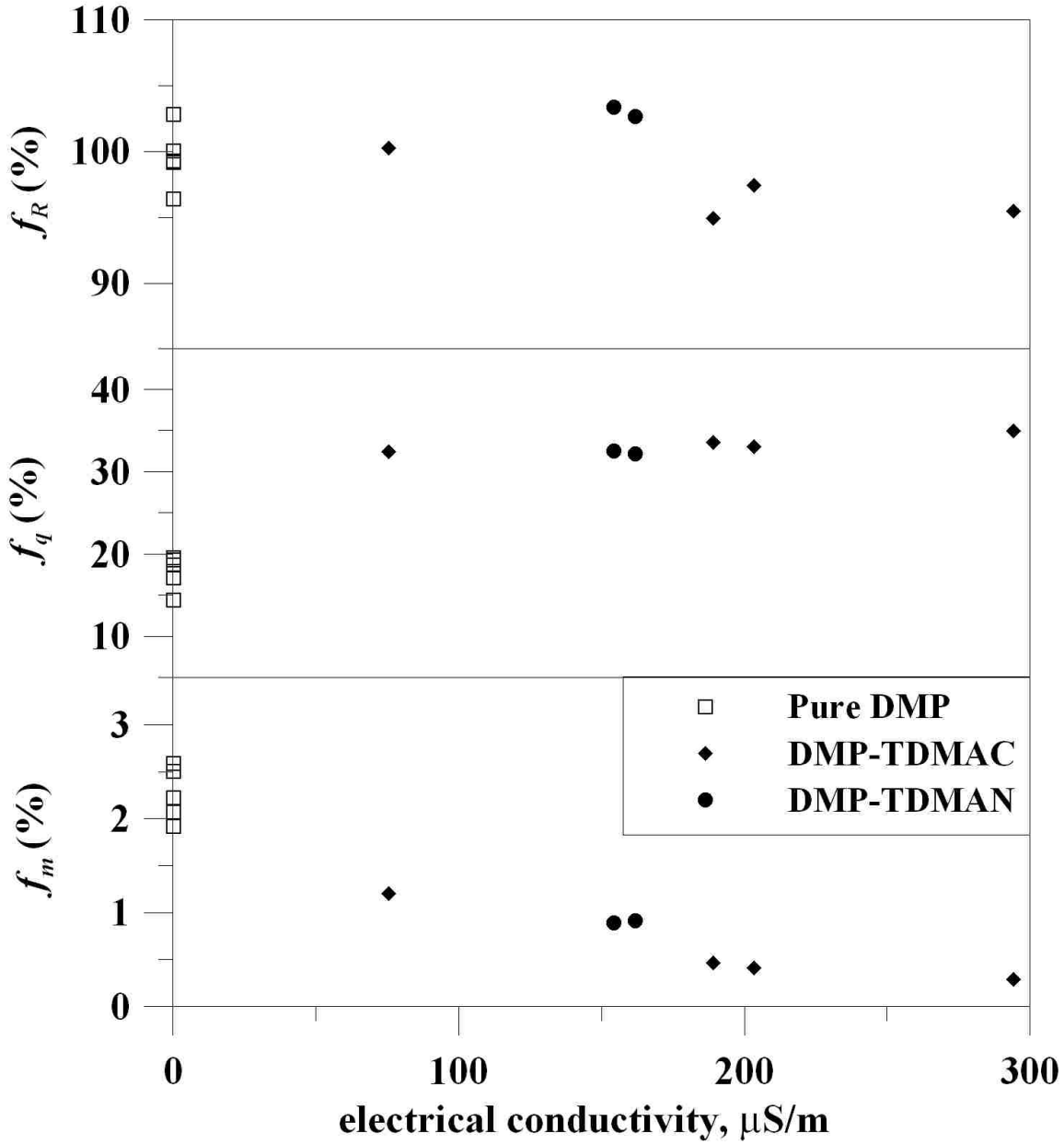

Figure 5.4 The effects of electrical conductivity on f_m, f_q, and f_R for droplets of DMP doped with either TDMAC or TDMAN.

The data presented in Figure 5.4 again clearly indicate that increasing the electrical conductivity of a dielectric droplet effects the percentages of mass and charge emitted during break-ups via Coulombic fission, but has no observable effect on the corresponding charge limits at which the break-ups occurred. Here again, an increase in the electrical conductivity of a dielectric droplet is seen to decrease the percentage of mass emitted and increase, to a point, the amount of charge emitted during a break-up via Coulombic fission, regardless of the type of ionic dopant used. The percentage of mass emitted is decreased from 2.26 ± 0.28% (pure DMP average) to below 0.3% and the percentage of charge emitted is increased from 17.79 ± 2.09% (pure DMP average) to over 35%.

In a separate study, a charged droplet of DMP doped TDMAN was observed to undergo two successive break-ups at charge limits significantly above the corresponding Rayleigh limits. Here, the initial concentration of TDMAN in the DMP droplet was 5.28 $g \cdot l^{-1}$, and was much higher than that of the initial concentrations of the two DMP-TDMAN droplets represented in figure 5.4. The resulting percentages of the Rayleigh limit from the 1st and 2nd fissions were 157.3% and 143.5%, respectively, and occurred when the droplet had electrical conductivities of 331 $\mu S \cdot m^{-1}$ and 481 $\mu S \cdot m^{-1}$, respectively. The resulting amounts of mass and charge emitted during the 1st and 2nd fissions from this particular droplet were 0.30% and 0.16% for mass and 24.12% and 26.77% for charge, respectively. Li and Ray (2004) have previously shown that the charge limits of droplets containing a precipitate at the instant prior to a Coulombic fission are significantly higher than the corresponding Rayleigh limits. As such, here it is assumed that the concentration of TDMAN in the DMP droplet at the instants prior to the two Coulombic fissions was greater than the solubility limit and therefore some of the TDMAN existed as a solid.

A single experiment was conducted to observe the effect of increased electrical conductivity on TEG. Although the percentage of mass emitted by a charged droplet of pure TEG during its break-up via Coulombic fission was already determined to occur near the detectable limit (<0.10%) and a reduction in such would be undetectable, the

goal here was to observe how much the percentage of charge emitted would possibly increase. Here, a single charged droplet of TEG was doped with TDMAC at an initial concentration of 5.35 g·l-1 and observed through 2 successive break-ups via Coulombic fission. The percentages of mass emitted during the break-ups were below the detectable limit (<0.10%) as expected. In fact, the theoretical and observed intensity spectra were nearly indistinguishable in the region where the break-ups occurred. Only a slight distortion in the observed intensity spectrum could be seen; likely due to the change in the droplet geometry prior to its break-up. The times at which the break-ups occurred were determined from the observed intensity spectra and used to determine the percentages of charge emitted during each break-up. The values of f_q were determined to be 43.27% and 49.18% for the 1st and 2nd fissions, respectively. These values are comparable to those of pure TEG given in Table 5.1 although the electrical conductivities at the instants prior to the 1st and 2nd break-ups were estimated to be 4000 $\mu S \cdot m^{-1}$ and 8700 $\mu S \cdot m^{-1}$, respectively. The electrical conductivity of pure TEG was measured to be 21.4 $\mu S \cdot m^{-1}$ during this study. Here again it appears that at some point the amount of charge emitted during the break-up of a charged droplet via Coulombic fission reaches a maximum value regardless of the amount of electrical conductivity as previously shown in figures 5.3 and 5.4 for droplets of DEP and DMP, respectively.

A study was also conducted to examine the effects of electrical conductivity on the break-up characteristics of charged droplets of PNN. Only the static dissipator Stadis 450 was found to work as an ionic dopant in PNN. It is important to note that no relationship between the concentration of Stadis 450 in PNN and electrical conductivity could be determined. The problem here arises from a combination of factors. First, Stadis 450 is a proprietary blend of dinonylnapthalene sulfonic acid, barium salt dissolved in toluene and isopropanol and therefore the exact amount of the active salt per unit of Stadis 450 could not be determined. Second, during the evaporation of a charged droplet containing Stadis 450, the toluene and isopropanol will evaporate and change the concentration of Stadis 450 in the droplet. Finally, the solubility of the active salt in Stadis 450 is unknown in PNN, but is likely insoluble without a suitable co-solvent.

Therefore, as the toluene and isopropanol are lost during the evaporation of a charged droplet, the active salt in Stadis 450 will precipitate out.

Despite an inability to exactly relate the amount of Stadis 450 in PNN to an electrical conductivity value, two charged droplets of PNN doped with an equal, but unspecified initial concentration of Stadis 450 were observed through a multitude of successive break-ups via Coulombic fission. The data collected from the two droplets are presented in Table 5.2. Each break-up is again identified by a pair of numbers given in the column labeled 'ID' where the first number corresponds to the droplet that was observed and the second number corresponds to the order in which break-ups occurred. The values of f_m and f_q determined for each droplet break-up are also given. Here, the values listed in the column labeled f_R are equivocal to the percentages of the Rayleigh limit, but were determined by first computing the constant, c, using (4.71) for each droplet break-up and then dividing that value by the average value of c for pure PNN given in Table 5.1.

Table 5.2 Data collected from the break-ups of two PNN droplets doped with Stadis 450.

ID	f_m(%)	f_q(%)	f_r(%)
1,1	0.98	10.85	121.1
1,2	0.97	11.72	125.7
1,3	1.14	13.11	126.0
1,4	1.17	14.32	130.8
1,5	1.22	19.17	137.7
1,6	1.37	20.11	145.0
1,7	1.48	21.57	151.6
1,8	1.87	27.09	167.1
1,9	1.54	32.30	195.8
2,1	1.045	14.99	133.4
2,2	1.255	15.55	139.5
2,3	1.461	14.17	143.2
2,4	1.605	21.61	158.8

The values of f_m, f_q, and f_R presented in Table 5.2 reveal that Stadis 450 had a much different effect on the break-up characteristics of PNN droplets than expected from the results previously obtained by dielectric droplets containing an ionic dopant. Here, the values of f_m can be seen to increase with each successive break-up whereas they had previously been shown to decrease for droplets of DEP and DMP containing an ionic dopant. In the studies involving DEP and DMP, the ionic dopants remained dissolved in the solvents during droplet evaporation and therefore the electrical conductivity was increased. As such, it would appear that the Stadis 450 did not remain soluble in the PNN droplets as the toluene and isopropanol evaporated out of the droplet as proposed earlier. As such, the electrical conductivity of the droplet would have decreased during evaporation. This could explain why f_m was observed to increase with each successive droplet break-up. As f_R was also observed to increase with each successive break-up, the logical assumption is that a precipitate formed during droplet evaporation and supports the assumption that the active salt in Stadis 450 is not soluble in PNN. The trend observed for f_q however, must be more closely examined. Here, the percentages of charge lost during each successive break-up were observed to increase as had been previously shown for charged droplets of DEP and DMP containing an ionic dopant. However, the percentages of charge emitted from the two aforementioned droplets of DMP doped with an initial concentration of 5.28 $g \cdot l^{-1}$ of TDMAN where a precipitate was believed to be formed were also observed to increase relative to that of pure DMP droplets. Furthermore, it would make sense that droplets having break-ups at charge limits in excess of their Rayleigh limits would need to emit more charge in order to return to a stable geometry. As such, here it is asserted that charged droplets of PNN doped with Stadis 450 possessed their highest electrical conductivity upon generation and that the electrical conductivity decreased with subsequent evaporation of the solvent and that a precipitate was formed from the active salt in the Stadis 450. The resulting decrease in electrical conductivity increased the percentages of mass emitted during successive droplet break-ups and the formation of the precipitate increased both the percentages of charge emitted during successive break-ups and the charge limit at which such break-ups occurred. However, further investigation into this phenomenon would be required to truly understand all the factors involved.

5.1.3 Role of Electrical Conductivity

To better understand the role of electrical conductivity, along with the role of other relevant physical properties, the data collected from 79 break-ups of charged droplets of DEG, TEG, DEP, DMP, DEP-TDMAC, DEP-IL1, DEP-IL2, DMP-TDMAC, and DMP-TDMAN that occurred via Coulombic fission at the Rayleigh limit were dimensionally analyzed using the Buckingham Pi theorem. Initially, the amounts of charge and mass emitted during each droplet break-up were calculated. Next, the possible relevant factors affecting the break-up of an individual charged droplet were assumed to be density, surface tension, relative permittivity, dynamic viscosity, electrical conductivity, charge, and size. Since the effects of the ionic dopants on the physical properties, excluding electrical conductivity, were not determined, the values for the pure solvents were used. The values for density and surface tension of DEP and DMP are given in Table 5.1. The relative permittivities of DEP and DMP were found to be 7.86 and 8.66, respectively, from Lide (2004) and were incorporated into the dimensionless analysis after multiplication with the permittivity of free space. The viscosity of DEP was found to be 0.0105 $kg \cdot m^{-1} \cdot s^{-1}$ from Lorenzi et al. (1997) and the viscosity of DMP was found to be 0.0144 $kg \cdot m^{-1} \cdot s^{-1}$ from Lide (2004).

To ascertain the role of the individual fluid properties on the amounts of charge and mass emitted during the break-up of charged droplets via Coulombic fission at their Rayleigh limit, the relationships given by (5.2 and 5.3) were developed. Since the data being analyzed were collected from droplets having break-ups via Coulombic fissions very near their Rayleigh limit, the charge and size of the droplet immediately before a break-up could be related using Rayleigh theory. Therefore, either the radius or the charge of a droplet was used during regression, but not both.

$$\Delta q = f\left(\rho, \varepsilon\varepsilon_0, \gamma, \mu, K, q\right) \tag{5.2}$$

$$\Delta m = f\left(\rho, \varepsilon\varepsilon_0, \gamma, \mu, K, a\right) \tag{5.3}$$

$$f_q = f\left(\rho, \varepsilon\varepsilon_0, \gamma, \mu, K, q\right) \tag{5.4}$$

$$f_m = f\left(\rho, \varepsilon\varepsilon_0, \gamma, \mu, K, a\right) \tag{5.5}$$

The variables given in (5.2) through (5.5) were expressed in terms of their fundamental units and are given by

$$\Delta q = [Q] \tag{5.6}$$

$$\Delta m = [M] \tag{5.7}$$

$$f_q = \left[\frac{Q}{Q}\right] \tag{5.8}$$

$$f_m = \left[\frac{M}{M}\right] \tag{5.9}$$

$$q = [Q] \tag{5.10}$$

$$a = [L] \tag{5.11}$$

$$K = \left[\frac{Q^2 t}{ML^3}\right] \tag{5.12}$$

$$\varepsilon\varepsilon_0 = \left[\frac{Q^2 t^2}{ML^3}\right] \tag{5.13}$$

$$\rho = \left[\frac{M}{L^3}\right] \tag{5.14}$$

$$\mu = \left[\frac{M}{Lt}\right] \tag{5.15}$$

$$\gamma = \left[\frac{M}{t^2}\right] \tag{5.16}$$

where M is mass (in kg), L is length (in m), t is time (in s), and Q is charge (in C). Note, that (5.8) and (5.9) are both already in a dimensionless form. Since (5.2) through (5.5) each contain seven variables possessing a total of four fundamental units they can expressed using three dimensionless groups having the form

$$\Pi_1 = f(\Pi_2 \Pi_3) \tag{5.17}$$

where each Π term represents a dimensionless group containing an experimental variable and a specific combination of the core variables. Here, Δq, Δm, f_q, f_m, q, a, and K were selected as the experimental variables and were each formed into a dimensionless group containing the core variables $\varepsilon\varepsilon_0$, ρ, μ, and γ given by

$$\Pi_{\Delta q} = \left[\frac{\Delta q \rho^{3/2} \gamma}{(\varepsilon \varepsilon_0)^{1/2} \mu^3} \right] \tag{5.18}$$

$$\Pi_{\Delta m} = \left[\frac{\Delta m \rho^2 \gamma^3}{\mu^6} \right] \tag{5.19}$$

$$\Pi_{f_q} = \lfloor f_q \rfloor \tag{5.20}$$

$$\Pi_{f_m} = \lceil f_m \rceil \tag{5.21}$$

$$\Pi_q = \left[\frac{q \rho^{3/2} \gamma}{(\varepsilon \varepsilon_0)^{1/2} \mu^3} \right] \tag{5.22}$$

$$\Pi_a = \left[\frac{a \rho \gamma}{\mu^2} \right] \tag{5.23}$$

$$\Pi_K = \left[\frac{K \mu^3}{\rho \varepsilon \varepsilon_0 \gamma^2} \right] \tag{5.24}$$

Using the Π terms given by (5.18) through (5.24), the relationships given by (5.2) through (5.5) were linearly recast in a dimensionless form as

$$\ln(\Pi_{\Delta q}) = \ln(A_1) + A_2 \ln(\Pi_q) + A_3 \ln(\Pi_K) \tag{5.25}$$

$$\ln(\Pi_{\Delta m}) = \ln(B_1) + B_2 \ln(\Pi_m) + B_3 \ln(\Pi_K) \tag{5.26}$$

$$\ln(\Pi_{f_q}) = \ln(C_1) + C_2 \ln(\Pi_q) + C_3 \ln(\Pi_K) \tag{5.27}$$

$$\ln(\Pi_{f_m}) = \ln(D_1) + D_2 \ln(\Pi_m) + D_3 \ln(\Pi_K) \tag{5.28}$$

where $A_{1\text{-}3}$ through $D_{1\text{-}3}$ are constants.

Prior to regressing the data inputted for the Π terms given by (5.18) through (5.24), a simple check was conducted to insure that the charge and size values calculated for each droplet immediately before a break-up were correctly paired. According to Rayleigh theory, charge is equal to the droplet radius raised to the 3/2 power times some constant. Since all the data being used were collected from the break-ups of charged droplets via Coulombic fission very near their Rayleigh limits, this relationship was

tested by fitting the values calculated for (5.22) and (5.23) for each droplet break-up using

$$\ln\left(\Pi_q\right) = \ln\left(x\right) + \left(3/2\right)\ln\left(\Pi_a\right) \tag{5.29}$$

Here, the fitted equation was found to have R^2=0.9728 and validates that the values for charge and size are correctly paired for each droplet break-up.

Assuming that the remainder of the values calculated for (5.18) through (5.24) are correct, (5.25) through (5.28) were regressed to determine the constants $A_{1\text{-}3}$ through $D_{1\text{-}3}$ and found to be

$$\ln\left(\Pi_{\Delta q}\right) = -1.1248 + 0.9904\ln\left(\Pi_q\right) + 0.1169\ln\left(\Pi_K\right) \tag{5.30}$$

$$\ln\left(\Pi_{\Delta m}\right) = -3.6154 + 3.2188\ln\left(\Pi_a\right) - 0.2924\ln\left(\Pi_K\right) \tag{5.31}$$

$$\ln\left(\Pi_{f_q}\right) = -1.1248 - 0.0096\ln\left(\Pi_q\right) + 0.1169\ln\left(\Pi_K\right) \tag{5.32}$$

$$\ln\left(\Pi_{f_m}\right) = -5.0478 + 0.2188\ln\left(\Pi_a\right) - 0.2924\ln\left(\Pi_K\right) \tag{5.33}$$

with R^2 values of 0.9798, 0.9046, 0.8355, and 0.5638 respectively. Here, only (5.30) was found to have an acceptable value of R^2 to validate the expression. However, as both (5.32) and (5.33) can be developed by rearrangement of (5.30) and (5.31), respectively, the significant decrease in the R^2 values determined for (5.32) and (5.33) are likely due to the fewer number of significant figures used for f_q and f_m. Furthermore, the coefficients determined for (5.30) through (5.33) suggest that f_q and f_m are strongly dependent on q and a as initially shown by Figures 5.1 and 5.2, respectively, and are only weakly dependent on K.

5.1.4 Determining the Electrical Conductivity at the Droplet Surface

In the previous analysis, the amounts of charge and mass emitted during the break-ups of charged droplets via Coulombic fission were found to be only weakly related to electrical conductivity. However, the electrical conductivity used for that analysis was the bulk electrical conductivity of the solvent. Several investigators however, have asserted that a droplet's excess ionic charges reside either on the surface on in a diffuse layer just below the surface (De Juan and De la Mora, 1997; Labowsky, 1998; Zhou and Cook, 2000;

Mylan and Oldham, 2002; Storozhev, 2004) and follow a Poisson-Boltzmann distribution (Mylan and Oldham, 2002). This assertion has also been applied to dielectric droplets (Labowsky, 1998; Storozhev, 2004) and droplets containing ionic species (Zhou and Cook, 2000; Myland and Oldham, 2002) as were studied as part of this dissertation. Therefore, it is a logical assumption that the electrical conductivity within a charge droplet would follow the same distribution. Moreover, it follows that the electrical conductivity at the surface of dielectric droplets would be much greater than the bulk electrical conductivity of the corresponding solvent. As such, the role of electrical conductivity at the droplet surface on the amounts of charge and mass emitted during the break-ups of charged droplets via Coulombic fission was examined. The following results and discussion are presented as found in Hunter and Ray (2009). Here, only the data from the break-ups of charged droplets of DEP-IL1, DEP-TDMAC, and DMP-TDMAN were evaluated.

The electrical conductivity, K, of a charged droplet immediately before a break-up via Coulombic fission was related to the molar concentration of dissociated ions, C_{diss}, in the droplet using

$$K = n^{+}u^{+} + n^{-}u^{-} = \Lambda C_{diss} \tag{5.34}$$

where Λ is the conductance, $n^{\pm}$ are the ion concentrations, and $u^{\pm}$ are the corresponding ion mobilities. Here, the ion mobilities were assumed to be inversely proportional to the square root of their molecular weights and calculated using

$$u^{+} = \frac{\sqrt{M_{B^-}/M_{A^+}}}{1+\sqrt{M_{B^-}/M_{A^+}}}\Lambda \tag{5.35}$$

$$u^{-} = \frac{1}{1+\sqrt{M_{B^-}/M_{A^+}}}\Lambda \tag{5.36}$$

where M_{A^+} and M_{B^-} are the molecular weights of the cations and anions, respectively, formed by the dissociation of the ionic dopant.

The molar concentration of dissociated ions, C_{diss}, present in a droplet at the instant prior to break-up was determined from the total molar concentration of ionic

dopant, C_{AB}, present in a droplet at the instant it was generated. Here, it is assumed that the total concentration of ionic dopant in the droplet is equal to that of the bulk solution from which the droplet was generated. Therefore, C_{AB} is given by

$$C_{AB} = C_{A^+B^-} + C_{diss} \tag{5.37}$$

where $C_{A^+B^-}$ is the molar concentration of ionic dopant that is undissolved and where $C_{diss} = C_{A^+} = C_{B^-}$ since all of the ionic dopants used during this study possess a single cation and a single anion. Their equilibrium with $C_{A^+B^-}$ was expressed assuming a fully reversible dissociation using

$$A^+B^- \xleftrightarrow{K_{eq}} A^+ + B^- \tag{5.38}$$

where K_{eq} is the equilibrium constant given by

$$K_{eq} = \frac{C_{diss}^2}{C_{A^+B^-}} = \frac{C_{diss}^2}{C_{AB} - C_{diss}} \tag{5.39}$$

Chapter 4 has previously described in detail how C_{AB} was determined and related to the electrical conductivity, K, for each solvent-ionic dopant pairing. Incorporating (5.34) and (5.39) gives

$$C_{AB} = xK^2 + yK \tag{5.40}$$

where x and y are given by

$$x = \frac{1}{K_{eq}\Lambda^2} \tag{5.41}$$

$$y = \frac{1}{\Lambda} \tag{5.42}$$

The coefficients x and y were determined via regression of ionic dopant concentration versus electrical conductivity for each solvent-dopant mixture. The values of K_{eq} were determined to be 0.27, 5.21, and 5.45 $mol \cdot m^{-3}$ for DEP-TDMAC, DEP-IL1, and DMP-TDMAN, respectively. Likewise, the values of Λ were determined to be 48.6, 86.5, and 47.0 $\mu S \cdot m^2 \cdot mol^{-1}$ for DEP-TDMAC, DEP-IL1, and DMP-TDMAN, respectively. The corresponding values of K_{eq} and C_{AB} were then used to determine C_{diss} using

$$C_{diss} = -\frac{K_{eq}}{2} + \frac{\sqrt{\left(K_{eq}^2 + 4K_{eq}C_{AB}\right)}}{2} \tag{5.43}$$

Here it is appropriate to note that molar concentrations of cations and anions produced from the dissociation of the ionic dopants are assumed to be equal and that C_{diss} is more accurately the molar concentration of either the cationic species or the anionic species, but not their combined concentration.

To determine the number of ions present at the droplet surface, their location within a droplet was assumed to follow a Boltzmann distribution where cations and anions that posses a single charge are related to the electrostatic potential by

$$n^{\pm}(r) = n_0^{\pm} \exp\left[\mp \frac{e}{k_B T} (\phi - \phi_0) \right] \tag{5.44}$$

where $n^{\pm}(r)$ are the number density ion concentrations at a radial position r, ϕ is the local potential, e is the charge on an electron, k_B is Boltzmann's constant, T is the absolute temperature of the droplet, and $n_0^{\pm}$ are the ion concentrations at the reference potential, ϕ_0. The distribution of the potential was assumed to follow a Poisson distribution given by

$$\frac{1}{r^2} \frac{d}{dr} \left(r^2 \frac{d\phi}{dr} \right) = -\frac{\rho_e(r)}{\varepsilon} \tag{5.45}$$

where ε is the permittivity of the droplet and ρ_e is the charge density given by the difference between the ion concentrations of the cations and anions according to

$$\rho_e(r) = e\left[n^+(r) - n^-(r) \right] \tag{5.46}$$

The boundary conditions applied to solve the Poisson-Boltzmann equation are given by

$$\left. \frac{d\phi}{dr} \right|_{r=0} = 0 \tag{5.47}$$

$$\left. \frac{d\phi}{dr} \right|_{r=a} = -\frac{q_R}{4\pi\varepsilon a^2} \tag{5.48}$$

where (5.47) is given by the symmetry at the center of a spherical droplet and (5.48) is Gauss' law. Two additional relations were developed from the conservation of charge and mass to account for the ion concentrations at the reference potential and are given, respectively, by

$$4\pi\int_0^a n^-(r)r^2dr = \frac{1}{3}4\pi a^3 C_{diss} + \left|\frac{q_R}{e}\right| \tag{5.49}$$

(5.50)

Here, it should be noted that the excess anions are solely those of the solvent molecule produced during droplet generation and not those of the dissociated ionic dopant. Also, the number of excess charges is assumed to be equal to the number of elementary charges present within the droplet at the Rayleigh limit. Finally, the reference potential was taken as zero at the droplet center since (5.49) is not truly independent as it can be developed by integrating (5.45) using (5.47) and (5.48). The solution of the Poisson-Boltzmann equation was solved by Ray of Hunter and Ray (2009) wherein a finite difference method was used to determine $n_0^{\pm}$ and $\phi(r)$, given a and C_{diss}, and Newton's method was used to determine $n_0^{\pm}$ such that (5.50) was satisfied and $\phi(0)=\phi_0=0$.

To determine the electrical conductivity at the droplet surface, Ks, the ion concentrations were calculated for a thin layer at the droplet surface having a thickness, δ, given by

$$\delta \approx 5\lambda_D \tag{5.51}$$

where λ_D is the Debye length given by

$$\lambda_D = \sqrt{\frac{\varepsilon k_B T}{2n_0 e^2}} \tag{5.52}$$

where n_0 is the ion concentration in the core. The results obtained from the numerical analyses were validated by comparing them to the results from an analytical analysis developed by approximating the thin surface layer as a planar film. After determining the ion concentrations at the surface for each break-up, the corresponding surface electrical conductivities were calculated using

$$K_s = n_s^+ u^+ + n_s^- u^- \tag{5.53}$$

where $n_s^{\pm}$ are the surface ion concentrations.

Hunter and Ray (2009) have provided an example of the results obtained from this analysis. Here, it is repeated. Consider a negatively charged droplet of DEP-TDMAC having a=10 μm and C_{diss}=0.05 mol·m^{-3}. Such a droplet would have n_s^+=3.27×10^{21} and n_s^-=2.80×10^{23} ions·m^{-3}, respectively, wherein the concentration of surface anions is nearly two orders of magnitude greater than the concentration of surface cations. Furthermore, such a droplet would have a bulk electrical conductivity of K=2.43 μS·m^{-1} and a surface electrical conductivity of K_s=5.01 μS·m^{-1}. This example provides an initial understanding of why the previous data analysis using bulk electrical conductivity values returned a weak dependence on electrical conductivity.

Myland and Oldham (2002) have also presented solutions to the Poisson-Boltzmann equation for the distribution of electrolytic ions in a charged droplet determined by a numerical simulation and an algebraic series. Here, the thickness of the thin layer at the surface of the droplet was taken to be 0.31073 nm and was determined from the cubic root of the molecular volume of a molecule of water as water was the droplet solvent chosen for study in their investigation. They reported that a positively charged droplet having a radius of 1 μm and an electrolyte concentration of 5.002 eq·m^{-3} would have 17,062 cations and 8096 anions at the surface. Here, the number ions possessing a like charge to the overall droplet charge are again significantly higher than those of the opposite sign.

5.1.5 Role of Surface Electrical Conductivity on the Characteristics of Charged Droplet Break-ups

The role of electrical conductivity at the surface of charged droplets on the characteristics of progeny microdroplets was also examined and is presented here as found in Hunter and Ray (2009). Here, the conservation of charge and mass was again employed to relate the amounts of charge, Δq, and mass, Δm, emitted by a charged droplet during its break-up via Coulombic fission at the Rayleigh limit to the characteristics of the progeny microdroplets formed during such break-up by

$$\Delta q = n_p q_p \tag{5.54}$$

$$\Delta m = n_p m_p \tag{5.55}$$

where n_p is the number of progeny microdroplets and q_p and m_p are the charge and mass of a progeny microdroplet, respectively. Li et al. (2005) have previously determined the characteristics of progeny microdroplets under the same assumption and photographs of the formation of progeny microdroplets have shown that they are approximately equal in size (Macky, 1931; Duft et al, 2003). Konermann (2009) however, has disputed the claim that progeny microdroplets would carry equal charge and suggests that each successive progeny microdroplet would carry slightly less charge.

Assuming that progeny microdroplet are formed having equal charge and mass, it was assumed that the charge to mass ratio of a progeny microdroplet could be related to the surface electrical conductivity of the mother droplet immediately before a break-up by

$$\frac{q_p}{m_p} = \frac{\Delta q}{\Delta m} = BK_s \tag{5.56}$$

where B is a constant. Assuming the charge on the primary droplet immediately before a break-up can be given by Rayleigh theory, (5.55) was recast in terms of the percentages of charge, f_q, and mass, f_m, emitted by a droplet using

$$\frac{f_q}{f_m} = \frac{\rho}{6\sqrt{\varepsilon_0 \gamma}} BK_s a^{3/2} \tag{5.57}$$

Linear regression of the f_q/f_m versus $K_s \cdot a^{3/2}$ data obtained from break-ups of charged droplets of DEP-TDMAC, DEP-IL1, and DMP-TDMAN using (5.57) yielded slopes of 4.70±0.19, 4.71±0.14, and 3.92±0.51, respectively. What is intriguing about these results is that the slopes determined for linear fits of the DEP-IL1 and DEP-TDMAC data were nearly identical at 4.70 and 4.71 although the ionic dopants used were very different. Furthermore, (5.57) is nearly identical to a previous postulation by de la Mora (1996) given by

$$\frac{(\Delta m/m)}{(\Delta q/q)} \approx \left(\frac{12\sqrt{2}}{f(\varepsilon)}\right)\left(\frac{d_{\min}}{D}\right)^{3/2} \tag{5.58}$$

where D is the droplet diameter, $f(\varepsilon)$ is a function given by de la Mora and Loscertales (1994), and $d_{min} \sim d_m$ given by (2.1). In fact, after incorporation of d_m and a slight rearrangement, (5.58) can be given by

$$\frac{f_q}{f_m} \approx c\sqrt{\frac{\rho}{\gamma}}\frac{Ka^{3/2}}{\varepsilon} \tag{5.59}$$

and differs from (5.57) only by a constant and the use of bulk electrical conductivity rather than surface electrical conductivity.

To determine values for q_p, m_p, and n_p, an assumption was made relating q_p to q_R since droplets were observed to break-up precisely at their Rayleigh limits. Previous investigators have reported that the charge on progeny microdroplets can range from 60% to 100% of the charge on the primary droplet immediately before break-up via Coulombic fission (de la Mora, 1996; Tang and Smith, 1999; Li et al., 2005, Gu et al., 2007). However, none of these findings have been theoretically substantiated. Here, the relationship between q_p and q_R was developed by Ray of Hunter and Ray (2009) by minimizing the Gibbs free energy change associated with the emission of charge and mass during the break-up of a charged droplet via Coulombic fission at the Rayleigh limit according to

$$\Delta G = n_p \frac{q_p^2}{8\pi\varepsilon_0 a_p} + 4\pi m_p a_p^2 \gamma - \left[1-\left(1-f_q\right)^2\right]\frac{q_R^2}{8\pi\varepsilon_0 a} \tag{5.60}$$

assuming that f_m is small and therefore the change in the size of the primary droplet is negligible. To evaluate (5.60), q_p, a_p, and n_p were all expressed in terms of f_q, f_m, and f_{RP}, where f_{RP} is the percentage of the Rayleigh limit on a progeny, as

$$q_p = f_{RP} q_R = 8\pi f_{RP}\sqrt{\varepsilon_0 \gamma a_p^3} \tag{5.61}$$

$$a_p = a\left(f_{RP}\frac{f_m}{f_q}\right)^{2/3} \tag{5.62}$$

$$n_p = \frac{1}{f_m}\left(\frac{f_q}{f_{RP}}\right)^2 \tag{5.63}$$

and incorporated into (5.60) to give

$$\Delta G = 8\pi a^2\gamma\left(f_q^2 f_m f_{RP}^4\right)^{1/3} + 4\pi a^2\gamma\left(\frac{f_q^2 f_m}{f_{RP}^2}\right)^{1/3} - 8\pi a^2\gamma\left[1-\left(1-f_q\right)^2\right] \qquad (5.64)$$

After differentiating (5.64) with respect to f_{RP}, the minimum in ΔG is found to occur where f_{RP}=50% from

$$\frac{\partial \Delta G}{\partial f_{RP}} = 4\pi a^2\gamma\left[\frac{8}{3}\left(f_q^2 f_m f_{RP}\right)^{1/3} - \frac{2}{3}\left(\frac{f_q^2 f_m}{f_{RP}^5}\right)^{1/3}\right] = 0 \qquad (5.65)$$

Therefore, progeny microdroplets are assumed to carry 50% of the charge of the primary droplet immediately before a break-up via Coulombic fission at the Rayleigh limit. Using f_{RP}=50%, q_p, a_p, and n_p were determined for each of the 32 observed break-ups where droplets produced progenies having

$$a_p \le \frac{a}{8} \qquad (5.66)$$

The values of a_p were regressed according to

$$a_p = \alpha\left(\frac{K_s}{\varepsilon}\sqrt{\frac{\rho}{\gamma}}\right)^{\beta} \qquad (5.67)$$

which was developed by incorporating (5.59) and (5.62) where α and β are constants. Here, α and β were found to be 0.394 and -0.664, respectively. The coefficient β is essentially -2/3 which is required for validation of (5.67).

5.1.6 Comparison of the Bulk and Surface Electrical Conductivity Results

Comparison of the results obtained from the Buckingham Pi theorem using the bulk electrical conductivity of the droplet and the solution of the Poisson-Boltzmann equation using the electrical conductivity at the surface of the droplet reveal two dramatically different relationships. Here, the differences in the role of electrical conductivity and droplet size will be primarily discussed as they are the only two variable droplet properties that were examined. To more equally compare the two analyses, the relationships for f_q/f_m will be examined. Although this relationship was not initially determined using dimensionless analysis, it can be developed using (5.32) and (5.33) and is given by

$$\frac{f_q}{f_m} = \frac{\exp(-1.1248)\left[\frac{q\rho^{3/2}\gamma}{(\varepsilon\varepsilon_0)^{1/2}\mu^3}\right]^{-0.0096}\left[\frac{K\mu^3}{\rho\varepsilon\varepsilon_0\gamma^2}\right]^{0.1169}}{\exp(-5.0478)\left[\frac{a\rho\gamma}{\mu^2}\right]^{0.2188}\left[\frac{K\mu^3}{\rho\varepsilon\varepsilon_0\gamma^2}\right]^{-0.2924}} \tag{5.68}$$

Assuming that the power term for Π_q is zero, and reducing the number of significant figures, (5.68) can be simplified and given by

$$\frac{f_q}{f_m} = 50.55\left[\frac{a\rho\gamma}{\mu^2}\right]^{-0.22}\left[\frac{K\mu^3}{\rho\varepsilon\varepsilon_0\gamma^2}\right]^{0.41} \tag{5.69}$$

which is further simplified to give

$$\frac{f_q}{f_m} = 50.55\left[\frac{\mu^{1.67}}{\rho^{0.63}(\varepsilon\varepsilon_0)^{0.41}\gamma^{1.04}}\right]a^{-0.22}K^{0.41} \tag{5.70}$$

Here it is important to note that (5.70) does not return the correct value for f_q/f_m when the corresponding values for μ, ρ, $\varepsilon\varepsilon_0$, γ, a, and K are inputted; likely due to the large amount of error incorporated by the reduction of significant figures. As such, only a generic comparison can be made. Comparison of (5.70) to (5.57) reveals that f_q/f_m is significantly more dependent on K_s as opposed to K. Moreover, when the role of K_s is considered, the role of a also becomes more dominant. Finally, only the analysis using K had any dependence on μ.

It is evident that the distribution of charge within a dielectric droplet significantly affects the role of electrical conductivity and size on the characteristics of charged droplet break-ups via Coulombic fission at the Rayleigh limit. This further suggests that the characteristics of charged droplet break-ups are almost completely dominated by their surface properties and can only be estimated from bulk properties. As such, a more in-depth analysis of how ρ, ε, μ, and γ exist at the droplet surface may reveal a more detailed illustration of the break-up process.

5.1.7 Prediction of Ion Emission

A common theme in literature pertaining to the break-ups of charged droplets and the formation of progeny microdroplets is discussion regarding the ability of charged droplets to emit gas phase ions (Iribarne and Thomson, 1976; Rollgen et al., 1987; Schmelzeisen-Redeker et al., 1989; Fenn, 1993; Loscertales and de la Mora, 1995; de la Mora, 1996; Labowsky et al., 2000; Rohner et al., 2004; Ichiki and Consta, 2006; Hogan et al., 2009; Consta, 2010. Here, the relationships developed are used to estimate the droplet characteristics necessary for ion emission.

Given the error associated with (5.70), the relationships given by (5.30) and (5..31) were used to estimate the conditions required for a charged droplet of pure DEP to emit only ions during its break-up via Coulombic fission at the Rayleigh limit. Here, (5.30) and (5.31) are recast as

$$\Delta q = 0.3327 q \left[\frac{K \mu^3}{\rho \varepsilon \varepsilon_0 \gamma^2} \right]^{0.1169} \tag{5.71}$$

$$\Delta m = 0.0269 a^{3.1288} \left[\frac{\rho^{1.2188} \gamma^{0.2188}}{\mu^{0.2576}} \right] \left[\frac{K \mu^3}{\rho \varepsilon \varepsilon_0 \gamma^2} \right]^{-0.2924} \tag{5.72}$$

assuming the power originally assigned to Π_q can be considered equal to one. Assuming that the charge term, q, in (5.71) can be expressed using Rayleigh theory, (5.71) is rewritten as

$$\Delta q = 0.3327 (8\pi) \sqrt{\varepsilon_0 \gamma a^3} \left[\frac{K \mu^3}{\rho \varepsilon \varepsilon_0 \gamma^2} \right]^{0.1169} \tag{5.73}$$

To predict the droplet radius, a, where only ions will be emitted during the break-up of a charged droplet via Coulombic fission at the Rayleigh limit, the number of molecules emitted must equal the number of ions emitted. Assuming each ionized solvent molecule will possess only a single charge, the number of ions emitted was determined by dividing (5.73) by the charge on an electron, e^-. The number of molecules emitted during the break-up of a charged droplet was determined by multiplying (5.72) by Avogadro's number, N_A, and dividing by the molecular weight, M_W, of the solvent. The equations

representing the number of ions and solvent molecules were then equated in terms of the droplet radius to give

$$a_{ion} = \left(12.368 \frac{M_w}{N_A e^-} \frac{8\pi\sqrt{\varepsilon_0 \gamma}}{\left[\frac{\rho^{1.2188} \gamma^{0.2188}}{\mu^{0.2576}} \right]} \left[\frac{K\mu^3}{\rho \varepsilon \varepsilon_0 \gamma^2} \right]^{0.4093} \right)^{\frac{1}{1.6288}} \tag{5.74}$$

where a_{ion} is the radius at which a charged droplet will break-up via Coulombic fission at its Rayleigh limit and only ions will be emitted. When (5.74) is applied to pure DEP (K=0.69 $\mu S \cdot m^{-1}$), a_{ion} is found to be 5.76 nm which represents a cluster of 2420 solvent molecules of which 39 are ionized with a single charge. Such a droplet is predicted to emit seven ionized solvent molecules during its break-up via Coulombic fission at the Rayleigh limit. The value of a_{ion} indicates that dielectric droplets are not likely to proceed through an ion evaporation mechanism until they are small clusters of molecules and ions. For a droplet of DEP having an artificially increased electrical conductivity of K=2000 $\mu S \cdot m^{-1}$, the upper limit of electrical conductivity for DEP droplets containing an ionic dopant observed in this study, a_{ion} is increased to 38.42 nm and calculated to emit 320 of its 667 ionized molecules during its break-up. In fact, for a droplet of DEP to have a_{ion} = 100 nm, its electrical conductivity would have to be 120000 $\mu S \cdot m^{-1}$. This hypothetical droplet would emit 2230 of its 2880 charges during a break-up via Coulombic fission representing a charge loss of 77%, but a mass loss of less than 0.02%.

When (5.74) is applied to a more electrically conductive droplet however, the droplet size is reduced although the electrical conductivity is significantly increased. For example, when the properties of sulfuric acid are applied (K=500000 $\mu S \cdot m^{-1}$), a_{ion} is found to be 59.25 nm and to emit 80% of its charge whereas a DEP droplet having an equivalent electrical conductivity would have a_{ion}=143.10 nm and emit 92% of its charge. Here, the role of other relevant physical properties of charged droplets become apparent. Moreover, this example demonstrates why dielectric droplets may have more application in the generation of nanoparticles.

Although (5.74) has no underlying physical basis, the estimated values determined for a_{ion} are supported by the findings of Labowsky et al. (2000) who predicted that ion evaporation would occur for small droplets having 12 or less individual charges and by Hogan et al. (2009) who have reported that droplets having diameters between 10 and 40 nm, well within the size range determined here, emitted only ions during their break-ups.

When the droplet characteristics required for ion emission are determined using the results obtained for surface electrical conductivity however, the findings are much different. Here, consider a charged droplet of DEP-IL1 having a_{ion}=100 nm. Assuming that only ions are emitted by such a droplet during its break-up via Coulombic fission at the Rayleigh limit, f_q/f_m can be determined in the following manner. First, f_q/f_m will be expressed using

$$\frac{f_q}{f_m} = \frac{\Delta q}{\Delta m}\frac{m}{q} \tag{5.75}$$

Next, assuming that all ions are singly charged solvent molecules, the ratio of $\Delta q/\Delta m$ can be given by

$$\frac{\Delta q}{\Delta m} = e^{-}\frac{N_A}{M_W} \tag{5.76}$$

Note that (5.76) is independent of the number of ions emitted. The droplet charge, q, can be determined using (1.1) where a is given by a_{ion} and the droplet mass, m, can be determined using

$$m = \rho\frac{4}{3}\pi a_{ion}^3 \tag{5.77}$$

Such a droplet is found to have f_q/f_m=4530.55. Using the fit previously given by (5.57) where the slope has been determined to be 4.71±0.14 for charged droplets of DEP-IL1, the $K_s \cdot a^{3/2}$ term is found to be 961.90 pS·m$^{1/2}$. Therefore, the surface electrical conductivity, K_s, required for ion emission is determined to be 30.42 S·m^{-1}. Here, K_s is found to be two orders of magnitude greater than the bulk electrical conductivity previously determined for an equivocal droplet.

What is intriguing about this result is that when the droplet characteristics previously determined for ion emission using bulk conductivity are inputted, the value for K_s is again determined to be precisely 30.42 $S \cdot m^{-1}$ regardless of a_{ion}. For example, the aforementioned droplet of pure DEP having a_{ion}=5.76 nm has f_q=(7/39) and f_m=(7/2420). Here, f_q/f_m is found to be 62.57 from which K_s=30.42 $S \cdot m^{-1}$ is again determined. Although the droplet size was significantly reduced from the previous example, the value of K_s remained constant whereas K was previously found to decrease as a_{ion} decreased. As such, the results from this analysis indicate that the surface electrical conductivity of a charged droplet must reach a certain point determined by the physical properties of the solvent before ion emission can occur. Moreover, here K_s is eight orders of magnitude greater than K. Therefore, charged droplets of dielectric solvents such as DEP are unlikely to emit only ions during their break-ups via Coulombic fission at the Rayleigh limit. Here, the findings are more in support of the charge residue model of Dole (1968) in that gas phase ions would only result from dielectric droplets by the evaporation of their neutral solvent molecules and that an ionic dopant would be required for the ion evaporation model of Iribarne and Thomson (1976) to be applicable. In fact, the study by Ichiki and Consta (2006) in support of the ion evaporation model was conducted using water doped with chloride ions. However, Ichiki and Consta (2006) and Consta (2010) have both shown that Rayleigh theory is no longer valid for very small droplets. As such, the earlier assumptions that break-ups would occur precisely at the Rayleigh limit may not have been valid for the very small droplet sizes examined.

5.2 Conclusions

In this chapter, the role of electrical conductivity on the characteristics of break-ups of negatively charged droplets via Coulombic fission at the Rayleigh limit has been examined. Initially, pure component droplets of DEG, TEG, T4EG, DMP, DEP, NNA, and PNN were observed through multiple break-ups and the percentages of charge and mass emitted and the charge limits at which break-ups occurred were recorded. Here, droplets of DEG, TEG, and T4EG were observed to emit 37% to 52% of their charge and

0.7% to less than 0.1% of their mass during break-ups via Coulombic fission that occurred precisely at the Rayleigh limit. Droplets of DMP and DEP however, were observed to emit only 12% to 20% of their charge, but 1.7% to 2.7% of their mass during break-ups via Coulombic fission that occurred precisely at the Rayleigh limit. Droplets of NNA were observed to have charge and mass emissions similar to DMP and DEP droplets, but to have break-ups that occurred above the Rayleigh limit. Finally, droplets of PNN were observed to emit 7% to 16% of their charge and 0.6% to 1.7% of their mass during break-ups via Coulombic fission. Although the charge level at which break-ups were observed could not be directly determined, they were observed to occur at a reproducible charge level.

To examine the role of electrical conductivity, the ionic dopants TDMAC, TDMAN, IL1, IL2, and Stadis 450 were used. All of the ionic dopants, except for Stadis 450, were found to completely dissolve in and predictably increase the electrical conductivity of the solvents used. Here, droplets of DEP and DMP were doped with known amounts of either TDMAC, TDMAN, IL1, or IL2 and observed through multiple break-ups and the percentages of charge and mass emitted and the charge limits at which break-ups occurred were again recorded. Here, the percentages of charge and mass emitted were observed to increase to 40% and decrease to below 0.1% as the amount of ionic dopant was increased. Also, the increase in the percentage of charge emitted by doped droplets was found to increase to a certain point and then remain nearly constant. No effect on the charge level at which break-ups occurred however, with one exception, was observed. The exception noted here was for a single droplet of DMP doped with a high concentration of TDMAN. In this situation, the charge level was observed to increase to 150% of the corresponding Rayleigh limit and assumed to be the result of solid TDMAN present in the droplet.

In separate studies, charged droplets of TEG-TDMAC and PNN-Stadis 450 were observed during their break-ups via Coulombic fission. The TEG-TDMAC droplet was observed to have charge and mass emissions similar to pure TEG droplets and to again have break-ups that occurred at the Rayleigh limit, although its electrical conductivity

was increased. Here again, the results indicate that the percentage of charge emitted by a droplet may be limited. The PNN-Stadis 450 droplets were observed to give very dissimilar results to those obtained from other droplets containing an ionic dopant. Here, the percentages of charge and mass emitted and the charge levels at which break-ups occurred were all observed to increase with each successive break-up. It is assumed that the Stadis 450 precipitated out of the PNN during evaporation and that the electrical conductivity of the droplets actually decreased as a result of evaporation of the co-solvents found in the ionic dopant. However, no tests were performed to verify this assumption.

To evaluate the role of electrical conductivity, as well as other physical droplet properties, a dimensionless analysis was performed using the Buckingham Pi theorem. Here, both the amounts and percentages of charge and mass emitted during break-ups were expressed as functions of density, relative permeability, surface tension, viscosity, electrical conductivity, and either the radius or the charge of the droplet. Data collected from the break-ups of pure and doped droplets were used to fit the equations. Both the amounts and percentages of charge and mass emitted during break-ups were found to have a weak dependence on the electrical conductivity relative to the other physical droplet properties.

A more detailed inspection into the role of electrical conductivity was performed by determining the electrical conductivity of droplets over a narrow layer at their surface. Here, the Poisson-Boltzmann equation was used to determine the distribution and therefore the densities of ions at the droplet surface for droplets of DEP-TDMAC, DEP-IL1, and DMP-TDMAN. The ratio of the percentages of charge emitted to mass emitted, f_q/f_m, was found to be linearly related to the surface electrical conductivity droplet times the radius to the 3/2 power, $K_s \cdot a^{3/2}$. An extension of this analysis also found that the radius of the progeny microdroplets, a_p, produced from the mass emitted during a break-up was dependent on K_s to the -2/3 power. To equivocally compare the results using surface electrical conductivity to those obtained using bulk electrical conductivity, f_q/f_m

was determined using the results the Buckingham Pi theorem. Here, fq/fm was found to be linearly related to $a^{0.22} \cdot K^{0.41}$.

The results from both analyses were used to predict the droplet characteristics required for charged droplets to emit only gas phase ions. Here, the relationship determined using bulk electrical conductivity found that a charged droplet of DEP would have a radius of less than 6 nm before ion emission could occur and that its electrical conductivity would have to be artificially increased to 120000 $\mu S \cdot m^{-1}$ before ion emission would occur for a droplet having a radius of 100 nm. When the relationship determined for f_q/f_m as a function of $K_s \cdot a^{3/2}$ is used however, a much different trend appears. Here, charged droplets are only found to undergo an ion emission when Ks=30.42 $S \cdot m^{-1}$, regardless of the droplet size. This finding suggests that dielectric droplets are unlikely to ever emit only gas phase ions.

In conclusion, electrical conductivity has been found to significantly affect how much charge and mass are emitted during the break-ups of charged droplets via Coulombic fission, but to have no effect on the charge levels at which such break-ups occur. However, electrical conductivity alone is not solely responsible for all the effects observed as part of this study. Physical droplet properties such as size, density, surface tension, and relative permeability all affect the characteristics of charge droplet break-ups. To fully understand the break-up phenomena, a more detailed investigation of how each of the physical properties of a charged droplet are related to its break-up is required.

Chapter 6: Role of Water Insoluble Materials on the Hygroscopic Behavior of Atmospherically Relevant Inorganic Salts

6.1 Results

6.1.1 Hysteresis of Pure NaCl and NaBr Particles

Charged particles of NaCl and NaBr were each individually levitated in an electrodynamic balance and observed during cycles of humidification and dehumidification over a specified range of relative humidity (RH). Using the data analysis procedure described in Chapter 4, hysteresis loops were constructed for the two inorganic salts. The goal here was not to determine the deliquescence relative humidities (DRH), crystallization relative humidities (CRH), or hygroscopic growth for the pure component inorganic salts, but to establish a baseline from which change could be ascertained. Since the hysteresis loops of both inorganic salts will be repeatedly given in the following figures along with their mixed component counterparts, they are not given independently. Furthermore, an example of the hysteresis loop for pure NaCl has been previously given in Chapter 2 by Figure 2.3. Although multiple hysteresis loops were constructed for both of the inorganic salts, only a representative sample for each inorganic salt will be shown for comparison with mixed particles.

During some experiments, the DRH and CRH of the pure component salts were observed to 'shift' below the values previously established for the individual salts. This was found to occur when the battery for the relative humidity meter was nearly depleted. As such, hysteresis loops for pure component NaBr and NaCl particles were routinely constructed to monitor this problem. To maintain consistency between experiments, the data collected from the pure component inorganic salt particles were calibrated using the DRH and CRH values found in current literature. Here, the DRH and CRH of NaCl were taken as 75% and 45% RH, respectively, and the DRH and CRH of NaBr were taken as 45% and 22% RH, respectively (Cohen et al., 1987a; Tang and Munkelwitz, 1994; Martin, 2000; and Wise et al., 2005; Biskos et al., 2006a). The post-deliquescent

hygroscopic growth of the particles was taken from the equilibrium data given by Hamer and Wu (1972) and is presented in all relevant subsequent figures.

6.1.2 Hygroscopic Behavior of NaCl and NaBr Particles Containing a Water Insoluble Solid

Here, the effects on the hygroscopic behavior of NaCl and NaBr particles internally mixed with a water insoluble solid are reported. The two inorganic salts were each individually combined with each of three selected water insoluble solids. Here, the water insoluble solids selected for study were a carbon black (BC) provided by Contintental Carbon (lot N234, Phenix City, Al plant), lauric acid (LA), and anthracene (AN). Each of the water insoluble solids was combined, although in different amounts, to both of the inorganic salts. The mixed particles generated from each of the inorganic salt-water insoluble solid pairs were each observed through a cycle of humidification and dehumidification over a specific range of RH. The data analysis procedure described in Chapter 4 was used to construct hysteresis loops for all the mixed particles that were observed.

Three NaCl-BC particles were individually generated from three different solutions having known dry-mass ratios of NaCl to BC. The hysteresis loops constructed from the mixed particles are presented in Figure 6.1 along with a hysteresis loop for a pure NaCl particle and data points representing the hygroscopic growth of pure NaCl obtained from Hamer and Wu (1972). Since the hygroscopic growth of both the pure and mixed particles were in agreement with that given by Hamer and Wu (1972), the raw data points obtained from Hamer and Wu (1972) given by hollow diamonds cannot be easily seen. The raw data points used to construct the hysteresis loop for pure NaCl are given by a solid circle and connected by a solid line. The raw data points used to construct the hysteresis loops for the three NaCl-BC particles are given by a solid diamond, a solid square, and a solid triangle and correspond to mixed particles having a dry-mass mixtures containing 40% NaCl and 60% BC, 57% NaCl and 43% BC, and 70 % NaCl and 30% BC, respectively, and are all connected by a solid line.

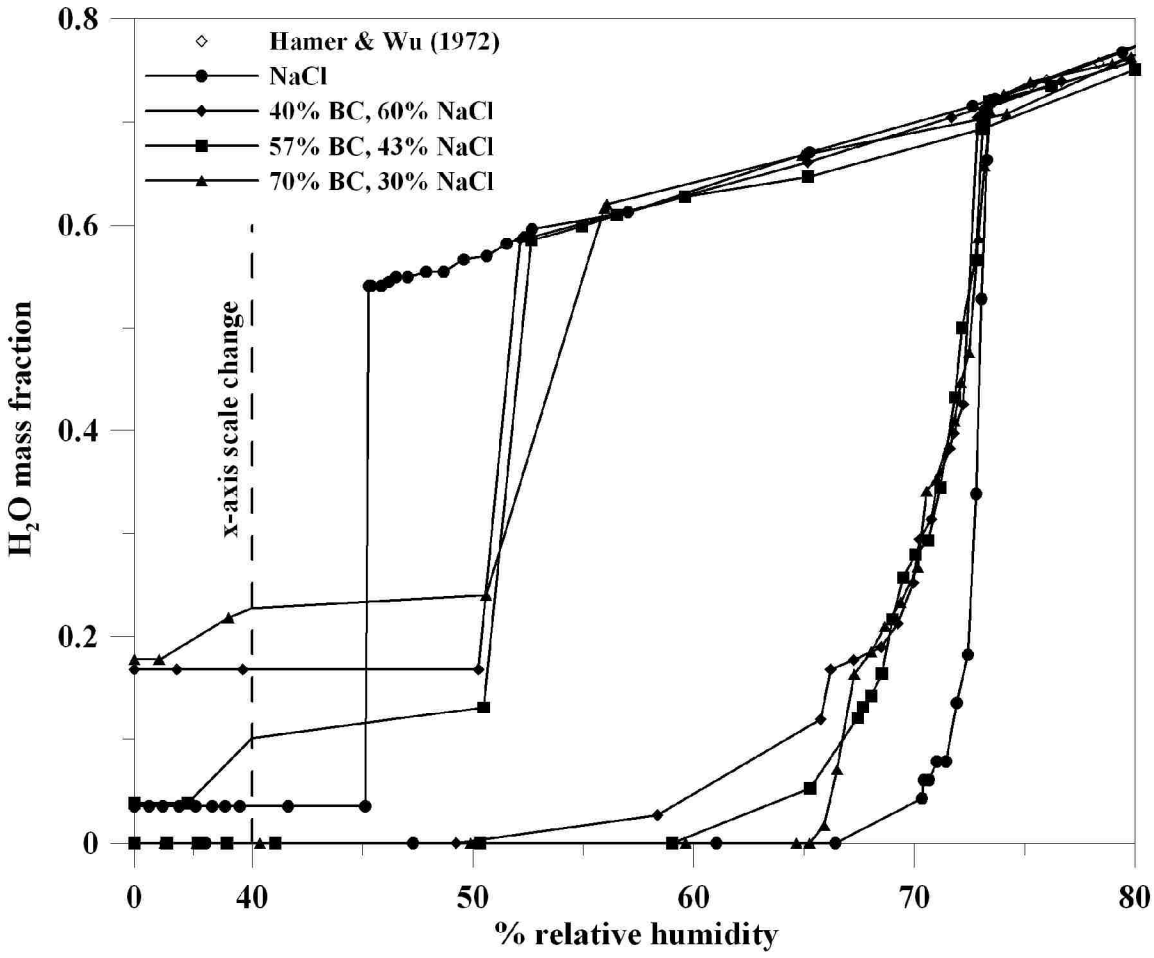

Figure 6.1 Effect of BC on the hysteresis of NaCl particles.

All three NaCl-BC particles were observed to begin their initial water uptake at a lower RH than pure NaCl, but eventually exhibited the same DRH as pure NaCl. After deliquescence, all three particles showed no noticeable difference in the amount of water absorbed or desorbed as compared to pure NaCl until they crystallized. All mixed particles were observed to crystallize at a much higher RH than the pure NaCl particle. The particle containing a dry-mass content of 70% BC was observed to crystallize between 55% and 50% RH and the particles containing dry-mass contents of 40% and 57% were observed to crystallize between 52% and 50% RH. After crystallization, all three mixed particles appeared to retain some fraction of water. No relationship between the amount of water retained after crystallization and the dry-mass ratios of the NaCl-BC particles was observed.

A separate study was performed in which three NaCl-BC particles having dry-mass contents of 43% NaCl and 57% BC were individually examined. Here, the particles were subjected to different rates of change in the surrounding RH. The hysteresis loops constructed from the mixed particles are presented in Figure 6.2 along with a hysteresis loop for a pure NaCl particle. The raw data points used to construct the hysteresis loop for pure NaCl are given by a solid circle and connected by a solid line. The raw data points used to construct the hysteresis loops for the three NaCl-BC particles are given by a solid diamond, a solid square, and a solid triangle and correspond to mixed particles having a dry-mass mixtures containing 57% NaCl and 43% BC that were observed under ‘fast’, ‘normal’, and ‘slow’ rates of change to the surrounding RH, respectively, and are all connected by a solid line. Here, the hysteresis loop for the ‘normal’ NaCl-BC particle is the same as the NaCl-BC particle having a dry-mass content of 57% BC in Figure 6.1. The ‘normal’ rate of change in the surrounding RH is consistent with the rate of change in all other related studies and corresponds to increasing the RH by about 1% per minute. The ‘fast’ and ‘slow’ rates correspond to a change in the RH by about 5% per minute and 1% per 5 minutes, respectively.

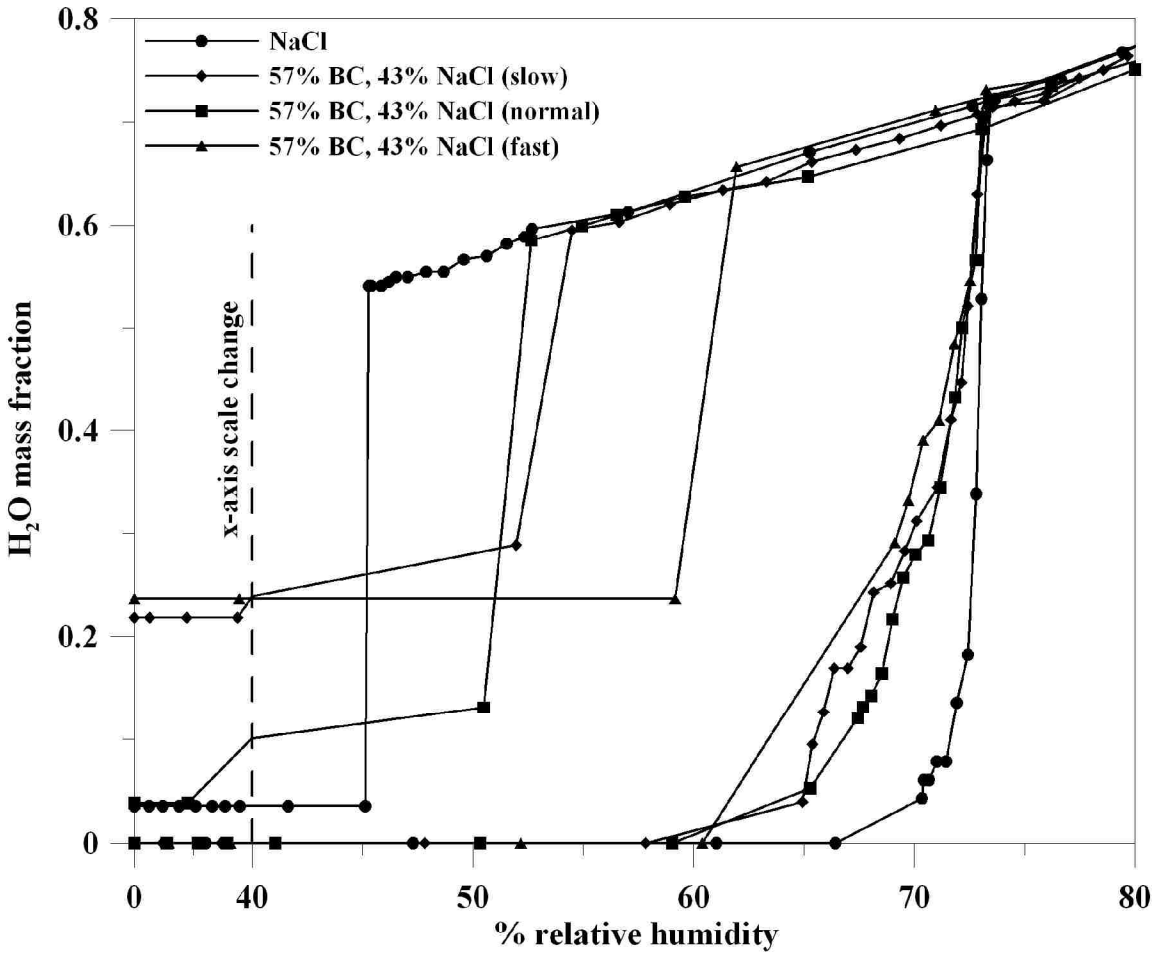

Figure 6.2 Effect of the rate of change in the surrounding RH on the hysteresis of NaCl-BC particles.

All three particles were observed to initiate water uptake at a much lower RH than pure NaCl, but eventually exhibited the same DRH and hygroscopic growth as pure NaCl. Also, all mixed particles were again observed to crystallize at a much higher RH than the pure NaCl particle. The particle labeled 'fast' was observed to crystallize between 62% and 59% RH and the particles labeled 'normal' and 'slow' were observed to crystallize between 53% and 50% RH. After crystallization, the three particles appeared to retain some fraction of water. No relationship between the amount of water retained after crystallization and the rate of change in the surrounding RH was observed.

Two NaBr-BC particles were individually generated from a solution having a dry-mass composition of 75% NaBr and 25% BC. The hysteresis loops constructed from the mixed particles are presented in Figure 6.3 along with a hysteresis loop for a pure NaBr particle and data points representing the hygroscopic growth of pure NaBr obtained from Hamer and Wu (1972) given by hollow diamonds. Here, the hygroscopic growth of the pure and mixed particles appears to differ slightly from that given by Hamer and Wu (1972). The raw data points used to construct the hysteresis loop for pure NaBr are given by a solid circle and connected by a solid line. The raw data points used to construct the hysteresis loops for the two NaBr-BC particles labeled (1) and (2) are given by a solid diamond and a solid square, respectively, and are both connected by a solid line.

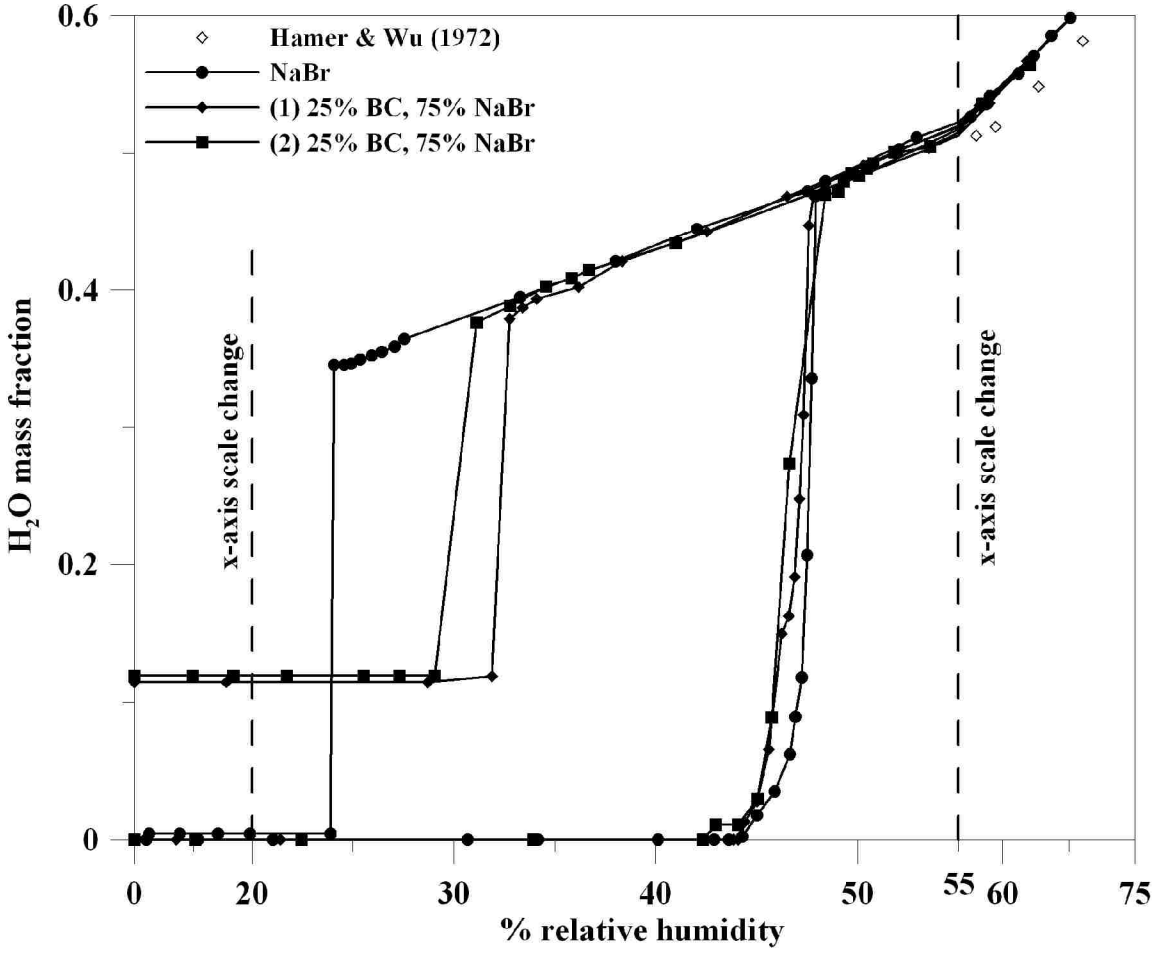

Figure 6.3 Effect of BC on the hysteresis of NaBr particles.

Both mixed particles were observed to begin their initial water uptake at the same RH as pure NaBr and exhibited the same DRH as pure NaBr. After deliquescence, the two mixed particles showed no noticeable difference in the amount of water absorbed or desorbed as compared to pure NaBr until they crystallized. Both the mixed particles were observed to crystallize at a much higher RH than the pure NaBr particle. Here, the two mixed particles were observed to crystallize between 33% and 29% RH. After crystallization, both mixed particles appeared to retain some fraction of water.

Two NaCl-LA particles were individually generated from a solution having a dry-mass composition of 51% NaCl and 49% LA. The hysteresis loops constructed from the mixed particles are presented in Figure 6.4 along with a hysteresis loop for a pure NaCl particle and data points representing the hygroscopic growth of pure NaCl obtained from Hamer and Wu (1972). Since the hygroscopic growth of both the pure and mixed particles were in agreement with that given by Hamer and Wu (1972), the raw data points obtained from Hamer and Wu (1972) given by hollow diamonds cannot be easily seen. The raw data points used to construct the hysteresis loop for pure NaCl are given by a solid circle and connected by a solid line. The raw data points used to construct the hysteresis loops for the two NaCl-LA particles labeled (1) and (2) are given by a solid diamond and a solid square, respectively, and are both connected by a solid line.

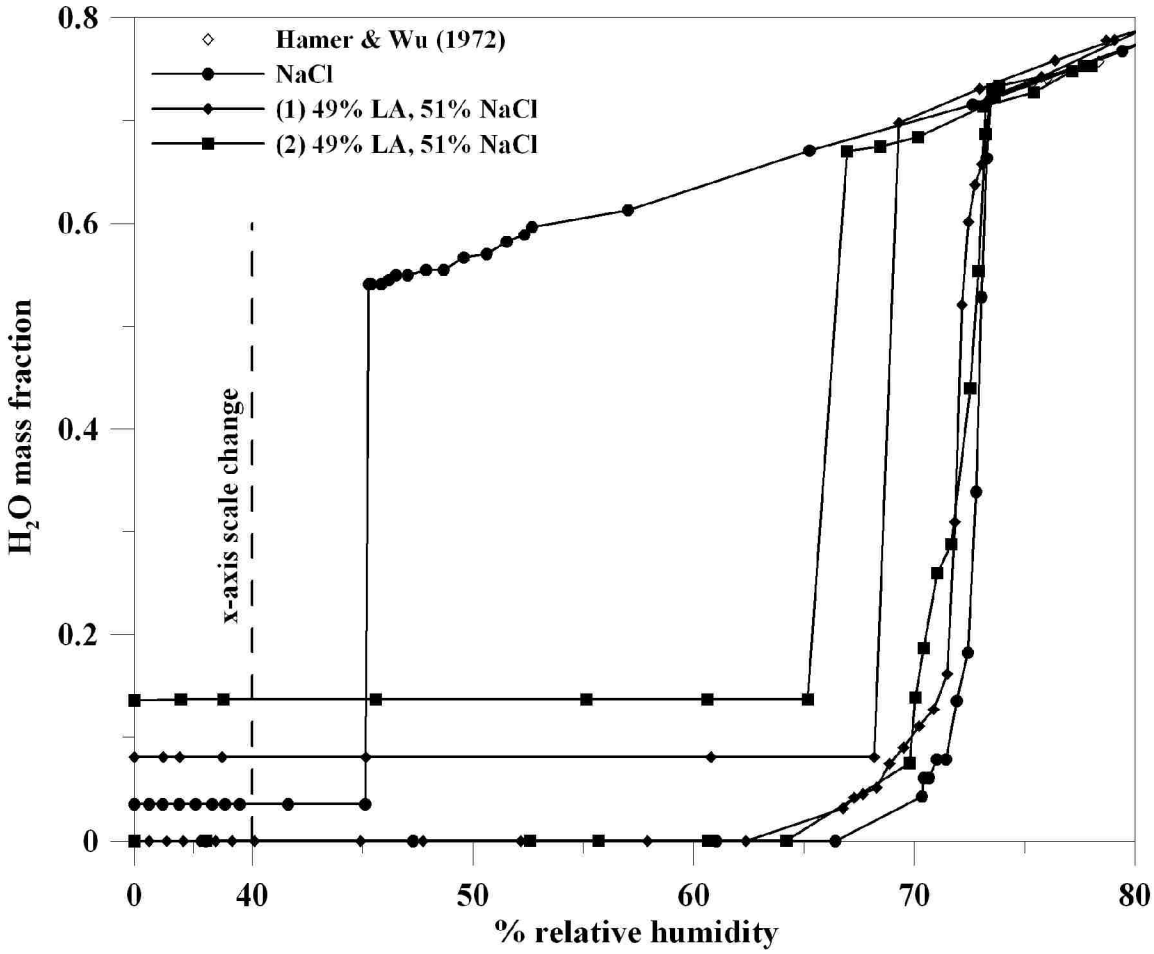

Figure 6.4 Effect of LA on the hysteresis of NaCl particles.

Both mixed particles were observed to begin their initial water uptake at a slightly lower RH than pure NaCl, but eventually exhibited the same DRH as pure NaCl. After deliquescence, the two mixed particles showed no noticeable difference in the amount of water absorbed or desorbed as compared to pure NaCl until they crystallized. Both the mixed particles were observed to crystallize at a RH significantly higher than the pure NaCl particle. Here, the two mixed particles were observed to crystallize between 68% and 65% RH which is just below their DRH. After crystallization, both mixed particles appeared to retain some fraction of water.

Two NaBr-LA particles were individually generated from a solution having a dry-mass composition of 82% NaBr and 18% BC. The hysteresis loops constructed from the mixed particles are presented in Figure 6.5 along with a hysteresis loop for a pure NaBr particle and data points representing the hygroscopic growth of pure NaBr obtained from Hamer and Wu (1972) given by hollow diamonds. Here, the hygroscopic growth of the pure and mixed particles appears to differ slightly from that given by Hamer and Wu (1972). The raw data points used to construct the hysteresis loop for pure NaBr are given by a solid circle and connected by a solid line. The raw data points used to construct the hysteresis loops for the two NaBr-LA particles labeled (1) and (2) are given by a solid diamond and a solid square, respectively, and are both connected by a solid line.

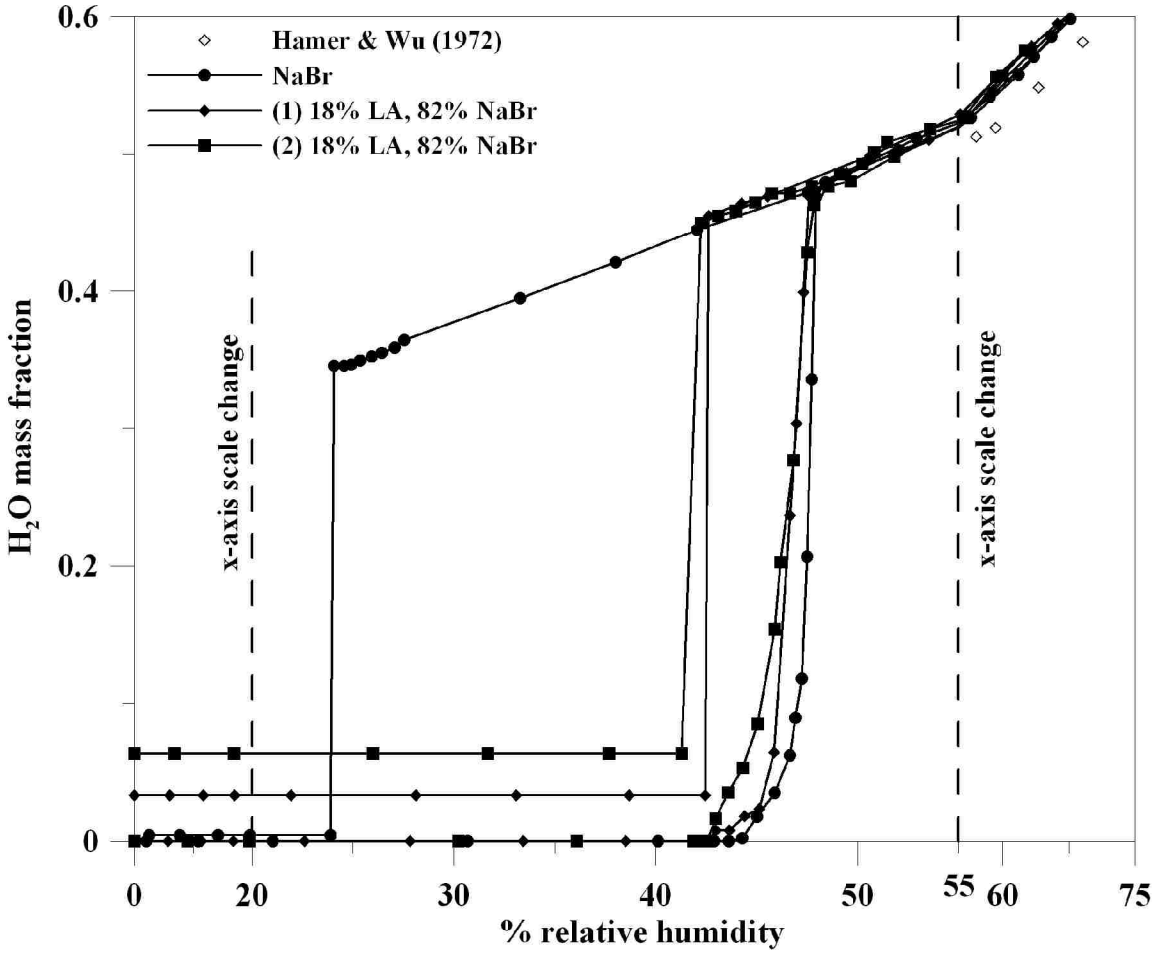

Figure 6.5 Effect of LA on the hysteresis of NaBr particles.

Both mixed particles were observed to begin their initial water uptake at approximately the same RH as pure NaBr and exhibited the same DRH as pure NaBr. After deliquescence, the two mixed particles showed no noticeable difference in the amount of water absorbed or desorbed as compared to pure NaBr until they crystallized. Both the mixed particles were observed to crystallize at a RH significantly higher than the pure NaBr particle. Here, the two mixed particles were observed to crystallize between 43% and 41% RH which is just below their DRH. After crystallization, both mixed particles appeared to retain some fraction of water.

A separate study was performed in which three NaBr-LA particles having dry-mass contents of 82% NaBr and 18% LA were individually examined. Here, two of the particles were subjected to multiple cycles of humidification and dehumidification. The hysteresis loops constructed from the mixed particles are presented in Figure 6.6. The raw data points used to construct the hysteresis loop for pure NaBr are given by a solid circle and connected by a solid line. Here, the particle labeled (1) is identical to the particle labeled (1) in figure 6.5 whereas the particles labeled (2) and (3) are unique to Figure 6.6. The subscripts ‘a’, ‘b’, and ‘c’ attached to particles (2) and (3) indicate the order of the cycles of humidification and dehumidification experienced by the particle where ‘a’ is the first cycle, ‘b’ is the second cycle, and ‘c’ is the third cycle. Particle (2) and particle (3) were exposed to two and three cycles of humidification and dehumidification, respectively. Particle (1) is represented by a solid diamond, particle (2) is represented by a solid square for its first cycle (2a) and by a hollow square for its second cycle (2b), particle (3) is represented by a solid triangle for its first cycle (3a), by a hollow triangle for its second cycle (3b), and by an inverted hollow triangle for its third cycle (3c). The data points representing each cycle of humidification and dehumidification are connected by a solid line.

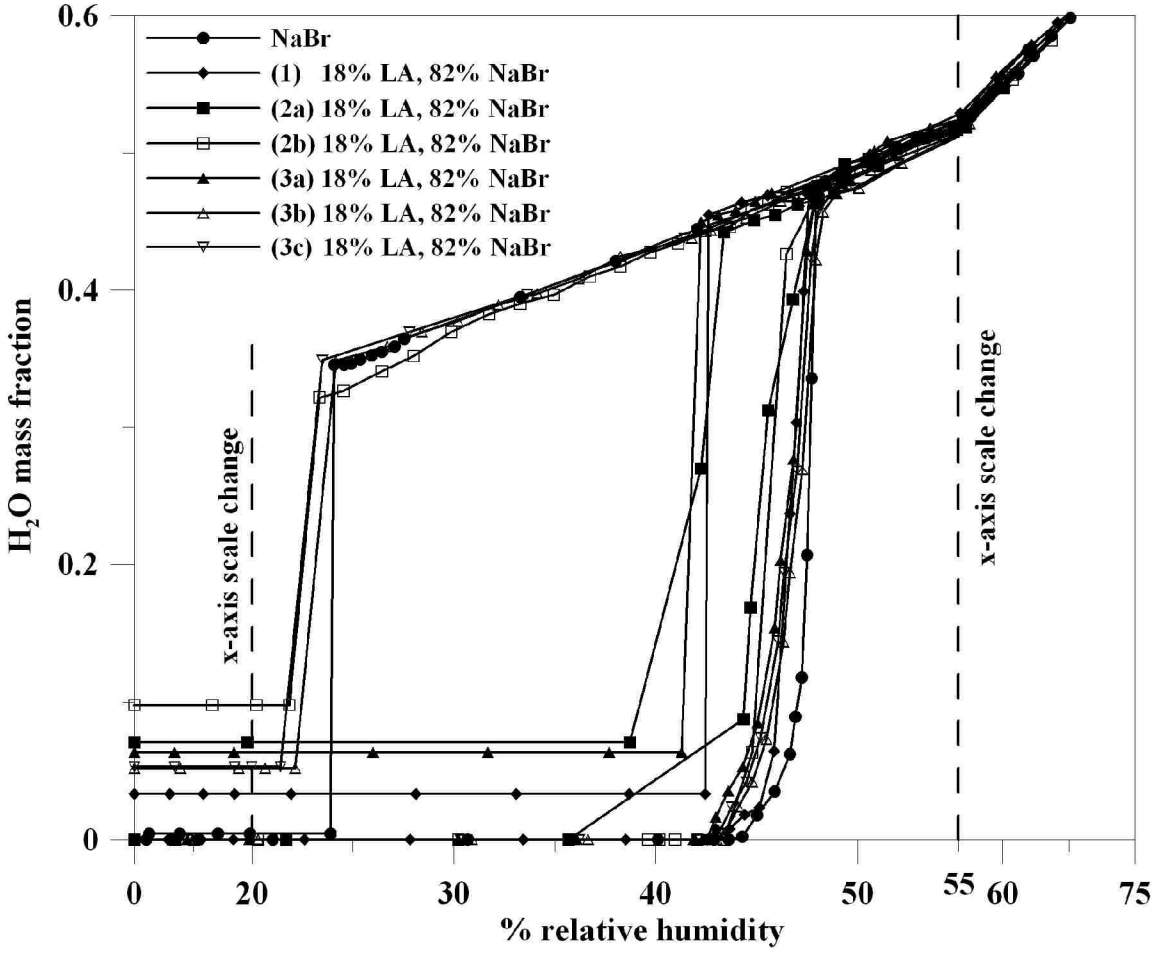

Figure 6.6 Effect of exposing mixed particles of LA and NaBr to repeated hysteresis on the CRH of the mixed particles.

With the exception of particle (2) during its first cycle, all particles during all cycles of humidification and dehumidification were observed to have the same initial water uptake, DRH, and post-deliquescence water absorption and desorption as pure NaBr. During their first dehumidification cycle, all mixed particles were observed to crystallize at a significantly higher RH than the particle of pure NaBr. Particle (1), and the first cycles of particles (2) and (3) given by (2a) and (3a), respectively, were observed to crystallize between 43% and 38% RH which is just below their DRH. However, when particles (2) and (3) were again subjected to a cycle of humidification and dehumidification given by (2b) and (3b), respectively, they were both observed to crystallize at the same CRH as the pure NaBr particle. Furthermore, this behavior was observed again by particle (3) when it was exposed to a third cycle given by (3c). After crystallization, all mixed particles appeared to retain some fraction of water at the end of each cycle.

Three NaCl-AN particles were individually generated from a solution having a dry-mass composition of 57% NaCl and 43% LA. The hysteresis loops constructed from the mixed particles are presented in Figure 6.7 along with a hysteresis loop for a pure NaCl particle and data points representing the hygroscopic growth of pure NaCl obtained from Hamer and Wu (1972) given by hollow diamonds. The raw data points used to construct the hysteresis loop for pure NaCl are given by a solid circle and connected by a solid line. The raw data points used to construct the hysteresis loops for the three NaCl-AN particles labeled (1), (2), and (3) are given by a solid diamond, a solid square, and a solid triangle, respectively, and are all connected by a solid line.

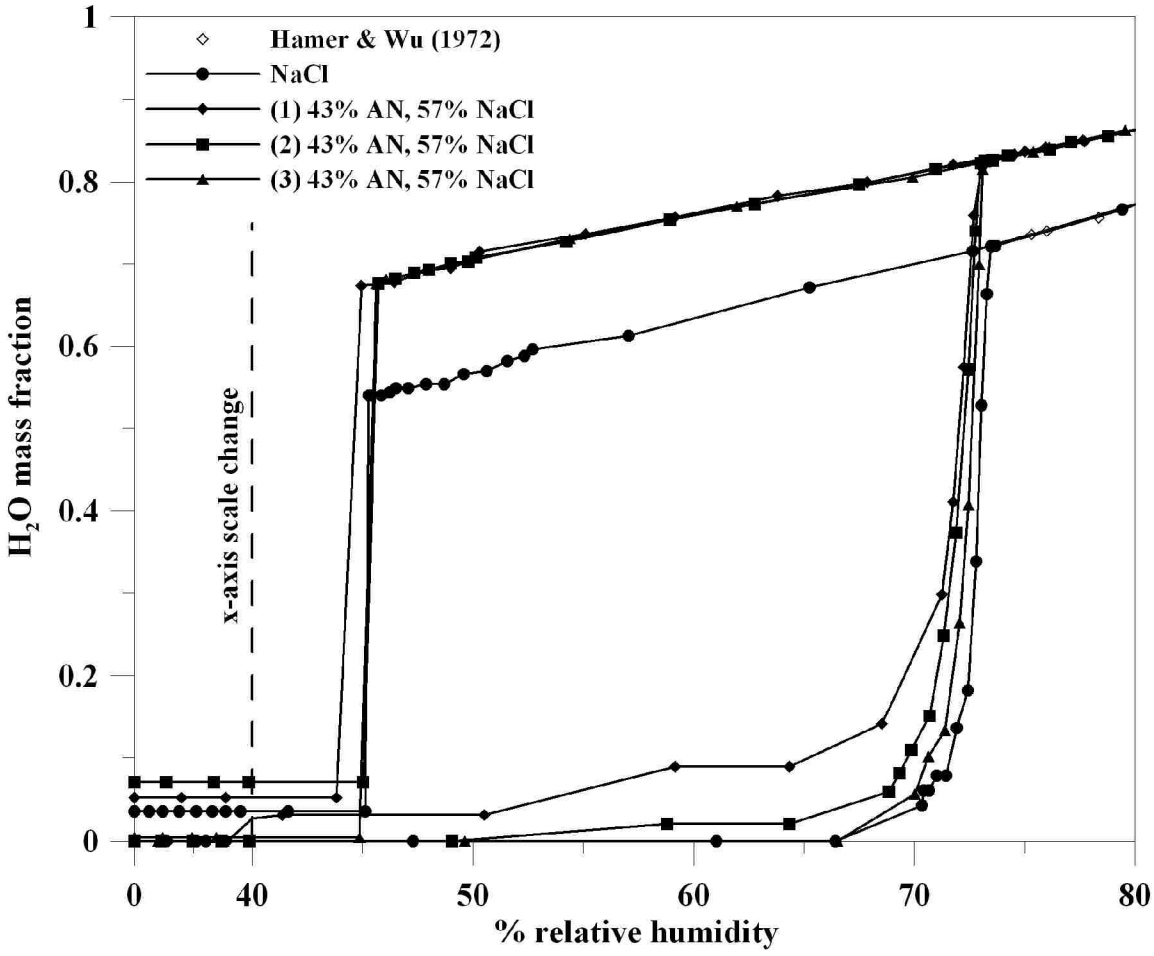

Figure 6.7 Effect of AN on the hysteresis of NaCl particles.

The mixed particles labeled (1) and (2) were observed to begin their initial water uptake at a slightly lower RH than pure NaCl, whereas particle (3) began its initial water uptake identically to the particle of pure NaCl. All particles however, eventually exhibited the same DRH as pure NaCl. After deliquescence, all three mixed particles showed a noticeable difference in the amount of water absorbed or desorbed as compared to pure NaCl. Here, the water mass fraction of the mixed particles appeared to be much higher than that of the pure NaCl particle. The three particles however, were observed to crystallize at the same CRH as pure NaCl. After crystallization, two of the three mixed particles appeared to retain some water after crystallization

As the behavior of the three NaCl-AN was dramatically different from that of the other mixed particles in relation to their pure component counterparts, an alternative analysis of the collected data was performed. Here, it was assumed that no AN was in fact present ion the mixed particle. Therefore, the raw data used to construct the hysteresis loops in Figure 6.7 was re-analyzed to construct the hysteresis loops given in Figure 6.8. Here, the mixed particles are identical to those in Figure 6.7 where particles (1), (2), and (3) are relabeled as (1a), (2a), and (3a), respectively. Furthermore, the dry-mass compositions of the particles are listed in the figure as 00% AN and 100% NaCl to reflect the assumption used to re-analyze the data.

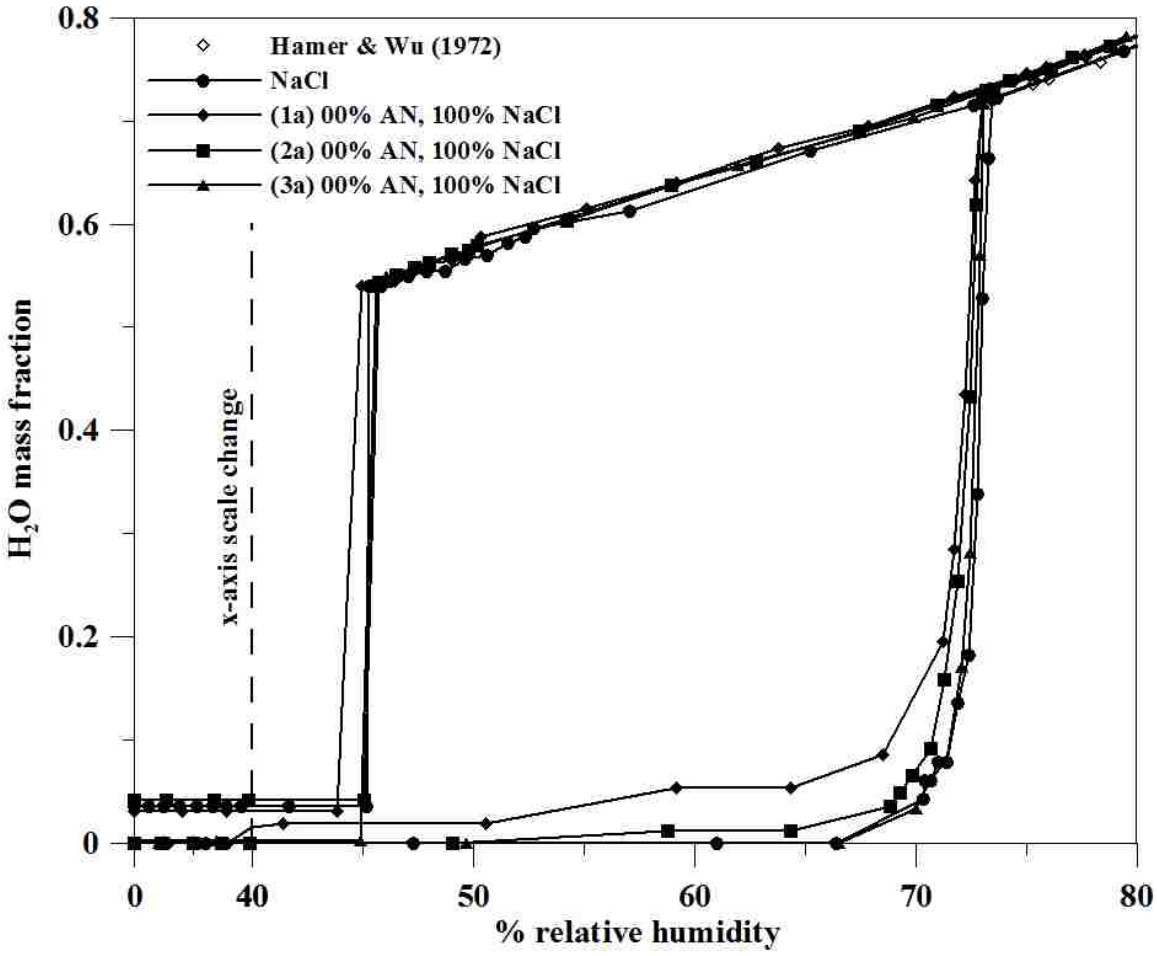

Figure 6.8 Alternative analysis of AN-NaCl data presented in figure 6.7.

After re-analyzing the data originally presented in Figure 6.7, the data presented in Figure 6.8 suggest that no AN was likely present in any of the mixed particles generated from a solution containing 57% NaCl and 43% AN on a dry-mass basis as all particles are nearly identical. While it is possible that significant settling of the AN could have occurred prior to the instant that the mixed particles were generated, no further tests were conducted to verify this assumption.

Three NaBr-An particles were individually generated from three solutions having different dry-mass ratios of NaBr to AN. The hysteresis loops constructed from the mixed particles are presented in Figure 6.9 along with a hysteresis loop for a pure NaBr particle and data points representing the hygroscopic growth of pure NaBr obtained from Hamer and Wu (1972) given by hollow diamonds. Here, the hygroscopic growth of the pure and mixed particles appears to differ slightly from that given by Hamer and Wu (1972). The raw data points used to construct the hysteresis loop for pure NaCl are given by a solid circle and connected by a solid line. The raw data points used to construct the hysteresis loops for the three NaBr-An particles are given by a solid diamond, a solid square, and a solid triangle and correspond to mixed particles having a dry-mass mixtures containing 90% NaBr and 10% AN, 60% NaBr and 40% AN, and 25 % NaBr and 75% AN, respectively, and are all connected by a solid line.

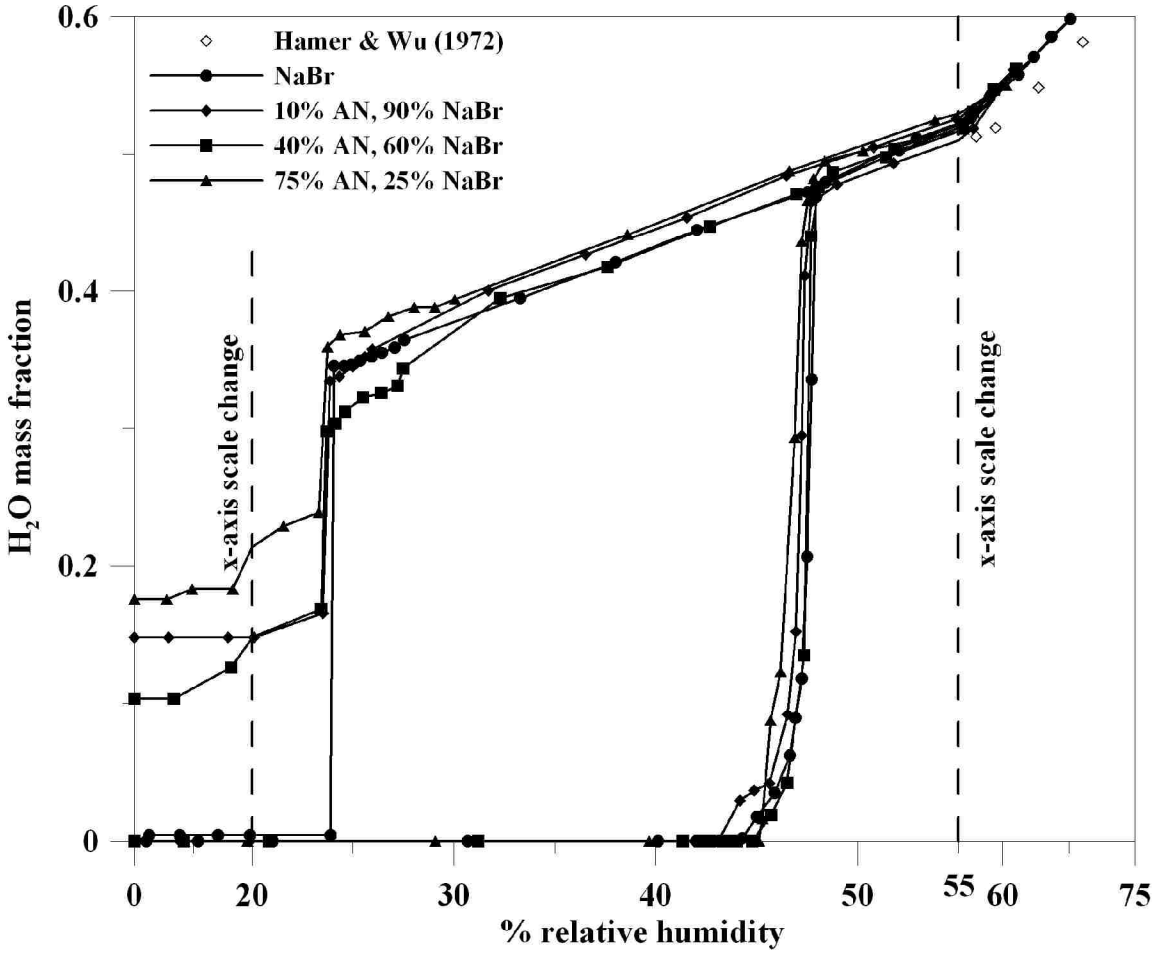

Figure 6.9 Effect of AN on the hysteresis of NaBr particles.

All three NaBr-AN particles were observed to begin their initial water uptake at approximately the same RH as pure NaBr and exhibited the same DRH as pure NaBr. After deliquescence, the mixed particle having a dry-mass composition of 40% AN showed no noticeable difference in the amount of water absorbed or desorbed as compared to pure NaCl until about 34% RH where it begin desorbing water at a faster rate. The other two mixed particles appeared to absorb slightly more water than the pure NaBr particle. However, all three mixed particles crystallized at the same CRH as the pure NaBr particle. All three mixed particles were observed to retain a noticeable amount of water after crystallization, but no relationship was observed between the amount of water retained and the dry-mass composition of the particles.

6.1.3 Hygroscopic Behavior of NaCl and NaBr Particles Containing a Water Insoluble Liquid

Here, the effects on the hygroscopic behavior of NaCl and NaBr particles internally mixed with a water insoluble liquid are reported. The two inorganic salts were each individually combined with one of three selected water insoluble liquids. Here, the water insoluble liquids selected for study were dioctyl phthalate (DOP), Invoil 704 silicone diffusion pump fluid (SIL), and Santovac-5-oil, a polyphenyl ether (PPE). Each of the water insoluble liquids was combined, although in different amounts, to both of the inorganic salts. The mixed particles generated from each of the inorganic salt-water insoluble liquid pairs were each observed through a cycle of humidification and dehumidification over a specific range of RH. The data analysis procedure described in Chapter 4 was used to construct hysteresis loops for all the mixed particles that were observed. For figures involving NaCl mixed with a liquid additive, a different pure component NaCl particle hysteresis is given as a reference than was seen in figures involving NaCl with a solid additive. The change in the pure NaCl particle hysteresis shown in the following corresponding figures reflects a recalibration of the humidity meter used.

A single NaCl-DOP particle was generated from solutions having a dry-mass ratios composition of 33% NaCl and 67% DOP. The hysteresis loops constructed from the mixed particle is presented in Figure 6.10 along with a hysteresis loop for a pure NaCl particle and data points representing the hygroscopic growth of pure NaCl obtained from Hamer and Wu (1972). Since the hygroscopic growth of both the pure and mixed particles were in agreement with that given by Hamer and Wu (1972), the raw data points obtained from Hamer and Wu (1972) given by hollow diamonds cannot be easily seen. The raw data points used to construct the hysteresis loop for pure NaCl are given by a solid circle and connected by a solid line. The raw data points used to construct the hysteresis loops for the NaCl-DOP particle is given by a solid diamond and connected by a solid line.

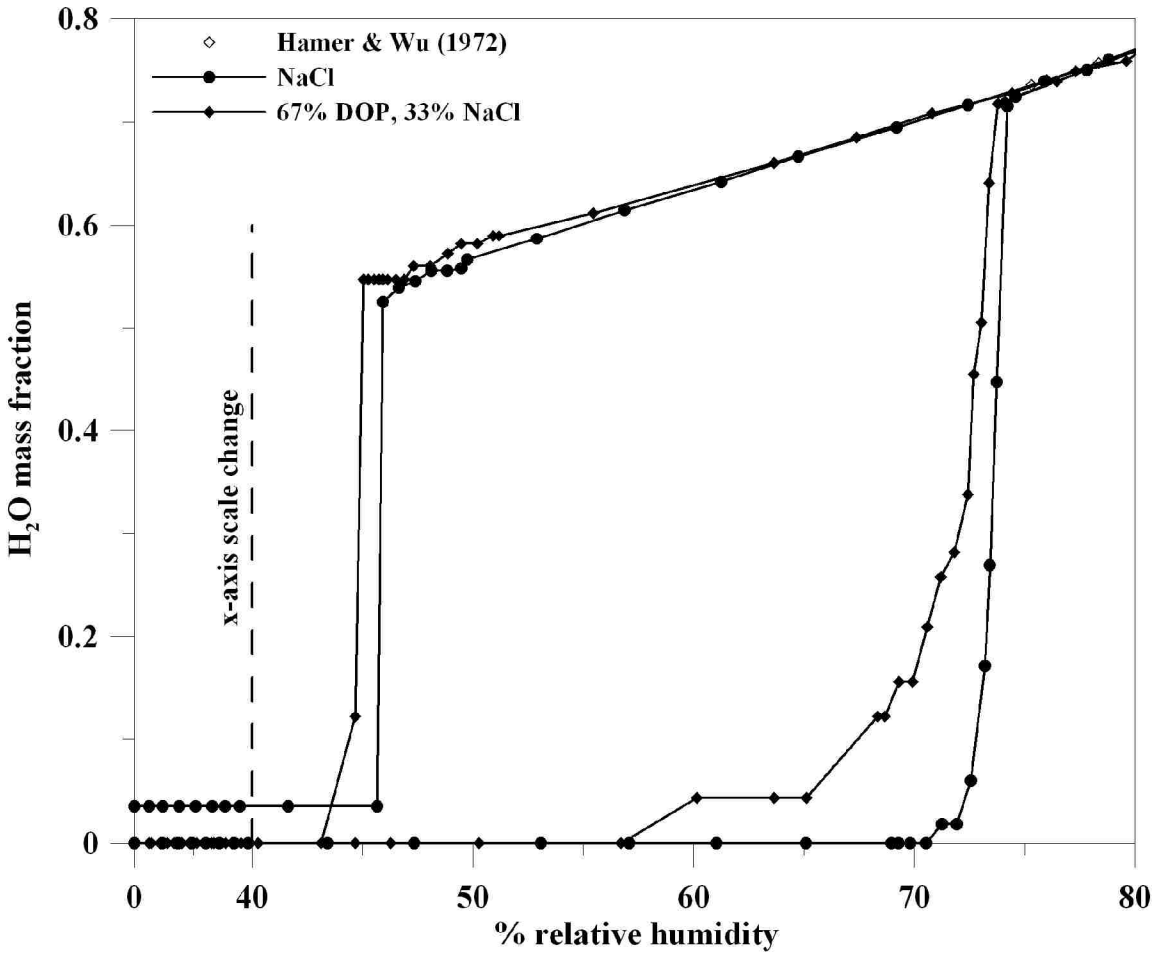

Figure 6.10 Effect of DOP on the hysteresis of NaCl particles.

The NaCl-DOP particle was observed to begin its initial water uptake at a much lower RH than pure NaCl and had a DRH that was slightly reduced (about 1%) as compared to pure NaCl. After deliquescence, the mixed particle showed no noticeable difference in the amount of water absorbed or desorbed as compared to pure NaCl. The mixed particle was observed to crystallize at a slightly lower RH than the pure NaCl particle (about 2%). After crystallization, the mixed particle appeared to retain some fraction of water.

A single NaBr-DOP particle was generated from solutions having a dry-mass ratios composition of 64% NaBr and 36% DOP. The hysteresis loops constructed from the mixed particle is presented in Figure 6.11 along with a hysteresis loop for a pure NaBr particle and data points representing the hygroscopic growth of pure NaCl obtained from Hamer and Wu (1972) given by hollow diamonds. Here, the hygroscopic growth of the pure and mixed particles appears to differ slightly from that given by Hamer and Wu (1972). The raw data points used to construct the hysteresis loop for pure NaBr are given by a solid circle and connected by a solid line. The raw data points used to construct the hysteresis loops for the NaBr-DOP particle is given by a solid diamond and connected by a solid line.

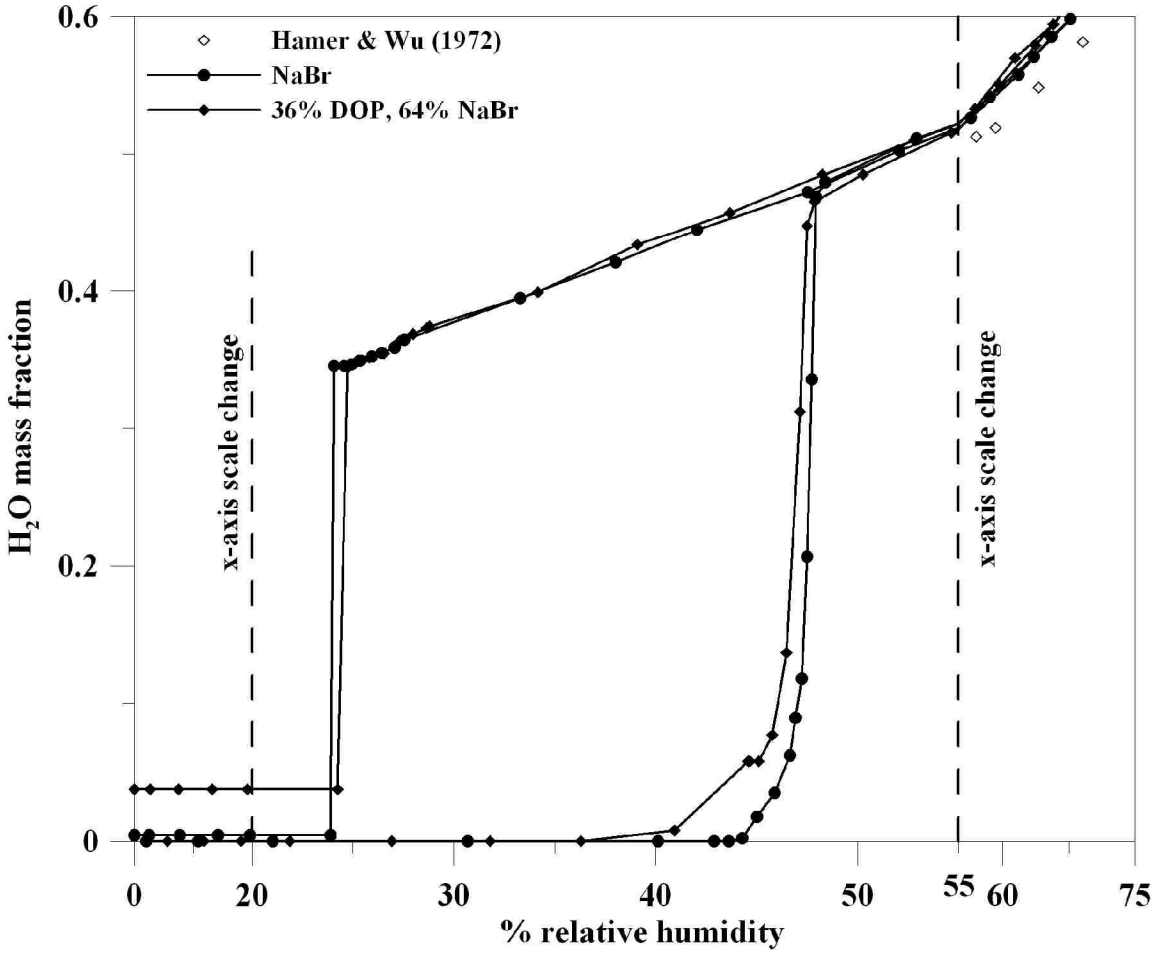

Figure 6.11 Effect of DOP on the hysteresis of NaBr particles.

The NaBr-DOP particle was observed to begin its initial water uptake at a somewhat lower RH than pure NaCl and had a DRH that was slightly reduced (about 1%) as compared to pure NaCl. After deliquescence, the mixed particle showed no noticeable difference in the amount of water absorbed or desorbed as compared to pure NaBr. The mixed particle was observed to crystallize at essentially the same RH as the pure NaBr particle. After crystallization, the mixed particle appeared to retain some fraction of water.

A single NaCl-SIL particle was generated from solutions having a dry-mass ratios composition of 68% NaCl and 32% SIL. The hysteresis loops constructed from the mixed particle is presented in Figure 6.12 along with a hysteresis loop for a pure NaCl particle and data points representing the hygroscopic growth of pure NaCl obtained from Hamer and Wu (1972). Since the hygroscopic growth of both the pure and mixed particles were in agreement with that given by Hamer and Wu (1972), the raw data points obtained from Hamer and Wu (1972) given by hollow diamonds cannot be easily seen. The raw data points used to construct the hysteresis loop for pure NaCl are given by a solid circle and connected by a solid line. The raw data points used to construct the hysteresis loops for the NaCl-SIL particle is given by a solid diamond and connected by a solid line.

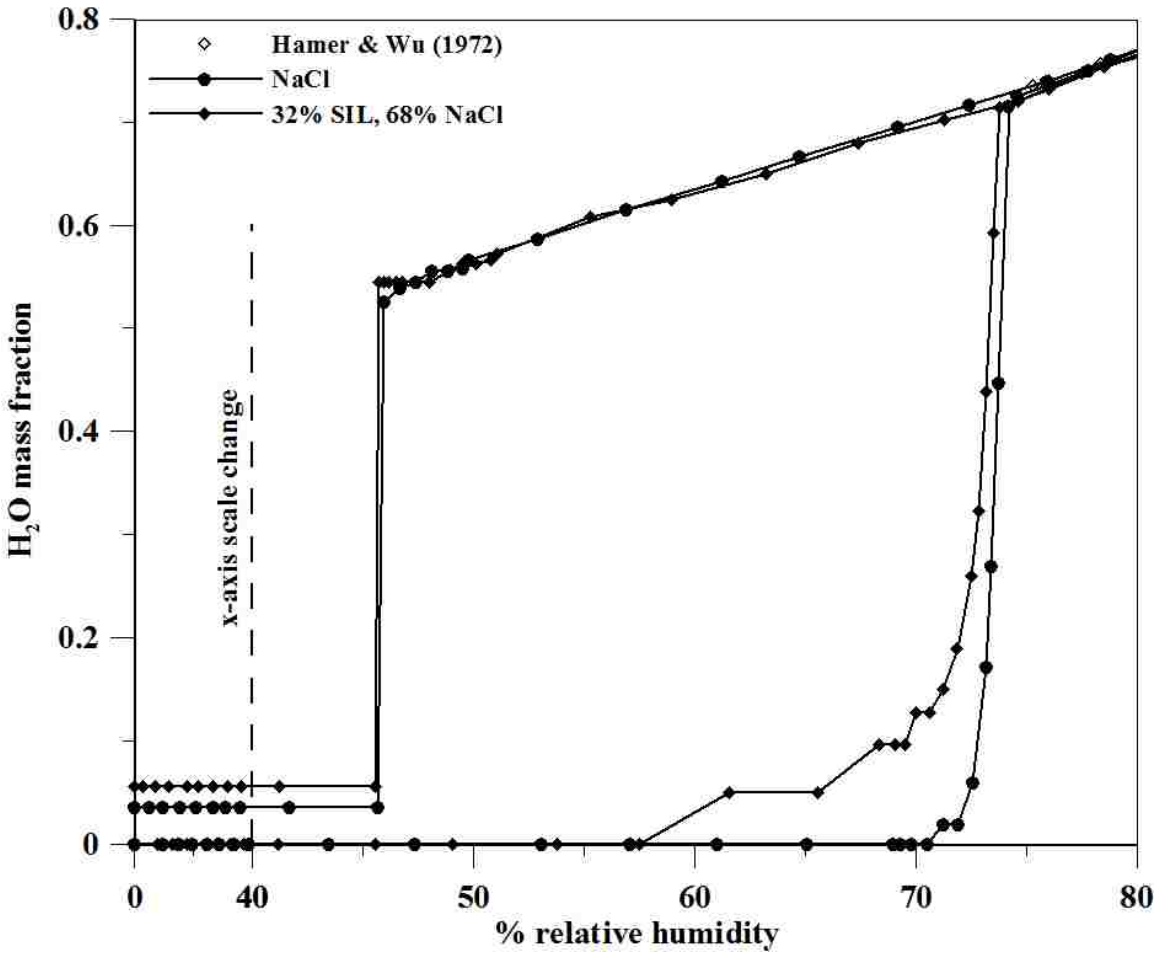

Figure 6.12 Effect of SIL on the hysteresis of NaCl particles.

The NaCl-SIL particle was observed to begin its initial water uptake at a much lower RH than pure NaCl and had a DRH that was slightly reduced (about 1%) as compared to pure NaCl. After deliquescence, the mixed particle showed no noticeable difference in the amount of water absorbed or desorbed as compared to pure NaCl. The mixed particle was observed to crystallize at precisely the same RH as the pure NaCl particle. After crystallization, the mixed particle appeared to retain some fraction of water.

A single NaBr-SIL particle was generated from solutions having a dry-mass ratios composition of 58% NaBr and 42% SIL. The hysteresis loops constructed from the mixed particle is presented in Figure 6.13 along with a hysteresis loop for a pure NaBr particle and data points representing the hygroscopic growth of pure NaCl obtained from Hamer and Wu (1972) given by hollow diamonds. Here, the hygroscopic growth of the pure and mixed particles appears to differ slightly from that given by Hamer and Wu (1972). The raw data points used to construct the hysteresis loop for pure NaBr are given by a solid circle and connected by a solid line. The raw data points used to construct the hysteresis loops for the NaBr-SIL particle is given by a solid diamond and connected by a solid line.

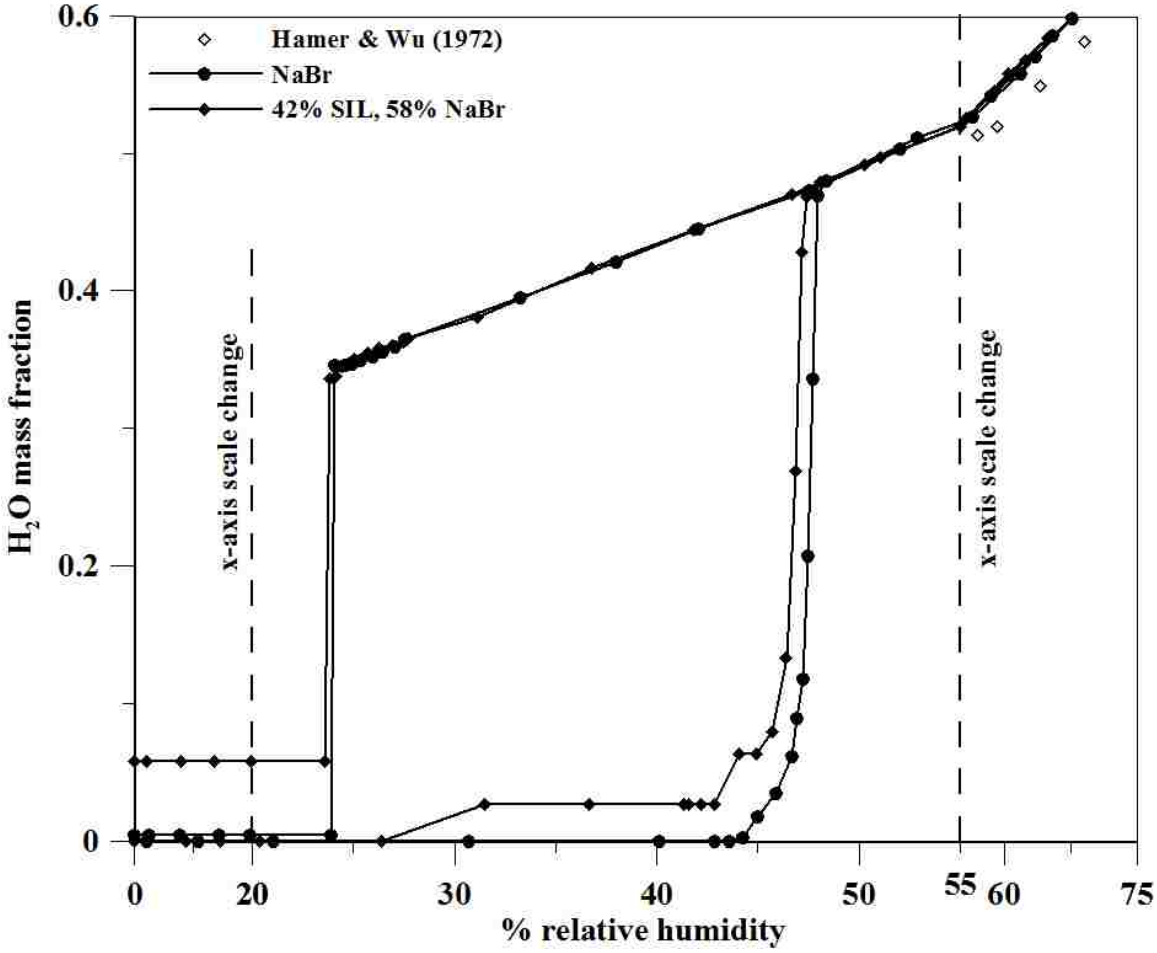

Figure 6.13 Effect of SIL on the hysteresis of NaBr particles.

The NaBr-SIL particle was observed to begin its initial water uptake at a significantly lower RH than pure NaBr and had a DRH that was slightly reduced (about 1%) as compared to pure NaBr. After deliquescence, the mixed particle showed no noticeable difference in the amount of water absorbed or desorbed as compared to pure NaBr. The mixed particle was observed to crystallize at precisely the same RH as the pure NaBr particle. After crystallization, the mixed particle appeared to retain some fraction of water.

A single NaCl-PPE particle was generated from solutions having a dry-mass ratios composition of 62% NaCl and 38% PPE. The hysteresis loops constructed from the mixed particle is presented in Figure 6.14 along with a hysteresis loop for a pure NaCl particle and data points representing the hygroscopic growth of pure NaCl obtained from Hamer and Wu (1972). Since the hygroscopic growth of both the pure and mixed particles were in agreement with that given by Hamer and Wu (1972), the raw data points obtained from Hamer and Wu (1972) given by hollow diamonds cannot be easily seen. The raw data points used to construct the hysteresis loop for pure NaCl are given by a solid circle and connected by a solid line. The raw data points used to construct the hysteresis loops for the NaCl-PPE particle is given by a solid diamond and connected by a solid line.

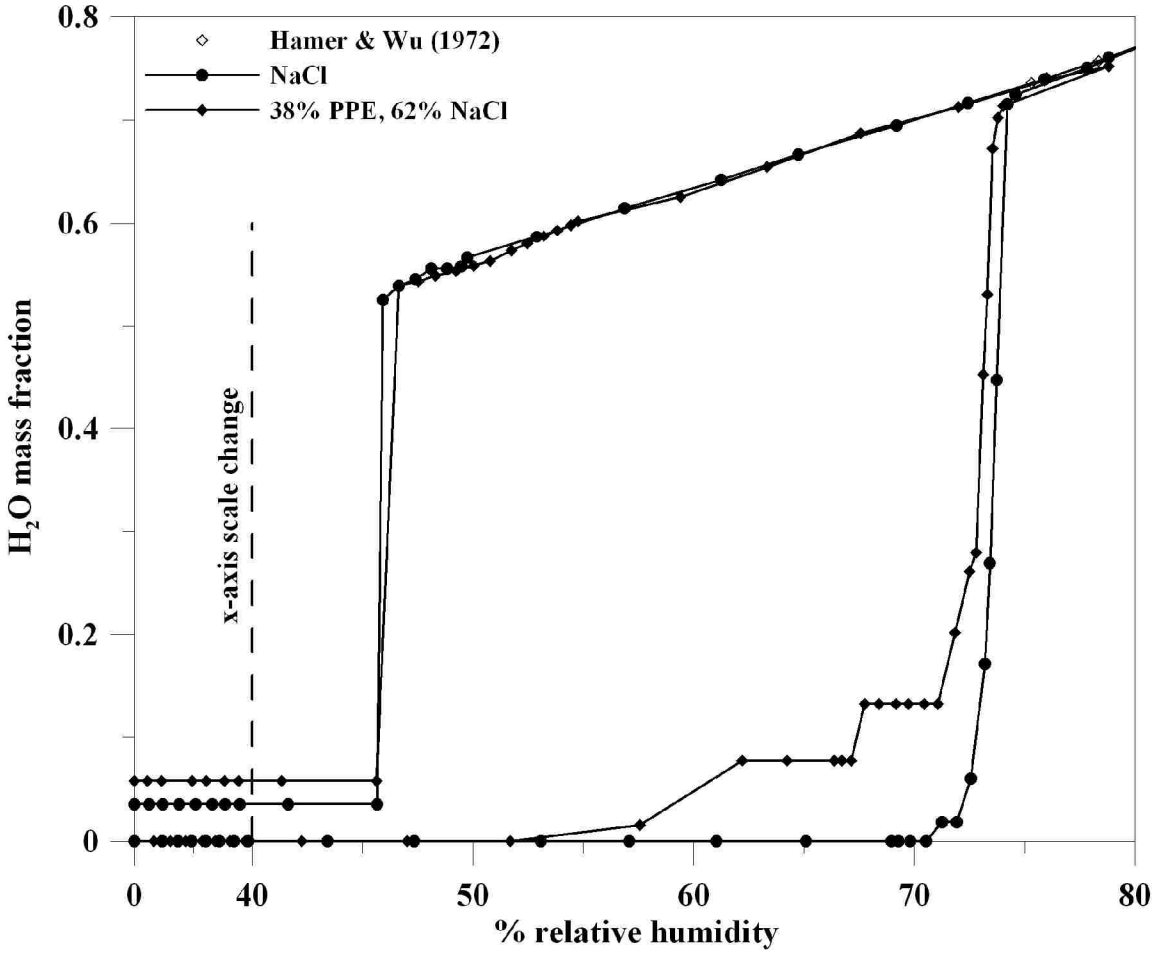

Figure 6.14 Effect of PPE on the hysteresis of NaCl particles.

The NaCl-PPE particle was observed to begin its initial water uptake at a much lower RH than pure NaCl and had a DRH that was slightly reduced (about 1%) as compared to pure NaCl. After deliquescence, the mixed particle showed no noticeable difference in the amount of water absorbed or desorbed as compared to pure NaCl. The mixed particle was observed to crystallize at precisely the same RH as the pure NaCl particle. After crystallization, the mixed particle appeared to retain some fraction of water.

A single NaBr-PPE particle was generated from solutions having a dry-mass ratios composition of 57% NaBr and 43% PPE. The hysteresis loops constructed from the mixed particle is presented in Figure 6.15 along with a hysteresis loop for a pure NaBr particle and data points representing the hygroscopic growth of pure NaCl obtained from Hamer and Wu (1972) given by hollow diamonds. Here, the hygroscopic growth of the pure and mixed particles appears to differ slightly from that given by Hamer and Wu (1972). The raw data points used to construct the hysteresis loop for pure NaBr are given by a solid circle and connected by a solid line. The raw data points used to construct the hysteresis loops for the NaBr-PPE particle is given by a solid diamond and connected by a solid line.

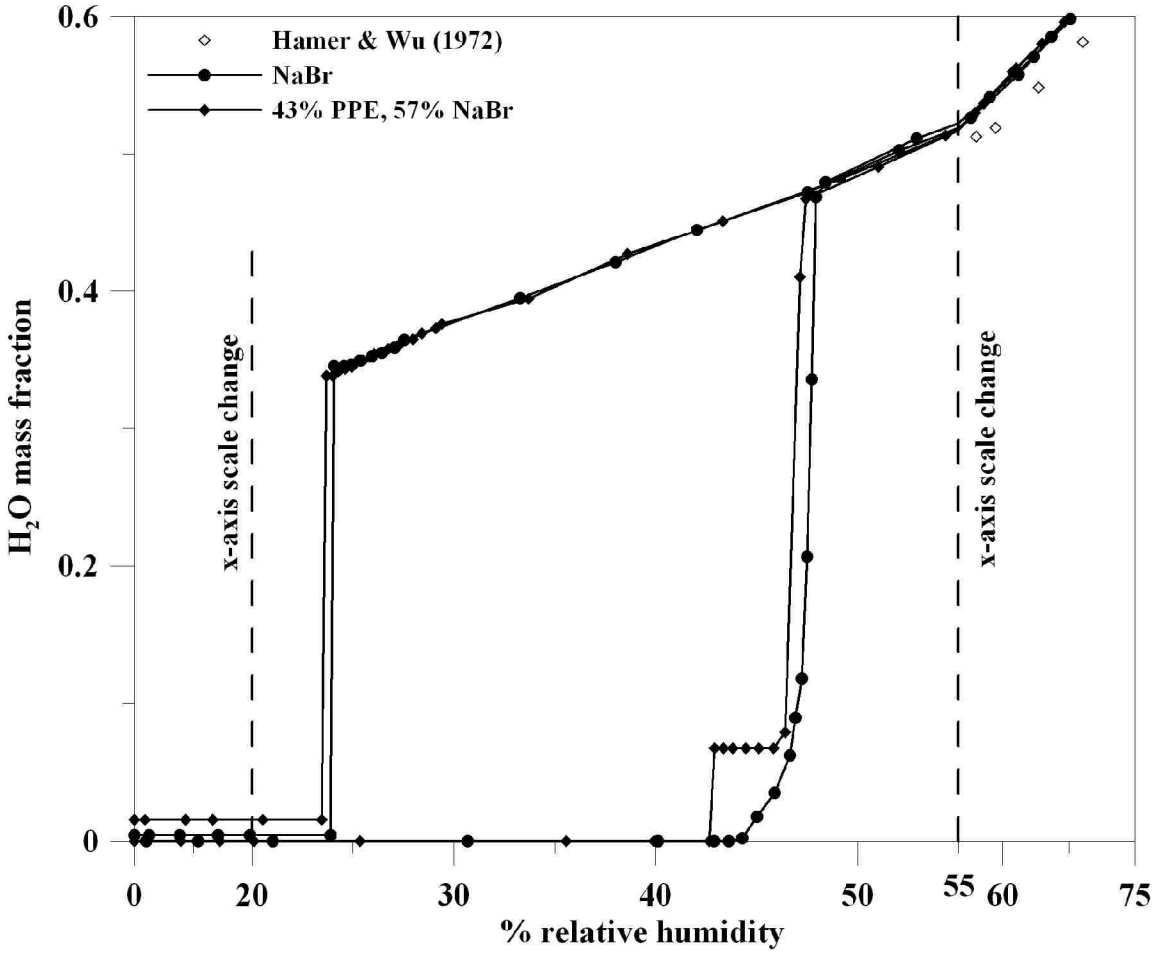

Figure 6.15 Effect of PPE on the hysteresis of NaBr particles.

The NaBr-PPE particle was observed to begin its initial water uptake at about the same RH as pure NaBr, but exhibited a sharp 'jump' in its initial water uptake. The water mass fraction of the mixed particle then remained nearly constant over a range of about 5% RH before beginning to deliquesce at a DRH that was slightly reduced (about 1%) as compared to pure NaBr. After deliquescence, the mixed particle showed no noticeable difference in the amount of water absorbed or desorbed as compared to pure NaBr. The mixed particle was observed to crystallize at very near the same RH as the pure NaBr particle. After crystallization, the mixed particle appeared to retain a small fraction of water.

6.2 Discussion

The initial water uptakes of nearly all the mixed particles observed during this study were observed to occur at noticeably lower relative humidities than what were observed for the corresponding pure component inorganic salts regardless of the additive used. This finding is fairly common within relevant literature, although more so for particles containing slightly soluble organics (Andrews & Larson, 1993; Lightstone et al., 2000; Choi & Chan, 2002a; Chan & Chan, 2003; Prenni et al., 2003; Braban & Abbatt, 2004; Brooks et al., 2004; Badger et al., 2005; Semeniuk et al., 2007a; Sjogren et al., 2007; Wise et al., 2007). Sjogren et al. (2007) have commented on the initial water uptake of pure $(NH_4)_2SO_4$ particles mixed with adipic acid. They have suggested that veins of the inorganic salt exist within the mixed particle and that the initial water uptake is aided by capillary forces that allow partial dissolution of the inorganic salt prior to deliquescence.

The deliquescence relative humidities and subsequent hygroscopic growth of all the mixed particles observed during this study were observed to be nearly identical to those of the corresponding pure component inorganic salts regardless of the additive used, within the range of error specified for the humidity meter (±1.5% RH). Previous investigators have reported similar findings for a wide variety of organic-inorganic particle mixtures. Cruz and Pandis (2000) and Choi and Chan (2002a) reported that the

water soluble organic acids they studied had no effect of the DRH of NaCl particles. Chan and Chan (2003), Brooks et al. (2004), and Parsons et al. (2004) have reported similar findings for NaCl particles containing humic and fulvic acids. Moreover, Semeniuk et al. (2007a) have reported that the inorganic fractions of naturally collected atmospheric particles dominated their hygroscopic behavior.

Slight disagreement was observed between NaBr-bearing particles and the literature data given by Hamer and Wu (1972). However, such disagreement is not unreasonable as the raw data points taken from Hamer and Wu (1972) are for bulk solutions and not particles. The disparity between bulk solutions and individual particles has been previously discussed by Tang et al. (1986) and Cohen et al. (1987a).

Some variance was also observed between the hygroscopic growth of NaBr-AN particles and pure NaBr particles. Here, two of the three mixed particles were observed to have increased water mass fractions relative to pure NaBr particles. The deviations noted here are most likely the result of assuming that the particles retained the same dry-mass ratio of NaBr to AN as the bulk solution they were generated from as even a slight change in the ratio could account for the differences observed.

The crystallization relative humidities of the mixed particles containing either BC or LA were observed to occur at much higher relative humidities than those of the corresponding pure component inorganic salts whereas mixed particles containing either AN, DOP, SIL, or PPE had crystallization relative humidities nearly identical to the corresponding pure component inorganic salts. Previous investigators have reported that the crystallization relative humidities of atmospherically relevant inorganic salts were affected by the inclusion of an organic, although such organics were typically water soluble. Lightstone et al. (2000) have reported they observed an increase in the crystallization relative humidities of NH_4NO_3 particles internally mixed with succinic acid. Furthermore, Choi and Chan (2002a) have reported they observed the same effect NaCl and $(NH_4)_2SO_4$ particles when internally mixed with succinic acid. Both investigators have attributed the increase in the crystallization relative humidity to the

heterogeneous nucleation of the corresponding inorganic salt by the organic. However, these effects are not mentioned by investigators who have used water insoluble liquids and solids (Otani and Wang, 1984; Hansson et al., 1990;1998; Hameri et al., 1992; Garland et al., 2005; Chan and Chan, 2007). Garland et al. (2005) have specifically stated that palmitic acid, a slightly soluble organic, did not act as heterogeneous nuclei for $(NH_4)_2SO_4$ particles. Furthermore, heterogeneous nucleation does not explain why the crystallization relative humidities of the NaBr-AN particles and the NaBr-LA particles exposed to repeated cycles of humidification and dehumidification were unaffected. The effect of water insoluble solids on the hygroscopic behavior of atmospherically relevant inorganic salts is discussed in greater detail in the following section of this chapter.

Nearly all particles observed during this study were observed to retain some amount of water after crystallization. Numerous investigators have also previously reported this finding (Cohen et al., 1987b; Chan et al., 1997; Peng & Chan, 2001; Choi & Chan, 2002; Colberg et al., 2004; Badger et al., 2005; Rosenoern et al., 2008). However, no independent tests were conducted to verify if the particles truly contained water after crystallization or if the particles emitted some portion of their charge during crystallization. Since the mass of the particles was determined via their DC null point levitation potential, both are possible. As such, no conclusions can be drawn from this aspect of the hygroscopic behavior of the particles.

6.3 Examination of the Water Insoluble Solids Used During this Study

During examinations conducted as part of this study, water insoluble solids were observed to affect the crystallization relative humidities of NaCl and NaBr particles. Namely, three types of water insoluble solids were examined, but only two were found to significantly increase the relative humidity at which the crystallization occurred. Since the three solids are completely different from each other, the physical and chemical properties of the three water insoluble solids used during this study were more closely examined. The goal here is to ascertain which, if any, of the physical and chemical

properties of the three solids affected the hygroscopic behavior of the NaCl and NaBr particles. As such, the contact angle, solubility, crystallinity, and functional groups associated with each of the water insoluble solids used as part of this study were more closely examined.

The role of contact angle has been previously reported by Gao et al. (2007) to affect the deliquescence relative humidity of NaCl nanoparticles residing on a substrate. However, no effect on the deliquescence relative humidity of any of the mixed particles was observed. The contact angle of AN and water is 93° - 94° (Fox et al., 1953; Maleki et al., 2006) and of LA and water is 78.5° - 111° (Nietz, 1928; De Keyser & Joos, 1984; Minami et al., 2008). The contact angle for the BC used in this study is unknown. Moreover, the contact angles of BC have been previously observed to be between 0° and 180° depending on composition (Studebaker & Snow, 1955) making it unreasonable to assume a probable value. However, as the contact angle of AN falls within the range given for LA, and only LA affected the crystallization relative humidity of the two inorganic salts, it is unlikely that the contact angle is a significant factor. It is noted here however, that the contact angles cited are for interaction with pure water, whereas the solids used this study were in contact with water containing dissolved ions from the inorganic salts which may significantly affect their wettability.

Lightstone et al. (2000) and Choi and Chan (2002a) have reported that succinic acid, a slightly soluble organic with a solubility of 83.5 $g \cdot l^{-1}$ (Lide, 2004), increased the crystallization relative humidities of atmospherically relevant inorganic salt particles. Although BC and AN are completely insoluble in water and none of the solids exhibited any hygroscopic growth as pure particles at relative humidities up to 95%, LA in fact has a very slight solubility of 0.055 $g \cdot l^{-1}$ (Lide, 2004) and was observed to increase the crystallization relative humidities of NaCl and NaBr particles. However, assuming that slightly soluble organics can affect the crystallization relative humidities of atmospherically relevant inorganic salt particles, why then where they not affected for the successive cycles of humidification and dehumidification of NaBr-LA particles and why where the crystallization relative humidities of NaC-BC and NaBr-BC particles also

increased? As these questions remained unanswered, it is unlikely that the solubility of an additive is a significant factor.

The crystallinity of the three solids was considered. Here, the LA and AN used in this study were most likely in a crystalline or microcrystalline form (Robertson, 1933; Vand et al., 1951; Lomer & Spanswick, 1961; Lomer, 1963; Bordat & Brown, 2009), whereas the BC would be considered non-crystalline (Biscoe & Warren, 1942; Zhu et al., 2004). It should be noted here that the exact composition and physical structure of the BC used as part of this study are unknown. Regardless, as BC and LA were observed to affect the crystallization of the NaCl and NaBr particles and AN was not, no relationship between the physical structure of the additive and its effect on the crystallization relative humidities of atmospherically relevant inorganic salts can be inferred.

The functional groups present in each of the water insoluble solids were also evaluated. Although the exact composition of the BC used as part of this study is not known, other forms of BC have been consistently observed to contain a wide variety of functional groups and metal ions (Hallum & Drushel, 1958; O'Reilly & Mosher, 1983; Boehm, 1994). O'Reilly & Mosher (1983) have reported they observed $COOH^+$ functional groups in commercially available BC. This same functional group is also present in LA. In fact, the $COOH^+$ functional groups is also present in the succinic acid reported to increase the crystallization relative humidities of atmospherically relevant inorganic salts by Lightstone et al. (2000) and Choi and Chan (2002a). Furthermore, the $COOH^+$ functional group is not found in AN. In fact, AN possess no functional groups at all, but is rather a highly stable, planar, aromatic hydrocarbon. Here at last, an inference can be made between the two water insoluble solids that affected the crystallization relative humidities of the NaCl and NaBr particles and the one that did not. Namely, the presence of a chemical functional group, more specifically the $COOH^+$ group, appears to increase the crystallization relative humidities of atmospherically relevant inorganic salts. However, no explanation still exists for why the crystallization relative humidities of NaBr-LA particles were unaffected when they were exposed to repeated cycles of humidification and dehumidification. Here it is proposed that a more specific array of

water insoluble solids containing a single, but known, functional group should be examined.

6.4 Conclusions

In this chapter, the effects of water insoluble materials on the hygroscopic behavior of atmospherically relevant inorganic salts have been discussed. Particles of NaCl and NaBr were examined both as pure components and when internally mixed with one of six different water insoluble materials; three of which were solids and three of which were liquids. Hysteresis loops for both the pure and mixed particles were constructed to examine the effects of the water insoluble materials on their hygroscopic behavior.

The deliquescence relative humidities and subsequent hygroscopic growth of all mixed particles were observed to be unaffected by the presence of any of the water insoluble materials. However, the crystallization relative humidities of NaCl and NaBr particles were observed to be increased when they were internally mixed with either BC or LA. However, no such effect was observed for mixtures involving AN, DOP, SIL, or PPE. Furthermore, the crystallization relative humidities of NaBr-LA particles were only observed to be affected during their first cycle of humidification and dehumidification.

The results ascertained from this study indicate that the hygroscopic behavior of atmospherically relevant inorganic salts can be affected by water insoluble solids. Specifically, the crystallization relative humidities of NaCl and NaBr particles can be significantly increased when a water insoluble solid is present. These results suggest that the solid additive somehow alters the point where it is more energetically favorable for the particle to exist in a solid state. However, the morphology of the mixed particle may also play a role in the observed effects to hygroscopic behavior. The particles observed during this study were internally mixed whereas previous investigations have examined atmospherically relevant salts that were externally coated with water insoluble solids and have not reported changes in the crystallization relative humidities (Otani and Wang, 1984; Hansson et al., 1990;1998; Hameri et al., 1992, Garland et al., 2005). Moreover,

not all the water insoluble solids examined as part of this study were found to affect the hygroscopic behavior of the NaCl and NaBr particles and none of the water insoluble liquids were found to affect the hygroscopic behavior of the NaCl and NaBr particles. Therefore, the particle morphology developed between an atmospherically relevant inorganic salt and a specific additive may have a greater effect on the hygroscopic behavior of the particle than the additive itself.

An in-depth study was performed to ascertain why only two of the three water insoluble solids used as part of this study were observed to increase the crystallization relative humidities of the NaCl and NaBr particles. Here, the contact angle, solubility, crystallinity, and functional groups associated with each of the three solids were more closely examined. No inferences could be made regarding the effects of the contact angle, solubility, or crystallinity of the three solids. However, the presence of a $COOH^+$ functional group in both the BC and LA additives, but absent in the AN additive, was attributed to the increases observed by BC and LA to the crystallization relative humidities of the NaCl and NaBr particles as it has also been found to be present in previous literature where such an increase has been reported (Lightstone et al., 2000; Choi and Chan, 2002a).

Chapter 7: Conclusions

In an effort to better understand the role of electrical conductivity on the break-ups of charged droplets via Coulombic fission and the hygroscopic behavior of mixed particles, two independent studies were conducted. The first of these studies examined the role of electrical conductivity on the amounts of charge and mass emitted by charged droplets during their break-ups via Coulombic fission and the charge limit at which break-ups occurred. Here, increasing the electrical conductivity of dielectric droplets via an ionic dopant was found to increase the amount of charge emitted and decrease the amount of mass emitted during droplet break-ups via Coulombic fission, but not to affect the charge limit at which the break-ups occurred. Two different analyses of the data revealed that droplet size, electrical conductivity, viscosity, density, and permittivity all play a role in determining the characteristics of charged droplet break-ups.

The second study examined how certain water insoluble materials affected the hygroscopic behavior of atmospherically relevant inorganic salts. Here, some water insoluble solids were found to increase the relative humidity at which crystallization occurs for NaCl and NaBr particles. However, the effects were only observed to occur for the first cycle of humidification and dehumidification for one of the solids. As such, many questions remain unanswered in this portion of the study. An analysis of the water insoluble solids found to elicit a change in the crystallization relative humidities of the NaCl and NaBr particles indicated that the presence of a $COOH^+$ functional group may play a role. Further study in this area however, would be required to assume a more formal relationship.

In conclusion, both studies discussed herein have contributed to the basic understanding of charged aerosols and the results obtained have promising applications in both modern industry and atmospheric research.

Nomenclature

A projected area of an aerosol

A_n grouping term

a droplet radius

a_n scattering coefficient

a_w activity of water

B_n grouping term

b_n scattering coefficient

C molar concentration

C_0 geometric constant

C_D drag coefficient

C_{Kelvin} Kelvin correction factor

C_n grouping term

D_{AB} diffusion coefficient of species A in species B

D_n grouping term

d droplet diameter

d_m charge relaxation length

E electric field

F force

f_{AC} AC frequency

f_m percentage of mass

f_q percentage of charge

f_R percentage of Rayleigh limit

f_{water} water fraction

g acceleration due to gravity

I intensity

J_r radial diffusive flux

K electrical conductivity

K_{eq} equilibrium constant

k grouping constant

k_B Boltzmann constant

l order number

M_w molar mass

m mass

N number

N_r radial flux

n degree of Legendre function

P pressure

P_n^1 1st order Legendre function of degree n

q charge on an aerosol

q_R Rayleigh limit charge

R ideal gas constant

r radial distance from the center of a droplet

r_{jet} radius of the initial cone-jet

S_w saturation ratio of water

T temperature

U characteristic velocity

V potential

X mass fraction

x size parameter

$Y(\omega)$ sum of squares

y vapor mole fraction

z distance between two electrodes

Greek symbols

α	grouping constant
β	field strength parameter
γ	surface tension of a liquid droplet
γ_{Kelvin}	influence of surface tension from Kelvin effect
γ_{sol}	surface tension of a bulk solution
δ	drag parameter
ε	dielectric constant
ε_0	permittivity of free space
η	grouping constant
θ	scattering angle
κ	grouping constant
λ	wavelength
μ	dynamic viscosity of fluid surrounding a levitated aerosol
Π	pi term used in dimensionless analysis
π_n	1^{st} angular function term for a grouping with an n^{th} degree Legendre function
ρ	density of a liquid droplet
ρ_f	density of the fluid displaced by a levitated aerosol
s	grouping constant
τ_n	2^{nd} angular function term for a grouping with an n^{th} degree Legendre function
χ_n	n^{th} order Ricatti-Bessel functions of the 2^{nd} kind
ψ_n	n^{th} order Ricatti-Bessel functions of the 1^{st} kind
ω	refractive index

References:

Abbas, M. A. and Latham, J., The instability of evaporating charged droplets, *J. Fluid Mech.*, Vol. 30, p. 663-670. (1967).

Achtzehn, T., Muller, R., Duft, D., and Leisner, T., The Coulomb instability of charged microdroplets: Dynamics and scaling, *Eur. Phys. Journal D.*, Vol. 34, p. 311-313. (2005).

Adachi, K., and Buseck, P. R., Internally mixed soot, sulfates, and organic matter in aerosol particles from Mexico City, *Atmos. Chem. Phys.*, Vol. 8, p. 6469-6481. (2008).

Adornato, P. M. and Brown, R. A., Shape and stability of electrostatically levitated drops, *Proc. Royal. Soc. Lond. Ser. A-Math. Phys. Engin. Sci.*, Vol. 389, p. 101-117. (1983).

Ali, M., Mazumder, M. K., and Martonen, T. B., Measurements of electrodynamic effects on the deposition of MDI and DPI aerosols in a replica cast of human oral–pharyngeal–laryngeal airways, *J. Aerosol Med. Pulmonary Drug Delivery*, Vol. 22, p. 35-44. (2009).

Allen, T. M., Taflin, D. C., and Davis, E. J., Determination of activity coefficients via microdroplet evaporation experiments, *Ind. Eng. Chem. Res.*, Vol. 29, p. 682-690. (1990).

Andrews, E. and Larson, S. M., Effect of surfactant layers on the size changes of aerosol particles as a function of relative humidity, *Environ. Sci. Technol.*, Vol. 27, p. 857-865. (1993).

Ansari, A. S. and Pandis, S. N., Prediction of multicomponent inorganic atmospheric aerosol behavior, *Atmos. Environ.*, Vol. 33, p. 745-757. (1999).

Ansari, A. S. and Pandis, S. N., Water absorption by secondary organic aerosol and its effect on inorganic aerosol behavior, *Environ. Sci. Technol.*, Vol. 34, p. 71-77. (2000).

Ataman, S. and Hanson, D. N., Measurement of charged drops, *Ind. Engin. Chem. Fund.*, Vol. 8, p. 833-836. (1969).

Bakhoum, S. F. W. and Agnes, G. R., Study of chemistry in droplets with net charge before and after Coulomb explosion: Ion-induced nucleation in solution and implications for ion production in electrospray, *Amal. Chem.*, Vol. 77, p. 3189-3197. (2005).

Badger, C. L., George, I., Griffiths, P. T., Braban, C. F., Cox, R. A., and Abbatt, J. P. D., Phase transitions and hygroscopic growth of aerosol particles containing humic acid and mixtures of humic acid and ammonium sulphate, *Atmos. Chem. Phys. Discuss.*, Vol. 5, p. 9581-9620. (2005).

Barber, P. W. and Hill, S. C., *Light Scattering by Particles: Computational Methods*, World Scientific, Singapore. (1990).

Berg, T. G. O., Trainor, R. J., and Vaughan, U., Stable, unstable, and metastable charged droplets, *J. Atmos. Sci.,* Vol. 27, p. 1173-1181. (1970).

Bilde, M. and Svenningsson, B., CCN activation of slightly soluble organics: the importance of small amounts of inorganic salt and particle phase, *Tellus*, Vol. 56B, p. 128-134. (2004).

Biskos, G., Malinowski, A., Russell, L. M., Buseck, P. R., and Martin, S. T., Nanosize effect on the deliquescence and the efflorescence of sodium chloride particles, *Aerosol Sci. Technol*., Vol. 40, p. 97-106. (2006a).

Biskos, G., Paulsen, D., Russell, L. M., Buseck, P. R., and Martin, S. T., Prompt deliquescence and efflorescence of aerosol nanoparticles, *Atmos. Chem. Phys*., Vol. 6, 4633-4642. (2006b).

Biskos, G., Russell, L. M., Buseck, P. R., and Martin, S. T., Nanosize effect on the hygroscopic growth factor of aerosol particles, *Geophys. Res. Lett*., Vol. 33, L07801. (2006c).

Blanchard, D. C., Electrically charged drops from bubbles in sea water and their meteorological significance, *J. Atmos. Sci.,* Vol. 15, p. 383-396. (1958).

Boehm, H. P., Some aspects of the surface chemistry of carbon blacks and other carbons, *Carbon*, Vol. 32, p. 759-769. (1994).

Bohren, C. F. and Huffman, D. R., *Absorption and Scattering of Light by Small Particles*, Interscience, New York. (1983).

Bordat, P. and Brown, R., Structure and molecular dynamics of crystalline and liquid anthracene and naphthalene: Possible transient rotator phase of naphthalene, *J. Chem. Phys*., Vol. 130, 124501. (2009).

Born, M. and Wolf, E., *Principles of Optics 6th Ed.,* Pergamon Press, Oxford. (1980).

Braban, C. F. and Abbatt, J. P. D., A study of the phase transition behavior of internally mixed ammonium sulphate – malonic acid aerosols, *Atmos. Chem. Phys*., Vol. 4, p. 1451-1459. (2004).

Brechtel, F. J. and Kreidenweis, S. M., Predicting particle critical supersaturation from hygroscopic growth measurements in the humidified TDMA. Part I: Theory and Sensitivity Studies, *J. Atmos. Sci*., Vol. 57, p. 1854-1871. (2000a).

Brechtel, F. J. and Kreidenweis, S. M., Predicting particle critical supersaturation from hygroscopic growth measurements in the humidified TDMA. Part II: Laboratory and ambient studies, *J. Atmos. Sci*., Vol. 57, p. 1872-1887. (2000b).

Biscoe, J. and Warren, B. E., An x-ray study of carbon black, *J. Appl. Sci*., Vol. 13, p. 364-371. (1942).

Brooks, S. D., Wise, M. E., Cushing, M., and Tolbert, M. A., Deliquescence behavior of organic/ammonium sulfate aerosol, *Geophys. Res. Letters*, Vol. 29, GL014733. (2002).

Brooks, S. D., DeMott, P. J., and Kreidenweis, S. M., Water uptake by particles containing humic materials and mixtures of humic materials with ammonium sulfate, *Atmos. Environ*., Vol. 38, p. 1859-1868. (2004).

Bustin, W. M. and Dukek, W. J., *Electrostatic Hazards in the Petroleum Industry*, Research Studies Press Ltd., England. (1983)

Cantrell, W., McCrory, C., and Ewing, G. E., Nucleated deliquescence of salt, *J. Chem. Phys*., Vol. 116, p. 2116-2120. (2002).

Carslaw, K. S., Clegg, S. L., and Brimblecombe, P., A thermodynamic model of the system HCl-HNO_3-H_2SO_4-H_2O, including solubilities of HBr from <200 to 328 K, *J. Phys. Chem.*, Vol. 99, p. 11557-11574. (1995).

Cederfelt, S-I., Martinsson, B. G., and Hansson, H-C., On the charge limit for crystallizing particles, *J. Aerosol Sci.*, Vol. 21, p. S127-130. (1990).

Chan, C. K., Kwok, C. S., and Chow, A. H. L., Study of hygroscopic properties of aqueous mixtures of disodium fluorescein and sodium chloride using an electrodynamic balance, *Pharm. Res*., Vol. 14, p. 1171-1175. (1997a).

Chan, C. K., Liang, Z., Zheng, J., Clegg, S. L., and Brimblecombe, P., Thermodynamic properties of aqueous aerosols to high supersaturation: I-Measurements of water activity of the system Na^+-Cl^--NO_3^--SO_4^{2-}-H_2O at ~ 298.15 K, *Aerosol Sci. Technol.*, Vol. 27, p. 324-344. (1997).

Chan, M. N. and Chan, C. K., Hygroscopic properties of two humic-like substances and their mixtures with inorganics of atmospheric importance, *Environ. Sci. Technol*., Vol. 37, p. 5109-5115. (2003).

Chan, M. N. and Chan, C. K., Mass transfer effects on the hygroscopic growth of ammonium sulfate particles with a water-insoluble coating, Atmos. Environ., Vol. 41, p. 4423-4433. (2007).

Chan, M. N., Choi, M. Y., Ng, N. L., and Chan, C. K., Hygroscopicity of water-soluble organic compounds in atmospheric aerosol: Amino acids and biomass burning derived organic species, *Environ. Sci. Technol*., Vol. 39, p. 1555-1562. (2005).

Chan, M. N., Kreidenweis, S. M., and Chan, C. K., Measurements of the hygroscopic and deliquescence properties of organic compounds of different solubilities in water and their

relationship with cloud condensation nuclei activities, *Environ. Sci. Technol.*, Vol. 42, p. 3602-3608. (2008).

Charlson, R. J., Lovelock, J. E., Andreae, M. O., and Warren, S. G., Oceanic phytoplankton, atmospheric sulphur, cloud albedo and climate, *Nature*, Vol. 326, p. 655-661. (1987).

Charlson, R. J., Seinfeld, J. H., Nenes, A., Kulmala, M., Laaksonen, A., and Facchini, M. C., Reshaping the theory of cloud formation, *Science*, Vol. 292, p. 2025-2026. (2001).

Chen, Y.-Y and Lee, W.-M. G., Hygroscopic properties of inorganic-salt aerosol with surface-active organic compounds, *Chemosphere*, Vol. 38, p. 2431-2448. (1999).

Chen, Y.-Y. and Lee, W.-M. G., The effect of surfactants on the deliquescence of sodium chloride, *J. Environ. Sci. Health*, Vol. A36, p. 229-242. (2001).

Choi, M. Y. and Chan, C. K., The effect of organic species on the hygroscopic behaviors of inorganic aerosols, *Environ. Sci. Technol*., Vol. 36, p. 2422-2428. (2002a).

Choi, M. Y. and Chan, C. K., Continuous measurements of the water activities of aqueous droplets of water-soluble organic compounds, *J. Phys. Chem. A*, Vol. 106, p. 4566-4572. (2002b).

Chylek, P., Large-sphere limits of the Mie-scattering functions, *J. Opt. Soc. Amer.*, Vol. 63, p. 699-706. (1973).

Chylek, P., Ramaswamy, V., Ashkin, A., and Dziedzic, J. M., Simultaneous determination of refractive index and size of spherical dielectric particles from light scattering data, *Appl. Opt.*, Vol. 22, p. 2302-2307. (1983).

Clegg, S. L. and Brimblecombe, P., A generalized multicomponent thermodynamic model applied to the $(NH_4)_2SO_4$-H_2SO_4-H_2O system to high supersaturation and low relative humidity at 298.15 K, *J. Aerosol Sci.*, Vol. 26, p. 19-38. (1995).

Clegg, S. L., Pitzer, K. S., and Brimblecombe, P., Thermodynamics of multicomponent, miscible, ionic solutions. 2. Mixtures including unsymmetrical electrolytes, *J. Phys. Chem.*, Vol. 96, p. 9470-9479. (1992).

Clegg, S. L., Brimblecombe, P., Liang, Z., and Chan, C. K., Thermodynamic properties of aqueous aerosols to high supersaturation: II-A model of the system Na^+-Cl^--NO_3^--SO_4^{2-}-H_2O at 298.15 K, *Aerosol Sci. Technol.*, Vol. 27, p. 346-366. (1997).

Clegg, S. L., Brimblecombe, P., and Wexler, A. S., Thermodynamic model of the system H^+-NH_4^+-SO_4^{2-}-NO_3^--H_2O at tropospheric temperatures, *J. Phys. Chem. A*, Vol. 102, p. 2137-2154. (1998a).

Clegg, S. L., Brimblecombe, P., and Wexler, A. S., Thermodynamic model of the system H^+-NH_4^+-Na^+-SO_4^{2-}-NO3$^-$-CL$^-$-H_2O at 298.15 K, *J. Phys. Chem. A*, Vol. 102, p. 2155-2171. (1998b).

Clegg, S. L., Seinfeld, J. H., and Brimblecombe, P., Thermodynamic modeling of aqueous aerosols containing electrolytes and dissolved organic compounds, *J. Aerosol Sci.*, Vol. 32, p. 713-738. (2001).

Cloupeau, M. and Prunet-Foch, B., Electrostatic spraying of liquids in cone-jet mode, *J. Electrostatics*, Vol. 22, p. 135-159. (1989).

Cloupeau, M. and Prunet-Foch, B., Electrostatic spraying of liquids – Main functioning modes, *J. Electrostatics*, Vol. 25, p. 165-184. (1990).

Cloupeau, M. and Prunet-Foch, B., Electrohydrodynamic spraying functioning modes – A critical review, *J. Aerosol Sci.*, Vol. 25, p. 1021-1036. (1994).

Cohen, M. D., Flagan, R. C., and Seinfeld, J. H., Studies of concentrated electrolyte solutions using the electrodynamic balance. 1. Water activities for single-electrolyte solutions, *J. Phys. Chem*., Vol. 91, p. 4563-4574. (1987a).

Cohen, M. D., Flagan, R. C., and Seinfeld, J. H., Studies of concentrated electrolyte solutions using the electrodynamic balance. 2. Water activities for mixed-electrolyte solutions, *J. Phys. Chem*., Vol. 91, p. 4575-4582. (1987b).

Cohen, M. D., Flagan, R. C., and Seinfeld, J. H., Studies of concentrated electrolyte solutions using the electrodynamic balance. 3. Solute nucleation, *J. Phys. Chem*., Vol. 91, p. 4583-4590. (1987b).

Colberg, C. A., Krieger, U. K., and Peter, T., Morphological investigations of single levitated H2SO4/NH3/H2O aerosol particles during deliquescence/efflorescence experiments, *J. Phys. Chem. A*, Vol. 108, p. 2700-2709. (2004).

Consta, S., Manifestation of Rayleigh instability in droplets containing multiply charged macroions, *J. Phys. Chem. B*, Vol. 114, p. 5263-5268. (2010).

Constable, G. and Somerville, B., *A Century of Innovation: Twenty Engineering Achievements that Transformed our Lives*, Joseph Henry Press. (2003).

Conwell, P. R., Barber, P. W., and Rushforth, C. K., Resonant spectra of dielectric spheres, *J. Opt. Soc. Amer. A*, Vol. 1, p. 62-67. (1984).

Crutzen, P. J. and Andreae, M. O., Biomass burning in the tropics: Impact on atmospheric chemistry and biogeochemical cycles, *Science*, Vol. 250, p. 1669-1678. (1990).

Cruz, C. N., Dassios, K. G., and Pandis, S. N., The effect of dioctyl phthalate films on the ammonium nitrate aerosol evaporation rate, *Atmos. Environ.*, Vol. 34, p. 3897-3905. (2000).

Cruz, C. N. and Pandis, S. N., The effect of organic coatings on the cloud condensation nuclei activation of inorganic atmospheric aerosol, *J. Geophys. Res.*, Vol. 103, p. 13111-13123. (1998).

Cruz, C. N. and Pandis, S. N., Deliquescence and hygroscopic growth of mixed inorganic-organic atmospheric aerosol, *Environ. Sci. Technol.*, Vol. 34, p. 4313-4319. (2000).

Davis, E. J., Electrodynamic balance stability characteristics and applications to the study of aerocolloidal particles, *Langmuir*, Vol. 1, p. 379-387. (1985).

Davis, E. J., A history of single aerosol particle levitation, *Aerosol Sci. Tech.*, Vol. 26, p. 212-254. (1997).

Davis, E. J. and Bridges, M. A., The Rayleigh limit of charge revisited: Light scattering from exploding droplets, *J. Aerosol Sci.*, Vol. 25, p. 1179-1199. (1994).

Davis, E. J. and Chorbajian, E., The measurement of evaporation rates of submicron aerosol droplets, *Ind. Eng. Chem. Fund.*, Vol. 13, p. 272-277. (1974).

Davis, E. J. and Periasamy, R., Light-scattering and aerodynamic size measurements for homogeneous and inhomogeneous microspheres, *Langmuir*, Vol. 1, p. 373-379. (1985).

Davis, E. J. and Ravindran, P., Single particle light scattering measurements using the electrodynamic balance, *Aerosol Sci. Tech.*, Vol. 1, p. 337-350. (1982).

Davis, E. J. and Ray, A. K., Determination of diffusion coefficients by submicron droplet evaporation, *J. Chem. Phys.*, Vol. 67, p. 414-419. (1977).

Davis, E. J. and Ray, A. K., Submicron droplet evaporation in the continuum and non-continuum regimes, *J. Aerosol Sci.*, vol. 9, p. 411-422. (1978).

Davis, E. J. and Ray, A. K., Single aerosol-particle size and mass measurements using an electrodynamic balance, *J. Colloid Inter. Sci.*, Vol. 75, p. 566-576. (1980).

de Juan, L. and de la Mora, J. F., Charge and size distributions of electrospray drops, *J. Coll. Inter. Sci.*, Vol. 186, p. 280-293. (1997).

de Keyser, P. and Joos, P., Kinetics of monolayer collapse as a nucleating process, *J. Phys. Chem.*, Vol. 88, p. 274-280. (1984).

de la Mora, J. F., On the outcome of the Coulombic fission of a charged isolated drop, *J. Colloid Inter. Sci.*, Vol. 178, p. 209-218. (1996).

de la Mora, J. F., The fluid dynamics of Taylor cones, *Annu. Rev. Fluid Mech.*, Vol. 39, p. 217-243. (2007).

de la Mora, J. F. And Loscertales, I. G., The current emitted by highly conducting Taylor cones, *J. Fluid Mech.*, Vol. 260, p. 155-184. (1994).

de Lorenzi, L., Fermeglia, M., and Torriano, G., Density, refractive index, and kinematic viscosity of diesters and triesters, *J. Chem. Eng. Data*, Vol. 42, p. 919-923. (1997).

Dole, M., Mack, L. L., Hines, R. L., Mobley, R. C., Ferguson, L. D., and Alice, M. B., Molecular beams of macroions, *J. Chem. Phys.*, Vol. 49, p. 2240-2249. (1968).

Donaldson, D. J. and Vaida, V., The influence of organic films at the air-aqueous boundary on atmospheric processes, *Chem. Rev*., Vol. 106, p. 1445-1461. (2006).

Donaldson, D. J., Tuck, A. F., and Vaida, V., Spontaneous fission of atmospheric aerosol particles, *Phys. Chem. Chem. Phys.*, Vol. 3, p. 5270-5273. (2001).

Doyle, A., Moffett, D. R., and Vonnegut, B., Behavior of evaporating electrically charged droplets, *J. Colloid Sci.*, Vol. 19, p. 136-143. (1964).

Duft, D., Lebius, H., and Huber, B. A., Shape oscillations and stability of charged microdroplets, *Phys. Rev. Lett.*, Vol. 89, 084503. (2002).

Duft, D., Achtzehn, T., Muller, R., Huber, B. A., and Leisner, T., Rayleigh jets from levitated microdroplets, *Nature*, Vol. 42, p. 128. (2003).

Dusek, U., Reischl, G. P., and Hitzenberger, R., CCN activation of pure and coated carbon black particles, *Environ. Sci. Technol*., Vol. 40, p. 1223-1230. (2006).

Eichler, H., Cheng, Y. F., Birmili, W., Nowak, A., Wiedensohler, A., Bruggemann, E., Gnauk, T., Herrmann, H., Althausen, D., Ansmann, A., Engelmann, R., Tesche, M., Wendisch, M., Zhang, Y. H., Hu, M., Liu, S., and Zeng, L. M., Hygroscopic properties and extinction of aerosol particles at ambient relative humidity in South-Eastern China, *Atmos. Environ*., Vol. 42, p. 6321-6334. (2008).

Ellison, G. B., Tuck, A. F., and Vaida, V., Atmospheric processing of organic aerosols, *J. Geophys. Res*., Vol. 104, p. 11633-11641. (1999).

Ewing, G. E., H2O on NaCl: From single molecule, to clusters, to monolayer, to thin film, to deliquescence, *Struct. Bond*, Vol. 116, p. 1-25. (2005).

Facchini, M. C., Mircea, M., and Fuzzi, S., Comments on "Influence of soluble surfactant properties on the activation of aerosol particles containing inorganic solute", *J. Atmos. Sci*., Vol. 58, p. 1465-1567. (2001).

Fenn, J. B., Ion formation from charged droplets: Roles of geometry, energy, and time, *J. Am. Soc. Mass Spec.*, Vol. 4, p. 524-535. (1993).

Feng, X., Bogan, M. J., and Agnes, G. R., Coulomb fission event resolved progeny droplet production from isolated evaporating methanol droplets, *Anal. Chem.*, Vol. 73, p. 4499-4507. (2001).

Finlayson-Pitts, B. J. and Hemminger, J. C., Physical chemistry of airborne sea salt particles and their components, *J. Phys. Chem. A*, Vol. 104, p. 11463-11477. (2000).

Fox, H. W., Hare, E. F., and Zisman, W. A., The spreading of liquids on low-energy surfaces. VI. Branched-chain monolayers, aromatic surfaces, and thin liquid films, *J. Colloid Sci*., Vol. 8, p. 194-203. (1953).

Fuzzi, S., Andreae, M. O., Huebert, B. J., Kulmala, M., Bond, T. C., Boy, M., Doherty, S. J., Guenther, A., Kanakidou, M., Kawamura, K., Kerminen, V.-M., Lohmann, U., Russell, L. M., and Poschl, U., Critical assessment of the current state of scientific knowledge, terminology, and the research needs concerning the role of organic aerosols in the atmosphere, climate, and global change, Atmos. Chem. Phys., Vol. 6, p. 2017-2038. (2006).

Gao, Y., Yu, L. E., and Chen, S. B., Theoretical investigation of substrate effect on deliquescence relative humidity of NaCl particles, *J. Phys. Chem. A*, Vol. 111, p. 633-639. (2007a).

Gao, Y., Yu, L. E., and Chen, S. B., Efflorescence relative humidity of mixed sodium chloride and sodium sulfate particles, *J. Phys. Chem. A*, Vol. 111, p. 10660-10666. (2007b).

Gao, Y., Chen, S. B., and Yu, L. E., Efflorescence relative humidity of airborne sodium chloride particles: A theoretical investigation, *Atmos. Environ*., Vol. 41, p. 2019-2023. (2007c).

Gao, Y., Yu, L. E., and Chen, S. B., Effects of organics on efflorescence relative humidity of ammonium sulfate or sodium chloride particles, *Atmos. Environ*., Vol. 42, p. 4433-4445. (2008).

Gibson, E. R., Gierlus, K. M., Hudson, P. K., and Grassian, V. H., Generation of internally mixed insoluble and soluble aerosol particles to investigate the impact of atmospheric aging and heterogeneous processing on the CCN activity of mineral dust aerosol, *Aerosol Sci. Technol*., Vol. 41, p. 914-924. (2007).

Giglio, E., Gervais, B., Rangama, J., Manil, B., Huber, B. A., Duft, D., Muller, R., Leisner, T., and Guet, C., Shape deformations of surface-charged microdroplets, *Phys. Rev. E.*, Vol. 77, 036319. (2008).

Gomez, A. and Tang, K., Charge and fission of droplets in electrostatic sprays, *Phys. Fluids*, Vol. 6, p. 404-414. (1994).

Grimm, R. L. and Beauchamp, J. L., Evaporation and discharge dynamics of highly charged droplets of heptane, octane, and p-xylene generated by electrospray ionization, *Anal. Chem.*, Vol. 74, p. 6291-6297. (2002).

Grimm, R. L. and Beauchamp, J. L., Dynamics of field-induced droplet ionization: Time resolved studies of distortion, jetting, and progeny formation from charged and neutral methanol droplets exposed to strong electric fields, *J. Phys. Chem. B*, Vol. 109, p. 8244-8250. (2005).

Gu, W., Singh, R., and Kim, K., Flow-limited field-injection electrostatic spraying for controlled formation of charged multiple jets of precursor solutions: Theory and application, *Appl. Phys. Lett.*, Vol. 87, 084107. (2005).

Gu, W., Heil, P. E., Choi, H., and Kim, K., Comprehensive model for fine Coulomb fission of liquid droplets charged to Rayleigh limit, *Appl. Phys. Lett.*, Vol. 91, 064104. (2007).

Guenther, A., Hewitt, C. N., Erickson, D., Fall, R., Geron, C., Graedel, T., Harley, P., Klinger, L., Lerdau, M., McKay, W. A., Pierce, T., Scholes, B., Steinbrecher, R., Tallamraju, R., Taylor, J., and Zimmerman, P., A global model of natural volatile organic compound emissions, *J. Geophys. Res*., Vol. 100, p. 8873-8892. (1995).

Gysel, M., Weingartner, E., and Baltensperger, U., Hygroscopicity of aerosol particles at low temperatures. 2. Theoretical and experimental hygroscopic properties of laboratory generated aerosols, *Environ. Sci. Technol*., Vol. 36, p. 63-68. (2002).

Hallum, J. V. and Drushel, H. V., The organic nature of carbon black surfaces, *J. Phys. Chem*., Vol. 62, p. 110-117. (1958).

Hamer, W. J. and Wu, Y.-C., Osmotic coefficients and mean activity coefficients of uni-univalent electrolytes in water at 25 C, *J. Phys. Chem. Ref. Data*, Vol. 1, p. 1047-1099. (1972).

Hameri, K., Rood, M., and Hansson, H.-C., Hygroscopic properties of a NaCl aerosol coated with organic compounds, *J. Aerosol. Sci*., Vol. 23, p. S437-S440. (1992).

Hameri, K., Charlson, R. J., Hansson, H.-C., and Jacobson, M., Hygroscopic properties of ammonium sulfate aerosols mixed with slightly soluble organic compound, *J. Aersol. Sci*., Vol. 28, p. S153-S154. (1997).

Hameri, K., Charlson, R. J., Hansson, H.-C., and Jacobson, M., Hygroscopic properties of ammonium sulfate aerosols mixed with slightly soluble organic compound, *J. Aersol. Sci*., Vol. 29, p. S587-S588. (1998).

Hameri, K., Charlson, R., and Hansson, H.-C., Hygroscopic properties of mixed ammonium sulfate and carboxylic acids, *AICHE Journal*, Vol. 48, p. 1309-1316. (2002).

Hansson, H.-C., Wiedensohler, A., Rood, M. J., and Covert, D. S., Experimental determination of the hygroscopic properties of organically coated aerosol particles, *J. Aerosol Sci*., Vol. 21, p. S241-244. (1990).

Hansson, H.-C., Rood, M. J., Koloutsou-Vakakis, S., Hameri, K., Orsini, D., and Wiedensohler, A., NaCl aerosol particle hygroscopicity dependence on mixing with organic compounds, *J. Atmos. Chem*., Vol. 31, p. 321-346. (1998).

Hartung, W. H. and Avedisian, C. T., On the electrodynamic balance, *Proc. Royal Soc. Lond. Ser. A-Math. Phys. Engin. Sci.*, Vol. 437, p. 237-266. (1992).

Hatch, C. D., Gierlus, K. M., Schuttlefield, J. D., and Grassian, V. H., Water adsorption and cloud condensation nuclei activity of calcite and calcite coated with model humic and fulvic acids, *Atmos. Environ*., Vol. 42, p. 5672-5684. (2008).

Hatch, C. D. and Grassian, V. H., 10th anniversary review: Applications of analytical techniques in laboratory studies of the chemical and climatic impacts of mineral dust aerosol in the Earth's atmosphere, *J. Environ. Monit*., Vol. 10., p. 919-934. (2008).

Haywood, J. M., Ramaswamy, V., and Soden, B. J., Tropospheric aerosol climate forcing in clear-sky satellite observations over the oceans, *Science*, Vol. 283, p. 1299-1303. (1999).

Henson, B. F., An adsorption model of insoluble particle activation: Application to black carbon, *J. Geophys. Res*., Vol. 112, D24S16. (2007).

Hines, R. L., Electrostatic ionization and spray painting, *J. Appl. Phys.*, Vol. 37, p. 2730-2736. (1966).

Hitzenberger, R., Berner, A., Dusek, U., and Alabashi, R., Humidity-dependent growth of size-segregated aerosol samples, *Aerosol Sci. Technol*., Vol. 27, p. 116-130. (1997).

Hobbs, P. V., Reid, J. S., Kotchenruther, R. A., Ferek, R. J., and Weiss, R., Direct radiative forcing by smoke from biomass burning, *Science*, Vol. 275, p. 1776-1778. (1997).

Hogan, C. J., Biswass, P., and Chen, D-r., Charged droplet dynamics in the submicrometer size range, *J. Phys. Chem. B*, Vol. 113, p. 970-976. (2009).

Huckaby, J. L. and Ray, A. K., Layer formation on microdroplets: A study based on resonant light scattering, *Langmuir*, Vol. 11, p. 80-86. (1995).

Huckaby, J. L., Ray, A. K., and Das, B., Determination of size, refractive index, and dispersion of single droplets from wavelength-dependent scattering spectra, *Appl. Optics*, Vol. 33, p. 7112-7125. (1994).

Hunter, H. C. and Ray, A. K., On progeny droplets emitted during Coulombic fission of charged microdrops, *Phys. Chem. Chem. Phys.*, Vol. 11, p. 6156-6165. (2009).

Iribarne, J. V. and Thomson, B. A., On the evaporation of small ions from charged droplets, *J. Chem. Phys.*, Vol. 64, p. 2287-2294. (1976).

Jacobson, M. C., Hansson, H.-C., Noone, K. J., and Charlson, R. J., Organic atmospheric aerosols: Review and state of the science, *Rev. Geophys*., Vol. 38, p. 267-294. (2000).

Johnson, B. R., Theory of morphology-dependent resonances: Shape resonances and width formulas, *J. Opt. Soc. Amer. A*, Vol. 10, p. 343-352. (1993).

Kanakidou, M., Seinfeld, J. H., Pandis, S. N., Barnes, I., Dentener, F. J., Facchini, M. C., Van Dingenen, R., Ervens, B., Nenes, A., Nielson, C. J., Swietlicki, E., Putaud, J. P., Balkanski, Y., Fuzzi, S., Horth, J., Moortgat, G. K., Winterhalter, R., Myhre, C. E. L., Tsigaridis, K., Vignati, E., Stephanou, E. G., and Wilson, J., Organic aerosol and global climate modeling: a review, *Atmos. Chem. Phys*., Vol. 5, p. 1053-1123. (2005).

Kerker, M., *The Scattering of Light and Other Electromagnetic Radiation,* Academic, New York. (1983).

Kohler, H., The nucleus in and the growth of hygroscopic droplets, *Trans. Farad. Soc.*, Vol. 32, p. 1152-1161. (1936).

Konermann, L., A simple model for the disintegration of highly charged solvent droplets during electrospray ionization, *J. Amer. Soc. Mass Spectrom.*, Vol. 20, p. 496-506. (2009).

Kramer, L,. Poschl, U., and Niessner, R., Microstructural rearrangement of sodium chloride condensation aerosol particles on interaction with water vapor, *J. Aerosol Sci*., Vol. 31, p. 673-685. (2000).

Kreidenweis, S. M., Petters, M. D., and DeMott, P. J., Single-parameter estimates of aerosol water content, *Environ. Res. Lett*., Vol. 3, 035002. (2008).

Kulmala, M., Korhonen, P., Vesala, T., Hansson, H.-C., Noone, K., and Svenningsson, B., The effect of hygroscopicity on cloud droplet formation, *Tellus*, Vol. 48B, p. 347-360. (1996).

Laaksonen, A., Korhonen, P., Kulmala, M., and Charlson, R. J., Modification of the Kohler equation to include soluble trace gases and slightly soluble substances, *J. Atmos. Sci*., Vol. 55, p. 853-862. (1998).

Labowsky, M., Discrete charge distributions in dielectric droplets, *J. Coll. Inter. Sci.*, Vol. 206, p. 19-28. (1998).

Labowsky, M., Fenn., J. B., and de la Mora, J. F., A continuum model for ion evaporation from a dropl: Effect of curvature and charge on ion salvation energy, *Anal. Chim. Acta*, Vol. 406, p. 105-118. (2000).

Lachiver, E. D., Abatzoglou, N., Cartilier, L., and Simard, J-S., Insights into the role of electrostatic forces on the behavior of dry pharmaceutical particulate systems, *Pharm. Res.*, Vol. 23, p. 997-1007. (2006).

Langsdorf. A., A continuously sensitive diffusion cloud chamber, *Rev. Sci. Instrum.* Vol. 10,p. 91-. (1939).

Latif, M. T., and Brimblecombe, P., Surfactants in atmospheric aerosols, *Environ. Sci. Technol*., Vol. 38, p. 6501-6506. (2004).

Lauk, C. and Erb, K-H., Biomass consumed in anthropogenic vegetation fires: Global patterns and processes, *Ecol. Econ.*, Vol. 69, p. 301-309. (2009).

Law, S. E., Agricultural electrostatic spray application: a review of significant research and development during the 20th century, *J. Electrostatics*, Vol. 51-52, p. 25-42. (2001).

Lehtinen, K. E. J., Kulmala, M., Ctyroky, P., Futschek, T., and Hitzenberger, R., Effect of electrolyte diffusion on the growth of NaCl particles by water vapour condensation, *J. Phys. Chem. A*, Vol. 107, p. 346-350. (2003).

Lenard, P., Ueber die electricitat der wasserfalle, *Ann. Phys. Chem.*, Vol. 282, p. 584-636. (1892).

Li, K-Y., Tu, H., and Ray, A. K., Charge limits on droplets during evaporation, *Langmuir*, Vol. 21, p. 3786-3794. (2005).

Li, K-Y. and Ray, A. K., Charge limits on evaporating droplets during precipitation of solutes, *J. Aerosol Sci.*, Vol. 35, p. S53-S54. (2004).

Lide, D. R., *Handbook of Chemistry and Physics 85th ed*., CRC press LCC, Boca Raton, Florida. (2004).

Lightstone, J. M., Onasch, T. B., Imre, D., and Oatis, S., Deliquescence, efflorescence, and water activity in ammonium nitrate and mixed ammonium nitrate/succinic acid microparticles, *J. Phys. Chem. A*, Vol. 104, p. 9337-9346. (2000).

Liu, Y. J., Zhu, T., Zhao, D. F., and Zhang, Z. F., Investigation of the hygroscopic properties of $Ca(NO_3)_2$ and internally mixed $Ca(NO_3)_2/CaCO_3$ particles by micro-Raman spectroscopy, *Atmos. Chem. Phys*., Vol. 8, p. 7205-7215. (2008).

Loscertales, I. G. and de la Mora, J. F., Experiments on the kinetics of field evaporation of small ions from droplets, *J. Chem. Phys.*, Vol. 103, p. 5041-5060. (1995).

Lomer, T. R., The crystal and molecular structure of lauric acid (Form A1), *Acta. Cryst*., Vol. 16, p. 984-988. (1963).

Lomer, T. R. and Spanswick, R. M., A new crystalline form of lauric acid, *Acta. Cryst*., Vol. 14, p. 312-313. (1961).

Lorenz, L.V., Lysvevaegelsen i og uden for en af plane lysbolger belyst kugle, *K. Dan. Vidensk. Selsk. Forh.*, Vol. 6, p. 1-62. (1890).

Macky, W. A., Some investigations on the deformation and breaking of eater drops in strong electric fields, *Proc. Royal. Soc. Lond. A*, Vol. 133, p. 565-587. (1931).

Maleki, N., Safavi, A., and Tajabadi, F., High-performance carbon composite electrode based on an ionic liquid as a binder, *Anal. Chem*., Vol. 78, p. 3820-3826. (2006).

Manil, B., Ntamack, G. E., Lebius, H., Huber, B. A., Duft, D., Leisner, T., Chandezon, F., and Guet, C., Charge emission and decay dynamics of highly charged clusters and micro-droplets, *Nuclear Instrum. Meth. Phys. Res. B*, Vol. 205, p. 684-689. (2003).

Marcolli, C. and Krieger, U. K., Phase changes during hygroscopic cycles of mixed organic/inorganic model systems of tropospheric aerosols, *J. Phys. Chem. A*, Vol. 110, 1881-1893. (2006).

Marcolli, C., Luo, B., and Peter, T., Mixing of the organic aerosol fractions: Liquids as the thermodynamically stable phases, *J. Phys. Chem. A*, Vol. 108, p. 2216-2224. (2004).

Martin, S. T., Phase transitions of aqueous atmospheric particles, *Chem. Rev*., Vol. 100, p. 3403-3453. (2000).

Maxwell, J. C., A dynamical theory of the electromagnetic field, *Phil. Trans. Royal Soc. Lond.*, Vol. 155, p. 459-512. (1865).

Mazumder, M. K. and Kirsch, K. J., Single-particle aerodynamic relaxation-time analyzer, *Rev. Sci. Instru.*, Vol. 48, p. 622-624. (1977).

Melcher, J. R. and Taylor, G. I., Electrohydrodynamics – A review of role of interfacial shear stresses, *Annu. Rev. Fluid Mech.*, Vol. 1, p. 111-146. (1969).

Mie, G., Beitrage zur optic truber medien speziell kolloidaler metallosungen, *Ann. Phys.*, Vol. 25, p. 377-445. (1908).

Mikhailov, E., Vlasenko, S., Niessner, R., and Poschl, U., Interaction of aerosol particles composed of protein and salts with water vapor: Hygroscopic growth and microsctructural rearrangement, *Atmos. Chem. Phys*., Vol. 4, p. 323-350. (2004).

Millikan, R. A., A new modification of the cloud method of determining the elementary electrical charge and the most probable value of that charge, *Phil. Mag. XIX*, Vol. 6, p. 209-228. (1910).

Minami, T., Mayama, H., and Tsujii, K., Spontaneous formation of super water-repellent fractal surfaces in mixed wax systems, *J. Phys. Chem. B*, Vol. 112, p. 14620-14627. (2008).

Ming, Y. and Russell, L. M., Predicted hygroscopic growth of sea salt aerosol, *J. Geophys. Res*., Vol. 106, p. 28259-28274. (2001).

Moore, R. H. and Raymond, T. M., HTDMA analysis of multicomponent dicarboxylic acid aerosols with comparison to UNIFAC and ZSR, *J. Geophys. Res*., Vol. 113, D04206. (2008).

Myland, J. C. and Oldham, K. B., Overcoming electroneutrality: concentrative and electrical conditions inside a charged droplet of electrolyte solution, *J. Electroanalytical Chem.*, Vol. 522, p. 115-123. (2002).

Nakajima, Y., A measuring system for the time variation of size and charge of a single spherical particle and its applications, *Chem. Engin. Sci.*, Vol. 61, p. 2212-2229. (2006).

Niedermeier, D., Wex, H., Voigtlander, J., Stratman, F., Bruggemann, E., Kiselev, A., Henk, A., and Heintzenberg, J., LACIS-measurements and parameterization of sea-salt particle hygroscopic growth and activation, *Atmos. Chem. Phys*., Vol. 8, p. 579-590. (2008).

Nietz, A. H., Molecular orientation at surfaces of solids I. Measurement of contact angle and the work of adhesion of organic substances for water, *J. Phys Chem*., Vol. 2, p. 255-269. (1928).

Nohmi, T. and Fenn, J. B., Electrospray mass-spectrometry of poly(ethylene glycols) with molecular-weights up to 5 million, *J. Am. Chem. Soc.*, Vol. 114, p. 3241-3246. (1992).

O'Reilly, J. M. and Mosher, R, A., Functional groups in carbon black by FTIR spectroscopy, *Carbon*, Vol. 21, p. 47-51. (1983).

Orr, C., Hurd, F. K., and Corbett, W. J., Aerosol size and relative humidity, *J. Colloid Sci*., Vol. 13, p. 472-482, (1958),

Otani, Y. and Wang, C. S., Growth and deposition of saline droplets covered with a monolayer of surfactant, *Aerosol Sci. Technol*., Vol. 3, p. 155-66. (1984).

Parsons, M. T., Knopf, D. A., and Bertram, A. K., Deliquescence and crystallization of ammonium sulfate particles internally mixed with water-soluble organic compounds, *J. Phys. Chem. A*, Vol. 108, p. 11600-11608. (2004).

Paul, W. and Raether, M., Das elektrische massenfilter, *Zeitschrift fur Physik*, Vol. 140, p. 448-450. (1955).

Paul, W. and Steinwedel, H., Ein neues massenspektrometer ohne magnetfeld, *Zeitschrift fur Naturforschung Sec. A, J. Phys. Sci*., Vol. 8, p. 448-450. (1953).

Peng, C. and Chan, C. K., The water cycles of water-soluble organic salts of atmospheric importance, *Atmos. Environ*., Vol. 35, p. 1183-1192. (2001).

Peng, C., Chan, M. N., and Chan, C. K., The hygroscopic properties of dicarboxylic and multifunctional acids: Measurements and UNIFAC predictions, *Environ. Sci. Technol*., Vol. 35, p. 4495-4501. (2001a).

Peng, C., Chow, A. H. L., and Chan, C. K., Hygroscopic study of glucose, citric acid, and sorbitol using an electrodynamic balance: Comparison with UNIFAC predictions, *Aersosol Sci. Technol*., Vol. 35, p. 753-758. (2001b).

Petters, M. D. and Kreidenweis, S. M., A single parameter representation of hygroscopic growth and cloud condensation nucleus activity, *Atmos. Chem. Phys*., Vol. 8, p. 1961-1971. (2007).

Petters, M. D. and Kreidenweis, S. M., A single parameter representation of hygroscopic growth and cloud condensation nucleus activity – Part 2: Including solubility, *Atmos. Chem. Phys*., Vol. 8, p. 6273-6279. (2008).

Pfeifer, R. J. and Hendricks, C. D., Charge-to-mass relationships for electrohydrodynamically sprayed liquid droplets, *Phys. Fluids,* Vol. 10, p. 2149-2154. (1967).

Pilinis, C., Pandis, S. N., and Seinfeld, J. H., Sensitivity of direct climate forcing by atmospheric aerosols to aerosol-size and composition, *J. Geophys. Res.-Atmos.,* Vol. 100, p. 18739-18754. (1995)

Posfai, M., Anderson, J. R., and Buseck, P. R., Soot and sulfate aerosol particles in the remote marine troposphere, *J. Geophys. Res.*, Vol. 104, p. 21685-21693. (1999).

Posfai, M., Gelencser, A., Simonics, R., Arrato, K., Li, J., Hobbs, P. V., and Buseck, P. R., Atmospheric tar balls: Particles from biomass and biofuel burning, *J. Geophys. Res*., Vol. 109, D06213. (2004).

Prather, K. A., Hatch, C. D., and Grassian, V. H., Analysis of atmospheric aerosols, *Annu. Rev. Anal. Chem*., Vol. 1, p. 485-514. (2008).

Prenni, A. J, DeMott, P. J., and Kreidenweis, S. M., Water uptake of internally mixed particles containing ammonium sulfate and dicarboxylic acids, *Atmos. Environ*. Vol. 37, p. 4243-4251. (2003).

Probert-Jones, J. R., Resonance component of backscattering by large dielectric spheres, *J. Opt. Soc. Amer. A*, Vol. 1, p. 823-830. (1984).

Raes, F., Van Dingenen, R. V., Vignatti, E., Wilson, J., Putaud, J., Seinfeld, J. H., and Adams, P., Formation and cycling of aerosols in the global troposphere, *Atmos. Environ*., Vol. 34, p. 4215-4240. (2000).

Ramanathan, V., Crutzen, P. J., Kiehl, J. T., and Rosenfeld, D., Aerosols, climate, and the hydrological cycle, *Science*, Vol. 294, p. 2119-2124. (2001).

Randles, C. A., Russell, L. M., and Ramaswamy, V., Hygroscopic and optical properties of organic sea salt aerosol and consequences for climate forcing, *Geophys. Res. Lett*., Vol. 31, L16108, (2004).

Ray, A. K. and Huckaby, J. L., Absorption of sparingly soluble vapor in microdroplets: A study based on light scattering, *Langmuir*, vol. 9, p. 2225-2231. (1993).

Ray, A. K. and Nandakumar, R., Simultaneous determination of size and wavelength-dependent refractive indices of thin-layered droplets from optical resonances, *Appl. Opt.*, Vol. 34, p. 7759-7770. (1995).

Ray, A. K., Souyri, A., Davis, E. J., and Allen, T. M., Precision of light scattering techniques for measuring optical parameters of microspheres, *Appl. Opt.*, Vol. 30, p. 3974-3983. (1991).

Rayleigh, J. W. S., *The Theory of Sound*, Dover Pub., New York. (1945).

Rayleigh, L., On the equilibrium of liquid conducting masses charged with electricity, *Pli. Mag. Ser. 5*, Vol. 14, p. 184-86. (1882).

Raymond, T. M. and Pandis, S. N., Formation of cloud droplets by multicomponent organic particles, *J. Geophys. Res*., Vol. 108, JD003503. (2003).

Renninger, R. G., Mazumder, M. K., and Testerman, M. K., Particle sizing by electrical single-particle aerodynamic relaxation-time analyzer, *Rev. Sci. Instru.*, Vol. 52, p. 242-246. (1981).

Richardson, C. B., Pigg, A. L., and Hightower, R. L., On the stability of charged droplets, *Proc. Royal Soc. Lond. A*, Vol. 422, p. 319-328. (1989).

Robertson, J. M., The crystalline structure of anthracene. A quantitive x-ray investigation, *Proc. Royal Soc. London A*, Vol. 140, p. 79-98. (1933).

Robinson, R. A. and Stokes, R. H., Tables of osmotic and activity coefficients of electrolytes in aqueous solutions at 25-degrees-C, *Tran. Farad. Soc.*, Vol. 45, p. 612-624. (1949).

Rohner, T. C., Lion, N., and Girault, H. H., Electrochemical and theoretical aspects of electrospray ionization, *Phys. Chem. Chem. Phys.*, Vol. 6, p. 3056-3068. (2004).

Rollgen, F. W., Bramer-Weger, E., and Butfering, L., Field ion emission from liquid solutions: Ion evaporation against electrohydrodynamic disintegration, *J. Phys. Coll. 6*, Vol. 48, p. 253-254. (1987).

Roulleau, M . and Desbois, M., Study of evaporation and instability of charged water droplets, *J. Atmos. Sci.*, Vol. 29, p. 565-569. (1972).

Rosenoern, T., Schlenker, J. C., and Martin, S. T., Hygroscopic growth of multicomponent aerosol particles influenced by several cycles of relative humidity, *J. Phys. Chem. A*, Vol. 112, p. 2378-2385. (2008).

Roth, D. G. and Kelly, A. J., Analysis of the disruption of evaporating charged droplets, *IEEE Trans. Ind. Appl.*, Vol. 19, p. 771-775. (1983).

Rubel, G. O. and Gentry, J. W., Measurement of the kinetics of solution droplets in the presence of adsorbed monolayers: Determination of water accommodation coefficients, *J. Phys. Chem*, Vol. 88, p. 3142-3148. (1984).

Ryce, S. A. and Wyman, R. R., Two sphere model for the asymmetric division of electrically charged liquid drops, *Can. J. Phys.*, Vol. 48, p. 2571-2576. (1970).

Saxena, P., and Hildemann, L. M., Water-soluble organics in atmospheric particles: a critical review of the literature and application of thermodynamics to identify candidate compounds, *J. Atmos. Chem*., Vol. 24, p. 57-109. (1996).

Saxena, P., Hildemann, L. M., McMurry, P. H., and Seinfeld, J. H., Organics alter hygroscopic behavior of atmospheric particles, *J. Geophys. Res*., Vol. 100, p. 18755-18770. (1995).

Schmelzeisen-Redeker, G., Butfering, L., and Rollgen, F. W., Desolvation of ions and molecules in thermospray mass spectrometry, *Int. Journal. Mass Spec. Ion Proc.*, Vol. 90, p. 139-150. (1989).

Semeniuk, T. A., Wise, M. E., Martin, S. T., Russell, L. M., and Buseck, P. R., Water uptake characteristics of individual atmospheric particles having coatings, *Atmos. Environ*., Vol. 41, p. 6225-6235. (2007a).

Semeniuk, T. A., Wise, M. E., Martin, S. T., Russell, L. M., Buseck, P. R., Hygroscopic behavior of aerosol particles from biomass fires using environmental transmission electron microscopy, J. *Atmos. Chem*., Vol. 56, p. 259-273. (2007b).

Shrimpton, J. S., Dielectric charged drop break-up at sub-Rayleigh limit conditions, *IEEE Trans. Dielectrics Elec. Insul.*, Vol. 12, p. 573-578. (2005).

Sjogren, S., Gysel, M., Weingartner, E., Baltensperger, U., Cubison, M. J., Coe, H., Zardini, A. A., Marcolli, C., Krieger, U. K., and Peter, T., Hygroscopic growth and water uptake kinetics of two-phase aerosol particles consiting of ammonium sulfate, adipic and humic acid mixtures, *Aerosol Sci*., Vol. 38, p. 151-171. (2007).

Smith, J. N., Flagan, R, C., and Beauchamp, J. L., Droplet evaporation and discharge dynamics in electrospray ionization, *J. Phys. Chem. A*, Vol. 106, p. 9957-9967. (2002).

Stephan, K., Krauss, R., and Laesecke, A., Viscosity and thermal conductivity of nitrogen for a wide range of fluid states, *J. Phys. Chem. Ref. Data*, Vol. 16, p. 993-1023. (1987).

Stokes, R. H. and Robinson, R. A., Standard solutions for humidity control at 25-degrees C, *Ind. Engin. Chem.*, Vol. 41, p. 2013-2013. (1949).

Stokes, R. H. and Robinson, R. A., Interactions in aqueous nonelectrolyte solutions. 1. Solute-solvent equilibria, *J. Phys. Chem.*, Vol. 70, p. 2126-2131. (1966).

Stokes, R. H. and Robinson, R. A., Solvation equilibria in very concentrated electrolyte solutions, *J. Sol. Chem.*, Vol. 2, p. 173-184. (1973).

Storozhev, V. B., Electrostatic field and charge distribution in small charged dielectric droplets, *J. Nanoparticle Res.*, Vol. 6, p. 383-393. (2004).

Storozhev, V. B. and Nikolaev, E, N., Computer simulations of the fission process of charged nanometre droplets, *Philos. Mag.*, Vol. 11, p. 157-171. (2004).

Studebaker, M. L. and Snow, C. W., The influence of ultimate composition upon the wettability of carbon blacks, *J. Phys. Chem*., Vol. 59, p. 973-976. (1955)

Svenningsson, B., Rissler, J., Swietlicki, E., Mircea, M., Bilde, M., Facchini, M. C., Decesari, S., Fuzzi, S., Zhou, J., Monster, J., and Rosenorn, T., Hygroscopic growth and critical supersaturations for mixed aerosol particles of inorganic and organic compounds of atmospheric relevance, *Atmos. Chem. Phys*., Vol. 6, p. 1937-1952. (2006).

Swietlicki, E., Hansonn, H.-C., Hameri, K., Svenningsson, B., Massling, A., McFiggans, G., McMurry, P. H., Petaja, T., Tunved, P., Gysel, M., Topping, D., Weingartner, E., Baltensperger, U., Rissler, J., Wiedensohler, A., and Kulmala, M., Hygroscopic properties of submicrometer atmospheric aerosol particles measured with H-TDMA instruments in various environments – a review, *Tellus*, Vol. 60B, p. 432-469. (2008).

Taflin, D. C., Ward, T. L., and Davis, E. J., Electrified droplet fission and the Rayleigh limit, *Langmuir*, Vol. 5, p. 376-384. (1989).

Taflin, D. C., Zhang, S. H., Allen, T., and Davis, E. J., Measurement of droplet interfacial phenomena by light-scattering techniques, *AIChE Journal*, Vol. 34, p. 1310-1320. (1988).

Takahama, S., Pathak, R. K., and Pandis, S. N., Efflorescence transitions of ammonium sulfate particles coated with secondary organic aerosol, *Environ. Sci. Technol*., Vol. 41, p. 2289-2295. (2007).

Tang, I. N., Phase transformation and growth of aerosol particles composed of mixed salts, *J. Aerosol Sci*., Vol. 7, p. 361-371. (1976).

Tang, I. N. and Munkelwitz, H. R., An investigation of solute nucleation in levitated solution droplets, *J. Coll. Inter. Sci.*, Vol. 98, p. 430-438. (1984).

Tang, I. N. and Munkelwitz, H. R., Composition and temperature dependence of the deliquescence properties of hygroscopic aerosols, *Atmos. Environ*., Vol. 27A, p. 467-473. (1993).

Tang, I. N. and Munkelwitz, H. R., Aerosol phase transformation and growth in the atmosphere, *J. Appl. Meteor*., Vol. 33, p. 791-796. (1994).

Tang, I. N., Munkelwitz, H. R., and Davis, J. G., Aerosol growth studies – IV. Phase transformation of mixed salt aerosols in a moist atmosphere, *J. Aerosol Sci.*, Vol. 9, p. 505-511. (1978).

Tang, I. N., Munkelwitz, H. R., and Wang, N., Water activity measurements with single suspended droplets: The NaCl-H2O and KCl-H2O systems, *J. Colloid Interface Sci*., Vol. 114, p. 409-415. (1986).

Tang, K. and Smith, R. D., Theoretical prediction of charged droplet evaporation and fission in electrospray ionization, *Inter. Journal Mass Spec.*, Vol. 185-187, p. 97-105. (1999).

Taylor, G., Disintegration of water drops in an electric field, *Proc. Roy. Soc. Lond. A*, Vol. 280, p. 383-397. (1964).

Taylor, G., Studies in electrohydrodynamics. I. Circulation produced in a drop by an electric field, *Proc. Royal Soc. Lond. A-Math. Phys. Sci.*, Vol. 291, p. 159-166. (1966).

Taylor, G., Electrically driven jets, *Proc. Royal Soc. Lond. A-Math. Phys. Sci.*, Vol. 313, p. 453-475. (1969).

Tsamopoulos, J. A., Akylas, T. R., and Brown, R. A., Dynamics of charged drop break-up, *Proc. Royal Soc. Lond. A*, Vol. 401, p. 67-88. (1985).

Tu, H. H., *Application of Light Scattering in Studies of Transport, Thermodynamics, Light Adsorption and Electrical Properties of Single Droplets*, PhD thesis, University of Kentucky, (2000).

Tu, H. and Ray, Analysis of time-dependent scattering spectra for studying processes associated with microdroplets, *Appl. Opt*., Vol. 40, p. 2522-2534. (2001).

Tu, H., and Ray, A. K., Measurement of activity coefficients from unsteady state evaporation and growth of microdroplets, *Chem. Eng. Comm.*, Vol. 192, p. 474-498. (2005).

Vand, V., Morley, W. M., and Lomer, T. R., The crystal structure of lauric acid, Acta Cryst., Vol. 4, p. 324-329. (1951).

van de Hulst, H. C., *Light Scattering by Small Particles,* Dover, New York. (1981).

Weingartner, E., Baltensperger, U., and Burtscher, H., Growth and structural change of combustion aerosols at high relative humidity, *Environ. Sci., Technol*., Vol. 29, p. 2982-2986. (1995).

Weingartner, E., Burtscher, H., and Baltensperger, U., Hygroscopic properties of carbon and diesel soot particles, *Atmos. Environ*., Vol. 31, p. 2311-2327. (1997).

Wex, H., Stratman, F., Hennig, T., Hartmann, S., Niedermeier, D., Nilsson, E., Ocskay, R., Rose, D., Salma, I., and Ziese, M., Connecting hygroscopic growth at high humidities to cloud activation for different particle types, *Environ. Res. Lett*., Vol. 3, 035004. (2009).

Wexler, A. S. and Seinfeld, J. H., Second-generation inorganic aerosol model, *Atmos. Environ*., Vol. 25A, p. 2731-2748. (1991).

Widmann, J. F., Aardahl, C. L., and Davis, E. J., Observations of non-Rayleigh limit explosions of electrodynamically levitated microdroplets, *Aerosol Sci. Technol.*, Vol. 27, p. 636-648. (1997).

Wise, M. E., Biskos, G., Martin, S. T., Russell, L. M., and Buseck, P. R., Phase transitions of single salt particles studied using a transmission electron microscope with an environmental cell, *Aerosol Sci. Technol*. Vol. 39, p. 849-856. (2005).

Wise, M. E., Semeniuk, T. A., Bruintjes, R., Martin, S. T., Russell, L. M., and Buseck, P. R., Hygroscopic behavior of NaCl-bearing natural aerosol particles using environmental transmission electron microscopy, *J. Geophys. Res*., Vol. 112, D10224. (2007).

Wise, M. E., Martin, S. T., Russell, L. M., and Buseck, P. R., Water uptake by NaCl particles prior to deliquescence and the phase rule, *Aerosol Sci. Technol*., Vol. 42, p. 281-294. (2008).

Woods, E., Kim, H. S., Wivagg, C. N., Dotson, S. J., Broekhuizen, K. E., and Frohardt, E. F., Phase transitions and surface morphology of surfactant-coated aerosol particles, *J. Phys. Chem. A*, Vol. 111, p. 11013-11020. (2007).

Xiong, J. Q., Zhong, M., Fang, C., Chen, L. C., and Lippmann, M., Influence of organic films on the hygroscopicity of ultrafine sulfuric acid aerosol, *Environ. Sci. Technol*., Vol. 32, p. 3536-3541. (1998).

Zardini, A. A., Sjogren, S., Marcolli, C., Krieger, U. K., Gysel, M., Weingartner, E., Baltensperger, U., and Peter, T., A combined particle trap/HTDMA hygroscopy study of mixed inorganic/organic aerosol particles, Atmos. *Chem. Phys. Discuss*., Vol. 8, p. 5235-5268. (2008).

Zdanovskii, A. B., Novyi metod rascheta rastvorimostei elektrolitov v mnogokomponentnykh sistemakh. 1., *Zhurnal Fizicheskoi Khimii*, Vol. 22, p. 1478-1485. (1948a).

Zdanovskii, A. B., Novyi metod rascheta rastvorimostei elektrolitov v mnogokomponentnykh sistemakh. 2., *Zhurnal Fizicheskoi Khimii*, Vol. 22, p. 1486-1495. (1948b).

Zhou, S. and Cook, K. D., A mechanistic study of electrospray mass spectrometry: Charge gradients within electrospray droplets and their influence on ion response, *J. Am. Soc. Mass Spectrom.*, Vol. 12, p. 206-214. (2001).

Zhu, W., Miser, D. E., Chan, G., and Hajaligol, M. R., HRTEM investigation of some commercially available furnace carbon blacks, *Carbon*, Vol. 42, p. 1841-1845. (2004).

VITA

Harry Cook Hunter, III was born on May 28, 1975 in Elizabethtown, Kentucky. He received the Bachelor of Science degree in Chemical Engineering in May of 2005 at the University of Kentucky in Lexington, Kentucky. In May of 2005, he began his pursuit of a Doctorate of Philosophy in Chemical Engineering at the University of Kentucky.

Harry Cook Hunter, III